Characterisation of Inflammasome-Induced Extracellular Vesicles, Their Uptake by and Effect on Bystander Cells

Lena Standke

ORCID ID:

0000-0003-3113-125X

from Bergisch Gladbach, Germany

Submitted in total fulfilment of the requirements of the joint degree of Doctor of Philosophy (PhD)

of

The Medical Faculty

The Rheinische Friedrich-Wilhelms-Universität Bonn

and

The Department of Microbiology and Immunology

The University of Melbourne

Bonn/Melbourne, 2023

Performed and approved by The Medical Faculty of The Rheinische Friedrich-Wilhelms-Universität Bonn and The University of Melbourne

1. Supervisor: Prof. Dr. Eicke Latz
2. Supervisor: Prof. Dr. Paul Hertzog
Co-Supervisor: Prof. Dr. Sammy Bedoui

Month and year of the original thesis submission: 03/2023
Month and year of the oral examination: 12/2023

Institute in Bonn: Institute of Innate Immunity
Directors: Prof. Dr. Eicke Latz
Prof. Dr. Felix Meissner
Prof. Dr. Dagmar Wachten

Table of Contents

Abbreviations

°C	degree Celsius
10KL	10K EVs from LPS treated cells
10KLN	10K EVs from LPS and nigericin treated cells
2KL	2K EVs from LPS treated cells
2KLN	2K EVs from LPS and nigericin treated cells
Å	angstrom (1 Å = 10^{-10} m)
ACTB	actin beta
adj.	adjusted
AEC	alveolar epithelial cell
AIM2	absent in melanoma 2
ALI	air-liquid interface
ALR	absent in melanoma 2 (AIM2)-like receptor
AMP	adenosine monophosphate
ampi	ampicillin
AP-1	activator protein 1
APOA1	apolipoprotein A-I
APOB	apolipoprotein B
Appli	application
ASC	apoptosis-associated speck-like protein containing a CARD
ATP	adenosine triphosphate
avg.	average
Aβ	amyloid-β
Bact Resis	bacterial resistance
BALF	bronchoalveolar lavage fluid
BCR	B cell receptor
BEGM	bronchial epithelial cell growth medium
Blast	blasticidin
BSA	bovine serum albumin
CA2	carbonic-anhydrase 2
Ca^{2+}	calcium ion

CANX	calnexin
CAPS	cryopyrin-associated periodic syndromes
CARD	carboxy-terminal caspase activation and recruitment domain
CC	coiled-coil
CCL	C-C motif chemokine ligand
CD	cluster of differentiation
cDNA	complementary DNA
CFSE	carboxyfluorescein diacetate succinimidyl ester (CFDA-SE)
CFTR	cystic fibrosis transmembrane conductance regulator
CLR	C-type lectin receptor
CMV	cytomegalovirus
CO_2	carbon dioxide
CoA	coenzyme A
COPD	chronic obstructive pulmonary disease
CRID3	cytokine release inhibitory drug 3
CRP	C-reactive protein
CS	cigarette smoke
CSF	colony stimulating factor
CVD	cardiovascular disease
CXCL	C-X-C motif chemokine ligand
DALYs	disability-adjusted life years
DAMP	danger-associated molecular pattern
DC	dendritic cell
DD	death domain
DE	differentially expressed
DMEM	Dulbecco's Modified Eagle Medium
DMSO	dimethyl sulfoxide
DNA	deoxyribonucleic acid
dsDNA	double stranded DNA
DTT	dithiothreitol
e.g.	*exempli gratia* (for example)
EBM-2	Endothelial Basal Medium-2

ECM	extracellular matrix
EDTA	ethylenediaminetetraacetic acid
EGFP	enhanced green fluorescent protein
EGM-2	Endothelial Growth Medium-2
ER MCS	ER membrane contact site
ERK	extracellular signal-regulated kinase
ESCRT	endosomal sorting complexes required for transport
Euk Resis	eukaryotic resistance
EV	extracellular vesicle
EVL	EVs from LPS treated cells
EVLN	EVs from LPS and nigericin treated cells
FACS	fluorescence-activated cell sorting
FADD	Fas-associated protein with death domain
FBS	foetal bovine serum
FCAS	familial cold autoinflammatory syndrome
FDR	False Discovery Rate
FGM-2	Fibroblast Growth Medium-2
fw	forward
g	gram (for weight), gravitational constant (for centrifugal force)
GlcNAc	N-acetylglucosamine
GM3	monosialodihexosyl ganglioside
GO	gene ontology
GSDMD	gasdermin D
GTP	guanosine-5'-triphosphate
h	hour
H^+	hydrogen ion
H3	histone group H3
HAMP	homeostasis-altering molecular process
HCO_3^-	bicarbonate
HDL	high-density lipoprotein
HEK293T	human embryonic kidney cell line; immortalised with the SV40 large T antigen

HIV	human immunodeficiency virus
HMGB1	high mobility group box 1
HSP	heat shock protein
HTA	human transcriptome array
HTRF	homogeneous time resolved fluorescence
HUVEC	human umbilical vein endothelial cells
ICAM1	intercellular adhesion molecule 1
IDL	intermediate density lipoprotein
IFIT	Interferon Induced Protein With Tetratricopeptide Repeats
IFN	interferon
IFNAR	IFN-α/β receptor
III	Institute of Innate Immunity
IL	interleukin
IL-18BP	IL-18 binding protein
IL-1R	IL-1 receptor
IL-1RA	IL-1 receptor antagonist
IL-1RAP	IL-1 receptor accessory protein
IL-18Ra	IL-18 alpha chain
IL-18Rβ	IL-18 beta chain
ILC	innate lymphoid cell
ILV	intraluminal vesicle
IRF	interferon regulatory factor
ISEV	International Society for Extracellular Vesicles
ISG	interferon-stimulated gene
JNK	c-Jun N-terminal kinase
K^+	potassium ion
l	litre
LB	Luria-Bertani
LDL	low-density lipoprotein
LDL-R	LDL receptor
LDS	lithium dodecyl sulphate
lfc	$\log_2$ fold change threshold

log_2CPM	log_2-counts per million
log_2FC	log_2 fold change
LPS	lipopolysaccharide
LRR	leucine-rich repeat
M	molar
m	metre
MAPK	mitogen-activated protein kinase
MD	mean-difference plot, also known as MA plot
MDS	multidimensional scaling
MHC	major histocompatibility complex
min	minute
miRNA	microRNA
MISEV	minimal information for studies of extracellular vesicles
mito-SEP	mitochondrially localised sORF-encoded peptides
MMP	matrix metalloproteinase
MOCCI	modulator of cytochrome C oxidase during inflammation
mRNA	messenger RNA
MSigDB	Molecular Signature Database
mtDNA	mitochondrial DNA
mTORC1	mechanistic target of rapamycin complex 1
MUC	mucin
MVB	multivesicular body
MW	molecular weight
MWS	Muckle-Wells syndrome
MyD88	myeloid differentiation primary response 88
MX1	MX Dynamin Like GTPase 1
MΦ	macrophage
n.a.	not applicable
Na^+	sodium ion
NBD	nucleotide-binding domain
NCD	non communicable disease
NET	neutrophil extracellular trap

NETosis	NET-based cell death
NF-κB	nuclear factor kappa B
NHBEC	normal human bronchial epithelial cells
NHLFs	normal human lung fibroblasts
Nig	nigericin
NK	natural killer
NLR	nucleotide-binding domain, LRR-containing receptor
NLRC	NLR family CARD domain containing
NLRP	NACHT, LRR and PYD domains-containing
NLuc	nano luciferase
NO	nitric oxide
NOMID	neonatal-onset multisystem inflammatory disorder
ns	not significant
NSCLC	non-small cell lung cancer
NTA	nanoparticle tracking analysis
OAS2	2'-5'-Oligoadenylate Synthetase 2
OPN	osteopontin
$P2X_7$	P2X purinoreceptor 7
PAMP	pathogen-associated molecular pattern
PBMC	peripheral blood mononuclear cell
PBS	phosphate-buffered saline
PCR	polymerase chain reaction
PFA	paraformaldehyde
PGK	phosphoglycerate kinase
PI3K	Phosphoinositide 3-kinase
PIP2	phosphatidylinositol 4,5-bisphosphate
PIT	pore-induced intracellular trap
PMA	phorbol 12-myristate-13-acetate
PRR	pattern recognition receptor
puro	puromycin
PVDF	polyvinylidene difluoride
PYD	pyrin domain

rev	reverse
RIG-I	retinoic acid-inducible gene I
RIPA	radioimmunoprecipitation assay buffer
RIPK	kinase receptor-interacting serine/threonine-protein kinase
RLR	RIG-I-like receptor
RMA	robust multichip average algorithm
RNA	ribonucleic acid
ROS	reactive oxygen species
RPMI	Roswell Park Memorial Institute
RSAD2	Radical S-Adenosyl Methionine Domain Containing 2
s	second
S100A9	S100 calcium-binding protein A9
SD	standard deviation
SDS	sodium dodecyl sulphate
SEC	size-exclusion chromatography
SECL	SEC EVs from LPS treated cells
SECLN	SEC EVs from LPS and nigericin treated cells
SELE	Selectin E
SLE	systemic lupus erythematosus
SLR	sequestosome 1-like receptor
SOD2	superoxide dismutase 2
sORF	small open reading frame
SP	surfactant protein
STAT	signal transducer and activator of transcription
TAE	tris-acetate-EDTA
TBS	tris-buffered saline
TBST	tris-buffered saline with 0.1% Tween 20 detergent
TCA	tricarboxylic acid
TCR	T cell receptor
td	tandem dimer
TGF-β	transforming growth factor beta
T_H1	T helper type 1

T_H2	T helper type 2
TIR	Toll/IL-1 receptor homology
TLR	toll-like receptor
TMM	trimmed mean of M-values
TNF	tumour necrosis factor
TRIF	TIR-domain-containing adaptor inducing interferon-β
tRNA	transfer RNA
TSG101	tumour susceptibility 101
TUBB	tubulin beta class I
TWIK2	two-pore domain K^+ channel (K_{2P})
UC	ultracentrifuge
v	version
VCAM-1	Vascular Cell Adhesion Molecule 1
vs	*versus* (against or in contrast to)
VIM	vimentin
VLDL	very low density lipoprotein
vWF	von Willebrand factor
WCL	whole cell lysate
wt	wild type
WTA	whole transcriptome amplification

List of Tables

List of Figures

Abstract

Inflammasomes are multimeric complexes whose activation triggers caspase-1 cleavage resulting in processing of the cytokines interleukin (IL)-1β and IL-18, and the pore-forming protein gasdermin D. This, in turn, initiates programmed inflammatory cell death (pyroptosis). However, even in the absence of IL-1β and IL-18 signalling, inflammation develops, pointing towards the importance of other factors released upon inflammasome activation, such as activated inflammasome itself or extracellular vesicles (EVs). We therefore hypothesised that EVs enhance the paracrine inflammatory effects of inflammasome-activated cells.

To investigate this, we isolated EVs from inflammasome-activated cells using differential centrifugation and size-exclusion chromatography. We next analysed the ribonucleic acid (RNA) and protein content of EVs and investigated their uptake by and their effect on different bystander cells.

Our results show that EV secretion is increased in macrophages stimulated with inflammasome activators relative to controls. Inflammasome-elicited EVs can be identified by the presence of N-terminal gasdermin D, as well as by their distinct RNA signatures. Thus, they have the potential to be used as biomarkers in clinical settings.

EVs can exert their effects over long distances and may therefore contribute to the propagation of inflammatory signals from one part of the body to cells at distant sites. We could show that inflammasome-elicited EVs are taken up by diverse recipient cells, including macrophages, endothelial cells, epithelial cells, fibroblasts, and T cells (primarily activated T cells). We then used transcriptomics to determine the effect of inflammasome-elicited EVs on these recipient cells. They for example induced inflammatory gene sets in endothelial cells and led to the upregulation of marker genes of activated endothelium, including adhesion molecules, which are known to facilitate the attachment and tissue invasion of immune cells. Upon interaction with fibroblasts EVs have the potential to induce inflammatory signalling, further propagating inflammation. Gene sets such as

interferon (IFN)-α/-γ, and tumour necrosis factor (TNF)-α signalling were enriched in these cells.

Taken together, these findings indicate that EVs may not only serve as diagnostic markers for inflammatory disease, but also play an important role in the systemic response towards inflammasome activation.

Acknowledgements

This work would not have been possible without the kindness and support of so many people that I have had the privilege to meet along the way. I have spent quite a while thinking about the best way to acknowledge everyone and express my thankfulness. In the end, the most appropriate way seems to be to work my way through the last years chronologically, which leads me to start with my family.

I would like to thank my siblings, and especially my sister **Julia Standke**. You have always looked out for your bigger sister and are always there for me. There are not many people with whom I can talk so openly. I would also like to thank my parents **Renate Standke-Nissen** and **Olaf Standke** as well as my stepparents **Hans-Georg Nissen** and **Bauke van der Velden**. Mom, you have taught me to believe in myself, to always strive for the best, and be empathetic. Dad, you have taught me to be independent, to stand up for myself and be persistent. All these traits helped me during my PhD. The four of you have enabled me to the point of doing a PhD in the first place, supporting me all the way through. This also included supporting me when I came to you and told you that I wanted to pursue an exchange year during high school.

Living abroad not only teaches one a lot about oneself; it also provides opportunities that would not have existed otherwise. For me, one of these opportunities was taking my first Biomedical Science class with Lynne Coté at Mountain View High School in Arizona, USA. I can truly say that it has been because of this class and the most amazing and inspiring teacher, **Lynne Coté**, that I decided to become a Scientist in the first place.

Coming home after this adventure I met a very special person—my fiancé **Alexander Schuy**. I can truly say that he is the most supportive and amazing partner I could have ever asked for and I feel truly blessed to have met him this early in my life. Not only did he decide to move to Rheinbach with me, but he also supported me throughout all these years—from my bachelor to my master studies and throughout my PhD. Thank you so much for being the most supportive and loving partner I could have asked for. For being such a caring, empathetic, understanding, and entertaining person, for being the best travel buddy ever, the

best deal finder, technician, and de-escalator/mediator, for being my partner and at the same time my best friend.

Through meeting Alex, I was lucky enough to become part of his family and to meet his mom **Claudia Schuy-Rohnke**. Thank you so much for welcoming me into your life, for always supporting us, and for being the best mother-in-law (well, soon) ever!

This brings me to some other very important people in my life—**Sandra Schröder**, **Katrin Ciupka**, **Carina Beuck**, and **Charlotte Hunkler**. Having met Sandra during high school, she has been one of my best friends ever since. Thank you so much for all the support throughout these years, the adventures we have had together (it's just a small hill!), your ability to always stay in contact, your SMS support, and your support when it came to getting that partner visa—those words meant a lot to me (and Alex). Along those lines I also want to thank Katrin, Carina, and Charlotte. We have met during our Bachelor studies and been friends ever since. Thank you so much for the amazing trip around Scotland, for being an amazing flatmate, Katrin, for all those "group therapy" calls, dinners, sleepovers, and brunches!

This, finally, brings me to my master's and the beginning of my PhD and to thanking **Dr. Tomasz Prochnicki**. Tom has been the one introducing me to the Institute of Innate Immunity and Eicke's group. He definitely is one of the smartest people I have ever met and has been a great mentor. Thank you, Tom, for introducing me to how science really works, for teaching me how to come up with a hypothesis, plan experiments, and present everything in a structured way. Thank you for supervising me during my lab rotation and my master's thesis, and for allowing me to be part of your project. At this point, I also want to thank **Dr. Verena von Born**. While I was still early in my career, just thankful to be employed at all, she has taught me my value and I am incredibly thankful for that. Thank you, Verena, for being a great mentor, for showing me how to stand up for myself and not to put up with everything—a very important lesson for a young Scientist in academia.

This, finally, brings me to my PhD project and to thanking everyone involved in the project. And as the project started with **Dr. Christina Budden** and **Prof. Dr. Eicke Latz**, those are the people I would like to thank first.

I first met Eicke in one of my lectures during my master studies. Eicke had quite a different approach to others when it came to his lectures: instead of just teaching the current knowledge, he taught us how this knowledge came to be, starting with the story of the discovery of TLR4. I quite liked that approach as it taught me how to interpret the information, understand how it came to be, and whether it can be trusted. I want to thank you, Eicke, for sharing your approach to, and view of science with me. Thank you, for allowing me to approach my PhD with a great deal of autonomy. I have learned a lot from coming up with my own ideas, planning my experiments, and organising my work. I also want to thank you for always applying for grants and making sure that your lab is well equipped. I very much appreciate having been in a position where I could come up with ideas and then actually follow up on these as we always had the necessary equipment or financial means. Finally, I want to thank you for giving me the opportunity to work with and continue Christina's work on inflammasome-elicited EVs.

This brings me to Christina. Christina started work on inflammasome-elicited EVs in our lab and has established many of the techniques used for experiments described in this thesis. Thank you, Christina, for teaching me how to work with vesicles, for sharing your knowledge, protocols, and enthusiasm about EVs. It has made the start into my PhD so much easier. You have always approached science in a structured way, which made it easy for me to understand what you had done so far—and that was quite a lot. I have really enjoyed all our discussions and loved working in our little vesicle team.

This vesicle team would not have been the same without **Romina Kaiser**. Romy has helped me a lot in the lab. She has isolated vesicles, ran qPCRs, Western Blots, done antibody stainings, and so much more. Importantly, when I was in Melbourne, she has run the complete laboratory part for the microarray experiment. But above all, she has become one of my best friends. Thank you so much Romy, for making my time at the Institute of Innate Immunity so enjoyable.

Even when things did not go well in the lab, I would still enjoy coming to work to spend time with you. Thank you for countless adventures outside the lab and for being an amazing friend.
Thank you also to all other **AG Latz lab members** and **Institute of Innate Immunity members**. Thank you for your support, the evenings spent together, coffee chats in the kitchen, and fun times in the lab. Thank you, **Fraser Duthie**, for great train rides together (whenever I managed to join you with your crazy working times) and for a lot of talks (and discussions) in the office. Thank you, and **Rainer Stahl**, for all the cloning you guys have done. Thank you, **Marta Lovotti**, **Dr. Wei Wang**, **Dr. Tobias Dierkes**, **Ornina Marma**, and **Fraser** for being great office mates. I have really enjoyed our office atmosphere, and especially the evening talks with you, Marta. Big thanks also to **Dr. Dalila Silva Ribeiro**. Without you, my time at the Institute of Innate Immunity would not have been the same. Thank you for reading through parts of this thesis and for your countless support during the last years, especially for those times in the evening when an experiment did not work as planned! Thank you for all the fun time we have spent together, the great food, wine evenings, and IKEA furniture assembly sessions. I would also like to thank **Dr. Ibrahim Hawwari** for teaching Romy and me how to draw blood and always jumping in whenever it got too difficult and, along these lines, a big thank you to everyone who donated blood. I would also like to thank **Dr. Pia Langhoff**, **Andrea Schlichting**, and **Leonie Verwohlt** for all their support.

I would further like to thank the Microscopy Core Facility. Thank you, **Dr. Hannes Beckert**, for your help with the Zeiss AxioScan.Z1 slide scanner (financed by the DFG project number 388168919) and **Dr. Gabor Horvath** for all your help with the Leica SP5 (financed by the DFG project number 169331223), Leica SP8 with Lightning (388159768), and all my microscopy questions in general. Thank you also to **Peter Wurst** from the flow cytometry core facility for your help with fluorescent cell sorting using the BD FACS Aria III (216372545) and to the Histology Platform, especially **Vanessa Barabasch**, for help with many of my cryosections.

I would also like to thank **Prof. Dr. Natalio Garbi** and **Lara Oberkircher** for their support with ALI cultures, **Prof. Dr. Christoph Wilhelm** and **Marcel Michla** for their help with experiments not shown in this thesis, but which were very insightful nevertheless, and **Prof. Dr. Jonathan Schmid-Burgk** and **Marius Jentzsch** for performing the library preparation and sequencing for the experiments shown here.

Many of the above-mentioned people from my lab and the Institute of Innate Immunity have become friends during the last years. But being part of the Bonn & Melbourne Research and Graduate School, I also got to meet many people outside of my own institute. Thank you to all the **Bonn- and Melbourne-based IRTG students** for all the fun times and for all your support. I especially want to thank **Andrea Maione** and **Carolina Santillano Téllez** for being the best flatmates and friends Alex and me could have asked for and Marcel and Lara for countless fun times throughout the years.

Being part of said graduate school also meant that I spent part of my time in Melbourne. I would like to thank **Prof. Dr. Paul Hertzog** for welcoming me in his lab and being my Melbourne-based supervisor. I have experienced you as a very passionate, inspiring Scientist. Thank you for the trust in me and for letting me choose the direction of my project while offering me so many different possibilities for my work in Melbourne. I really enjoyed being part of your lab. Especially, as I got to work with **Dr. Linden James Gearing**. Jamie is a post doc in Paul's lab and a great bioinformatician. Not only have you helped me extensively with my bioinformatic analysis, Jamie, but you have helped me so much beyond: proofreading this thesis, my poster, presentations, joining my oration committee, my thesis committee meetings, discussing my results and my project, teaching me proper British English, and helping me make the best of my not-so-great sequencing data while staying sane. You have been an incredible mentor and have become a valued friend along the way. I will always remember our table tennis matches, the great office chocolate and tea selection, bird collection, and the hot chocolate at Mörk.

I also want to thank **Prof. Dr. Sammy Bedoui**. Sammy has been my Melbourne-based supervisor from the Peter-Doherty Institute and as such been part of all my thesis committee meetings and my oration. Thank you, Sammy, for giving me input on my project throughout the years and for taking the time to be an important member of my committee. Furthermore, I would like to thank you for initiating the IRTG program in the first place and thus allowing so many students, including me, to experience the research and working culture in two different countries—a very valuable experience.

With regards to my Melbourne-based committee, I also want to thank **Prof. Dr. Patrick Reading**. Patrick has been the chair during all the aforementioned committee meetings. Thank you for always ensuring that all the guidelines were followed, that these meetings could take place, and for your scientific input. I have really appreciated your support.

Participating in an international graduate program results in a lot of bureaucracy. I want to thank **Sandra Rathmann**, **Lucie Delforge**, **Dr. Annabelle Blum**, and **Dr. Marie Greyer** for always helping me to navigate through the different guidelines and requirements from both Universities. It further results in not only one committee, but two. Besides thanking the members of my Melbourne based committee, I thus want to thank all my German thesis examination committee members (Dissertationskomitee). I want to thank **Prof. Dr. Christian Kurts** for being a member of this committee and, as such, for taking the time to read through my work and listen to my presentation. Thank you also for initiating the IRTG program. As mentioned above, this gives so many students the incredible opportunity of getting to know different cultures. Furthermore, it allowed the formation of a great group spirit and the establishment of bonds between different labs.

Finally, I would like to acknowledge that part of the work presented here was carried out on the lands of the Wurundjeri Woi-wurrung and the Bunurong Wurrung People in Naarm (Melbourne). They belong to the greater Kulin Nation that consists of five major nations including the two aforementioned as well as

the Dja Dja Wurrung, Wathaurung, and Taungurung. I recognise their continuing connection to the land and waters of this beautiful place I got to know this past year. I pay my respects to Aboriginal and Torres Strait Islander cultures and to Elders past, present, and emerging.

List of Publications

Próchnicki T, Vasconcelos MB, Robinson KS, Mangan MSJ, De Graaf D, Shkarina K, Lovotti M, **Standke L**, Kaiser R, Stahl R, *et al* (2023) Mitochondrial damage activates the NLRP10 inflammasome. *Nat Immunol*: 1–9

Budden CF, Gearing LJ, Kaiser R, **Standke L**, Hertzog PJ & Latz E (2021) Inflammasome-induced extracellular vesicles harbour distinct RNA signatures and alter bystander macrophage responses. *Journal of Extracellular Vesicles* 10: e12127

Erazo AB, Wang N, **Standke L**, Semeniuk AD, Fülle L, Cengiz SC, Thiem M, Weighardt H, Strugnell RA & Förster I (2021) CCL17-expressing dendritic cells in the intestine are preferentially infected by Salmonella but CCL17 plays a redundant role in systemic dissemination. *Immunity, Inflammation and Disease* 9: 891–904

1 Introduction

From the moment one is born, one is surrounded by microorganisms and it is currently estimated that the ratio of bacterial to host cells is around 1:1 (Sender *et al*, 2016). While microorganisms can cause harm – these are called pathogens – not all do so. Instead they can constantly colonise a host without causing damage and form microbial communities called the microbiome (Murphy *et al*, 2017).

The microorganisms that make up the microbiome, also called commensals, consist of archaea, bacteria, and fungi. They live in a symbiotic relationship with their host. Pathogenic microorganisms, on the other hand, can be divided into four classes: viruses, bacteria, fungi and parasites (Murphy *et al*, 2017).

The human immune system has evolved to defend against these damaging microorganisms, while allowing the presence of commensals at the same time. Besides being crucial in the defence against pathogens, the immune system is also involved in other processes, including homeostatic and developmental processes, such as the clearance of dead cells (Pradeu, 2020). It achieves all of this through the orchestration of its two branches: the innate and the adaptive immune system.

The role of the innate immune system is to act as a first line of defence against pathogens (Murphy *et al*, 2017), as well as a sensor for imbalances in homeostasis (Liston & Masters, 2017). The first level of defence employed by the innate immune system includes anatomic and chemical barriers, such as the skin and mucosal tissues. These barriers act to prevent exposure of internal tissues to pathogens (Murphy *et al*, 2017). If this level of defence is breached, the second line of defence comes into play: the complement system. It consists of around 30 different plasma proteins that target invading microorganisms for phagocytosis and lysis (Murphy *et al*, 2017). If these first two lines of defence fail, innate immune cells are activated through the engagement of pattern recognition receptors (PRRs). Most innate immune cells develop from common myeloid

progenitor cells, which give rise to dendritic cells (DCs), neutrophils, eosinophils, basophils, mast cell precursor cells and monocytes. Mast cell precursor cells then give rise to mast cells and monocytes differentiate into macrophages (MΦs). Additionally, natural killer (NK) cells and innate lymphoid cells (ILCs) are important innate immune cells. They develop from common lymphoid progenitor cells (Murphy *et al*, 2017).

While all the above-described mechanisms are employed within minutes and are essential for the defence against pathogens, they rely on germline-encoded receptors, resulting in limited variability. This variability is immensely expanded by the adaptive immune system: the primary immune cells of the adaptive immune system are T and B lymphocytes with T cell receptors (TCR) and B cell receptors (BCR) respectively. These receptors are created through somatic recombination and, in the case of BCRs, subsequent mutagenesis (Murphy *et al*, 2017). This generation of antigen-specific receptors results in highly specific and efficient immune responses, but also in the formation of antigen-specific memory (Murphy *et al*, 2017).

While the human immune system is commonly described as being divided into the innate and the adaptive part, in the end, there is a lot of crosstalk between both systems: innate immunity is needed to mount an adaptive immune response, with the main player being DCs that present antigens to T cells. Once mounted, adaptive immunity then influences innate immunity, for example through the secretion of cytokines (Murphy *et al*, 2017).

1.1 The Innate Immune System and the Role of PRRs

Recognition of both pathogens and homeostatic imbalances by the innate immune system relies on a range of receptors, which are called PRRs. PRRs can be further grouped into five families: Toll-like receptors (TLRs), Absent in melanoma 2 (AIM2)-like receptors (ALRs), nucleotide-binding domain, leucine-rich repeat (LRR)-containing (or NOD-like) receptors (NLRs), C-type lectin

receptors (CLRs), and retinoic acid-inducible gene I (RIG-I)-like receptors (RLRs) (Brubaker *et al*, 2015). Sometimes, the sequestosome 1-like receptors (SLRs) are also included in the definition of PRRs, resulting in six families of PRRs (Deretic *et al*, 2013).

PRRs respond to pathogens through recognition of pathogen-associated molecular patterns (PAMPs) and to imbalances in homeostasis through sensing of danger-associated molecular patterns (DAMPs) and homeostasis-altering molecular processes (HAMPs) (Murphy *et al*, 2017; Liston & Masters, 2017).

1.2 Inflammasomes

Inflammasomes are protein complexes of high molecular weight (MW) that act as signalling platforms for activation of caspase-1. Active caspase-1 cleaves the cytokines interleukin (IL)-1β and IL-18, and gasdermin D (GSDMD), thereby initiating a form of cell death known as pyroptosis (Martinon *et al*, 2002; Broz & Dixit, 2016).

Inflammasomes typically consist of an inflammasome sensor molecule, an adaptor protein called apoptosis-associated speck-like protein containing a carboxy-terminal caspase activation and recruitment domain (CARD) (ASC), and pro-caspase-1 (Figure 1).

Inflammasome sensor molecules usually consist of a variable C-terminal sensor domain and an N-terminal death domain (DD), either a pyrin domain (PYD) or CARD. They recognise PAMPs, DAMPs, or HAMPs with their sensor domain and, upon recognition, are believed to form a homomultimer seed and thereby cluster the PYD domains. Most inflammasomes employ these PYD domains to recruit ASC. ASC consists of two DDs, an N-terminal PYD, and a C-terminal CARD domain. The N-terminal PYD domain allows interaction with the homomultimer seed PYD domains and, additionally, with the PYD domains of other ASC molecules. This capability of ASC molecules to interact with one another allows a prion-like polymerisation of basically all ASC proteins in the cell, which is seen upon inflammasome-activation and leads to the formation of an

ASC speck about 1 μm in size (Masumoto *et al*, 1999; Richards *et al*, 2001; Franklin *et al*, 2014). When fluorescently tagged, these ASC specks can be observed under the microscope to quantify inflammasome activation (Stutz *et al*, 2013). The resulting clustering of ASC CARD domains leads to the recruitment of pro-caspase-1 to the ASC speck (Fernandes-Alnemri *et al*, 2007; Cai *et al*, 2014; Lu *et al*, 2014). Pro-caspase-1 molecules are brought into close proximity of each other, resulting in dimerisation and auto-activation (Wilson *et al*, 1994; Elliott *et al*, 2009).

Active caspase-1 then cleaves pro-IL-1β to IL-1β (Thornberry *et al*, 1992) and pro-IL-18 to IL-18 (Ghayur *et al*, 1997). Additionally, caspase-1 cleaves GSDMD, allowing its N-terminal domain to mediate pore formation in the plasma membrane (Shi *et al*, 2015). GSDMD pores provide a pathway for the release of IL-1β and IL-18 into the extracellular space (Kayagaki *et al*, 2015; Shi *et al*, 2015; He *et al*, 2015). However, caspase-1-dependent IL-1β release does not have to depend on GSDMD pore formation but can be both GSDMD-dependent and GSDMD-independent (Monteleone *et al*, 2018).

ASC specks have been found to persist in the extracellular space after cells have undergone pyroptosis and have even been shown to remain active when phagocytosed by surrounding MΦs, thus continually leading to the activation of caspase-1 (Franklin *et al*, 2014; Baroja-Mazo *et al*, 2014). However, caspase-1 undergoes proteolytic self-inactivation, thus acting as a negative feedback signal in inflammasome activation (Boucher *et al*, 2018).

Inflammasome sensors can be grouped based on their structure (Figure 1). The largest group consists of members of the NLR family. Several NACHT, LRR and PYD domains-containing (NLRP) proteins, as well as the NLR family CARD domain-containing (NLRC) protein 4, can assemble inflammasomes (Poyet *et al*, 2001; Martinon *et al*, 2002; Agostini *et al*, 2004; Yu *et al*, 2006a; Franchi *et al*, 2006; Miao *et al*, 2006; Faustin *et al*, 2007; Roberts *et al*, 2009; Bürckstümmer *et al*, 2009; Fernandes-Alnemri *et al*, 2009; Hornung *et al*, 2009). Inflammasome-

forming NLRs contain an N-terminal DD (CARD in case of NLRC4, PYD in case of the NLRPs), a central nucleotide-binding domain (NBD), and a C-terminal LRR domain (Latz *et al*, 2013). In case of the NLRP3 sensor molecule, the NBD is a NACHT domain with adenosine triphosphate(ATP)ase activity (Duncan *et al*, 2007) and the LRR domain is thought to have an autoinhibitory function (Swanson *et al*, 2019) (Figure 1).

Besides the NLR family of inflammasome sensors, additional inflammasome-forming receptors have been recognised to date: pyrin, which contains a PYD, a B-box region, a coiled-coil domain, and a B30.2 domain (Xu *et al*, 2014; Broz & Dixit, 2016), AIM2, which contains a PYD and a HIN-200 domain (Roberts *et al*, 2009; Bürckstümmer *et al*, 2009; Fernandes-Alnemri *et al*, 2009; Hornung *et al*, 2009) (Figure 1), and CARD8, which consists of a small N-terminal region, a function-to-find domain (FIIND), and a CARD domain (Ball *et al*, 2020; Linder *et al*, 2020; Barnett *et al*, 2023). Furthermore, caspases-4 and -5 (murine caspase-11) have been shown to form an inflammasome (non-canonical inflammasome, section 1.3.2; Kayagaki *et al*, 2013; Shi *et al*, 2014).

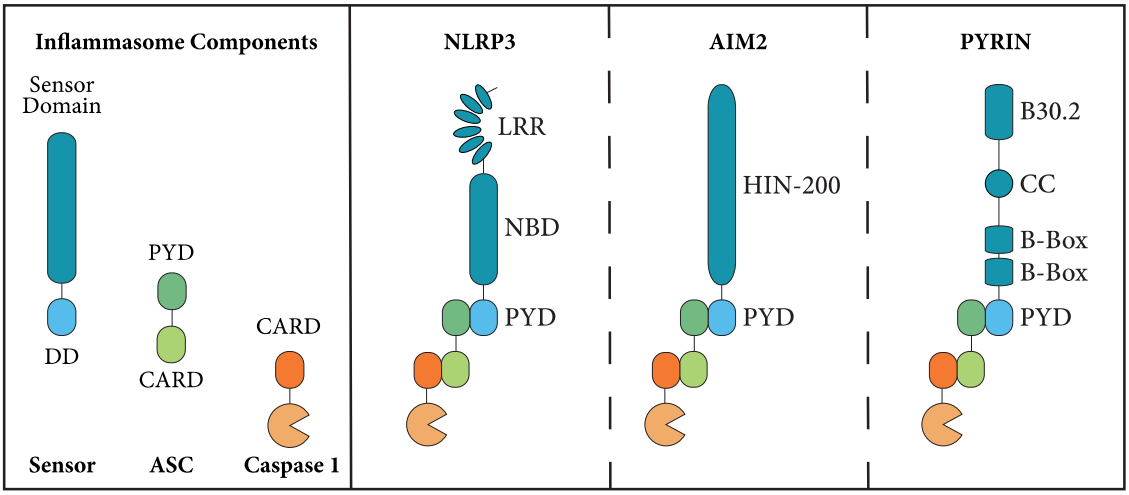

Figure 1: Inflammasome sensor structure and assembly. Inflammasomes consist of an inflammasome sensor molecule that contains a sensor domain and a death domain (DD). They interact with apoptosis-associated speck-like protein containing a carboxy-terminal caspase activation and recruitment domain (CARD) (ASC) via their DD. ASC has two DDs: a pyrin domain (PYD) interacting with the inflammasome sensor and a CARD interacting with the CARD of pro-caspase-1. A member of the nucleotide-binding domain, leucine-rich repeat

(LRR)-containing receptor (NLR) family is NLRP3. It consists of a PYD, a nucleotide-binding domain (NBD), and a LRR domain. A member of the absent in melanoma 2 (AIM2)-like receptor (ALR) family is AIM2. It consists of a PYD and a HIN-200 domain. Pyrin consists of a PYD, a B-box region, a coiled-coil (CC) domain, and a B30.2 domain.

1.3 The NLRP3 Inflammasome

NLRP3 is mainly expressed in monocytes, MΦs, and Schwann cells and to a lesser extent in DCs and T cells (The Human Protein Atlas; Karlsson *et al.*, 2021). In most cell types, including in both murine and human MΦs, NLRP3 is expressed at low levels under baseline conditions (Bauernfeind *et al*, 2009).

While the inflammasome sensor molecules have all been shown to lead to caspase-1 activation, they differ with regard to their activators. For the NLRP3 inflammasome, various activators have been identified that commonly induce cellular stress. They can be grouped into canonical NLRP3 activation, non-canonical NLRP3 activation, and alternative NLRP3 activation (Xu & Núñez, 2022).

1.3.1 Canonical NLRP3 Activation

Canonical NLRP3 activation is a two-step process comprising a priming and an activation step (Xu & Núñez, 2022; Figure 2):

To increase NLRP3 expression, but also to increase expression of pro-IL-1β and pro-IL-18, cells are usually treated with an activator of nuclear factor kappa B (NF-κB) like lipopolysaccharide (LPS). This is called “priming” (Bauernfeind *et al*, 2009; Latz *et al*, 2013; Franchi *et al*, 2009).
Additionally, priming leads to post-transcriptional changes like deubiquitylation or phosphorylation of NLRP3, which license NLRP3 for activation (Juliana *et al*, 2012; Schroder *et al*, 2012; Song *et al*, 2017; Song & Li, 2018).

After priming, a second treatment is needed to activate the licensed NLRP3 inflammasome. These stimuli are extremely diverse and include viral and bacterial proteins such as the bacterial pore forming toxin nigericin (Nig), intracellular molecules released into the extracellular fluid upon cellular damage such as ATP, and insoluble particles such as uric acid crystal or amyloid-β (Aβ) depositions (Coll *et al*, 2022). They usually perturb cellular homeostasis (e.g., ions or organelles) in addition to activating the NLRP3 inflammasome. This, and the fact that NLRP3 activation varies between cell types and species, makes it hard to elucidate the exact mechanism by which such diverse stimuli lead to the activation of NLRP3. While the exact mechanism is still unknown, it has been suggested that they lead to a common upstream cellular event, which then activates NLRP3.

One recognised signal upstream of NLRP3 activation is potassium ion (K^+) efflux. For example, extracellular ATP, a well-known NLRP3 activator, activates the P2X purinoreceptor 7 ($P2X_7$). $P2X_7$ promotes calcium ion (Ca^{2+}) and sodium ion (Na^+) influx and, in cooperation with the two-pore domain K^+ channel (K_{2P}) (TWIK2), K^+ efflux (Di *et al*, 2018). K^+ efflux then leads to the activation of the NLRP3 inflammasome.
The K^+ and hydrogen ion (H^+) ionophore nigericin, a model agonist commonly used in *in vitro* studies, also activates NLRP3 through induction of K^+ efflux (Perregaux & Gabel, 1994).

However, not all stimuli known to activate NLRP3 do so through potassium depletion: changes in metabolism can lead to activation of the NLRP3 inflammasome in a K^+-independent way (Groß & Groß, 2016; Sanman *et al*, 2016; Wolf *et al*, 2016; Groß *et al*, 2016). Chemical disruption of glycolysis was, for example, shown to activate NLRP3 (Sanman *et al*, 2016), as was inhibition of the mitochondrial electron transport chain complex I (e.g., by R837 ;Groß *et al*, 2016) or N-acetylglucosamine (GlcNAc)-induced hexokinase delocalisation into the cytosol (Wolf *et al*, 2016).

Other upstream signals described to be involved in NLRP3 inflammasome formation are lysosomal disruption and trans-Golgi disassembly (Swanson *et al*, 2019).

1.3.2 Non-Canonical NLRP3 Activation

During non-canonical activation of NLRP3, the bacterial PAMP LPS, once in the cytosol, leads to activation of caspase-11 (in mice), or caspases-4 and -5 (in humans; Kayagaki *et al*, 2013; Shi *et al*, 2014). Caspases-4/5 and -11 can then directly cleave GSDMD, leading to GSDMD pore formation. Of note, the non-canonical inflammasome cannot (or only to a limited extend) cleave pro-IL-1β and pro-IL-18 (Ramirez *et al*, 2018; Bibo-Verdugo *et al*, 2020). However, GSDMD pore formation results in potassium efflux, NLRP3 activation, ASC specking, caspase-1 activation and finally IL-1β and IL-18 cleavage and release through the pre-formed GSDMD pore (Kayagaki *et al*, 2013, 2015; Shi *et al*, 2015; Yang *et al*, 2015; Jorgensen *et al*, 2017).
While canonical NLRP3 activation requires an adaptor to link it to caspase-1, it is believed that non-canonical inflammasomes directly act as a receptor for LPS without the need for an adaptor. However, this hypothesis has been challenged in recent years, as several members of the GBP protein family have been linked to the formation of a caspase-4 signalling platform (Kutsch *et al*, 2020; Santos *et al*, 2020; Wandel *et al*, 2020; Fisch *et al*, 2020).

1.3.3 Alternative NLRP3 Activation

Certain cells are able to employ alternative NLRP3 activation. During alternative NLRP3 activation, stimulation of cells with TLR ligands directly leads to NLRP3 activation without the need for a second activation stimulus (Gaidt & Hornung, 2017). This is for example the case in human monocytes (but not in human MΦs or DCs): here, stimulation with TLR2 and TLR4 activators leads to direct activation of NLRP3 (Netea *et al*, 2009; Gaidt *et al*, 2016). Alternative NLRP3 activation is independent of K^+ depletion (Gaidt *et al*, 2016). Instead activation is mediated through Toll/IL-1 receptor homology (TIR)-domain-containing adaptor

inducing interferon-β (TRIF), kinase receptor-interacting serine/threonine-protein kinase (RIPK) 1, Fas-associated protein with death domain (FADD) and caspase-8 signalling (Gaidt *et al*, 2016). Caspase-8 then activates NLRP3 in a so far unknown mechanism. However, no ASC specking is observed, and no pyroptosis results. Instead, IL-1β is released in an pyroptosis-independent way (Gaidt & Hornung, 2017).

1.4 Pyroptosis

Activation of inflammasome sensors, and resulting cleavage of pro-caspases-1/4/5/11 and GSDMD, leads to a form of programmed cell death called pyroptosis (Shi *et al*, 2015; Kayagaki *et al*, 2015; Jorgensen *et al*, 2017).
There are two forms of cell death that can be distinguished: accidental cell death and programmed cell death (Nagata & Tanaka, 2017). Programmed cell death can be further grouped into non-lytic cell death, which is the case for apoptosis, and lytic cell death. Lytic cell death types include necroptosis, neutrophil extracellular trap (NET)-based cell death (NETosis), and pyroptosis (Jorgensen *et al*, 2017). Pyroptosis can be initiated by a range of signalling pathways. In the case of NLRP3, the canonical and non-canonical initiation pathways lead to pyroptosis while alternative NLRP3 activation does not lead to pyroptosis (Gaidt *et al*, 2016).
During pyroptosis osmotic lysis of cells occurs, resulting in plasma membrane tears that allow for the release of cytosolic contents but not cellular organelles (Jorgensen *et al*, 2016b). Instead, the collapsed organelles, together with the mostly intact cell membrane and other cellular structures, form a pore-induced intracellular trap (PIT) (Jorgensen *et al*, 2016a, 2016b). When pyroptosis has been initiated by bacteria, pyroptosis does not lead to their direct killing (Miao *et al*, 2010; Jorgensen *et al*, 2016b), but rather the still viable bacteria are trapped within these PITs, leading to activation of the complement system, release of IL-1β and IL-18 from the pyroptotic cell and eicosanoid production (Jorgensen *et al*, 2016a). This results in recruitment of neutrophils which, using phagocytic scavenger receptors and complement receptors, phagocytose PITs containing

entrapped bacteria in a process called efferocytosis. Neutrophils then kill phagocytosed bacteria through reactive oxygen species (ROS) production (Jorgensen *et al*, 2016a, 2016b).

There is a way to restrict pyroptosis as a result of GSDMD pore formation: Rühl and colleagues have found that cells have a mechanism to remove GSDMD pores from the membrane (Rühl *et al*, 2018). Upon GSDMD pore formation, Ca^{2+} influx occurs, which acts as a signal to recruit the endosomal sorting complexes required for transport (ESCRT) machinery to GSDMD pores. This leads to ESCRT-induced microvesicle formation which bud off the plasma membrane, thus allowing cells to remove GSDMD from their membranes and restrict pyroptosis (Rühl *et al*, 2018).

Pyroptosis has classically been described in the context of innate immune cells. However, it has also been shown for epithelial cells (Knodler *et al*, 2014; Shi *et al*, 2014), endothelial cells (Cheng *et al*, 2017), hepatocytes (Liu *et al*, 2020), keratinocytes (Shi *et al*, 2014), and other non-immune cells (Downs *et al*, 2020).

1.5 The IL-1 Family

IL-1β and IL-18 are both members of the IL-1 family. The IL-1 family consists of 11 soluble and 10 receptor molecules (Dinarello, 2018). While most cytokines (e.g., tumour necrosis factor (TNF)-α and IL-6) contain a signal sequence that directs them to the ER from which they are trafficked through the Golgi apparatus and released via the secretory pathway, most members of the IL-1 family lack this signal sequence. Instead, they are synthesised in the cytosol and released through mechanisms independent of the ER and Golgi apparatus (Monteleone *et al*, 2015; Rubartelli *et al*, 1990). As discussed above, one of these mechanisms is the release through GSDMD pores (Kayagaki *et al*, 2015; Shi *et al*, 2015; He *et al*, 2015), however, other pathways have been proposed as well (Monteleone *et al*, 2018).

The IL-1 receptors contain TIR domains (Dinarello, 2009). TIR domains are intracellular signalling domains also found in TLRs. Ligand binding leads to

dimerisation through the TIR domains, inducing recruitment of myeloid differentiation primary response 88 (MyD88), finally resulting in the activation of transcription factors NF-κB, activator protein 1 (AP-1), c-Jun N-terminal kinase (JNK), mitogen-activated protein kinases (MAPKs) such as p38, extracellular signal-regulated kinase (ERKs), and different interferon regulatory factors (IRFs) (Dinarello, 2009). Despite leading to the initiation of the same signalling pathways, the diversity of IL-1 receptor responses comes from the different expression of receptors and regulatory molecules (Mantovani *et al*, 2019).

1.5.1 IL-1α and IL-1β

IL-1β shares a receptor with IL-1α and IL-1 receptor antagonist (IL-1RA)—the IL-1 receptor (IL-1R) 1 (Dinarello, 2018). Upon IL-1α or IL-1β (IL-1 is commonly used to refer to both) binding to IL-1R1, a conformational change of IL-1R1 allows the binding of the co-receptor IL-1 receptor accessory protein (IL-1RAP), to the IL-1R1. This allows the initiation of signalling through the TIR domains (Dinarello, 2018). IL-1β can additionally bind to IL-1R2. IL-1R2 acts as a soluble or membrane bound (although without a cytoplasmic domain) decoy receptor for IL-1β (Dinarello, 2018). The receptor's decoy function is even enhanced upon complex formation with soluble IL-1RAP (Dinarello, 2018). Finally, IL-1R2 can bind IL-1α intracellularly to inhibit the release of IL-1α (Dinarello, 2018).

IL-1α is special in that it is constitutively expressed in mesenchymal cells (Mantovani *et al*, 2019). It is expressed in its precursor form and can be cleaved by proteases, however, does not need to be cleaved for its activity and for secretion (Kim *et al*, 2013a). Furthermore, it is special in that it has been found to localise to the nucleus, to the cytoplasm, and to the cell membrane (Broderick & Hoffman, 2022). When in the nucleus, IL-1α acts as a transcription factor and regulates cytokine expression (amongst others IL-6 and IL-8) downstream of NF-κB and AP-1 (Broderick & Hoffman, 2022; Wessendorf *et al*, 1993; Werman *et al*, 2004). In the cytosol, on the other hand, it has been proposed to bind to mitochondrial cardiolipin and thereby regulate the NLRP3 inflammasome (Dagvadorj *et al*, 2021). Finally, at the cell membrane, IL-1α can bind to IL-1R1

on neighbouring cells (Kurt-Jones *et al*, 1985; Broderick & Hoffman, 2022) or be released as part of the membrane of apoptotic bodies, spreading inflammation further (Berda-Haddad *et al*, 2011), or by itself, acting as a DAMP and resulting in pro-inflammatory signalling through IL-1R1 engagement (Di Paolo & Shayakhmetov, 2016). Location to the nucleus is generally induced by pro-apoptotic signals while location to the cytoplasm is induced by necrotic signals (Cohen *et al*, 2010). IL-1α is especially known to be a mediator of local and sterile inflammation and is not found in circulation under inflammatory conditions (Malik & Kanneganti, 2018; Mantovani *et al*, 2019).

IL-1β was discovered as an inducer of fever in rabbits and originally termed a pyrogen (Dinarello *et al*, 1974, 1977). While IL-1α is expressed constitutively in most cells, IL-1β expression is primarily found in monocytes, MΦs, and neutrophils in an inducible (Schindler *et al*, 1990a, 1990b), highly regulated fashion (Shi *et al*, 2020; Sneezum *et al*, 2020). Through binding of IL-1β to its receptor, it can lead to further expression of inflammatory proteins and, to expression of IL-1β itself, thus leading to a feed-forward loop (Warner *et al*, 1987a, 1987b; Dinarello *et al*, 1987). Of note, the induction of IL-1β messenger ribonucleic acid (mRNA) through IL-1 stimulation leads to a rapid (within 15 min) upregulation of mRNA levels that is sustained for over 24 h. In contrast, induction of IL-1β mRNA levels using a microbial stimulus such as LPS leads to the same rapid onset of mRNA upregulation, but levels are only increased for 4 h and decrease thereafter (Schindler *et al*, 1990a).

Unlike IL-1α, IL-1β cannot be secreted in its precursor form and instead needs cleavage to generate active IL-1β. Cleavage of IL-1β to its active form can be either caspase-1 dependent, or caspase-1 independent (Dinarello, 2018).

Locally, IL-1β leads to the activation of vascular endothelium and lymphocytes and to the recruitment of neutrophils (Murphy *et al*, 2017). Systemically, it contributes to fever and induces acute-phase protein production (Bode *et al*, 2012). While IL-1β-induced responses are generally beneficial during infection, they can be detrimental in case of uncontrolled production such as in genetic and acquired diseases (Monteleone *et al*, 2015).

One important regulator of IL-1β and IL-1α is IL-1RA (Hannum *et al*, 1990; Eisenberg *et al*, 1990). Like IL-1α, IL-1RA is expressed in all cells. It is induced by different inflammatory stimuli and acts as an anti-inflammatory cytokine through competitive binding to IL-1R1 (Seckinger *et al*, 1987). The importance of IL-1RA has especially become clear since the use of anakinra, a recombinant form of IL-1RA, as a therapeutic in autoinflammatory diseases (Broderick & Hoffman, 2022). Anakinra was introduced in 2002 for the treatment of rheumatoid arthritis.

1.5.2 IL-18

IL-18 was discovered in 1989 as an "interferon (IFN)-γ-inducing factor" (Nakamura *et al*, 1989) and later named IL-18 (Dinarello, 2018). IL-18 is structurally similar to IL-1β in that it is does not have a signal peptide for secretion and is synthesised as an inactive precursor that needs cleavage (e.g., by caspase-1) to become activated (Okamura *et al*, 1995; Bazan *et al*, 1996; Gu *et al*, 1997; Ghayur *et al*, 1997).

One of the main differences between IL-1β and IL-18 is that, while pro-IL-1β expression is inducible and absent in healthy human cells such as monocytes, MΦs, and epithelial cells, the precursor form of IL-18 is constitutively expressed in blood monocytes and MΦs of healthy subjects (Puren *et al*, 1999), as well as in endothelial cells, keratinocytes, and in epithelial cells of the gastrointestinal tract (Dinarello, 2018). The primary sources of active IL-18 are MΦs and DCs (Novick *et al*, 2013), although intestinal epithelial cells have recently been recognised as another important source of active IL-18 (Yasuda *et al*, 2019; Chiang *et al*, 2022).

IL-18 forms a low affinity complex with the IL-18 receptor alpha chain (IL-18Rα, encoded by *IL18R1*). This receptor is ubiquitously expressed. Upon joining of the co-receptor IL-18 receptor beta chain (IL-18Rβ, encoded by *IL18RAP*) to IL-18 and IL-18Rα, a high-affinity complex is formed, which allows signalling (Dinarello, 2018; Zhou *et al*, 2020). This signalling is similar to the signalling induced by IL-1β or IL-1α binding to IL-1R1 and its co-receptor IL-1RAP in that it induces TIR

domain-mediated MyD88 recruitment and signalling, leading to the release of NF-κB. However, expression of the co-receptor is restricted to certain cells and higher concentrations of IL-18 (cells expressing IL-18Rα and co-receptor IL-18Rβ require about ≥10–20 ng/mL IL-18) are needed to activate said signalling than in the case of IL-1α and IL-1β (concentrations in the low ng/mL range or even pg/mL range; Dinarello, 2018; Morel *et al*, 2001; Lee *et al*, 2004).

Interestingly, the affinity of IL-18 for IL-18 binding protein (IL-18BP) is higher than the affinity for the IL-18 receptor (Novick *et al*, 2013). IL-18BP is a secreted protein without a cytoplasmic domain and acts as a decoy receptor for IL-18 (Dinarello, 2018). It was first isolated and cloned in 1999 and shown to specifically bind and neutralise IL-18 activity (Novick *et al*, 1999). IL-18BP is a constitutively secreted protein, present in the serum of healthy humans at a level 20-fold higher than IL-18 (Novick *et al*, 2001). In diseases associated with higher levels of secreted IL-18, IL-18BP levels have also been found to be increased (Novick *et al*, 2010, 2009) and, as one molecule of IL-18 binds to one molecule of IL-18BP, it is worth investigating the ratio between IL-18 and IL-18BP and determining not only if overall IL-18 levels are increased but also levels of free IL-18 (Dinarello, 2018).

From the very moment of its discovery, IL-18 has been linked to the production of IFN-γ. For example, scientists treated wild type and caspase-1 knockout mice with LPS and attributed the absence of IFN-γ in caspase-1 knockout mice to the absence of IL-18 (Gu *et al*, 1997; Ghayur *et al*, 1997; Fantuzzi *et al*, 1998). Induction of IFN-γ was also absent in IL-18 knockout mice, further supporting this finding (Takeda *et al*, 1998).

Later, the mechanism of IFN-γ induction by IL-18 was revealed. IL-18, together with IL-12 and IL-15, was shown to be capable of inducing IFN-γ: both IL-12 and IL-15 lead to an increase in co-receptor IL-18R7 expression, enabling downstream signalling once IL-18 binds to its high affinity receptor consisting of IL-18R5 and IL-18R7 (Dinarello, 2018; Novick *et al*, 2013). IL-18 and IFN-γ are associated with several human autoimmune diseases, such as systemic lupus erythematosus (SLE), rheumatoid arthritis, type 1 diabetes, Crohn’s disease,

psoriasis, and graft-vs-host disease (Dinarello, 2018). In the context of T cell immune responses, IL-18 and IL-12 induce T helper type 1 (T_H1) immune responses (Nakanishi *et al*, 2001).

Without IL-12 and IL-15, on the other hand, IL-18 has been implicated in T helper type 2 (T_H2) diseases (Nakanishi *et al*, 2001). Generally, in the absence of IL-12 and IL-15, IL-18 responses are similar to those of other pro-inflammatory cytokines of the IL-1 family. Those include the upregulation of adhesion molecules, NO (nitric oxide) synthesis, as well as chemokine production (Dinarello, 2018). And as with anakinra for IL-1 signalling, the inhibition of IL-18 also leads to a reduction in disease severity (Dinarello, 2018). However, while IL-1α and IL-1β induce fever, this is not one of the significant outcomes of IL-18 signalling (Dinarello, 2018). When injected into mice or rabbits, IL-18 did not cause fever (Gatti *et al*, 2002; Li *et al*, 2003a), neither did it cause fever in most cancer patients when injected at low intravenous doses (Robertson *et al*, 2006). Additionally, while IL-18 has been shown to be pro-inflammatory when injected systemically, in the gut a constitutive release of IL-18 seems to promote barrier functions in some mouse models (Elinav *et al*, 2011; Levy *et al*, 2015).

1.6 Involvement of NLRP3 in Various Diseases

While NLRP3 inflammasome activation is an important mechanism of the immune system to protect against various pathogens, aberrant NLRP3 activation has been linked to various diseases.

1.6.1 NLRP3-Dependent Genetic Diseases

Cryopyrin-associated periodic syndromes (CAPS) are a group of genetic, NLRP3-dependent, autoinflammatory diseases. They are caused by gain-of-function mutations of the NLRP3 gene and include familial cold autoinflammatory syndrome (FCAS), Muckle-Wells syndrome (MWS), and neonatal-onset multisystem inflammatory disorder (NOMID) (Hoffman *et al*, 2001b, 2001a; Milhavet *et al*, 2008). All three involve recurrent systemic fever episodes, blood neutrophilia, and tissue-specific inflammation in the skin, joints, and conjunctiva

(Mangan *et al*, 2018). Symptom severity increases from FCAS to NOMID with patients suffering from NOMID experiencing the most severe symptoms (de Jesus *et al*, 2015; Xiao *et al*, 2018).
Mouse lines expressing CAPS-associated variants of NLRP3 for all three syndromes have been developed. They all show lethal inflammation that is dependent on ASC and caspase-1, but only partially dependent on IL-1β and IL-18 (Brydges *et al*, 2013).

1.6.2 The Role of NLRP3 and Western Diet in Inflammatory Diseases

While CAPS are very rare diseases with one to two cases per 1 million inhabitants in the USA (Kuemmerle-Deschner, 2015) and one case per 360,000 inhabitants in France (Cuisset *et al*, 2011), non-communicable diseases (NCDs) are very common. They lead to the death of 41 million people each year, accounting for an equivalent of 74 % of all deaths globally. Of those, 17 million people prematurely die from NCDs before the age of 70 (World Health Organisation, 2022).
NCDs are caused by a combination of genetic, physiological, environmental, and behavioural factors. They include cardiovascular disease (CVDs) such as heart attacks and stroke, chronic respiratory diseases such as asthma, diabetes, cancers (World Health Organisation, 2022), and neurodegenerative diseases (Christ & Latz, 2019).

The Global Burden of Diseases, Injuries, and Risk Factors Study provides data quantifying the health loss caused by hundreds of different diseases, injuries, and risk factors by systematically assessing published, publicly available, and contributed data (Vos *et al*, 2020). In their most recent study published in 2020, the authors have estimated the impact of 369 diseases and injuries (Vos *et al*, 2020). They showed that, in 1990, NCDs contributed to less than half (43.2 %) of the overall global health loss measured in the proportion of healthy years lost (DALYs: disability-adjusted life years). Since then, the global estimate for DALYs has increased to 63.8 % in 2019 (Global Burden of Disease, 2019, 2020). The strongest impact on DALYs was seen for CVDs (Global Burden of Disease,

2020). Cases of CVD nearly doubled from 271 million CVD cases in 1990 to 523 million CVD cases in 2019. Of all the deaths attributed to CVD in 2019, ischemic heart disease accounted for 49.2 %, followed by ischemic stroke accounting for 17.7 %, and intracerebral haemorrhage for 15.5 %. Highest risk factors were a high systolic blood pressure, dietary risks, high low-density lipoprotein (LDL) cholesterol, high body-mass index, tobacco exposure, high fasting plasma glucose, and kidney dysfunction (Roth *et al*, 2020).

Taking into account these risk factors, it is of no surprise that countries with a high prevalence of what is called a “western diet” have seen an increase in NCDs (Christ *et al*, 2019). The typical western diet consists of foods high in calories, simple sugars, trans and saturated fats, cholesterol, salt, and food additives. It is missing or low in complex carbohydrates, fibres, vitamins, and minerals (Christ & Latz, 2019).

A western diet, coupled to a sedentary lifestyle, leads to the accumulation of lipids such as LDL cholesterol or oxidised LDL: cholesterol is usually taken up by cells as LDL on an on-demand basis through the upregulation of the LDL receptor (LDL-R). However, if cells have taken up enough cholesterol, they downregulate the LDL-R, leading to the accumulation of cholesterol outside cells (Christ *et al*, 2019). In the presence of free radicals, LDL can be oxidised, forming oxidised LDL. Free radicals can increase through the consumption of trans fats and sugars, smoking or exposure to toxins such as pollutants or certain preservatives. Oxidised LDL is more reactive than LDL and can be taken up by MΦs through scavenger receptors such as cluster of differentiation (CD)36 or through TLRs. While LDL-R mediated uptake of LDL is dependent on a negative feedback loop, limiting the amount of cholesterol in cells, uptake of oxidised LDL through scavenger receptors and TLRs does not have a negative feedback loop and thus can lead to the accumulation of oxidised LDL in MΦs and finally to the formation of cholesterol crystals (Christ *et al*, 2019).

Lipids like oxidised LDL can act as a priming signal for NLRP3 through the activation of e.g., TLR4 (Shi *et al*, 2006; Saberi *et al*, 2009; Stewart *et al*, 2010;

Duewell *et al*, 2010). They can further activate NLRP3, for example through above mentioned cholesterol crystal formation: cholesterol crystals can form inside the phagolysosomal compartment of MΦs from previously internalised oxidised LDL and lead to the rupture of lysosomes (Duewell *et al*, 2010; Rajamäki *et al*, 2010). Lysosomal rupture leads to the release of the lysosomal protease cathepsin B into the cytoplasm, which has been linked to NLRP3 activation (Rajamäki *et al*, 2010). As a result, chronic, low-grade inflammation is triggered.
This chronic, low-grade inflammation contributes, for example, to atherosclerosis and it has been shown that NLRP3 indeed plays an important role in atherosclerosis: Duewell and colleagues have demonstrated that cholesterol crystals are found early in the development of atherosclerosis and that these cholesterol crystals can prime and activate NLRP3. This leads to IL-1β release, which allows recruitment of MΦs, DCs, and neutrophils to the intima space of atherosclerotic lesions (Duewell *et al*, 2010).

Not only cholesterol and oxidised LDL have been linked to NLRP-associated diseases and chronic, low-grade inflammation—dietary palmitate and ceramide have also been shown to lead to NLRP3 activation:
Wen and colleagues have shown that palmitate, a saturated fatty acid, can induce NLRP3 activation (Wen *et al*, 2011). Palmitate was shown to inhibit the activation of adenosine monophosphate (AMP)-activated protein kinase, leading to the inhibition of autophagy and mitochondrial ROS production. As a result, they saw NLRP3 activation, leading to IL-1β and IL-18 production, a decrease in insulin sensitivity, and a reduced glucose tolerance (Wen *et al*, 2011).
In addition to palmitate, ceramide has been linked to NLRP3 inflammasome activation in type 2 diabetes mellitus: ceramide is generated from fatty acids during obesity and has been linked to inflammation (Shah *et al*, 2008; Park *et al*, 2008; Håversen *et al*, 2009; Prieur *et al*, 2010) and it has been shown that NLRP3 can sense an increase in intracellular ceramide (Vandanmagsar *et al*, 2011).
Ablation of NLRP3 led to the prevention of obesity-induced inflammasome activation and an enhancement in insulin signalling, as well as to a reduction in IL-18 and IFN-γ expression (Vandanmagsar *et al*, 2011). Resulting chronic

inflammation reduces the size of the pancreatic beta-cell compartment, leading to insulin resistance (Mangan *et al*, 2018).

1.6.3 Inflammatory Diseases of the Lung Involving NLRP3

NLRP3 has further been shown to be involved in many lung-related NCDs, including pulmonary fibrosis, asthma, and COPD.

Pulmonary fibrosis is a result of a chronic and progressive tissue repair response that leads to tissue scarring and remodelling of the lung. It is caused by diverse fibrogenic triggers such as infections, cigarette smoke (CS), pollutants, obesity, or diabetes mellitus (Kolahian *et al*, 2016). Of interest, increased levels of IL-1β and IL-18 have been shown in pulmonary fibrosis (Zhang *et al*, 1993; Pan *et al*, 1996; Kitasato *et al*, 2004) and IL-1β has been shown to contribute to an increase of transforming growth factor beta (TGF-β) and the progression of pulmonary fibrosis (Kolb *et al*, 2001). In a common mouse model of pulmonary fibrosis, the administration of bleomycin, an increase in IL-1β has been observed, in addition to increased levels of TNF-α and TNF-β (Cavarra *et al*, 2004). Additionally, common triggers of pulmonary fibrosis are also triggers of NLRP3 inflammasome activation, such as silica, asbestos, and uric acid (Dostert *et al*, 2008; Cassel *et al*, 2008; Hornung *et al*, 2008; Gasse *et al*, 2009; Peeters *et al*, 2013).
Indeed, silica crystals have been shown to lead to silicosis, a progressive, irreversible and incurable form of lung fibrosis (Hornung *et al*, 2008). Silica crystals are naturally found in sand or quartz and, while the ingestion of silica crystals is harmless, their inhalation causes acute lung inflammation and, if exposure becomes chronic (e.g., due to occupational reasons), leads to pneumoconiosis (progressive massive fibrosis) silicosis (Hornung *et al*, 2008; Mossman & Churg, 1998). The inhaled silica crystals end up in the small airways of the lung where they cannot be cleared by mucocilial clearance. Instead, they are phagocytosed by resident MΦs. Once inside phagosomes, silica crystals activate NLRP3 in a mechanism common with cholesterol crystals (Duewell *et al*, 2010; Rajamäki *et al*, 2010) and other crystals such as uric acid (Gasse *et al*, 2009), Charcot-Leyden crystals (Rodríguez-Alcázar *et al*, 2019), or aluminium:

they induce lysosomal swelling and damage, and the release of the lysosomal cysteine protease cathepsin B. This activates the NLPR3 inflammasome and leads to the release of IL-1β (Hornung *et al*, 2008).

Asthma is a chronic inflammatory airway disease. Inflammation of the airways leads to mucous production, airway wall remodelling resulting in airway obstruction, and bronchial hyperresponsiveness. It manifests as coughing and wheezing, shortness of breath, and chest tightness (Hammad & Lambrecht, 2021). While previously only two main forms of asthma – allergic and non-allergic asthma – had been identified, nowadays asthma is classified into endotypes such as type 2-high and type 2-low which each include a spectrum of different phenotypes. The type 2-high endotype is characterised by T_H2 cell involvement and the corresponding T_H2 cytokines IL-4, IL-5, and IL-13 and the accumulation of type 2-associated cells like eosinophils and mast cells. Type 2-high asthma can be studied using ovalbumin-induced models. While these models are not very physiologically relevant, since the sensitisation happens through intraperitoneal administration of ovalbumin plus alum, these models lead to IL-4, IL-5, and IL-13 production and antigen-specific IgE. The type 2-low (also referred to as non-type 2) endotype is characterised by the lack of the above-mentioned type 2 biomarkers. It has been associated with a later onset of the disease, an unresponsiveness of patients to corticosteroids, and obesity. Of interest, the pathways most consistently linked to type 2-low asthma are linked to inflammasome signalling and IL-1β. Both IL-1β and IL-6 have been identified as mediators of some of the type 2-low asthma phenotypes (Hammad & Lambrecht, 2021).

The involvement of NLRP3 in asthma has been shown in more and more studies, however, the exact role it plays remains controversial (Wu *et al*, 2022).
Some evidence links the non-canonical inflammasome to asthma: caspase-11 has been shown to be elevated in the lungs of mice suffering from allergic airway inflammation and, similarly, caspase-4 has been shown to be elevated in alveolar MΦs from asthma patients (Zasłona *et al*, 2020).

The above-mentioned Charcot-Leyden crystals, which have been shown to activate the NLRP3 inflammasome and cause IL-1β release (Rodríguez-Alcázar *et al*, 2019), are formed from the eosinophilic and basophilic granular protein Galectin-10, also known as Charcot-Leyden protein (Golightly *et al*, 1992; Archer & Blackwood, 1965). They are found in tissues from patients with eosinophilic disorders including asthma and allergic reactions (Dor *et al*, 1984). This points towards an involvement of NLRP3 activation in allergic asthma.
Indeed, one study has shown that NLRP3 activation through mitochondrial ROS production in bronchial epithelial cells induces IL-1β production and contributes to allergic asthma (Kim *et al*, 2014b). The authors have additionally shown that NLRP3 and caspase-1 levels are increased in BAL fluids from patients with asthma compared to levels in healthy controls (Kim *et al*, 2014b).
Along the same lines, it has been shown that NLRP3 drives allergic airway inflammation and mucous hypersecretion: airway eosinophilia and T_H2 cytokine production after ovalbumin challenge is reduced in NLRP3, IL-1R1, IL-1β, and IL-1α knockout mice (Besnard *et al*, 2011).

In contrast, Allen and colleagues, as well as Kool and colleagues, have shown that airway inflammation after allergen challenge shows no difference between NLRP3 knockout and wild type mice (Allen *et al*, 2012; Kool *et al*, 2011). Finally, a study by Madouri and colleagues even found that NLRP3 activation can lead to a dampening of allergic lung inflammation in a house dust mite model (Madouri *et al*, 2015).

All of the above-mentioned studies - those pointing towards and those pointing against NLRP3 involvement in asthma - have looked at the type 2-high asthma endotype. While involvement of NLRP3 in this endotype remains controversial, evidence for the involvement of NLRP3 in the type 2-low endotype is less controversial and suggests involvement of NLRP3 in these phenotypes:
Kim and colleagues have for example studied obesity-related asthma, a phenotype of type 2-low asthma. They have shown that obesity-related asthma

is independent of T and B cells and dependent on NLRP3, and IL-17A (Kim *et al*, 2014a). Kim and colleagues further showed that NLRP3 seems to play a role in severe, steroid-resistant asthma (Kim *et al*, 2017), yet another phenotype belonging to the type 2-low asthma endotype.

Chronic obstructive pulmonary disease (COPD) is characterised by chronic airway inflammation, alveolar destruction, and limitation of airflow (Kaur *et al*, 2022). Risk factors for COPD include exposure to CS, air pollution (Kaur *et al*, 2022), and occupational particular matter, gases, and fumes (Murgia & Gambelunghe, 2022).
COPD is commonly modelled with CS in animal models and cell culture. In mice, CS induces TLR4-, MyD88-, NLRP3-, and IL-1R1-dependent neutrophil recruitment (Doz *et al*, 2008; Eltom *et al*, 2011), as well as NLRP3-dependent IL-1β and IL-18 production (Eltom et al. 2011, 2014). CS has furthermore been shown to induce pyroptosis in human bronchial epithelial cells in a ROS-, NLRP3-, and caspase-1-dependent manner (Zhang *et al*, 2021) and, in an *in vitro* model of COPD exacerbation in A549 cells, NLRP-3 and IL-1β levels increased in a dose-dependent manner (Nachmias *et al*, 2019).
The involvement of NLRP3 in COPD is further supported by a large lung gene expression study: Yi and colleagues demonstrated higher IL-1β gene expression in small airway epithelial cells from COPD patients compared to healthy controls. Interestingly, IL-1β gene expression was only increased in small airway epithelial cells and not in COPD lung tissue, sputum, and blood (Yi *et al*, 2018). This difference of IL-1β expression in the different parts of the lung might for example explain why Di Stefano and colleagues, contrary to the above-mentioned studies, could not identify a role of NLRP3 in COPD, as they looked at caspase-1 activation, IL-1, and IL-18 levels in samples from the bronchial mucosa and from bronchoalveolar lavage (Di Stefano *et al*, 2014).

While the above mentioned diseases already demonstrate that NLRP3 is involved in a very diverse set of diseases, it is involved in even more pathologies (Mangan *et al*, 2018), which would go beyond the scope of this introduction.

1.7 Extracellular Vesicles

1.7.1 Further Consequences of Inflammasome Activation

NLRP3 activation is primarily known for activation of caspase-1 and subsequent cleavage of IL-1β, IL-18, GSDMD, and the initiation of pyroptosis (Figure 2; Broz & Dixit, 2016). However, inflammasome activation has further consequences. An inducible NLRP3 gain-of-function mouse model has shown that, even in the absence of IL-1 receptor and IL-18 signalling, lethal inflammation develops (Brydges *et al*, 2013), suggesting that factors other than IL-1β and IL-18 are involved:

As discussed above, inflammasome activation—in most cases—results in the initiation of pyroptosis, a lytic form of cell death that involves the disruption of the plasma membrane and the release of intracellular content. As a consequence, DAMPS such as high mobility group box 1 (HMGB1) or LDH have been shown to be released (Kayagaki *et al*, 2021; Lamkanfi *et al*, 2010; Barlan *et al*, 2011; Craven *et al*, 2009; Lu *et al*, 2012; Volchuk *et al*, 2020). Extracellular HMGB1 acts as an inflammatory cytokine and is an important player in sepsis (Wang *et al*, 1999; Yang *et al*, 2004). It leads to the activation of macrophages (Yang *et al*, 2010; Lu *et al*, 2012) and endothelial cells (Xiang *et al*, 2011; Fiuza *et al*, 2003), and has been shown to play a role in priming of NLRP3 (Xiang *et al*, 2011; Yu *et al*, 2006b; Barnett *et al*, 2023). Other molecules released upon lytic cell death are ATP and DNA (Yang *et al*, 2015; Denning *et al*, 2019), which have the potential to activate inflammasomes (Sutterwala *et al*, 2006; Mariathasan *et al*, 2006; Hu *et al*, 2016; Jakobs *et al*, 2015; Lammert *et al*, 2020).

Furthermore, it has been shown that inflammasomes themselves, in the form of ASC specks, are released upon NLRP3 activation (Franklin *et al*, 2014; Baroja-Mazo *et al*, 2014). They accumulate in inflamed tissues and are able to continuously mature IL-1β (Franklin *et al*, 2014; Baroja-Mazo *et al*, 2014) or are even taken up by surrounding bystander macrophages, in which they can escape

from the endosome and nucleate further ASC specks (Franklin *et al*, 2018). Interestingly, although currently only hypothesised and not yet investigated, in combination with other intracellular content such as DNA released during pyroptosis, these extracellular ASC specks might even play a role in trapping bacteria for subsequent clearance by neutrophils (Franklin *et al*, 2018).

Finally, extracellular vesicles have been shown to be released upon NLRP3 activation (EVs; MacKenzie *et al*, 2001; Qu *et al*, 2007, 2009; Sarkar *et al*, 2009; Budden *et al*, 2021; Figure 2).

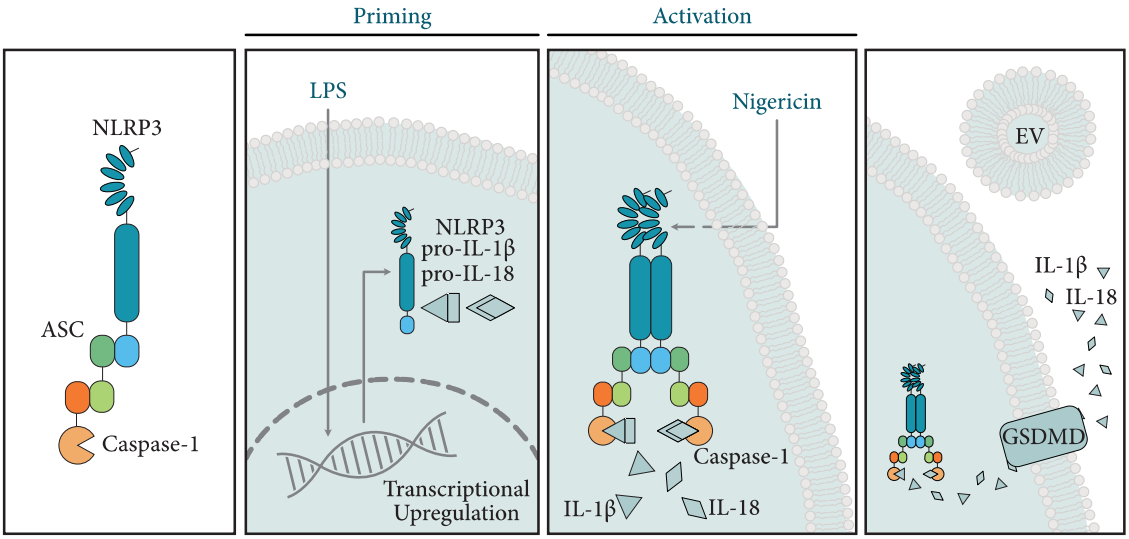

Figure 2: NLRP3 activation leads to the release of IL-1β and IL-18 through GSDMD pores as well as to an increase in EV secretion. The NLRP3 inflammasome recruits ASC through its PYD domain. With its CARD domain, ASC then recruits caspase-1. Canonical inflammasome activation requires a priming and an activation step. Upon stimulation of cells with an NF-κB activator, such as LPS, transcription of NLRP3, IL-1β, and IL-18 is upregulated. Additionally, priming leads to post-transcriptional changes, licensing NLRP3 for activation. A second stimulus, for example nigericin treatment, is needed to activate the NLRP3 inflammasome. Upon activation, NLRP3 forms a multimeric protein complex that results in the cleavage of IL-1β, IL-18, and GSDMD. IL-1β and IL-18 are released from the cell through GSDMD pores in the plasma membrane. An additional result of inflammasome activation is the release of extracellular vesicles (EVs).

EVs are lipid bilayer-encapsulated particles released from cells. They are composed of phospholipids, nucleic acids, and proteins (Lötvall *et al*, 2014; Théry *et al*, 2018). EVs were discovered in 1983 in the context of research on the transferrin receptor in reticulocytes (Pan & Johnstone, 1983; Harding *et al*, 1983).

At that time, EVs were thought to play a role in the removal of cell debris (Johnstone *et al*, 1987); however, they have nowadays been shown to play a role in signalling and cell-cell communication through the exchange of nucleic acids, lipids, and proteins (Raposo *et al*, 1996; Ratajczak *et al*, 2006; Valadi *et al*, 2007; Subra *et al*, 2010).

EVs are present in different bodily fluids including blood (Caby *et al*, 2005; Houali *et al*, 2007), bronchoalveolar lavage fluid (BALF; Admyre *et al*, 2003), urine (Pisitkun *et al*, 2004; Keller *et al*, 2007; Nilsson *et al*, 2009), saliva (Houali *et al*, 2007), nasal lavage fluid (Lässer *et al*, 2011), breast milk (Admyre *et al*, 2007), semen (Poliakov *et al*, 2009), amniotic fluid (Keller *et al*, 2007), cerebrospinal fluid (Vella *et al*, 2008), bile (Masyuk *et al*, 2010), ascites fluid (Andre *et al*, 2002), synovial fluid (Skriner *et al*, 2006), and tears (Grigor'eva *et al*, 2016). Especially the presence of EVs in blood offers an important advantage: these EVs can exert their effects over long distances while their content stays protected.

1.7.2 EV Biogenesis

EV subtypes can be defined based on their origin and biogenesis pathway (Figure 3): exosomes, the smallest EVs, range in size from 30–150 nm (Kalra *et al*, 2016; Turchinovich *et al*, 2019). They originate from the endosomal pathway: double invagination of the plasma membrane leads to the formation of multivesicular bodies (MVBs; Kalluri & LeBleu, 2020). MVBs contain intraluminal vesicles (ILVs), which are formed through inward budding into the lumen of the MVB. Once ILVs are secreted through fusion of the MVB with the plasma membrane, they are called exosomes (Harding *et al*, 1984; Pan *et al*, 1985; Johnstone *et al*, 1987). An alternative fate for MVBs is the fusion with lysosomes or autophagosomes, resulting in the degradation of their content (Van Niel *et al*, 2018). Exosome biogenesis has been described to involve proteins of the ESCRT machinery, tumour susceptibility 101 (TSG101), tetraspanins, ceramides, phospholipids, sphingomyelinases, and others (Kalluri & LeBleu, 2020).

Microvesicles are of intermediate size, ranging in average from 50 nm–1 µm but can also be bigger (up to 10 µm in the case of tumour-derived oncosomes; Van

Niel *et al*, 2018). They shed from the plasma membrane through outward budding (Figure 3; Cocucci *et al*, 2009). Microvesicles were originally called “platelet dust”, a term coined by Wolf *et al.* who demonstrated the presence of subcellular material in plasma through ultracentrifugation (Wolf, 1967). After the discovery of ectocytosis (Stein & Luzio, 1991), they were later called ectosomes, a term often used interchangeably with microvesicles.

Apoptotic bodies derive from apoptotic cells and are on average between 1–5 µm in size (Atkin-Smith *et al*, 2015; Atkin-Smith & Poon, 2017), making them the largest EV population (Figure 3). They can be formed by some cell types during later stages of apoptosis in a process called apoptotic cell disassembly (Atkin-Smith *et al*, 2015).

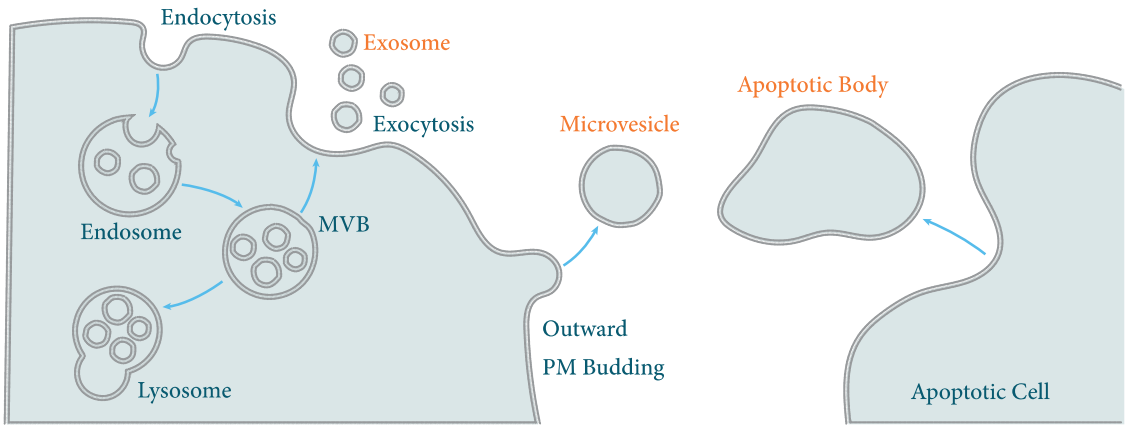

Figure 3: EVs are particles released from cells that are surrounded by a lipid bilayer. They are composed of phospholipids, nucleic acids, and proteins. EV subtypes can be defined based on their pathogenesis pathway: exosomes, the smallest EVs, range in size from 30–150 nm and derive from endosomes. Microvesicles are of intermediate size, ranging from 50 nm–1 µm. They are shed from the plasma membrane. Apoptotic bodies derive from apoptotic cells and are bigger than 1 µm, making them the largest EV population.

1.7.3 EV RNA Content

EVs harbour specific subsets of proteins, nucleic acids, and lipids that do not solely represent the donor cell content (Choi *et al*, 2015). Certain EV components have been shown to be commonly enriched within EV subsets and thus can provide information about EV cargo sorting and biogenesis. Other proteins,

nucleic acids, and lipids are cell-type specific and are therefore used as biomarkers or to study pathophysiological functions (Choi *et al*, 2015).

Interest in nucleic acids contained in EVs sparked in the late 2000s. In 2006, it was shown that microvesicles from embryonic stem cells are selectively enriched in mRNA for several pluripotent transcription factors and that EV mRNA was translated in recipient cells (Ratajczak *et al*, 2006). This knowledge was expanded from microvesicles to exosomes in 2007 when Valadi and colleagues showed that exosomes contain mRNA and small RNAs, such as microRNAs, that can be transferred to recipient cells. Utilising an *in vitro* transfer of mouse exosomal RNA to a human cell line, they could show that exosome-derived mRNA can be translated within the recipient cell (Valadi *et al*, 2007). While these early studies used array techniques and were thus limited in their analysis, especially of small RNAs, the rise of next-generation sequencing led to the identification of further nucleic acid species. Deep sequencing of small non-coding RNAs not only revealed that many of the RNAs found in EVs were enriched compared to the cellular RNA content, but also identified vault RNAs, Y-RNAs and transfer RNAs (tRNAs) as the most abundant small non-coding RNAs in EVs (Nolte-'t Hoen *et al*, 2012).

Besides RNA, deoxyribonucleic acid (DNA) is also contained within EVs. For example, dsDNA was identified within EVs released by tumour cells (Thakur *et al*, 2014) and mitochondrial DNA (mtDNA) was shown to be present in microvesicles from glioblastoma and astrocyte cells (Guescini *et al*, 2010).

1.7.4 EV Protein Content

Early mass spectrometry techniques used gel electrophoresis to isolate and analyse abundant proteins by mass spectrometry (Théry *et al*, 1999; Van Niel *et al*, 2001; Skokos *et al*, 2003; Choi *et al*, 2015). These studies were able to reveal proteins commonly enriched in EVs, such as tetraspanins, annexins, and heat shock proteins (HSPs) (Choi *et al*, 2015). However, few cell-type specific EV proteins were discovered (Choi *et al*, 2015). This has changed with new high-

throughput mass spectrometry-based techniques that allow for the cataloguing of thousands of EV proteins (Choi *et al*, 2013) and thus enable the identification of vesicle- and cell type-specific EV contents. These specific contents may serve as promising biomarkers, which is of particular interest in the field of tumour biology. For example, Hoshino and colleagues showed that tumour-derived exosomal membranes can be enriched in certain integrins and that distinct integrin expression patterns in these exosomes determine the site of tumour metastasis. Integrins $\alpha_6\beta_4$ and $\alpha_6\beta_1$ were demonstrated to be associated with lung metastasis while integrin $\alpha_v\beta_5$ was linked to liver metastasis (Hoshino *et al*, 2015). Thus, EVs could be studied to identify possible novel metastasis sites.

1.7.5 EV Lipid Content

Most studies investigate EV biology with regard to their RNA and protein content. However, some studies have focused on lipids present in EVs. They have revealed that while the EV lipid bilayer mainly resembles the lipid composition of the plasma membrane, including phospholipids, sphingomyelin, monosialodihexosyl ganglioside (GM3), and cholesterol (Choi *et al*, 2013), it is enriched in phosphatidylserine, desaturated phosphatidylethanolamine, desaturated phosphatidylcholine, sphingomyelin, GM3, and cholesterol (Choi *et al*, 2013).

Besides forming the lipid bilayer of EVs, some lipids also play a functional role. For example, sphingomyelin from tumour-derived EVs has angiogenic activity that has been demonstrated *in vitro* as well as *in vivo* (Kim *et al*, 2002). EV lipids can further function as signalling entities. A study using rat basophil-derived exosomes showed that these EVs transport guanosine-5'-triphosphate (GTP)-activatable phospholipase A_2 and phospholipase D_2, as well as the whole set of prostaglandins, and that they are able to modulate cell activation through their lipid contents (Subra *et al*, 2010).

Protein, lipid, and nucleic acid data is collected in field-specific databases. EVpedia (Kim *et al*, 2013b, 2015) and Vesiclepedia (Kalra *et al*, 2012; formerly ExoCarta [Mathivanan & Simpson, 2009]) are online databases on EVs. In

addition, the extracellular RNA (exRNA) Atlas (Subramanian *et al*, 2015) contains data on EVs.

1.7.6 EV Uptake Mechanisms

After being secreted from cells, EVs can travel to near (including autocrine [Matsumoto *et al*, 2017]) or distant sites to exert their effects on recipient cells. How cells interact with EVs – whether no interaction is seen, surface interaction without uptake takes place, or EVs are taken up – is yet to be fully understood.

There seems to be some target cell specificity through the interaction of EV surface proteins with receptors on the recipient cell's membrane (Van Niel *et al*, 2018). This has for example been shown for DC-derived exosomes that appear to be targeted to T cells (Nolte-'t Hoen *et al*, 2009). Other examples are oligodendroglia-derived exosomes that are taken up by microglia but not by astrocytes, neurons, or oligodendrocytes (Fitzner *et al*, 2011), or cortical neuron-derived exosomes that are taken up by neurons and not by glial cells (Chivet *et al*, 2014).
Neuroblastoma-derived exosomes on the other hand were bound by both neurons and glial cells and preferentially taken up by glial cells (Chivet *et al*, 2014), indicating that both mechanisms might be present: transfer of exosomes to specific cells and indiscriminate EV targeting.
More indiscriminate targeting has been further shown by studies that demonstrated that HeLa cells are for example able to take up EVs from a variety of cell types (Costa Verdera *et al*, 2017) and by other studies showing that both normal and transformed cell-lines were able to take up exosomes (Svensson *et al*, 2013), or by the fact that interspecies EV cargo transfer has been observed (Valadi *et al*, 2007).

It is important to note that, to be able to have an effect on recipient cells, EVs do not need to be taken up. The effect of EVs bound to recipient cells may be mediated through receptor signalling. An important example is the ability of B cell-

and DC-derived exosomes to present antigen to T cells to induce an antigen response (Raposo *et al*, 1996; Zitvogel *et al*, 1998; Tkach *et al*, 2017).

EV uptake may be mediated by membrane fusion or by endocytosis followed by fusion with the endosomal membrane (Figure 4).
While vesicle uptake through membrane fusion has for example been demonstrated for human melanoma cells (Parolini *et al*, 2009), for DCs (Montecalvo *et al*, 2012) or for platelets (del Conde *et al*, 2005), most studies have shown endocytosis to be the main mechanism of EV uptake (Escrevente *et al*, 2011; Fitzner *et al*, 2011; Svensson *et al*, 2013; Heusermann *et al*, 2016).
Endosomal pathways include phagocytosis and pinocytosis (Figure 4). Phagocytosis involves the endocytosis of large (> 1 µm) particles and is employed by professional phagocytes such as MΦs or DCs. EVs have been shown to be taken up by phagocytosis in several studies. For example, Feng and colleagues have shown that leukaemia cell line-derived exosomes are taken up through phagocytosis by professional phagocytes. Non-phagocytic cells on the other hand just bound exosomes to the plasma membrane but did not take them up (Feng *et al*, 2010).
While phagocytosis is mainly restricted to professional phagocytes, pinocytosis is not. There are different mechanisms of pinocytosis that can be broadly divided into clathrin-mediated endocytosis and clathrin-independent endocytosis. Clathrin-mediated endocytosis has been shown to be one of the uptake mechanisms of EVs. For example rat PC12 cell-derived exosomes have been shown to be taken up through clathrin-mediated endocytosis (as well as through macropinocytosis; Tian *et al*, 2014)
Forms of clathrin-independent endocytosis are macropinocytosis (often grouped separately from clathrin-independent endocytosis as another category of uptake), lipid raft-mediated endocytosis, and caveolar endocytosis (Nichols & Lippincott-Schwartz, 2001; Donaldson, 2019). All three pathways have been shown to be involved in EV uptake: using microscopy to look at co-localisation of the lipid raft marker cholera toxin subunit B with exosomes, Svensson and colleagues demonstrated that glioblastoma-derived exosomes are taken up through lipid raft-

dependent endocytosis in HUVECs and human glioblastoma cells (Svensson *et al*, 2013). Fitzner and colleagues reported that oligodendrocyte-derived exosomes are taken up by microglia through macropinocytosis (Fitzner *et al*, 2011). Finally, Qi and colleagues have demonstrated exosome uptake through caveolar endocytosis (together with uptake through clathrin-dependent endocytosis and macropinocytosis; Qi *et al*, 2023).

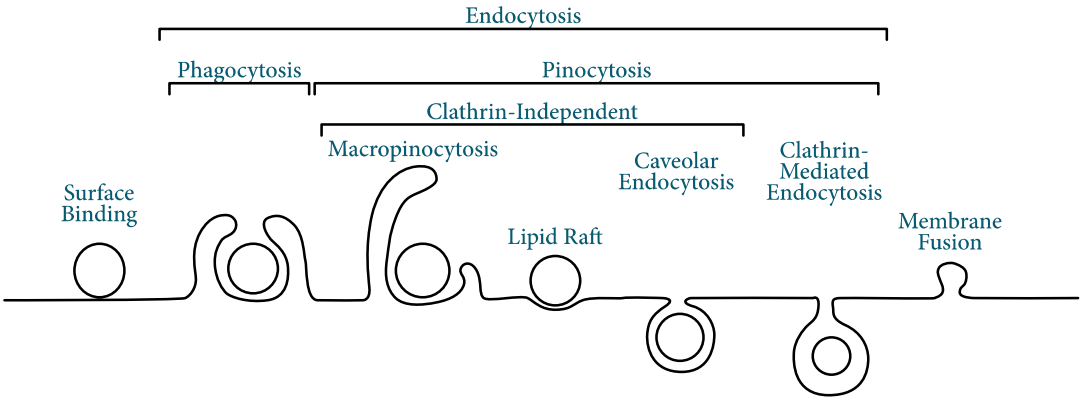

Figure 4: EV interaction with recipient cells. Upon initial contact of EVs with recipient cells, surface binding takes place. This interaction can already trigger changes in the recipient cell—even without uptake. EV uptake is mediated either by membrane fusion or through endocytosis. EVs can either be phagocytosed or taken up through pinocytosis. There are different forms of pinocytosis that can be grouped based on their dependence on clathrin: clathrin-mediated endocytosis and clathrin-independent endocytosis. Clathrin-independent forms of endocytosis are for example macropinocytosis, lipid raft-mediated uptake, and caveolar endocytosis.

1.8 Intracellular Fate of EVs

When taken up through an endocytic pathway, EVs are destined to be targeted to the lysosome for degradation (Tian *et al*, 2010). However, it is possible for EVs to escape digestion in the lysosome by back fusion with the MVB membrane, leading to the release of their contents into the cytoplasm (Bissig & Gruenberg, 2014).

Alternatively, once in the endocytic compartment, EV contents might directly be processed, thus release to the cytoplasm is not needed to exert an effect on recipient cells in this case (Van Niel *et al*, 2018). This has for example been

observed in DCs as well as in intestinal epithelial cells, in which exosomal content has been processed and used for antigen presentation in the endo-lysosomal compartment (Morelli *et al*, 2004; Mallegol *et al*, 2007).

When EVs fuse with the recipient cell's membrane, their contents are directly released into the recipient cell's cytoplasm (Mulcahy *et al*, 2014).

1.9 The Role of EVs in Immunology

In 1996, for the first time, a function of EVs in immunology was shown (Raposo *et al*, 1996). The study focused on the release of exosomes from Epstein-Barr virus-transformed B cell lines. Compared to the composition of the cell plasma membrane, the surface of these exosomes was enriched in major histocompatibility complex (MHC) class II molecules. They could induce antigen-specific MHC class II-restricted T cell responses *in vitro* (Raposo *et al*, 1996). In 1998, the first *in vivo* evidence was published (Zitvogel *et al*, 1998). Exosome release from DCs was studied. These exosomes were shown to express functional MHC class I and II and T cell costimulatory molecules. After peptide-pulsing of the DC-derived exosomes, they were able to prime specific cytotoxic T lymphocytes *in vivo*, leading to the eradication of murine tumours (Zitvogel *et al*, 1998).

1.9.1 MΦ-Derived EVs

In 2003, it was shown for the first time that primary human MΦs release EVs in the context of human immunodeficiency virus (HIV) infection (Nguyen *et al*, 2003). In addition to viral infection, infection of MΦs with mycobacteria, leads to an increase in EV release (Ramachandra *et al*, 2010). These EVs not only contain MHC Class II molecules capable of antigen presentation (Ramachandra *et al*, 2010), but are also loaded with RNA that has been shown to still be functional upon uptake by recipient MΦs (Singh *et al*, 2015). Mycobacteria-induced EVs are able induce a pro-inflammatory response in recipient cells (Bhatnagar & Schorey, 2007). Indeed, MΦs can release EVs containing pro-inflammatory microRNAs

(miRNAs) that have the ability to change the recipient cell's transcriptome (Hulsmans & Holvoet, 2013). MΦs were additionally shown to release mitochondria-containing EVs that can lead to the induction of type I IFN and TNF signalling (Puhm *et al*, 2019). All of this suggests that EVs play an important role in inflammation.

1.9.2 The Inflammasome and EVs

EVs were first linked to inflammasome activation in 2001, when IL-1β was shown to be released in microvesicles after ATP stimulation (MacKenzie *et al*, 2001). This finding was confirmed in 2007 in murine MΦs. Indeed, the release of IL-1β in EVs was demonstrated to be NLRP3 dependent (Qu *et al*, 2007). Besides IL-1β, caspase-1 is found in EVs after LPS stimulation and was shown to induce pyroptosis in recipient cells (Sarkar *et al*, 2009).

Microvesicle release has been shown to be increased by Ca^{2+}-related stimuli (Sidhu *et al*, 2004; Bianco *et al*, 2005; Pizzirani *et al*, 2007). This is of special interest with regard to inflammasome activation, as many NLRP3 activators induce changes in Ca^{2+} flux (Swanson *et al*, 2019). Indeed, in DCs and MΦs, it was shown that activation of the $P2X_7$ receptor, which leads to Ca^{2+} influx, leads to an increase in microvesicle release (MacKenzie *et al*, 2001; Pizzirani *et al*, 2007).

The NLRP3 inflammasome has not only been studied as a source of EVs—it has also been studied as a target of EVs: Bottino and colleagues studied EVs derived from head and neck squamous cells carcinoma. These tumour-derived EVs, when transferred to recipient MΦs, reduced the secretion of IL-1β and caspase-1 by inhibiting the induction of pro-IL-1β during the priming phase (Bottino *et al*, 2021).

Interestingly, in a study by Sur and colleagues looking at COVID-19 patient-derived EVs, it was shown that EVs trigger NLRP3 inflammasome activation in recipient endothelial cells (Sur *et al*, 2022): COVID-19 patient-derived EVs, from both patients with mild or severe COVID, were investigated with regards to their effect on endothelial cells. Compared to EVs from mild COVID-19 patients, EVs from severe COVID-19 patients lead to the strong induction of NLRP3,

caspase-1, and IL-1β mRNA expression in endothelial cells. COVID-19 patient-derived EVs furthermore lead to the secretion of IL-1β, thus playing a role in both priming and activation of the NLRP3 inflammasome (Sur *et al*, 2022).
Along these lines, exosomes from burn injury patient serum have been shown to contain S100 calcium-binding protein A9 (S100A9) and lead to an induction of IL-1β and IL-18 release in recipient cells, as well as to an increase in protein levels of NLRP3, caspase-1, GSDMD, and S100A9 itself in recipient cells, pointing towards an induction of pyroptosis in recipient cells (Wang *et al*, 2022).

Our lab has built on, and contributed to, the above-described knowledge on the role of EVs in the context of NLRP3 activation.
Work on inflammasome-derived EVs was originally started in our lab by Dr. Christina Budden during her work as a PhD student in the Bonn & Melbourne Research and Graduate School Immunosciences IRTG2168. Christina established EV isolation from cell culture supernatant and human blood samples (Budden *et al*, 2021). Combined differential centrifugation and size-exclusion chromatography (SEC) turned out to be the most efficient isolation technique, separating three different EV fractions: large EVs, intermediately sized EVs, and small EVs. Since EV origin was not investigated here and EV subtypes were solely classified based on their size, the nomenclature of exosomes, microvesicles, and apoptotic bodies, as suggested in the literature, could not be applied. Therefore, EVs were named based on their isolation procedure: large EVs pelleting at 2,000 g were called 2K EVs, intermediately sized EVs pelleting at 10,000 g were termed 10K EVs, and small EVs isolated using size exclusion chromatography were called SEC EVs. It can be noted, however, that 2K EVs fell roughly in the size range of apoptotic bodies, 10K EVs within the size range of microvesicles, and SEC EVs in the size range of exosomes.
Dr. Christina Budden studied EV release after inflammasome activation. She focused on EVs released from THP-1 MΦs after treatment with different inflammasome and TLR activators. She could show that inflammasome activation leads to secretion of EVs in an NLRP3-, caspase-1-, and GSDMD-dependent

way (Budden *et al*, 2021). TLR stimulation also triggered EV secretion, but in an NLRP3- and caspase-1-independent manner (Budden *et al*, 2021).

Additionally, the RNA content of 10K and SEC EVs released from inflammasome- and TLR-activated cells was investigated. Vast differences between the 10K and SEC subtypes became apparent, suggesting that the loading of cargo into EVs is a regulated process (Budden *et al*, 2021). For example, the 10K subtype of EVs derived from both TLR- and inflammasome-stimulated MΦs was enriched in mitochondrially encoded transcripts compared to the SEC subtype (Budden *et al*, 2021). Furthermore, EV content varied depending on the initial PRR trigger (Budden *et al*, 2021).

Next, Dr. Christina Budden transferred EVs from inflammasome-activated MΦs to recipient MΦs and investigated EV uptake and transcriptional changes induced in these cells. MΦs rapidly took up EVs. In contrast to TLR-induced EVs, inflammasome-elicited EVs induced an interferon signature in recipient MΦs (Budden *et al*, 2021). When transferring inflammasome-elicited EVs to un-primed primary MΦs the inflammasome response in these recipient cells was downregulated, suggesting a negative feedback loop that limits the detrimental effects of inflammasome activation in the body (Budden *et al*, 2021).

1.10 Aims

As mentioned above, NCDs pose a huge challenge to today's healthcare systems and are expected to increase in frequency even further. With western diet on the rise and air pollution worsening in many parts of the worlds, it is not surprising that NCDs related to the cardiovascular system are currently the main cause of premature death, closely followed by NCDs of the lung. Most NCDs are related to chronic, low-grade systemic inflammation, with the NLRP3 inflammasome playing a prominent role in many.
But how does this chronic, low-grade inflammation spread systemically and what can be done to intervene early enough to stop inflammation turning chronic and leading to cardiovascular or lung diseases in the first place?
Considering the state of current knowledge described above of inflammasome involvement in many NCDs and EV involvement in both inflammasome responses and diseases, as well as what we have learned from previous research in our lab, we believe that inflammasome-elicited EVs might play an important role. While they might not only explain how inflammation becomes systemic, they might also be used as biomarkers to diagnose low-grade systemic inflammation early on and thus prevent many NCDs before they even start causing problems.

Therefore, to gain an understanding of the effects of inflammasome-elicited EV release systemically and to investigate if they might serve as biomarkers for NCDs, we expanded our analysis from recipient MΦs to other cell types. In order to cover both cardiovascular and lung diseases, in addition to working with MΦs, we included fibroblasts, endothelial cells, epithelial cells, and both naïve and activated T cells. Additionally, we analysed EVs isolated after inflammasome activation from human plasma, trying to identify inflammasome-related EV RNA signatures or characteristic proteins that might be used in biomarker development.
To achieve all this, the project was divided into three main parts:

1.10.1 EV Characterisation

Upon inflammasome activation in THP-1 MΦs, a distinct set of EVs is released (Budden *et al*, 2021). So far, this set of EVs has been characterised extensively using microarray analysis of EV-enclosed RNA. Within this project, EVs were further characterised with regards to the EV protein content (Figure 5). Initial Western blotting experiments performed by Dr. Christina Budden needed very high amounts of samples and did not always lead to a positive result. Therefore, part of my PhD project was the establishment of Western blotting for EV proteins. Blotting for different EV marker proteins as well as for GSDMD was performed.

Additionally, the RNA and protein content of EVs derived from human blood after inflammasome stimulation was investigated in an attempt to detect a signature specific to inflammasome-elicited EVs (Figure 5). Originally, sequencing of blood-derived vesicle RNA was tried. However, several problems arose that made it favourable to switch back to a microarray-based analysis.

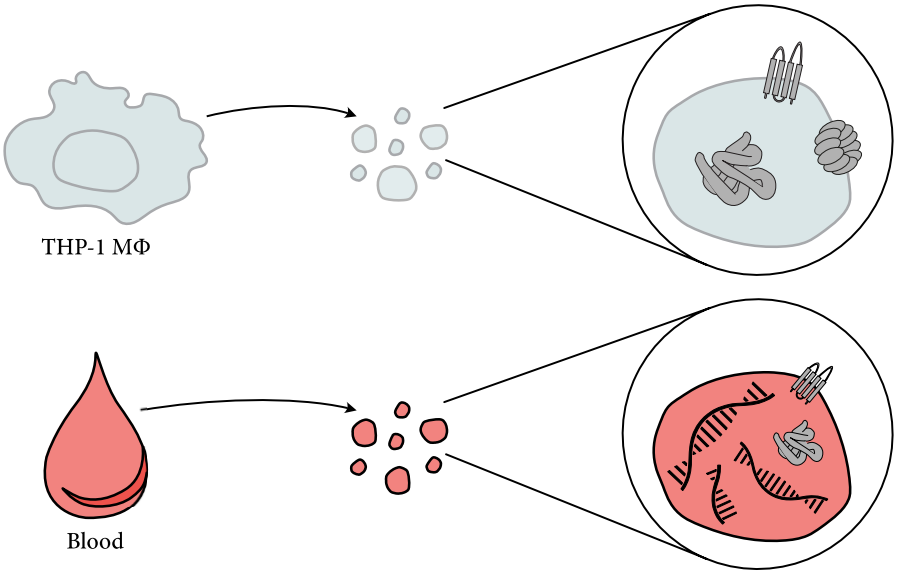

Figure 5: Inflammasome-elicited EV characterisation. Inflammasome-elicited EVs from THP-1 MΦs were analysed with regards to their protein content. Building on this cell culture knowledge, inflammasome-elicited EVs isolated from human blood were characterised for their RNA content and some proteins were investigated.

In the future, this may allow the diagnosis of inflammasome-related diseases through characterisation of patient blood-derived EVs.

1.10.2 Uptake Mechanism of Inflammasome-Elicited EVs

In order to elicit an effect, EVs must interact with recipient cells. Interaction with the surface of recipient cells already allows initiation of signalling cascades and can thus lead to several responses in these cells. Internalisation of EVs is another way of eliciting effects in recipient cells. EVs that are taken up by recipient cells may be degraded in the lysosome, recycled to the cell surface, or their intraluminal content may be released into the cell's cytoplasm (Van Niel *et al*, 2018).
To investigate how inflammasome-elicited EVs interact with recipient cells, different fluorescent EV stainings (R18 and CFSE) and pipelines to quantify EV uptake were established and used on THP-1 MΦs, as well as two lung epithelial cell lines—A549 and BEAS-2B (Figure 6).

EVs can be taken up through different mechanisms, e.g., through macropinocytosis, phagocytosis, through calveolae or clathrin-mediated uptake, uptake through lipid rafts, or by membrane fusion (Figure 4; Van Niel *et al*, 2018). To study how inflammasome-elicited EVs are taken up by recipient cells, EV uptake at 37 °C was compared to uptake at 4 °C. Furthermore, a competition assay, time-course experiments, and inhibition of EV uptake with Cytochalasin D were performed. The read-out for these experiments was confocal microscopy.

Confocal microscopy using fluorescence-based EV staining allowed us to study whether EVs just bind to the surface of recipient cells or if they are indeed taken up. However, it did not allow the investigation of whether or not the intraluminal content of EVs actually ended up in the cytosol. To determine if this is the case for inflammasome-elicited EVs, a cell line was created that expresses the cytoplasmic EV cargo protein HSP70 fused to luciferase (Figure 6). This cell line, together with different control cell lines, was used to study whether cytosolic release of EV cargo plays a role.

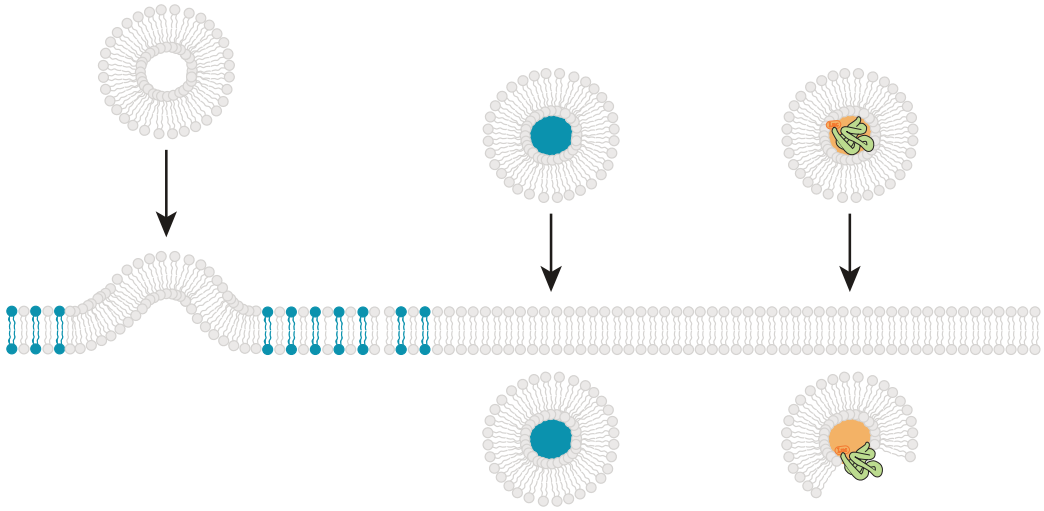

Figure 6: Uptake mechanism of inflammasome-elicited EVs. Inflammasome-elicited EVs from THP-1 MΦs were analysed with regard to their uptake by different recipient cells. EV staining with R18 (self-quenching dye, left) and CFSE (cytoplasmic and EV lumen dye, middle) were established and used to study uptake. Cell lines with luciferase-tagged EV proteins were used to investigate cytoplasmic release of EV contents (right).

1.10.3 THP-1 MΦ-Derived EVs and Their Effect on Different Cells

To gain an understanding of the systemic consequences of inflammasome-elicited EV release, we studied the response of epithelial and endothelial cells, fibroblasts, and T cells to inflammasome-elicited or control EVs (Figure 7).

Originally, we planned to use different cell lines as recipient cells. However, as A549 and BEAS-2B cells showed quite different uptake behaviours as opposed to THP-1 MΦs, possibly, amongst other reasons, due to the fact that they were immortalised or cancer cell line derived, we switched to primary human cells. These included normal human bronchial epithelial cells (NHBECs), normal human lung fibroblasts (NHLFs), human umbilical vein endothelial cells (HUVECs), and primary T cells (naïve and activated T cells).
To understand their response to inflammasome-elicited EVs, their mRNA content was investigated through sequencing.

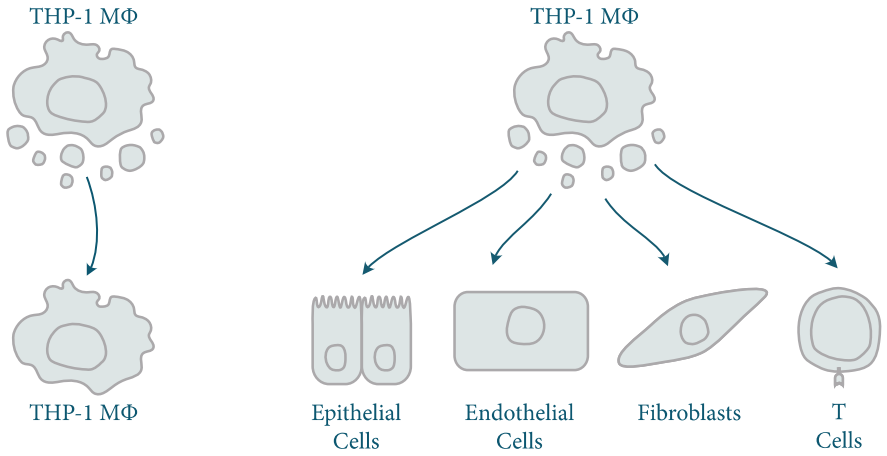

Figure 7: THP-1 MΦ-derived EVs and their effect on different human primary cells. So far, our lab has studied the effect of THP-1 MΦ-derived EVs released upon inflammasome activation in THP-1 MΦ recipient cells. In this project, the analysis was expanded to further recipient cells: epithelial cells, endothelial cells, fibroblasts, and T cells (activated and naïve).

2 Materials and Methods

2.1 Materials

2.1.1 Devices

The following devices were used for experiments shown in this thesis:

Device	Manufacturer
2200 Tape Station System	Agilent Technologies, Inc.
Attune NxT Acoustic Focusing Cytometer	Thermo Fisher Scientific Inc.
Balance, Sartorius Extend, (~0.001 g accuracy)	Sartorius AG
Biometra T3000 Thermocycler	Analytik Jena GmbH
Biometra TAdvanced Series	Analytik Jena GmbH
Biometra TProfessional TRIO Thermocycler	Analytik Jena GmbH
Centrifuge 5425	Eppendorf SE
Centrifuge 5430 R	Eppendorf SE
Centrifuge 5810 R	Eppendorf SE
Centrifuge 5810 R	Eppendorf SE
CO2 Incubator MCO-230AICUV	PHC Corporation
Cooling Thermoshaker CTM	HTA-BioTec
Cryostat Leica CM3050 S	Leica Microsystems GmbH
DynaMag-2 magnet	Thermo Fisher Scientific Inc.
EasySep Magnet	STEMCELL Technologies Inc.
Electronic E4 XLS+ multichannel pipettes	Mettler-Toledo International Inc.
Electrophoresis Power Supply Consort EV202	Thermo Fisher Scientific Inc.
ELMI orbital shaker DOS-10L	ELMI SIA
Epoch Microplate Spectrometer with Take3 Micro-Volume Plate	Agilent Technologies, Inc.
Freezer, -150 °C	Panasonic Holdings Corporation
Freezer, -20 °C	Liebherr-International AG
Freezer, -80 °C	Thermo Fisher Scientific Inc.
Fridge, 4 °C	Liebherr-International AG
HotPlate A3 with HP A3 Hot Plate Controller	Labotect Labor-Technik-Göttingen GmbH
LAB DANCER S000	IKA-Werke GmbH & CO KG
Labnet Spectrafuge Mini Centrifuge	Labnet International Inc
Leica DMi1	Leica Microsystems GmbH

Leica DMi8	Leica Microsystems GmbH
Leica SP5 AOBS with SMD Confocal Microscope	Leica Microsystems GmbH
Leica SP8	Leica Microsystems GmbH
MacBook Pro 13"	Apple Inc.
NanoDrop 1000	Thermo Fisher Scientific Inc.
NanoSight NS300	Malvern Panalytical
Neubauer Cell Counting Chamber	Paul Marienfeld GmbH & Co. KG
NextSeq 2000	Illumina, Inc.
Odyssey M	LI-COR, Inc.
Optima L-80 XP Ultracentrifuge	Beckman Coulter, Inc.
Pipet-Lite LTS Pipette L-1000XLS+, L-200XLS+, L-20XLS+, L-2XLS+	Mettler-Toledo International Inc.
PipetBoy Acu2	INTEGRA Biosciences GmbH
QuantStudio 6 Flex Real-Time PCR System	Thermo Fisher Scientific Inc.
Qubit 3.0 Fluorometer	Thermo Fisher Scientific Inc.
RM5 Roller	Ingenieurbüro CAT M. Zipperer GmbH
Rotator for immunoblotting RM5	Ingenieurbüro CAT M. Zipperer GmbH
Sapphire Biomolecular Imager	Azure Biosystems Inc.
SCANLAF MARS	LaboGene A/S
SpectraMax i3 Plate Reader with HTRF cartridge	Molecular Devices, LLC
Syringe Flow Pump	Malvern Panalytical
ThermoMixer C	Eppendorf SE
ThermoMixer comfort	Eppendorf SE
Unimax 1010 Inkubator 100	Heidolph Instruments GmbH & Co. KG
Vi-CeLL BLU cell viability analyzer	Beckman Coulter, Inc.
Vortex 3 S000	IKA-Werke GmbH & CO KG
VP100	Avantor, Inc.
Waterbath WNE 22	Memmert GmbH + Co. KG
Wes	Bio-Techne Corporation
XCell SureLock Mini-Cell and XCell II Blot Module	Thermo Fisher Scientific Inc.
ZX3 Vortexer	VELP Scientifica

2.1.2 Software

The following software was used for experiments shown in this thesis:

Software	Version	Supplier
Adobe Illustrator	27.1.1	Adobe Inc.
Affinity Designer	1.10.6	Serif Ltd
CellProfiler	4.2.4	(Carpenter *et al*, 2006)
Compass for Simple Western	6.1.0	Bio-Techne Corporation
FastQC High Throughput Sequence QC Report	0.11.9	Babraham
Fiji/ImageJ	2.3.0	Broad Institute, Inc.
Geneious R11	11.1.2	Biomatters Ltd.
ilastik	1.4.0	(Berg *et al*, 2019)
ImageStudio	4.0	LI-COR, Inc.
NanoSight NS300 NTA	3.4.4	Malvern Panalytical
Office 365	16.70	Microsoft Corporation
Prism 9	9.5.1	GraphPad Software, LLC.
QuantStudio 6 and 7 Flex Real-Time	1.3	Thermo Fisher Scientific Inc.
R	4.2.1	(R Core Team, 2022)
RStudio	2022.07.1	(RStudio Team, 2022)
SoftMax Pro	6.3	Molecular Devices, LLC
ZEN	2.0	Carl Zeiss AG
Zotero	6.0.22	Corporation for Digital Scholarship

2.1.3 Plasticware

The following plasticware was used for experiments shown in this thesis:

Product	Company
1 ml Luer Syringe	Becton, Dickinson and Company
10 ml Luer Syringe	Becton, Dickinson and Company
10ml Syringe Luer-Lok Tip	Becton, Dickinson and Company
12 Well Cell Culture Plate, sterile, with lid	Greiner Bio-One International GmbH
18G x 1.5 in. (1.2 mm x 40 mm) Blunt Fill Needle	B. Braun Melsungen AG
20 ml Luer Syringe	Becton, Dickinson and Company
24 Well Cell Culture Plate, sterile, with lid	Greiner Bio-One International GmbH
384 Well Microplate, polystyrol low volume	Labomedic GmbH

384 Well Plate, Nunc	Thermo Fisher Scientific Inc.
384 Well qRT-PCR plate	Thermo Fisher Scientific Inc.
48 Well Cell Culture Plate, sterile, with lid	Greiner Bio-One International GmbH
6 Well Cell Culture Plate, sterile, with lid	Greiner Bio-One International GmbH
96 Well Cell Culture Plate, F-bottom, Cell Carrier Ultra, black wells (for imaging)	PerkinElmer, Inc.
96 Well Cell Culture Plate, sterile, F-bottom, TPP	TPP Techno Plastic Products AG
96 Well Cell Culture Plate, sterile, F-bottom, with lid	Greiner Bio-One International GmbH
96 Well Cell Culture Plate, sterile, U-bottom, with lid	Greiner Bio-One International GmbH
96 Well, Cell Culture Microplate, PS, F-Bottom, Chimney Well, white, Cellstar TC, sterile	Greiner Bio-One International GmbH
Amicon Ultra - 15 Centrifugal Filters Ultracel - 10K, 10,000 NMWL	Merck KGaA
Amicon Ultra - 2mL Centrifugal Filters Ultracel, 10K, 10,000 NMWL	Merck KGaA
Cell Culture Dishes, PS, 145/20 mm, vents, TC, sterile	Greiner Bio-One International GmbH
Cell Culture Flask 250 ml, 75 cm2, PS, Red filter screw cap, clear, sterile	Greiner Bio-One International GmbH
Cell Culture Flask 50 ml, 25 cm2, PS, Red filter screw cap, clear, sterile	Greiner Bio-One International GmbH
Cell Culture Flask 550 ml, 175 cm2, PS, Red filter screw cap, clear, sterile	Greiner Bio-One International GmbH
Cell Strainer 70µm Nylon	Avantor, Inc.
CellCamper Mini-12	neoLab Migge GmbH
CellCamper Mini-30	neoLab Migge GmbH
CellCarrier 96 ultra	PerkinElmer, Inc.
Centrifuge Tubes Polycarbonate Thick Wall 16x76 mm, 13.5 mL	Beckman Coulter, Inc.
Corning 150 mL Vacuum Filter/Storage Bottle System, 0.22 µm Pore 54.5cm² PES Membrane, Sterile	Corning Incorporated
Corning 250 mL Vacuum Filter/Storage Bottle System, 0.22 µm Pore 54.5cm² PES Membrane, Sterile	Corning Incorporated
Costar 12 mm Transwell, 0.4 um Pore Polyester Membrane Inserts	STEMCELL Technologies Inc.
CRYO.S, PP, with screw cap, sterile, Cryopreservation vials	Greiner Bio-One International GmbH
Discardit II Syringe 10ml	Becton, Dickinson and Company

Discardit II Syringe 20ml	Becton, Dickinson and Company
Falcon Round Bottom Polystyrene Tube, 5 mL	Corning Incorporated
Ficoll-Paque Plus	Cytiva (Global Life Sciences Solutions)
Immobilon-FL PVDF Membrane	Merck KGaA
Leukoplast wasserfest Fixierpflaster 1,25cm x 5m	BSN medical GmbH
Microfuge Tube Polypropylene 1.5 mL	Beckman Coulter, Inc.
Millex-HP Filter Unit Fast Flow & Low Binding MIllipore Express PES Membrane	Merck KGaA
Opti-Seal optical disposable adhesive	BIOplastics BV
PCR 8er-Strip-Tubes, 0.2 mL, qPCR, Einzeldeckel	Labomedic GmbH
Pipette Tips 1000 uL BioClean Ultra, Filter, sterilized	Mettler-Toledo International Inc.
Pipette Tips 20 uL BioClean Ultra, Filter, sterilized	Mettler-Toledo International Inc.
Pipette Tips 200 uL BioClean Ultra, LR, Filter, sterilized	Mettler-Toledo International Inc.
Pipette Tips, LTS Green-Pak SpaceSaver 1000uL 768A/8	Mettler-Toledo International Inc.
Pipette Tips, LTS Green-Pak SpaceSaver 20uL 960A/10	Mettler-Toledo International Inc.
Pipette Tips, LTS Green-Pak SpaceSaver 250uL 960A/10	Mettler-Toledo International Inc.
qEVoriginal / 70 nm Gen 2	Izon Sciences Limited
qEVoriginal Rack	Izon Sciences Limited
Rechteckige Deckgläser aus reinweißem Glas der hydrolytischen Klasse 1, 22x50mm, thickness No. 1.5	Avantor, Inc.
Reservoirs, 12 channel, 12×5 ml	Carl Roth GmbH + Co. KG
Reservoirs, 50 mL	Avantor, Inc.
S-Monovette 9-NC, 8.2 mL	Sarstedt AG & Co. KG
S-Monovette K3 EDTA, 9 mL	Sarstedt AG & Co. KG
Safe-Lock Tubes 1.5 mL	Eppendorf SE
Safe-Lock Tubes 2 mL	Eppendorf SE
Safety-Multifly 20G tube200mm	Sarstedt AG & Co. KG
Safety-Multifly 21G tube200mm	Sarstedt AG & Co. KG
Serological Pipette 1 ml in 1/100 ml	Sarstedt AG & Co. KG
Serological Pipette 25 mL in 2/10ml, Costar Stripette 25 mL	Corning Incorporated
Serological Pipette, sterile, 10 ml in 1/10 ml	Greiner Bio-One International GmbH

Serological Pipette, sterile, 5 ml in 1/10 ml	Greiner Bio-One International GmbH
Sterican MIX blunt needle 18G x 1 1/2 1.20 x 40 mm	B. Braun Melsungen AG
SuperFrost Plus Objektträger	Avantor, Inc.
Surgical Gown	O&M Halyard, Inc.
TC-Schale 100, Standard	Sarstedt AG & Co. KG
Tissue-Tek Cryomold, Intermediate Cryomold, 15 mm x 15 mm x 5 mm	Avantor, Inc.
True North Freezer Boxes	Heathrow Scientific LLC
Tube, 15 ML, PP, 17/120 MM, conical bottom, blue screw cap, sterile	Greiner Bio-One International GmbH
Tube, 50 ML, PP, 30/115 MM, conical bottom, blue screw cap, sterile	Greiner Bio-One International GmbH
VWR Reagent Reservoirs	Avantor, Inc.
Whatman Chromatography Paper, 3 mm CHR, 46 x 57 cm	Cytiva (Global Life Sciences Solutions)
Whatman Puradisc FP 30/0.2 CA-S Filter Unit 0.2 um	Cytiva (Global Life Sciences Solutions)
Whatman Puradisc FP 30/0.45 CA-S Filter Unit 0.45 um	Cytiva (Global Life Sciences Solutions)
XCell II Blot Module	Thermo Fisher Scientific Inc.
XCell SureLock	Thermo Fisher Scientific Inc.

2.1.4 Kits

The following kits were used for experiments shown in this thesis:

Product	Company
Clariom D Pico Microarray	Thermo Fisher Scientific Inc.
EasySep™ Human T Cell Isolation Kit	STEMCELL Technologies Inc.
Gene Chip Hybridization Wash and Stain	Thermo Fisher Scientific Inc.
GLOBINclear Kit, human, for globin mRNA depletion	Thermo Fisher Scientific Inc.
Human IL-1b HTRF Kit, Cisbio	PerkinElmer, Inc.
Human TNFa HTRF Kit, Cisbio	PerkinElmer, Inc.
Nano-Glo In-Gel Detection System TM527	Promega GmbH
Nano-Glo Luciferase Assay System TM369	Promega GmbH
Pierce BCA Protein Assay Kit	Thermo Fisher Scientific Inc.
PureLink HiPure Plasmid Maxiprep Kit	Thermo Fisher Scientific Inc.
PureLink Quick Gel Extraction Kit	Thermo Fisher Scientific Inc.
PureLink Quick Plasmid Miniprep Kit	Thermo Fisher Scientific Inc.

Qubit HS RNA assay kit	Thermo Fisher Scientific Inc.
RNAeasy plus micro kit	QIAGEN N.V.

2.1.5 Chemicals

The following chemicals were used for experiments shown in this thesis:

Product	Manufacturer
12-230 kDa Separation 8x25 Capillary Cartridges	Bio-Techne Corporation
2-mercaptoethanol	Merck KGaA
Acti-Stain 488 Phalloidin	Cytoskeleton, Inc.
Agarose	Biozym Scientific GmbH
Ampicillin Ready Made Solution, 100 mg/mL, 0.2 um filtered	Merck KGaA
Animal Component-Free Cell Dissociation Kit	STEMCELL Technologies Inc.
Aqua-Poly/Mount	Polysciences, Inc.
Bovine serum albumin (BSA)	Merck KGaA
Bronchial Epithelial Cell Basal Medium (BEBM)	Lonza Group AG
Bronchial Epithelial Growth Medium (BEGM) Single Quots	Lonza Group AG
CellTrace Far Red	Thermo Fisher Scientific Inc.
cOmplete EDTA-free Protease-Inhibitor Cocktail Tablets	Roche Holding AG
Cultrex 3-D Culture Matrix Rat Collagen I	Bio-Techne Corporation
Cytochalasin D Ready Made Solution, from Zygosporium mansonii, 5 mg/mL in DMSO, 0.2 Œºm filtered	Merck KGaA
DAPI	Thermo Fisher Scientific Inc.
Dimethyl Sulfoxide (DMSO) for cell culture	AppliChem GmbH
DNA/RNA dye peqGREEN	Avantor, Inc.
dNTP mix	Thermo Fisher Scientific Inc.
DRAQ5 5mM	Thermo Fisher Scientific Inc.
Dulbecco's Modified Eagle's Medium (DMEM) (1X), 4.5 g/L glucose, 2 mM L-glutamine, with phenol red	Thermo Fisher Scientific Inc.
Dulbecco's phosphate-buffered saline (DPBS) (1X)	Thermo Fisher Scientific Inc.
Dynabeads Protein A	Thermo Fisher Scientific Inc.
eBioscience CFSE Proliferation Dye	Thermo Fisher Scientific Inc.
Endothelial Cell Basal Medium-2 (EBM-2)	Lonza Group AG

Endothelial Cell Growth Medium-2 (EGM-2) Single Quots	Lonza Group AG
Ethanol	AppliChem GmbH
Fetal Bovine Serum (FBS)	PAN-Biotech GmbH
Fibroblast Basal Medium (FBM)	Lonza Group AG
Fibroblast Growth Medium-2 (FGM-2) Bullet Kit	Lonza Group AG
Fibronectin Solution Bovine	PromoCell GmbH
Formaldehyde 16% (w/v), Methanol-free	Thermo Fisher Scientific Inc.
GeneJuice Transfection Reagent	Merck KGaA
Glycerol	Merck KGaA
Goat Serum, New Zealand origin	Thermo Fisher Scientific Inc.
Haut-Desinfiziens Cutasept F	BODE Chemie GmbH
Hexadimethrine bromide (Polybrene)	Merck KGaA
High Sensitivity RNA Screen Tape	Agilent Technologies, Inc.
High Sensitivity RNA Screen Tape Ladder	Agilent Technologies, Inc.
High Sensitivity RNA Screen Tape Sample Buffer	Agilent Technologies, Inc.
Hoechst 34580	Thermo Fisher Scientific Inc.
Hydrocortisone Stock Solution (200X)	STEMCELL Technologies Inc.
IFM-2384	IFM Therapeutics, LLC.
Interleukin-2, human (hIL-2), recombinant E.coli	Merck KGaA
Isopropanol (technical grade)	AppliChem GmbH
LB agar (Lennox L agar)	Thermo Fisher Scientific Inc.
LB Medium (Luria/Miller)	Carl Roth GmbH + Co. KG
Library preparation, Illumina, RNA with rRNA and globindepletion with ERCC spike-in, value package	Illumina, Inc.
Low Density Lipoprotein from Human Plasma, BODIPY™ FL complex (BODIPY™ FL LDL)	Thermo Fisher Scientific Inc.
MEM NEAA (100X) Minimum Essential Medium Non-Essential Amino Acids	Thermo Fisher Scientific Inc.
Methanol	Carl Roth GmbH + Co. KG
NaCl 5M solution	Merck KGaA
Nigericin, free acid 10mg	Thermo Fisher Scientific Inc.
Nuclease-free water	Thermo Fisher Scientific Inc.
NuPAGE 10X Sample Reducing Agent (10X)	Thermo Fisher Scientific Inc.
NuPAGE 4-12% Bis-Tris Gel 1.5mm X 10 well	Thermo Fisher Scientific Inc.
NuPAGE 4x LDS Sample Buffer (4X)	Thermo Fisher Scientific Inc.

NuPAGE MES SDS Running Buffer (20X)	Thermo Fisher Scientific Inc.
NuPAGE MOPS SDS Running Buffer (20X)	Thermo Fisher Scientific Inc.
octadecyl rhodamine B chloride (R18)	Thermo Fisher Scientific Inc.
oligo(dT)18 Primer	Thermo Fisher Scientific Inc.
Opti-MEM Reduced Serum Medium	Thermo Fisher Scientific Inc.
PageRuler Plus prestained protein ladder	Thermo Fisher Scientific Inc.
Penecillin / Streptomycin (10,000 U/mL)	Thermo Fisher Scientific Inc.
PfuUltra II Hotstart PCR Master Mix	Agilent Technologies, Inc.
Phorbol-12-myristate 13-acetate (PMA, TPA)	Merck KGaA
PhosSTOP phosphatase inhibitor tables	Roche Holding AG
Pierce BCA Protein Assay Kit	Thermo Fisher Scientific Inc.
Pierce TSG101 Antibody (4A10)	Thermo Fisher Scientific Inc.
PMSF	AppliChem GmbH
PneumaCult Ex Plus Basal Medium	STEMCELL Technologies Inc.
PneumaCult-Ali 10x Supplement	STEMCELL Technologies Inc.
PneumaCult-Ali Basal Medium	STEMCELL Technologies Inc.
PneumaCult-Ali Maintenance Supplement	STEMCELL Technologies Inc.
Potasium chloride solution 0.075M, sterile-filtered, BioXtra, suitable for cell culture	Merck KGaA
Power SYBR Green PCR Master Mix	Thermo Fisher Scientific Inc.
ProLong Glass Antifade Mountant	Thermo Fisher Scientific Inc.
PureLink Quick Gel Extraction Kit	Thermo Fisher Scientific Inc.
Puromycin (10 mg/mL)	Thermo Fisher Scientific Inc.
RPMI Medium 1640 (1X)	Thermo Fisher Scientific Inc.
SDS	Carl Roth GmbH + Co. KG
Sodium deoxycholate	Merck KGaA
Sodium Pyruvate 100mM (100X)	Thermo Fisher Scientific Inc.
SuperScript III Reverse Transcriptase	Thermo Fisher Scientific Inc.
T4 DNA Ligase, 5 U/uL	Thermo Fisher Scientific Inc.
TAE buffer 50X	Carl Roth GmbH + Co. KG
TBS 20X	Santa Cruz Biotechnology, Inc.
Tissue-Tek O.C.T. compound	Sakura Finetek Europe B.V.
Tris-Glycine Buffer 10X	Thermo Fisher Scientific Inc.
Tris-HCl	Merck KGaA
Triton X-100	Carl Roth GmbH + Co. KG
Trypan Blue Solution (0.4%)	Merck KGaA
TrypLE Express (1X) Stable Trypsin Replacement Enzyme	Thermo Fisher Scientific Inc.
Trypsin Neutralizing Solution, 100 mL	Lonza Group AG

Tween 20	Merck KGaA
UltraPure 0.5 M EDTA, pH 8.0	Thermo Fisher Scientific Inc.
Ultrapure LPS, E. coli 0111:B4	InvivoGen
Universal-Indikatorpapier pH 1-14	Macherey-Nagel GmbH & Co. KG
Water, nuclease free	Thermo Fisher Scientific Inc.

2.1.6 Antibodies

The following antibodies (except for those included in a kit [2.1.4]) were used:

Antibody	Clone	Manufacturer	Dilution	Application
Mouse anti-b-Actin, rabbit	926-42212	LI-COR, Inc.	1:2000	Western Blotting
Mouse anti-Calnexin, rabbit	MAB 3126	Merck KGaA	1:200, 1:800, 1:1000, 1:2000, 1:20 (WES)	Western Blotting
Gasdermin D (L60), rabbit	93709	Cell Signaling Technology, Inc.	1:20 (WES)	Western Blotting
Histone H3, rabbit	(D1H2) 4499T	Cell Signaling Technology, Inc.	1:2000	Western Blotting
IRDye® 680RD Donkey anti-Rabbit IgG (H + L), 0.5 mg; donkey anti rabbit	926-68073	LI-COR, Inc.	1:20000	Western Blotting
IRDye® 800CW Donkey anti-Mouse IgG (H + L), 0.5 mg; donkey anti-mouse	926-32212	LI-COR, Inc.	1:20000	Western Blotting
Ultra-LEAF Purified anti-human CD28, mouse	CD28.2	BioLegend, Inc.	4 µg/mL	T-cell activation
Ultra-LEAF Purified anti-human CD3, mouse	UCHT1	BioLegend, Inc.	2 µg/mL	T-cell activation
Rabbit anti-b-Tubulin, rabbit	2128	Cell Signaling Technology, Inc.	1:2000	Western Blotting
CD9 Monoclonal Antibody (Ts9), mouse	10626D	Thermo Fisher Scientific Inc.	1:200, 1:800, 1:1000, 1:2000, 1:20 (WES)	Western Blotting

CD63 Monoclonal Antibody (Ts63), mouse	10628D	Thermo Fisher Scientific Inc.	1:200, 1:800, 1:1000, 1:2000, 1:20 (WES)	Western Blotting
CD81 Monoclonal Antibody (M38), mouse	10630D	Thermo Fisher Scientific Inc.	1:200, 1:800, 1:1000, 1:2000, 1:20 (WES)	Western Blotting
TSG101 Monoclonal Antibody (4A10), mouse	MA1-23296	Thermo Fisher Scientific Inc.	1:200, 1:800, 1:1000, 1:2000, 1:20 (WES)	Western Blotting
HPS70 (N27F3-4), mouse	Sc-66049	Santa Cruz Biotechnology, Inc.	1:200, 1:800, 1:1000, 1:2000, 1:100 (WES)	Western Blotting
Apolipoprotein A I, goat	ab 7613	Abcam PLC	1:20 (WES)	Western Blotting
Apolipoprotein B, rabbit	ab 20737	Abcam PLC	1:40	EV Isolation from blood
Acetyl-alpha tubulin clone 6-11B-1, mouse	MABT 868	Merck KGaA	1:500	Microscopy
F(ab')2-Goat anti-Mouse IgG (H+L) Cross-Adsorbed Secondary Antibody, Alexa Fluor 647	A-21237	Thermo Fisher Scientific Inc.	1:500	Microscopy

2.1.7 Primers

The following oligonucleotides were used as qRT-PCR primers:

Target	Sequence
hBST2 fwd	TCTGCAGAGGTGGAGCGACT
hBST2 rev	GAGGCCCAGCAGCACAATCA
hHPRT fw	TCAGGCAGTATAATCCAAAGATGGT
hHPRT rev	AGTCTGGCTTATATCCAACACTTCG
hIFI35 fwd	CCAGGTGATGATGTCCAGCCAG
hIFI35 rev	CCACATCGCCACCTCCGTTC

hIFI6 fwd	GCTCCGGGCTGAAGATTGCT
hIFI6 rev	TTACCTGCCTCCACCCCACT
hIFITM3 fwd	TGCTGATCTTCCAGGCCTATGGA
hIFITM3 rev	GGCAGGGCGAGGAATGGAAG
hISG15 fwd	GCTGAGAGGCAGCGAACTCA
hISG15 rev	CGCCAGCATCTTCACCGTCA
hLY6E fwd	TTGGTTTGTGACCTCCAGGCAG
hLY6E rev	AGCAGGAGAAGCACATCAGCG
hMMP7 for	TGATTGGCTTTGCGCGAGGA
hMMP7 rev	CTGCTACCATCCGTCCAGCG
hMX2 fwd	GAACGTGCAGCGAGCTTGTC
hMX2 rev	GTAGGGCCAAGGCTTGTGGG
hOAS3 fwd	GCTGGTCACCCAGTACCGC
hOAS3 rev	GGATGATAGGCCTGGGCTTCTG
hTGFB1 for	AGTTGTGCGGCAGTGGTTGA
hTGFB1 rev	CCGGTAGTGAACCCGTTGATGT
hTNFa fw	CCCAGGCAGTCAGATCATCTTC
hTNFa rev	TCTCTCAGCTCCACGCCATT
hVIM for	ACGAGGAGGAGATGCGGGAG
hVIM rev	CTGCAATTTCTCCCGGAGGCG

The following oligonucleotides were used as PCR primers:

Target	Sequence
R4106	tttttGGCGCGCCTGCCACCATGGCGGTGGAAGGAGGAATGAAATG
R4107	aaaaaaaaaaaaGCGGCCGCTCACATCACCTCGTAGCCACTTCTGATACTC
R4108	tttttGGCGCGCCTGCCACCATGGCCAAAGCCGCGGCGATC
R4109	aaaaaaaaaaaaGCGGCCGCTCAATCTACCTCCTCAATGGTGGGGCCTG

2.1.8 Plasmids

The following plasmids were used for the generation of stable cell lines (section 2.3). The ID refers to their identifier in the institute of innate immunity (III) Plasmid Repository maintained by Rainer Stahl and Fraser Duthie.

ID	Plasmid	Appli	Bact Resis	*E. coli* Strain	Euk Resis	Original Vector
56	VSVG rbglobPA	Packaging of retroviral particles	amp	*E. coli*, NEB 5-alpha	no	pCMV-VSV-G

57	Gag Pol-rbglobPA	Entry of retroviral particles into cells	amp	*E. coli*, NEB 5-alpha	no	pCMV-GAG-POL
816	5' LTR-MHRRRSRS-mUNC93B (wt)-linker tdTomato-NHKKEKSS	Expression of tdTomato	amp	*E. coli*, NEB 5-alpha	no	pR
925	CAG Enhancer-GagPol-RRE-Rabbit Globulin Terminator	Entry of retroviral particles into cells	amp	*E. coli*, NEB 5-alpha	no	psPAX2
926	CAG Enhancer-VSV_G-Human beta Globulin Terminator	Packaging of retroviral particles	amp	*E. coli*, NEB 5-alpha	no	pMD2.G
1258	CMV-hPKC gamma-eGFP	Expression of EGFP	amp	*E. coli*, NEB 5-alpha	puro	pRP
2048	pInducer20 minus SV40-EF1-Palm signal-EGFP-mPGK-Blasticidin	EGFP targeted to membrane	amp	*E. coli*, NEB 5-alpha	blast	SV40, EF 1-alpha
2049	pInducer20 minus SV40-EF1-Palm signal-tdTomato-mPGK-Blasticidin	tdTomato targeted to membrane	amp	*E. coli*, NEB 5-alpha	blast	SV40, EF 1-alpha
2248	pInducer20 minus CMV-NanoLuc-hCD63-hPGK-Puromycin	NLuc tagged CD63	amp	*E. coli*, NEB 5-alpha	puro	CMV
2249	pInducer20 minus CMV-hCD63-hPGK-Puromycin	Control for 2248	amp	*E. coli*, NEB 5-alpha	puro	CMV
2250	pInducer20 minus CMV-NanoLuc-hHsp70-hPGK-Puromycin	NLuc tagged HSP70	amp	*E. coli*, NEB 5-alpha	puro	CMV
2251	pInducer20 minus CMV-hHsp70-hPGK-Puromycin	Control for 2249	amp	*E. coli*, NEB 5-alpha	puro	CMV

ID: identifier in the Institute of Innate Immunity (III) Plasmid Repository; Appli: application; Bact Resis: bacterial resistance; *E.coli*: *Escherichia coli*; Euk Resis: eukaryotic resistance; amp: ampicillin; blast: blasticidin; puro: puromycin; CMV: cytomegalovirus

2.1.9 Cell Lines and Primary Cells

The following human primary cells, human cell lines, and bacterial cells were used for experiments shown in this thesis. The ID refers to their identifier in the III cell line database maintained by Romina Kaiser.

ID	Name	Description	Preparation/ Origin
CL53	THP-1	Human monocytic cell line from an acute monocytic leukemia patient	ATCC
CL657	THP-1 2251	Derived from CL53 with 2251 insert	Myself
CL656	THP-1 2250	Derived from CL53 with 2250 insert	Myself
CL655	THP-1 2249	Derived from CL53 with 2249 insert	Myself
CL654	THP-1 2248	Derived from CL53 with 2248 insert	Myself
CL380	EGFP-Palmi THP-1	Derived from CL53 with 2048 insert	Myself
CL381	tdTomato-Palmi THP-1	Derived from CL53 with 2049 insert	Myself
CL23	293T HEK	Human embryonic kidney cell line; immortalised with the SV40 large T antigen	ATCC
CL91	A549	Human lung epithelial cancer cell line	Schmidt Lab
CL155	BEAS-2B	Human bronchial epithelial cell line	ATCC
n.a.	HUVEC	Human umbilical vein endothelial cells, pooled, in EGM-2	Lonza Group AG
n.a.	NHBECs	Normal human bronchial/tracheal epithelial cells for B-ALI culture	Lonza Group AG
n.a.	NHLFs	Normal human lung fibroblasts	Lonza Group AG
n.a.	DH5-α	chemically competent *E.coli*	New England Biolabs GmbH

ID: identifier in the III cell line database; n.a.: not applicable.

2.1.10 Cell Culture Media

The following cell culture media were used for cell culture work (section 2.2):

Name	Reagent	Conc
ALI complete base medium	PneumaCult-Ali Basal Medium	
	PneumaCult-Ali 10x Supplement	1X
ALI maintenance medium	ALI complete base medium	
	PneumaCult-Ali Maintenance Supplement (100X)	1X
	Heparin Solution	4 ug/mL
	Hydrocortison Stock Solution (200X)	1X
	P/S	1 %
BEAS-2B freezing medium	BEGM	80 %
	DMSO	10 %
	FBS	10 %
BEGM	BEBM Basal Medium	1X
	BEGM Single Quots	
Detaching Buffer	EDTA	5 mM
	FBS	1 %
	PBS	1X
DMEM 10 % FBS	DMEM	1X
	P/S	1 %
	FBS	10%
HUVEC freezing medium	EGM-2	80 %
	DMSO	10 %
	FBS	10 %
NHBEC basal medium	Pneumacult Ex-Plus Basalmedium	
	Pneumacult Ex-Plus Basalmedium 50X Supplement	1X
	Hydrocotison Stock Solution (200X)	0.2X
	P/S	1 %
NHBEC freezing medium	NHBEC basal medium	50 %
	FBS	40 %
	DMSO	10 %
NHLF freezing medium	FGM-2	80 %
	DMSO	10 %
	FBS	10 %
RPMI 10 % FBS	RPMI	1X
	P/S	1 %
	FBS	10%

Serum-free RPMI	RPMI	
	P/S	1 %
Standard Freezing Medium	FBS	90 %
	DMSO	10 %
T cell medium	RPMI	
	FBS	10 %
	P/S	1 %
	Sodium Pyruvate	1 mM
	NEM Non-Essential Amino Acids Solution	1X
	hIL-2	20 U/mL

2.1.11 Buffers

The following buffers were used for experiments shown in this thesis:

Application	Buffer	Reagent	Concentration
Antibody Staining	Permeabilisation	Triton X-100	0.1 %
		FBS	1 %
		PBS	
	Blocking	Triton X-100	0.1 %
		BSA	3 %
		FBS	1 %
		Goat Serum	1 %
		PBS	
Tissue Culture	Detaching	EDTA	5 mM
		FBS	1 %
		PBS	
	EasySep Buffer	PBS	
		FBS	2 %
		EDTA	1 mM
Western Blot	Transfer	Tris-Glycine Buffer 10X	1 X
		Methanol	20 %
	TBST	TBS	1 X
		Tween 20	0.05 %
	Blocking	TBS	1 X
		BSA	3 %
	RIPA Lysis	Tris-HCl	20 mM
		NaCl	150 mM
		EDTA	1 mM
		Triton X-100	1 %

Glycerol	10 %
SDS	0.1 %
Sodium deoxycholate	1 mM
cOmplete EDTA-free	1 X
PhosSTOP phosphatase inhibitor tablets	1 X
PMSF	0.2 mM

2.2 Cell Culture

All cells were cultured at 37 °C at 5 % CO_2 and 95 % humidity. Unless stated otherwise, cell culture media, phosphate-buffered saline (PBS), and trypsin were warmed to room temperature before use. Cells were regularly screened for mycoplasma contamination.

2.2.1 THP-1 Cells

THP-1 cells (Cell lines CL53, CL380, CL381, CL654, CL655, CL656, and CL657 in the III cell line database) were cultured in suspension flasks (25 cm^2 up to 175 cm^2 depending on cell number) in Roswell Park Memorial Institute (RPMI) medium supplemented with 10 % foetal bovine serum (FBS) (RPMI 10 % FBS medium) and kept at a concentration between 3 x 10^5 and 3 x 10^8 cells/mL. Cells were split every two to three days and kept for up to 20 passages. To split cells, THP-1 cells were transferred to 50 mL tubes and pelleted at 340 x g for 5 min before being resuspended in fresh RPMI 10 % FBS medium, counted, and seeded at a density of 3 x 10^5 cells/mL.

To freeze THP-1 cells, cells were harvested and counted. 10 x 10^6 cells were resuspended in 1 mL pre-chilled standard freezing medium and transferred to a cryovial. Cryovials were transferred to a CellCamper freezing box and frozen at −80 °C at a rate of 1 °C per minute. After 24 h, cryovials were transferred to a −150 °C freezer for long-term storage.

To thaw THP-1 monocytes, cryovials were taken from the −150 °C storage and transferred to a water bath. Cells were thawed for about 3 min, keeping medium

constantly in motion. Using a 10 mL pipette, cells were mixed with RPMI 10 % FBS medium and transferred to a 15 mL tube. Next, THP-1 cells were pelleted at 340 x g for 5 min, resuspended in 15 mL RPMI 10 % FBS and transferred to a 75 cm^2 suspension flask.

THP-1 monocytes were differentiated in 100 mm^2 and 150 mm^2 culture dishes with 100 nM phorbol 12-myristate-13-acetate (PMA) (in dimethyl sulfoxide [DMSO]) for 12–18 h. Cells were washed three times with PBS, and fresh PMA-free RPMI 10 % FBS was added. After leaving cells to rest for about 24 h, PMA-differentiated THP-1 MΦs were harvested using detaching buffer. The desired number of cells was seeded.

2.2.2 HEK293T and A549 Cells

HEK293T (CL23 in the III cell line database) and A549 (CL91 in the III cell line database) cells were cultured in Dulbecco's Modified Eagle Medium (DMEM) 10 % FBS medium in 25 cm^2 to 175 cm^2 adherent cell flasks. Cells were split every two to three days when ~80 % confluency was reached. To split cells, HEK293T cell medium was discarded, and cells were washed with PBS. 2–3 mL (depending on flask size) of TrypLE Express Enzyme (1X) was added, and cells were incubated at room temperature until detached as monitored using a phase contrast microscope (generally 1–5 min). 8–12 mL (depending on flask size) of fresh medium was added and cells were split between 1:5 and 1:15 (depending on confluency). Flasks were filled to a final volume of 12–25 mL (depending on flask size).

HEK293T and A549 cells were frozen and thawed as described above for THP-1 cells in standard freezing medium. Cells of one 175 cm^2 cell flask were typically split into three cryovials.

2.2.3 BEAS-2B Cells

Bronchial epithelial cell growth medium (BEGM) was prepared by adding BEGM Single Quots to Bronchial epithelial basal medium (BEBM). BEGM does not contain any FBS, since it induces epithelial-mesenchymal transition (Malm, Amouzougan & Klimecki 2018). BEAS-2B cells were purchased from ATCC (CRL-9609). Cells were cultured in BEGM medium in 25 cm^2 to 175 cm^2 adherent cell flasks and split every three to four days. Cells were seeded at a density of 3 x 10^3 cells/cm^2 and not allowed to grow to more than 70 % confluency. To passage BEAS-2B cells, medium was removed, cells were washed twice with PBS, and 3–5 mL (depending on flask size) of TrypLE Express Enzyme (1X) was added. Flasks were transferred to an incubator, and cells were incubated for 5–10 min until BEAS-2B cells had detached. 30 mL of medium was added, and cells were pelleted at 120 x g for 10 min to remove trypsin. BEAS-2B cells were resuspended in fresh BEGM and seeded.

BEAS-2B cells were frozen and thawed as described for THP-1 cells but in BEAS-2B freezing medium and only using centrifugation at 120 x g for 10 min. Cells of one 175 cm^2 cell flask were typically split into 3 cryovials.

2.2.4 NHLFs

Fibroblast Growth Medium-2 (FGM-2) was prepared by adding FGM-2 SingleQuots to Fibroblast Basal Medium (FBM). NHLFs were purchased from LONZA (CC-2512). NHLFs were cultured in FGM-2 in 75 cm^2 adherent cell flasks and split every two to three days whenever confluency reached 70-80 %. To split cells, the medium was removed, cells were washed with PBS twice, and 5 mL of TrypLE Express Enzyme (1X) was added. NHLFs were incubated at 37 °C for 2–6 min until cells started to detach. Trypsin was neutralised by adding 10 mL FGM-2 and cells were transferred to a 15 mL tube. The culture flask was rinsed with 2 mL PBS to collect residual cells. NHLFs were centrifuged at 220 x g for 5 min. 2 x 10^5 cells were seeded per 75 cm^2 flask. NHLFs were only used for up to five passages.

NHLFs were frozen as described for THP-1 cells but in NHLF freezing medium. 1 x 10^6 cells were frozen per cryovial. Cells were only frozen down after the initial purchase from Lonza at passages two and three.

To thaw NHLFs, 25 mL FGM-2 was added to a 75 cm^2 adherent cell flask and the flask was placed in an incubator for 30 min to allow for equilibration. Cryovials were removed from the −150 °C freezer and thawed in a 37° C water bath. Cells were directly added to the flask, without centrifugation. Medium was changed after 16–24 h to remove DMSO.

2.2.5 HUVECs

Endothelial Growth Medium-2 (EGM-2) was prepared by adding EGM-2 Single Quots to Endothelial Basal Medium-2 (EBM-2). Pooled HUVECs in EGM-2 were purchased from Lonza (C2519A). HUVECs were cultured in EGM-2 in 75 cm^2 adherent cell flasks and split every two to three days whenever confluency reached 70–80 %. To split cells, cells were washed with PBS and 5 mL of TrypLE Express Enzyme (1X) was added. HUVECs were placed into the incubator for 3–5 min until about 90 % of cells had rounded up. Trypsin was neutralised using 5 mL Trypsin Neutralising solution and cells were transferred to a 15 mL tube. The culture flask was rinsed with 2 mL PBS to collect residual cells. HUVECs were pelleted at 200 x g for 5 min, taken up in fresh medium and split 1:2 to 1:5. HUVECs were only used for up to two to three passages after initial thawing.

HUVECs were frozen as described for THP-1 cells but in HUVEC freezing medium. 5 x 10^5 cells were frozen per cryovial. They were only frozen down until passage four. HUVECs were thawed as described for NHLFs but with 15 mL of initial medium per 75 cm^2 flask.

2.2.6 NHBECs

NHBECs (CC-2540S) were purchased from Lonza. Cells were initially expanded, and aliquots were frozen down: 25 mL of NHBEC basal medium were added to

a 75 cm^2 adherent cell flask and placed into the incubator for 30 min. NHBECs were removed from the −150 °C freezer and thawed at 37 °C in a water bath. Cells were gently resuspended in the cryovial and added to the cell flask. No centrifugation was performed as per the manufacturer's recommendation. The cell flask was directly placed in the incubator and medium was changed after 16–24 h. After two to three days of culturing fresh NHBECs, when confluency was at about 60–80%, the first aliquots were frozen down and cells were split. To passage NHBECs, cells were washed with PBS and dissociated from the culture vessel using 5 mL Animal Component-Free Cell dissociation solution for 2–6 min at 37 °C. The reaction was stopped with Animal Component-Free enzyme inhibition solution and cells were collected in a 15 mL tube. Flasks were rinsed twice to collect the remaining cells. NHBECs were pelleted at 340 x g for 5 min, counted, and seeded or frozen. 5 x 10^5 cells were seeded per new 75 cm^2 flask and remaining cells were frozen at 1 x 10^6 cells per cryovial. NHBECs were frozen as described previously for THP-1 cells but in NHBEC freezing medium.

Before seeding NHBECs on transwell inserts, inserts were coated with collagen. Collagen was diluted 1:100 in deionised, sterile, cold water, and 100 µL was applied per insert. Transwells were incubated for 60 min at 37°C. Every 10 min, transwells were gently shaken. After incubation, the remaining collagen solution was aspirated, and inserts were dried under the hood for 2 h at room temperature. 1 mL of NHBEC basal medium was added per well in the lower chamber. About 8 x 10^4 cells were then seeded in 500 µL on transwells. In case of using frozen cells, cryovials were thawed in a water bath, transferred to fresh medium, and centrifuged at 340 x g for 5 min to remove DMSO, resuspended in medium and 8 x 10^4 cells were seeded per transwell.
NHBECs were expanded on transwells for about 5 days until full confluency was reached. Medium was changed in both chambers on day one and day three.
Once confluency was reached, cells were air lifted: medium from both chambers was aspirated and 1 mL of air-liquid interface (ALI) maintenance medium was added to the lower chamber. Medium was changed two to three times per week

and after about two weeks, cells were washed once a week with 1 mL PBS to wash away mucous.

2.2.7 T Cell Isolation and Culture

Circulating T cells were isolated from healthy donors. 20 mL of blood per donor was drawn using either a 20 or 21 safety multifly needle and K3 ethylenediaminetetraacetic acid (EDTA) S-Monovettes. Blood was transferred to a 50 mL tube and 20 mL PBS was added. Two 50 mL tubes were filled with 15 mL of Ficoll-Paque Plus. PBS-diluted blood was then carefully overlayed, and tubes were spun at 400 x g for 35 min with minimal acceleration and no brakes. The peripheral blood mononuclear cell (PBMC) layer was transferred to a new 50 mL tube, which was then filled up to 40 mL with PBS. Cells were pelleted at 400 x g for 20 min. Cells were resuspended in OptiMEM, filtered through a 70 µM cell strainer, and counted.

T cells were isolated according to manufacturer's instructions using the EasySep Human T Cell Isolation Kit from StemCell. In short, a volume of OptiMEM containing 5 x 10^7 cells was taken and centrifuged at 340 x g for 5 min to pellet cells. PBMCs were resuspended in 600 µL EasySep buffer and transferred to a 5 mL polystyrene round-bottom tube. 30 µL of EasySep Human T cell Isolation Cocktail was added and mixed with cells. After 5 min of incubation, 24 µL of EasySep Dextran RapidSpheres (vortexed for 30 sec) was added and mixed with the cells. Next, 1.41 mL EasySep buffer was added to a total volume of 2.5 mL and mixed gently. The tube was placed into an EasySep magnet and incubated for 3 min. Magnet and tube were inverted, pouring the enriched cell suspension into a new tube.

T cells were either kept in a naïve state or activated. For naïve T cells, 2 x 10^5 cells/well were added to a TPP 96-well plate in 200 µL T cell medium per well. They were used directly for experiments.

To activate T cells, a TPP 96-well plate was coated with 2 µg/mL CD3 and 4 µg/mL CD28: Appropriate volumes of CD3 and CD28 were mixed with PBS, and 50 µL were added per well. Plates were incubated for 2 h at 37 °C.

Afterwards, plates were washed two times with 200 µL PBS per well. Wells were kept covered with PBS until T cells were seeded. 1 x 10^5 cells/well were seeded in 200 µL T cell medium. T cell medium was changed every two to three days: 96-well plates were centrifuged at 300 x g for 5 min, medium was removed, and cells were resuspended in 200 µL/well of fresh medium. T cells were split through centrifugation at 300 x g for 5 min followed by resuspension in fresh medium and cell counting. Cells were seeded at 1 x 10^5 cells/well in 200 µL T cell medium/well.

2.2.8 EV-Free Medium

Cell Culture Medium for recipient cells for transfer experiments (section 2.5) was transferred to 1.5 mL or 13.5 mL ultracentrifuge (UC) tubes (depending on volume needed) and spun for 18 h at 100,000 x g. Medium was filtered through a 0.22 µm vacuum filter and stored at 4 °C until use.

2.3 Generation of Stable Cell Lines

Insert generation, backbone vector linearisation, ligation, transformation by heat shock, plasmid generation by mini- and maxiprep, and generation of glycerol stocks were performed by Fraser Duthie and Rainer Stahl.

2.3.1 Insert Generation

Inserts were generated either from the restriction digest of already available plasmids at the III Plasmid Repository, or from a precision LentiORF collection. The 2048 and 2049 inserts are based on (Sung *et al*, 2020, 2015) and were generated using plasmids 1258 and 816 from the III Plasmid Repository. The 2248, 2249, 2250, and 2251 inserts are based on Bonsergent *et al*. (2021), Gupta *et al*. (2020), and Hikita *et al*. (2018) and were cloned from the LentiORF: hCD63 was cloned by polymerase chain reaction (PCR) using primers R4106/R4107 and hHSP70 was cloned from the LentiORF by PCR using primers R4108/R4109.

PCR amplification was employed to amplify inserts. PfuUltra II Hotstart PCR Master Mix containing PfuUltra II Fusion HS DNA polymerase was mixed with forward and reverse primers (0.5 µM final concentration) and 100–500 ng DNA. Initial denaturation was performed for 1 min at 94 °C, followed by 35 or 40 cycles of denaturation for 30 sec at 94 °C, primer annealing for 30 sec at 58–65 °C (based on primer T_m), and elongation for 1 min/kb DNA at 72 °C. A final elongation for 5–10 min at 72 °C was performed. PCR products were then separated on a 1–1.5 % agarose gel in tris-acetate-EDTA (TAE) buffer at 120 V using the green DNA/RNA dye peqGREEN. Products were isolated from the gel using the PureLink Quick Gel Extraction kit according to the manufacturer's instructions. Using an appropriate pair of restriction enzymes, sticky ends were generated. Products were again run on a 1–1.5 % agarose gel and purified.

2.3.2 Backbone Vector Linearisation

Backbone vectors (SV40-EF1 for 2048 and 2049 and cytomegalovirus (CMV) for 2248–2251) were linearised using the same restriction enzymes used to generate the insert sticky ends. Vectors were run on a 1 % agarose gel and purified.

2.3.3 Ligation

On ice, insert and backbone vector were mixed at a ratio between 3:1 and combined with T4 DNA ligase and 1X T4 DNA Ligase Buffer. After 1 min of incubation on ice, the mix was incubated for 20 min at 22 °C, before being transferred back to ice again.

2.3.4 Transformation by Heat Shock

Having generated the plasmid, 3 µL of the ligation product was mixed with 50 µL chemically competent DH5α *E. coli* cells taken from a glycerol stock and thawed on ice. Bacteria/plasmid mixes were incubated for 30 min on ice before being transferred for 45 sec to 42 °C to administer the heat shock. This was followed by regeneration for 5 min on ice.

2.3.5 Plasmid Preparation Using MiniPrep

Freshly transformed *E. coli* were added to Luria-Bertani (LB) broth and were incubated for 60 min at 37 °C under shaking (1000 rpm). Subsequently, bacteria were plated on LB-agar plates with 100 µg/mL ampicillin and incubated overnight at 37 °C. The next day, single colonies were picked to inoculate bacterial cultures (6 mL LB broth containing 100 µg/mL ampicillin). Cultures were grown for 16 to 18 h at 37 °C under shaking (~360 rpm). Next, bacteria were harvested, and plasmids were isolated using the PureLink Quick Plasmid Miniprep kit according to the manufacturer's instructions. Plasmids were verified by Sanger Sequencing performed by Eurofins Genomics or GATC Biotech and pairwise alignment using Geneious software.

2.3.6 Glycerol Stocks

One of the positive clones was used to prepare a glycerol stock. To do so, 600 µL bacterial suspension in LB broth containing 100 µg/mL ampicillin was mixed with glycerol (final concentration 20 %) to a final volume of 1 mL and frozen at −80 °C.

2.3.7 Plasmid Preparation Using MaxiPrep

Glycerol stocks were used to inoculate 6 mL LB broth containing 100 µg/mL ampicillin for incubation overnight at 37 °C under shaking (~360 rpm) before then inoculating 150 mL LB broth containing 100 µg/mL ampicillin with 150 uL. Bacterial cultures were incubated for 16–18 h at 37 °C under shaking (~170 rpm). The PureLink HiPure Plasmid Maxiprep kit was then used according to the manufacturer's instructions to isolate plasmids, and Sanger Sequencing was performed by Eurofins Genomics or GATC Biotech followed by pairwise alignment using Geneious software to verify plasmids.

2.3.8 Production of Retroviruses in HEK293T Cells

All work was carried out under S2 biosafety conditions. HEK293T cells low in passage number were plated in a 6-well tissue culture plate and incubated

overnight at 37 °C. The next day in the evening, when cells were approximately at 70–80 % confluency, cells were transfected for retroviral production: for each well, a 10 µL DNA master mix was prepared consisting of the retroviral construct (1.5 µg of 2048 and 2049, 2 µg of 2248, 2249, 2250, and 2251), gag-pol plasmid (for packaging of the virus; 1 µg of plasmid 57 in case of CMV-based plasmid [for 2248–2251] and 0.65 µg of plasmid 925 in case of SV40-EF1 lentivirus-based plasmid [for 2048 and 2049]), vesicular stomatitis virus (VSV)-G plasmid (for entry into cells; 100 ng of plasmid 56 in case of CMV-based plasmid [for 2248–2251] and 0.35 µg of plasmid 926 in case of SV40-EF1 lentivirus-based plasmid [for 2048 and 2049]) in FBS-free DMEM. A transfection reagent master mix, consisting of GeneJuice (transfection reagent; 8 µL for 2248–2251 and 5.5 µL for 2048 and 2049) in FBS-free DMEM (100 µL/well for 2248–2251 and 150 µL/well for 2048 and 2049) was prepared and incubated for 5 min at room temperature. Next, the transfection reagent master mix was combined with the DNA mix and incubated for 20 min at room temperature to allow the complex formation of DNA and transfection reagent. Meanwhile, HEK293T cell medium was changed to fresh culture medium. Next, cells HEK293T cells were transfected with 100 µL of the DNA/transfection reagent (100 µL/well for 2248–2251 and 300 µL/well for 2048 and 2049), mixed and incubated overnight at 37 °C. The next morning, the media was replaced with 2 mL RPMI containing 30 % FBS. After 30 h of incubation the medium containing the retrovirus was harvested through an 18G blunt needle using a 10 mL Luer-lock syringe and filtered through a 0.45 µm filter into a 50 mL tube.

2.3.9 Retroviral Infection of Target Cells

Per transduction, 2 x 10^5 THP-1 monocytes and 4 µg/mL polybrene were added to the retrovirus containing HEK239T cell medium tubes and tubes were centrifuged for 90 min at 32 °C. Afterwards, the cells were carefully resuspended in the virus-containing media and transferred to a 24-well tissue culture plate. Cells were incubated with the virus overnight at 37 °C. The next morning, the THP-1 monocytes were transferred to a 50 ml tube and centrifuged at 350 x g for 5 min. The virus-containing supernatant was removed, and cells were

resuspended in fresh RPMI 10 % FBS and transferred to a new well of a 24-well plate. Cells were passaged four times before being switched to S1 biological safety conditions and selected.

2.3.10 Selection of Infected Cells Using FACS

In case of THP-1 monocytes transduced with 2048 and 2049, fluorescence-activated cell sorting (FACS) was employed to select for successfully transduced cells. THP-1 monocytes were grown in 150 mL in T175 culture flasks. Once confluent, cells were pelleted at 340 x g for 5 min. Supernatant was removed, cells were washed with PBS, centrifuged at 340 x g for 5 min, and resuspended in 2–3 mL RPMI 10 % FBS. Cells were filtered through a 70 µm cell strainer to remove cell aggregates and handed to the Flow Cytometry Core Facility (Medical Faculty, University of Bonn) for FACS using the BD FACS Aria III. Sorted cells were pelleted at 340 x g for 5 min and resuspended in RPMI 10 % FBS at a density of 3 x 10^5 cells/mL. Cells were expanded until cell numbers were high enough to freeze down aliquots.

2.3.11 Selection of Infected Cells Using Mammalian Selection Marker

THP-1 monocytes successfully transduced with 2248, 2249, 2250, and 2251 were selected through the addition of puromycin (10 µg/mL) to the culture medium and culturing for about seven days. Afterwards cells were expanded until cell numbers were high enough to freeze down aliquots.

2.4 Stimulation & Inhibitors

LPS only: Cells were stimulated with 200 ng/mL LPS in their respective media for 2 h at 37 °C. Next, cells were washed three times with PBS.
LPS + nigericin: To activate the NLRP3 inflammasome, cells were stimulated with 200 ng/mL LPS for 2 h at 37 °C. Cells were then washed three times with PBS to remove all remaining LPS. Next, cells were stimulated with 10 µM nigericin for 90 min at 37 °C.

Nigericin only: Cells were stimulated with 10 µM nigericin for 90 min at 37 °C.
DMSO + UT (23 h): Whole blood was mixed with DMSO (0.014 % final concentration) and incubated for 24 h at 37 °C.
DMSO + LPS (23 h): Whole blood was mixed with DMSO (0.014 % final concentration) and incubated for 1 h at 37 °C. LPS (1 µg/mL final concentration) was added and samples were incubated for 23 h at 37 °C.
CRID3 + LPS (23 h): Whole blood was mixed with cytokine release inhibitory drug 3 (CRID3) (5 µM final concentration) and incubated for 1 h at 37 °C. LPS (1 µg/mL final concentration) was added and samples were incubated for 23 h at 37 °C.
IFM-2384 + LPS (23 h): Whole blood was mixed with IFM-2384 (4 µM final concentration) and incubated for 1 h at 37 °C. LPS (1 µg/mL final concentration) was added and samples were incubated for 23 h at 37 °C.

2.5 Transfer Experiments

For all transfer experiments, the same relative EV concentrations were used: originally, experiments were carried out for THP-1 MΦ-derived EVs and their effect on THP-1 MΦs at a ratio of 40 EV donor cells to 1 EV recipient cell. EVs from 13 x 10^6 donor THP-1 MΦs were used to stimulate 325,000 recipient THP-1 MΦs in a volume of 300 µL in a 24-well plate. As the different cells used here were of different sizes and thus different cell numbers were plated in 24-well plates (or even other well plates were used), the concentration was left the same while the donor-to-recipient cell ratio changed. This would best represent the in vivo situation, where EV concentration levels would not change for cell types. It was thus ensured that for every 13 x 10^6 donor THP-1 MΦs, 300 µL of PBS was used to resuspend the final EV pellet. 300 µL was then applied to all 24-well plates (or 12-well plates with inserts the size of a 24-well), and 150 µL was applied to 96-well plates.
For microscopy experiments, originally 2.4 x 10^6 donor THP-1 MΦs were used to stimulate 60,000 recipient THP-1 MΦs in a volume of 50 µL (slightly different concentration). Thus, for microscopy experiments here, EVs from 2.4 x 10^6 donor

THP-1 MΦs, were applied to every well of a 96-well plate in a total volume of 50 µL.

2.5.1 For Microscopy

Per well, EVs from 2.6 x 10^6 PMA-differentiated THP-1 MΦs stimulated with LPS and nigericin were isolated and stained with R18 or CFSE (section 2.6.2) or isolated from enhanced green fluorescent protein (EGFP) THP-1 MΦs (section 2.6.1). Different recipient cell numbers were used as indicated in the figures.
EGFP THP-1 MΦ-derived 10K and SEC EVs were transferred to tandem dimer (td)Tomato THP-1 MΦs for 15 h.
CFSE/R18-stained 10K and SEC EVs were transferred to THP-1 MΦs and A549 and BEAS-2B epithelial cells at different time points (1 h, 3 h, 7 h, 15 h, 24 h), in competition with unstained 10K and SEC EVs (Either using different ratios of stained to unstained EVs at a constant overall EV concentration; or using stained EVs in the presence and absence of an excess of unstained EVs leading to an overall higher EV concentration), at different temperatures (4 °C vs 37 °C), and in the presence vs absence of 2 µM Cytochalasin D.
CFSE/R18-stained 10K and SEC EVs were transferred to NHBEC, HUBEC, NHLF, naïve T cells, and active T cells for 15 h.

2.5.2 For Sequencing

10K and SEC EVs from 6.5 x 10^7 PMA-differentiated THP-1 MΦs, stimulated with LPS only or with LPS and nigericin, were isolated as outlined in section 2.6.1:

- **UT** → untreated
- **10KL** → 10K EVs from LPS stimulated cells (15 h)
- **10KLN** → 10K EVs from LPS + nigericin stimulated cells (15 h)
- **SECL** → SEC EVs from LPS stimulated cells (15 h)
- **SECLN** → SEC EVs from LPS + nigericin stimulated cells (15 h)
- **LPS** → LPS only (2 h)
- **Nig** → Nigericin only (90 min)

These stimuli were used, in a reverse time course, to stimulate the following recipient cells:

- **NHBEC**: 8 x 10^4 cells/transwell were seeded one month before the experiment and expanded for one week. After expansion, cells were airlifted and allowed to differentiate for three weeks.
- **HUVEC**: 5 x 10^4 cells/well, seeded one week before the day of EV isolation and allowed to grow to full confluency on a transwell membrane.
- **NHLF**: 1 x 10^5 cells/well, seeded three days before the day of EV isolation and allowed to grow to 70 % confluency.
- **naïve T cells**: 2 x 10^5 cells/well were isolated on the day of EV isolation and cultured in an uncoated plate.
- **activated T cells**: 2 x 10^5 cells/well were isolated one week before the experiment and activated in a CD3/CD28-coated plate for one week.

To stimulate the different recipient cells, the old cell culture medium was removed and 290 µL (for HUVEC and NHLF) or 145 µL (for naïve and activated T cells) of EV-free medium was added. In case of NHBEC cells, the bottom chamber medium was exchanged to fresh medium. Stimuli were applied by addition to EV-free medium (or directly on top of air-exposed NHBEC side) at respective times in 10 µL (NHBEC, HUVEC, and NHLF cells) or 5 µL (naïve and activated T cells) PBS.

2.6 EV Isolation

2.6.1 From Cell Culture

THP-1 MΦ cell culture supernatants were spun at 340 x g for 10 min at 4 °C to remove cells. Supernatants were transferred to new tubes and spun at 2,000 x g for 20 min at 4 °C to remove cell debris and pellet the 2K fraction. 2K supernatants were transferred to new tubes. 2K pellets were either used directly (for nanoparticle tracking analysis (NTA) measurements, if not stated otherwise) or washed in PBS and pelleted at 2,000 x g for 20 min at 4 °C (for transfer experiments, protein, and RNA extraction). 2K supernatants were then spun at

10,000 x g for 45 min at 4 °C to pellet the 10K fraction. 10K supernatants were transferred to new tubes. 10K pellets were either used directly (for NTA measurements, if not stated otherwise) or washed in 1 mL PBS and pelleted at 10,000 x g for 45 min at 4 °C (for transfer experiments, protein, and RNA extraction). 10K supernatants were filtered through 0.22 µm filters and concentrated to a volume of 450–500 µL using Amicon tubes with a 10K cut-off according to the manufacturer's protocol. Samples were adjusted to exactly 500 µL using PBS and SEC was performed: room-temperature adjusted qEV original (70 nm Gen 2, IZON) SEC columns were washed with at least 10 mL PBS. 500 µL sample were applied to the column. Once absorbed by the column matrix, 2.5 mL PBS were added in steps of 500 µL. The flow through, consisting of fractions one to six, was discarded. Next, fractions seven, eight, and nine were collected by placing a 1.5 mL tube under the SEC column and applying another 1.5 mL of PBS to the column. Finally, columns were washed with at least 10 mL PBS. Captured SEC fractions were either used directly (for NTA measurements, if not stated otherwise) or spun at 10,000 x g for 90 min at 4 °C to concentrate SEC EVs (for transfer experiments, protein, and RNA extraction).

2.6.2 For Microscopy (Including Staining)

THP-1 MΦ cell culture supernatants were centrifuged at 340 x g for 10 min at 4 °C to remove cells. Supernatants were transferred to a new 50 mL tube and centrifuged at 2,000 x g for 20 min at 4 °C to remove the 2K fraction. Next, supernatants were transferred to UC tubes and centrifuged at 10,000 x g for 45 min to pellet the 10K fraction. The 10K pellet was resuspended in 1 mL PBS and 2 µL of CFSE was added to a final concentration of 20 µM CFSE in PBS. For an unstained control, the 10K pellet was resuspended in PBS without addition of CFSE and for a CFSE-only control, PBS (without EVs) was mixed with CFSE. Samples were incubated in the dark for 30 min at 37 °C, mixing tubes in between by flicking. Afterwards, tubes were centrifuged at 10,000 x g for 40 min and pellets were resuspended in PBS. 10K samples were kept on ice until transfer. The 10K supernatant (from the first 10,000 x g spin) was filtered through a 0.2 µm filter and centrifuged at 100,000 x g for 70 min. Thereafter, the pellet was

resuspended in 500 µL PBS. 0.5 µL of R18 was added to get a final concentration of R18 of 10 µM. As for the 10K pellet, a dye only control was generated by mixing PBS (without EVs) and R18 only, and an unstained control was generated by resuspending the pellet in PBS without the addition of R18. Samples were incubated in the dark for 30 min at 37 °C and mixed in between through flicking. After incubation with R18, SEC was performed as described above. Afterwards, samples were spun at 100,000 x g for 90 min at 4 °C to pellet SEC EVs.
In some experiments, both 10K and SEC EVs were stained with CFSE or R18. In those cases, the same concentration of dye was used for both EV fractions.

2.6.3 From Whole Blood

16 mL of blood was drawn from healthy donors using either a 20 or 21 safety multifly needle and citrated (9-NC) S-Monovettes. Blood was transferred to four 15 mL tubes (3.8 mL whole blood per tube). Whole blood was stimulated as described in section 2.4. After stimulation tubes were spun at 1,000 x g for 15 min with the brake off. Plasma was collected (about 2 mL per tube) and transferred to a new 15 mL tube. Tubes were centrifuged at 340 x g for 10 min to remove all remaining cells. Supernatant was transferred to new 15 mL tubes and spun at 2,500 x g for 15 min to remove platelets from the plasma. The spin was repeated once to remove platelets completely. Samples were transferred to 1.5 mL UC tubes (2 tubes per condition, 1 mL per tube) and spun at 10,000 x g for 45 min at 4 °C to pellet 10K EVs. Supernatant was removed and pooled (pooled per condition, different stimulations were still separate). 10K pellets were resuspended and pooled in a total of 1 mL PBS and used either directly (for NTA measurements) or pelleted at 10,000 x g for 45 min at 4 °C (for protein and RNA extraction). 100 µL of 10K supernatants was taken for TNFA and IL1B HTRFs. Remaining 10K supernatants were concentrated in Amicon tubes with a 10K cutoff. Concentrated 10K supernatants were then applied to SEC as described above. As only 500 µL of sample can be loaded per tube, SEC was performed twice per sample. SEC fractions were then filtered through a 0.22 µm filter and either used directly (for NTA measurements) or spun at 100,000 x g for 90 min at 4 °C to pellet SEC EVs. In case of one experiment, instead of spinning samples

directly at 100,000 x g, immunoprecipitation using an antibody against apolipoprotein B (APOB) was performed: to prepare antibody-coated beads, Dynabeads coated with recombinant protein A were vortexed for 30 s and transferred to a 2 mL tube. The tube was placed on a DynaMag-2 magnet and the supernatant was removed. For each sample, 5 µL of APOB antibody was mixed with 200 µL of PBS with 0.02 % Tween 20 and added to the 2 mL tube containing the Dynabeads. Beads were incubated with antibodies under rotation for 10 min. Afterwards, 2 mL tubes were placed on the DynaMag-2 magnet and supernatant was removed. Antibody-coated beads were washed three times with 200 µL of PBS with 0.02 % Tween 20 by removing the tube from the magnet, gently pipetting up and down, and then placing the tube back on the magnet and removing the supernatant. After the last wash, the PBS with 0.02 % Tween 20 was removed and 1,500 µL of sample was added to the tube. Sample and antibody-coated Dynabeads were mixed through gentle pipetting followed by incubation under rotation for 20 min. Afterwards the supernatant was transferred to an UC tube and centrifuged at 100,000 x g for 90 min.

2.7 Nanoparticle Tracking Analysis

NTA was used to determine the concentration and size distribution of EV samples (both cell culture and blood-derived EV samples). During NTA, EVs resuspended in PBS are illuminated with a laser beam. The light scattered at the particle's surface is detected by a camera, which enables visualisation of each individual particle. The particles in solution move due to Brownian motion, which directly correlates with particle size. Thus, the hydrodynamic diameter of particles can be calculated (Colombo *et al*, 2014). This is done using the Stokes-Einstein equation (Filipe *et al*, 2010).

NTA was performed using the NanoSight NS300 with a Syringe Flow Pump to generate a constant flow and NanoSight NS300 NTA software version 3.4.4. First, the NanoSight chamber was washed using 1 mL of PBS at a flow rate of 1,000. Samples were diluted in PBS to reach a concentration of about 50-100 vesicles/frame. Samples were taken up into a syringe and 100 µL were

injected into the system using a flow rate of 1000. Next, the infusion rate was decreased to 20 and settings were adapted to the sample. For each sample, three measurements were captured with a duration of 60 sec each at a continuous syringe pump flow of 20 at 25 °C. The camera focus was manually adjusted for each sample. For 2K and 10K EVs, a camera level of 9 was used; for SEC EVs a camera level of 14 was used. After each sample had been analysed, the chamber was cleaned using at least 1 mL of PBS. For analysis of measurements, different detection thresholds were chosen depending on the EV fraction: 20 was used for 2K EVs, 10 for 10K EVs, and 5 for SEC EVs.

2.8 Protein Biochemical Methods

2.8.1 Cell Lysis for Protein Isolation

Before lysis, cells were placed on ice and washed twice with PBS. Next, radioimmunoprecipitation assay buffer (RIPA) lysis buffer was added (50 µL per well in a 6-well plate, 20 µL per 1.5 mL tube for EV samples). Cells were scraped and transferred from plates to 1.5 mL tubes. Tubes were spun at 2,000 x g for 15 min at 4 °C to remove nuclei. Supernatants were collected and either frozen at −80 °C or used directly.

2.8.2 EV Lysis for Protein Isolation

EVs were lysed after washing with PBS and centrifugation at 10,000 x g for 10K EVs or 100,000 x g for SEC EVs. PBS was carefully removed after centrifugation, and EVs were lysed in 2X RIPA lysis buffer. Tubes were vortexed and either frozen at −80 °C or used directly.

2.8.3 Protein Measurements

For protein concentration measurements, the Pierce BCA Protein Assay Kit was used according to the manufacturer's instructions. In short, bovine serum albumin (BSA) standards were diluted to cover concentrations between 0 µg/mL and

2,000 µg/mL. An appropriate amount of working reagent was prepared by mixing 50 parts of BCA reagent A with 1 part of BCA reagent B. Based on the expected protein concentration, samples were either left undiluted or diluted with water. Samples and standards were transferred to a 96-well cell culture plate with a flat bottom. Working Reagent was added to each well and plates were incubated for 15 min at 37 °C in the dark. Absorbance was measured at 562 nm using the SpectraMax i3 Plate Reader. The average absorbance at 562 nm of the blank standard was then subtracted from the absorbance measurements of standards and samples. Using the standards, a standard curve was prepared and used to determine the protein concentration of the samples.

2.8.4 SDS-Polyacrylamide Gel Electrophoresis

For sodium dodecyl sulfate (SDS)-polyacrylamide gel electrophoresis, sample volumes resulting in the desired amount of protein were mixed with NuPAGE lithium dodecyl sulfate (LDS) Sample Buffer and NuPAGE Sample Reducing Agent and filled up with water to a final volume of 20 µL per sample. Samples were transferred to a heating block and incubated for 10 min at 85 °C, shaking. PageRuler Plus pre-stained protein ladder and samples were loaded onto a NuPAGE 4-12 % Bis-Tris Gel with either NuPAGE MES or MOPS Running Buffer. Gels were run at ~90 mA for 1.5 h.

2.8.5 Western Blotting

After running gel electrophoresis, Western blotting was performed using the Xcell II Blot Module with transfer buffer and stacked with sponges, chromatography paper, and an Immobilon-FL polyvinylidene difluoride (PVDF) membrane previously activated for 30 sec in methanol. Western blotting was performed at 32 V for 1.5 h.

After blotting, membranes were blocked with blocking buffer for 1.5–2 h at room temperature (or at 4 °C overnight). Primary antibodies were diluted in blocking buffer and membranes were incubated for 1.5–2 h at room temperature (or at 4 °C overnight). Afterwards, membranes were washed thrice with tris-buffered

saline (TBS) with 0.1% Tween 20 detergent (TBST) for 10 min at room temperature. Secondary antibodies were diluted in TBST and membranes were incubated for 1.5–2 h at room temperature (or at 4 °C overnight). Finally, membranes were washed two times in TBST and one time in TBS and imaged using the LICOR Odyssey.

2.8.6 Simple Western WES

Western blotting using the Simple Western WES system was performed as an alternative to the above-described standard Western blotting procedure, according to the manufacturer's instructions. In short, samples were lysed as described above. Lysates were diluted in 0.1 X sample buffer to the required protein amount. Generally, 3–5 µg of protein was used per sample. Samples were then mixed with 5X Fluorescent Master mix that had been previously prepared with either dithiothreitol (DTT; for reduced samples) or H_2O (for non-reduced samples). Samples were denatured for 10 min at 95 °C. Primary antibodies were diluted with antibody diluent. WES plates were pipetted according to the manufacturer's pipetting scheme with the exception of using 5 µL prepared sample instead of 3 µL (to ensure no air was later sucked into the system). A 12–230 kDa kit was used with a separation time of 25 min and 375 V, a primary antibody time of 90 min and a secondary antibody time of 30 min. Results were analysed using the Compass for Simple Western software.

2.8.7 Detergent-Free Cell Fractionation

1.5 x 10^6 THP-1 MΦs/well were seeded on a 6-well plate and stimulated. Cells were washed with PBS and detached from the cell culture plate using PBS with 0.5 mM EDTA. After pelleting cells at 350 x g for 10 min at 4 °C, cells were resuspended in either 50 µL or 200 µL PBS containing 1X cOmplete EDTA-free Protease-Inhibitor and 1X PhosSTOP phosphatase inhibitor. In case of the control (no fractionation possible as membranes disrupted), cells were resuspended in 200 µL of 1 % Triton-X-100 in PBS containing 1X cOmplete EDTA-free Protease-Inhibitor and 1X PhosSTOP phosphatase inhibitor. Cell

disruption was carried out by vortexing samples for 5 sec followed by using a Dounce homogeniser for five strokes. Centrifugation at 350 x g for 10 min at 4 °C was performed to pellet intact cells. Next, supernatants were centrifuged at 100,000 x g for 1 h at 4 °C to pellet membranes and to recover the cytosolic fraction (supernatant). Western blotting for calnexin (CANX) was performed to check for successful fractionation.

2.8.8 Luciferase Assay

To detect in-gel luciferase activity, the Nano-Glo In-Gel Detection System was used according to the manufacturer's instructions. In short, cells were lysed using RIPA lysis buffer and separated using SDS-polyacrylamide gel electrophoresis as described above (section 2.8.4). To remove SDS and allow refolding of nano luciferase (NLuc), SDS was removed by washing the gel three times in 25 % isopropanol and two times in water, each wash for 15 min. The gel was then immersed in Nano-Glo In-Gel Detection Reagent supplemented with Nano-Glo Luciferase Assay Substrate and placed into the chemiluminescent Sapphire Biomolecular Imager (Azure). An image was taken 35 min after immersion in the detection reagent with a 2-min exposure time.

To detect NLuc activity in solution, the Nano-Glo Luciferase Assay System was used according to the manufacturer's instructions. In short, 1.5 x 10^6 THP-1 MΦs or EVs from 30 x 10^6 THP-1 MΦs were resuspended in 1 mL or 30 µL PBS respectively. Nano-Glo Luciferase Substrate was prepared and both substrate and samples were equilibrated to room temperature. 30 µL of the sample was mixed with 30 µL of the substrate in a white 96-well cell culture plate (Cellstar). Beginning 3 min after mixing, luciferase activity was measured continuously using the SpectraMax i3 Plate Reader (Molecular Devices).

2.8.9 HTRF

Homogeneous time resolved fluorescence (HTRF) assays were performed to determine IL-1β and TNF-α protein levels. Experiments were carried out

according to the manufacturer's instructions. In short, the d2 antibody was mixed with the cryptate antibody at a 1:1 ratio. Standards were prepared using PBS. In case of hTNF-α, the highest standard had a concentration of 7,500 pg/mL. The highest standard for IL-1β had a concentration of 6,500 pg/mL. Blanks were included. 12 µL/well of standards, blanks, and samples were added to a low-volume 384-well plate. 3 µL of antibody mix was added to each well. Plates were centrifuged at 340 x g for 1 min and incubated for 3 h or overnight at room temperature. Fluorescence was read using the SpectraMax i3 Plate Reader with the HTRF cartridge.

2.9 Microscopy Experiments

2.9.1 Recipient Cell Staining With CellTrace Far Red

To stain recipient cells with CellTrace Far Red, different numbers of cells were seeded in a 96-well plate and allowed to attach overnight. The next day, culture medium was removed and cells were washed with PBS. 50 µL of 0.5 µM CellTrace Far Red in PBS was added per well and cells were incubated for 20 min at 37 °C. Staining solution was removed and cells were washed twice with culture medium containing FBS. After the last wash, FBS-containing culture medium was left on the cells for 10 min to allow the CellTrace Far Red reagent to undergo acetate hydrolysis. FBS containing medium was then removed, cells were washed once, and normal cell culture medium was added.

2.9.2 Cell Fixation

To fix cells, stimulation medium was removed from wells and cells were washed twice with PBS. 4 % paraformaldehyde (PFA) was applied for 30 min at room temperature. Afterwards, cells were washed two times with PBS.

2.9.3 Recipient Cell Staining With Hoechst 34580 and Fixation

After stimulation, before fixation, cells were stained with Hoechst 34580. Stimulation medium was removed and 100 µL of 0.4 µg/mL Hoechst 34580 in PBS was applied for 15 min at 37 °C. Afterwards, cells were washed with PBS and 100 µL of 4 % PFA was applied for 10–15 min at room temperature in the dark. Finally, PFA was replaced by PBS and cells were stored at 4 °C in the dark until imaging.

2.9.4 Recipient Cell Staining With DRAQ5 and Fixation

After stimulation, stimulation medium was removed, and cells were washed with PBS. After the wash, cells were fixed with 4 % PFA containing 5 µM DRAQ5 for 10 min at room temperature. Afterwards, PFA was removed and cells were washed with PBS. Finally, PBS was added to cells and cells were stored at 4 °C in the dark until imaging.

2.9.5 Cryo-Embedding of ALI Cultures

After fixation as described above, transwell inserts were removed. Using a scalpel, the membrane was cut out from the insert. The membrane was then put cell side up on the table and cut through the middle, creating two semicircles. An embedding chamber was filled about halfway with TissueTek and the two membrane halves were inserted so that they stood up (cut side faces bottom, round side up). More TissueTek was added to completely cover the membrane. Embedding chambers were then put on dry ice and allowed to solidify. Once solid, samples were moved to the −80 °C freezer.

2.9.6 Cryostat

Samples were cryosliced either in our lab using the Leica cryostat or at the Histology Platform (University Hospital Bonn, Dermatology Department). After preparing the cryostat, samples were thawed slightly to allow removal from the embedding chamber. Using TissueTek, samples were put on a stamp and

allowed to freeze. The stamp was put into the cryostat holder. The first slices were discarded until the membranes were visible. Slice thickness was set to 4 µm and slices were moved to glass slides. Slides were allowed to dry overnight at 4 °C.

2.9.7 Antibody Staining

After allowing slides to dry overnight, samples were moved to room temperature and quenched with 150 nm ammonium chloride for 30 min. Next, samples where permeabilised with permeabilisation buffer for 5–10 min. Permeabilisation buffer was removed, and samples were incubated with blocking buffer for 45 min at room temperature or overnight at 4 °C. After blocking, the primary antibody was applied in blocking buffer for 1 h at room temperature followed by two washes for 3 min each with blocking buffer. Next, the secondary antibody was applied in blocking buffer for 45 min at room temperature in the dark, followed by two washes for 3 min each with blocking buffer. Next, Acti-stain 488 was applied at a concentration of 100 nM for 30 min at room temperature in the dark. This was followed by three washes for 3 min each using PBS. Finally, samples were stained by applying Hoechst 34580 for 10 min at room temperature, two washes with PBS for 3 min each and mounting of samples using Aqua-Poly/Mount mounting medium. Samples were dried overnight at room temperature in the dark and moved the next day to 4 °C.

2.9.8 Image Acquisition

Images were acquired at the Microscopy Core Facility (Medical Faculty, University of Bonn) using the Leica TCS SP8 microscope with the Leica Application Suite X software version 3.5.5. A HC PL APO CS2 water objective with 63X magnification and 1.20 aperture was used for most experiments; for imaging ALI slices, a HC PL APO CS2 oil objective with 63X magnification and 1.40 aperture was used for image acquisition. The image format was set to have the proper sampling rate at the respective zoom factor. In some experiments, line averaging was set to 4. Images were acquired at room temperature, except for

imaging EGFP and tdTomato THP-1 MΦs; these cells were imaged at 37 °C and 5 % CO_2. The following lasers (with the argon laser set to 20 % power) were used for the indicated fluorophores/dyes: the Diode 405 laser was used for Hoechst 34580, the 496 nm argon laser line was used for CFSE and Acti-Stain 488, the DPSS 561 laser was used for R18, and the HeNe 633 laser was used for CellTracer Far Red, AF647, and DRAQ5.
HyD detectors were used to detect emitted light from fluorophores/dyes. In the last sequence, transmitted light detector (TLD) was enabled with the PMT voltage set to around 550 V.
Images were saved as Leica image files (.lif).

2.9.9 Fiji/ImageJ

Leica image files from confocal imaging were opened in Fiji/ImageJ. In case of z-stacks, five images from the middle of each stack (in order to exclude EVs attached to the cell surface and only analyse EVs taken up by cells) were selected manually and a maximum intensity projection was created. In all other cases (non-z-stack files), images were just opened in Fiji/ImageJ. Next, images were split into their individual channels and if needed, each channel was saved individually as TIF file. The individual channel images were then combined to create a composite image with or without a scale bar, saved either as TIF or PNG. Scale bar lengths are indicated in figure legends.

2.9.10 ilastik

For some images, instead of directly identifying nuclei in cell profiler, nuclei were first detected and enhanced using ilastik. ilastik employs machine learning for pixel classification. Nuclei channel images were used as input. σ_1 and σ_6 were used across Color/Intensity (Gaussian Smoothing), Edge (Laplacian of Gaussian, Gaussian Gradient Magnitude, Difference of Gaussians), and Texture (Structure Tensor Eigenvalues, Hessian of Gaussian Eigenvalues). Training was performed by labelling nuclei and background. Predictions were exported using probabilities as a source. The following image export options were adapted: the cutout

subregion for c was changed from all to start with 0 and stop at 1. The data type was converted from a float32 image to unsigned 8-bit. Renormalisation was performed from 0.00 and 1.00 to 0 and 255. The output file format was set to TIF.

2.9.11 Cell Profiler

Cell Profiler was used to quantify EV uptake. Three different pipelines were used. For all three pipelines, microscopy images were opened in Fiji/ImageJ, maximum projections of z-stacks were created, and images were split into their individual channels as described above (section 2.9.9). In case of the nuclei channel, ilastik (section 2.9.10) was used to find and enhance nuclei. The outputs of Fiji/ImageJ and ilastik were loaded into Cell Profiler as TIF files. Metadata was extracted from file names to identify channels 1, 2, and 3. Channel 1 was named DNA, channel 2 EV, and channel 3 Cell.

To quantify EV uptake in general by measuring the overall fluorescence per cell, the following pipeline was created and used:
The IdentifyPrimaryObjects module was used to identify cell nuclei using the DNA images as input. The typical diameter of objects was set to be between 120 and 290 pixels. Objects outside the diameter range and touching the border of the image were discarded. A Global Thresholding strategy with the Robust Background method was chosen, with the lower and upper outlier fractions being 0.02 each. A threshold smoothing scale of 1.3488 and a correction factor of 1.86 with lower and upper bounds of 0.001 and 1.0 respectively were chosen. The Shape method was used to distinguish clumped objects. Holes in identified objects were filled after both thresholding and declumping.
Based on the identified nuclei, recipient cells were identified using the IdentifySecondaryObjects module. The Propagation method with Adaptive Thresholding strategy using the Otsu method was chosen. Two-class thresholding with a smoothing scale of 1.5 and a correction factor of 0.8 and lower and upper bounds of 0.0 and 1.0 was chosen. An adaptive window of 50 was used.

Next, the MeasureObjectIntensity module was employed to measure EV fluorescence intensity per recipient cell.
Finally, the ExportToSpreadsheet module was used to create output Excel files.

To quantify EV uptake and to differentiate between EVs sticking to the outside of cells and EVs actually taken up by cells, the following pipeline was used:
Nuclei were identified using the IdentifyPrimaryObjects module selecting DNA as input. The typical diameter was set to be between 120 and 300 pixels. Objects outside the diameter range were discarded, as were objects touching the border of the image. A Global Threshold strategy was chosen using the Otsu Thresholding method with two-class thresholding. A threshold smoothing scale of 1.3488 with a threshold correction factor of 2 was chosen. The lower and upper bounds of the threshold were 0.0001 and 1.0 respectively. To distinguish clumped objects the Shape method was chosen. The size of the smoothing filter for declumping was calculated automatically, as was the allowed distance between local maxima. Holes in identified objects were filled after both thresholding and declumping.
Having identified the nuclei, the recipient cells were identified using the IdentifySecondaryObjects module on the Cell input image and taking the identified nuclei as input objects. The identified objects were named Recipients. The Propagation method was chosen to identify the secondary objects using an Adaptive Thresholding strategy with the Otsu Thresholding method and two-class thresholding. A smoothing scale of 1.5 was chosen and a correction factor of 0.8. The lower and upper bounds on the threshold were set to 0.0 and 1.0 respectively. The size of the adaptive window was set to 50. A regularisation factor of 0.05 was used. Holes in identified objects were filled, and secondary objects touching the border of the image were discarded together with the associated primary objects.
Next, the ExpandOrShrinkObjects module was used to shrink recipient cells by 20 pixels. The same module was then applied again to expand recipient cells by 100 pixels.

Using the module MaskImage twice in a row, two masks were created: Once for EVs inside of cells called InsideCellEVs and one for EVs sticking to the cell membrane called OutsideCellEVs. The first mask uses the EV image as input and the shrunken recipient cells as the object for the mask. The second mask inverts the first mask.

The IdentifyPrimaryObjects module was then used to identify EVs inside cells using the first mask as input. The typical diameter of objects was set between 5 and 100 pixels and objects outside the diameter range were discarded. An Adaptive Threshold strategy using the Robust Background method was chosen with a lower and upper outlier fraction of 0.05 each. The Mean Averaging method was chosen together with the Standard Deviation Variance method, allowing for 2.0 deviations. A threshold smoothing scale of 1.3488 was chosen with a correction factor of 1. Lower and upper bounds of 0.2 and 1.0 were chosen on the threshold. Clumped objects were distinguished by intensity and holes in identified objects were filled after both thresholding and declumping. The same module was then used again with exactly the same settings but using the second mask as input to identify vesicles surrounding the cell membrane.

Using the RelateObjects module twice, inside vesicles were related to shrunken recipients and vesicles surrounding cell membranes were related to expanded recipients.

Finally, EV signal intensity was measured using the MeasureObjectIntensity module on the EV channel and all data was exported to Excel spreadsheets using the ExportToSpreadsheet module.

While the above-described pipelines were used to originally gain an understanding of EV uptake with regards to EV binding vs actual uptake, a simpler pipeline that did not require recipient cell staining was used for later experiments: microscopy images were opened in Fiji/ImageJ, channels were split, and saved individually as TIF files. The nuclei and EV channels were loaded into Cell Profiler and named DNA and EV respectively.

The IdentifyPrimaryObjects module was used on the DNA channel image to identify cell nuclei allowing a typical diameter of objects between 80 and 200 and

discarding objects outside the diameter range but not those touching the border of the image. A Global Thresholding strategy was employed using the Robust Background method with a lower and upper outlier fraction of 0.02.
Next, the MeasureImageIntensity module was used to measure EV fluorescence intensity.
Finally, the ExportToSpreadsheet module was used to export data, in particular nuclei count and EV fluorescence intensity, to Excel spreadsheets.

2.10 Molecular Genetics

2.10.1 RNA Isolation (including gDNA removal)

To isolate RNA from EVs for qPCR and microarray analysis, EVs from 30 x 10^6 THP-1 MΦs per condition were isolated as described above (section 2.6.1). After the final centrifugation spin, 10K and SEC pellets were lysed in 350 µL Buffer RLT Plus containing β-ME (10 µL per mL). Samples were vortexed vigorously.
To isolate RNA from EVs derived from human blood, EVs from 2 mL plasma were isolated as described above (section 2.6.3). After the final centrifugation spin, EVs were lysed in 350 µL Buffer RLT Plus containing β-ME (10 µL per mL). Samples were vortexed vigorously.

To isolate RNA from cells for qPCR analysis, 1 x 10^6 THP-1 MΦs were seeded in 6-well plates. After stimulation, cells were washed once with PBS. 700 µL Buffer RLT Plus containing β-ME (10 µL per mL) was added. Samples were vortexed vigorously.

Samples in Buffer RLT were either frozen at −80 °C and stored for future use, or directly used for RNA isolation. RNA isolation was performed using the RNeasy Plus Micro Kit. In case of frozen samples, lysates were thawed on ice. From then on, work was carried out at room temperature. 350 µL of lysates were transferred to a gDNA eliminator spin column. Columns were spun at 8,000 x g for 30 sec.

The flow-through was kept and 525 µL of 100 % EtOH was added. After mixing, samples were transferred to a RNeasy MinElute spin column and centrifuged at 8,000 x g for 15 sec. The flow-through was discarded and the column was washed with 500 µL buffer RPE at 8,000 x g for 15 sec and then for 2 min. Afterwards, the column was centrifuged with an open lid at full speed for 5 min. Elution of RNA from the column was achieved through the addition of 14 µL RNase-free water directly to the column membrane. The column was then centrifuged at full speed for 1 min.

2.10.2 RNA Concentration Measurement

RNA concentrations were measured using the Qubit HS RNA assay kit according to the manufacturer's protocol. In short, a Qubit Working Solution was prepared by mixing Qubit Buffer with Qubit Reagent 200:1. 190 µL of Qubit Working Solution was then mixed with 10 µL of Qubit Calibration samples to calibrate the Qubit. Standard one acts as a blank (0 ng/mL RNA), while standard two has a final concentration of 500 ng/mL RNA. To determine sample RNA concentrations, 199 µL of Qubit Working solution was mixed with 1 µL of sample RNA. Samples and calibration samples were vortexed and incubated for 2 min followed by measuring of the RNA concentration using the Qubit instrument.

For microarray samples, RNA concentration and quality were determined using automated-electrophoresis with the high-sensitivity RNA Screen Tape of the 2200 Tape Station according to the manufacturer's instructions. In short, reagents were equilibrated to room temperature for 30 min. RNA samples were kept on ice. A ladder was prepared by adding 10 µL of RNase free water to the High Sensitivity RNA Ladder. Per run, 2 µL of the ladder was mixed with 1 µL High Sensitivity RNA Sample Buffer. Samples were prepared by mixing 1 µL of High Sensitivity RNA Sample Buffer with 2 µL of sample RNA. Samples and Ladder were spun down and vortexed at 2,000 rpm for 1 min. Next, samples and ladder were spun down and denatured for 3 min at 72 °C. Samples and ladder were immediately placed on ice for 2 min and spun down again before being loaded into the 2200 TapeStation instrument.

2.10.3 cDNA Synthesis

For cDNA synthesis, a master mix consisting of 5X first-strand buffer, 10 mM dNTP mix and 0.1 M DTT with a total volume of 6 µL per sample was prepared. A sample volume corresponding to 300 ng of RNA was taken and adjusted to 12.9 µL using nuclease-free water. The sample with the highest RNA concentration was additionally used for a no reverse transcriptase control. 1 µL of oligo dTs was added to each sample and samples were spun down. Next, samples were heated for 5 min at 65 °C. Afterwards, samples were immediately placed on ice for a minute and spun down. 6 µL of master mix was added to the no reverse transcriptase control. 0.1 µL SuperScript III Reverse Transcriptase was then added to the master mix. 6.1 µL of this master mix containing SuperScript was then added to each sample. Samples were heated for 50 min at 50 °C followed by heating for 5 min at 85 °C.

2.10.4 qPCR

qPCR was performed in duplicates. First, forward and reverse primers were mixed and diluted with nuclease-free water to a final primer concentration of 2 µM each. A master mix consisting of 1X Power SYBR Green PCR Master Mix, 2 µM primer mix, and nuclease-free water was generated. 8 µL of master mix was added per well to a 384-well plate and mixed with 2 µL of diluted cDNA per well. Plates were centrifuged at 1,000 x g for 5 min to remove air bubbles. qPCR was run using the QuantStudio 6 Flex System using the comparative CT method and standard run setting. Melting curves were included.

2.11 Bioinformatic Methods

2.11.1 Microarray

Samples were stimulated as described above (section 2.4) and EVs were isolated as described before (section 2.6.3). RNA was isolated from EVs as described (section 2.10.1) and RNA concentration and quality was checked using the Qubit

system (section 2.10.2). RNA was sent to the Gene Expression Affymetrix Facility at the Center for Molecular Medicine Cologne where samples were processed using the Clariom D Pico Microarray.

Samples were then analysed in Australia with the help of Dr. Jamie Gearing. Data analysis was performed using R version 4.2.1 (R Core Team, 2022) and RStudio version 2022.07.1 build 554 (RStudio Team, 2022). First, sample CEL files were imported using the oligo package version 1.58.0 (Carvalho & Irizarry, 2010). This creates a human transcriptome array (HTA) FeatureSet data object. Using the pData function of the Biobase package version 2.56.0 (Huber *et al*, 2015), sample group information was added to the HTAFeatureSet object. Robust multichip average algorithm (RMA) normalisation was performed with the rma function of the oligo package with target set to core. The rma function performs background correction, quantile normalisation and summarisation via median-polish on the core or probeset level (Irizarry *et al*, 2003b; Bolstad *et al*, 2003; Irizarry *et al*, 2003a). Summarisation on the core level allows analysis at the gene level, while summarisation on the probeset level allows the investigation of transcript isoforms.

Feature annotation was performed using the Thermo Fisher Scientific-provided Clariom_D_Human.ng36.hg38.transcript.csv file as well as EntrezID, gene symbol and gene name information derived from Bioconductor with help of the clariomdhumantranscriptcluster.db package version 8.8.0 (MacDonald, 2021).

Data was filtered to only consist of main category probes. According to ThermoFisher some transcripts show potentially anomalous behaviour. These transcripts were removed, together with non-coding and unassigned transcripts.

The limma package version 3.52.4 (Ritchie *et al*, 2015) was used for data analysis. Multidimensional scaling (MDS) plots were generated to examine the distances between the samples based on their gene expression profiles using the plotMDS function of the limma package. The 500 top genes were used to calculate pairwise distances. MDS plots were then assessed for clustering of samples according to experimental factors and batch effects. Initial MDS plots

showed a donor and a microarray batch effect. The batch effects were removed from the data using the removeBatchEffect function to re-generate MDS plots.

Linear modelling was performed. A design matrix without an intercept term was set up using the sample group, donor, and microarray date as factors. Using the donor and microarray date as a factor in the design matrix accounted for the observed batch effects. Model contrasts were set up for pairwise comparisons between the different stimuli and respective untreated samples (e.g., 10KL vs 10KD or 10KCL vs 10KD) as well as between uninhibited LPS stimulations and respective inhibited stimulations (e.g., 10KL vs 10KCL). Linear modelling was then performed on RMA-normalised values with the lmFit function. The contrast.fit function was then used to estimate coefficients and standard errors for the contrasts of interest, by subtracting relevant $\log_2$ expression values according to the contrast matrix, to create $\log_2$ fold changes ($\log_2$FC) for the different contrasts.

Two different methods were used to rank genes in order of evidence for differential expression: the eBayes and treat functions. Both use an empirical Bayes method and compute moderated t-statistics with corresponding two-sided p-values. The eBayes function additionally computes log-odds of differential expression, moderated F-statistics, and p-values corresponding to the F-statistics (Phipson *et al*, 2016). While eBayes tests for genes that have true $\log_2$FC different from zero, treat tests whether the true $\log_2$FC is greater than a set $\log_2$FC threshold (lfc) in absolute value (Mccarthy & Smyth, 2009). Here, lfc was set to 1.2. The decideTests function was used on the output of both the eBayes and treat function to analyse which genes were significantly up- or downregulated. The function applies a multiple testing procedure and a significance level cut-off to the statistics to determine whether a gene can be considered significant. A table of the top-ranked significant genes was generated using the topTable or topTreat functions (eBayes and treat results respectively) with the p.value cut-off set to 0.05.

For comparisons that showed differentially abundant transcripts, mean-difference plots (MD plots, also known as MA plots) were generated using the plotMD function with the eBayes results.
Expression plots of individual transcripts of interest were generated using the beeswarm function on the normalised expression data with removed batch effects.
A heatmap was generated using the pheatmap function of the pheatmap package (Raivo, 2019) with the normalised expression data with removed batch effects.
To compare our current data to previous microarray data generated by Dr. Christina Budden, we used the barcodeplot function. Transcripts that showed differential abundance when comparing THP-1-derived 10KLN EVs with 10KL EVs in data from Dr. Christina Budden were visualised: they were ranked based on their t-statistic calculated when comparing whole blood-derived 10KL vs 10KD EVs in this dataset and visualised as vertical bars in a barcode plot. Enrichment worms were calculated using the tricubeMovingAverage function to visualise the relative enrichment of these vertical bars and thus to show how the previously identified differentially abundant transcripts are distributed in the current data.

2.11.2 Sequencing

After stimulation (section 2.5.2), supernatants were collected for TNF-α and IL-1β measurements and recipient cells were washed three times with PBS followed by lysis in 50 µL (for naïve and activated T cells) or 100 µL lysis buffer (for NHBEC, HUVED, and NHLFs). EVs from 13 x 10^6 THP-1 MΦs per condition were lysed in 10 µL lysis buffer. The lysis buffer was provided by the Schmid-Burgk lab.

Whole cell lysates were then given to Dr. Jonathan Schmid-Burgk and Marius Jentzsch for library preparation (using 2 µL per sample) and sequencing. Libraries were prepared directly from whole cell lysates without previous RNA isolation and quantification. Paired-end sequencing was performed two times on the same library on the NextSeq 2000 platform using NextSeq 2000 P3 reagents for 50 cycles.

The data was then analysed by me with the help of Dr Jamie Gearing.
Sequencing quality control was performed using FastQC (Andrews *et al*, 2017) on all FASTQ files. To summarise FastQC results, MultiQC (Ewels *et al*, 2016) was used.

Data analysis was performed using R version 4.2.1 (R Core Team, 2022) and RStudio version 2022.07.1 build 554 (RStudio Team, 2022). Sequencing reads of both runs were aligned to the human reference genome (Homo sapiens GRCh38, release 107) downloaded from the Ensembl database (Cunningham *et al*, 2022) and BAM files were created using the align function of the Rsubread package version 2.10.5 (Liao *et al*, 2014, 2019) with default parameters. Gene-level counts were generated using the featureCounts function of the Rsubread package with BAM files of both runs as input and the Ensembl version 107 GTF file, setting isPairedEnd to TRUE and strandSpecific to 0 (unstranded).

The edgeR (Robinson *et al*, 2010; McCarthy *et al*, 2012; Chen *et al*, 2016b) and limma (Ritchie *et al*, 2015) packages (versions 3.38.4 and 3.52.4 respectively) were used for data pre-processing, linear modelling, and analysis:

The count table was transformed to a DGEList object using the featureCounts2DGEList function. Using the sumTechReps function the counts of the two library runs were combined. Genes that were not detected in any samples were removed. Finally, genes were annotated with the biomaRt package version 2.52.0 (Durinck *et al*, 2005, 2009).

For data pre-processing, samples were filtered to remove those with a library size smaller than or equal to 1×10^4, leading to the removal of 32 samples. After filtering, the library sizes ranged from 1.2×10^4 to 2.6×10^7. Next, using the filterByExpr function incorporating the sample group and with min.count set to 10, lowly expressed genes were removed. Normalisation by the method of trimmed mean of M-values (TMM; Robinson & Oshlack, 2010) was performed using the calcNormFactors function on the DGEList object. The function calculates scaling

factors to convert raw to effective library sizes. MDS plots were then generated using the plotMDS function of the limma package to access if samples cluster according to experimental factors and batch effects.

For linear modelling, a design matrix without an intercept term was set up using the sample group as a factor: model.matrix(~0 + group). Model contrasts were set up for pairwise comparisons between the different stimulations and respective untreated samples. Linear modelling was performed using the voomLmFit function, which calculates log_2CPM values with accommodated mean-variance relationships using precision weights calculated with the voom method (Law *et al*, 2014) and then returns group averages of individual log_2CPM values. The contrast.fit function was then used to estimate coefficients and standard errors for the contrasts of interest, by subtracting relevant log_2CPM values according to the contrast matrix, to create log_2FC for the different contrasts.

Two different methods were used to rank genes in order of evidence for differential expression: the eBayes and treat functions. Both use an empirical Bayes method and compute moderated t-statistics with corresponding two-sided p-values as described above (section 2.11.1). The lfc was set to 1 for the treat method. The decideTests function was used on the output of both the eBayes and treat function to analyse which genes were significantly up- or downregulated. A table of the top-ranked significant genes was generated using the topTable or topTreat functions (eBayes and treat results respectively) with the p.value cut-off set to 0.05.

For comparisons that showed differentially expressed (DE) genes, mean-difference plots were generated using the plotMD function with the eBayes or treat results.

Heat maps were generated using the pheatmap function of the pheatmap package (Raivo, 2019) with relative log_2CPM values. log_2CPM for each stimulation were normalised to the respective untreated condition. To do so, log_2CPM values per group for untreated conditions were calculated using the

edgeR function cpmByGroup with log = TRUE. These log_2CPM group values for untreated conditions were subtracted from the relevant sample log_2CPM values, resulting in relative log_2CPM values.). The top 20 most variable genes (ranked by p-value) between 10KLN and untreated samples were shown.

Gene set testing (Subramanian *et al*, 2005) was performed by applying the pre-ranked camera function (cameraPR; Wu & Smyth, 2012) of the limma package to the eBayes t-statistics as input to test whether genes in the following gene sets were highly ranked relative to genes not present in the set, taking inter-gene correlation into account. Molecular Signature Database (MSigDB) gene set collections were obtained using the msigdbr package version 7.5.1 and included the hallmark gene sets (h), which were derived by aggregation of many MSigDB gene sets to represent coherently expressed signatures that represent well-defined biological states or processes (Liberzon *et al*, 2015), the curated gene sets (c2) that took gene sets from online pathway databases such as the Reactome database, PubMed publications, and domain expert knowledge, and the gene ontology (GO) gene sets (c5) that includes gene sets with genes annotated by common GO terms. Camera results are shown as heat maps generated using the pheatmap function, displaying the average log_2FC of all genes in the set, annotated by significance of the camera results ($-log_{10}$ adjusted p-value; * $p < 0.05$).

Barcode plots were generated using the barcodeplot function of the limma package to check if up- or downregulated genes found in previous experiments (Budden et al. 2021) showed the same pattern in this experiment. Vertical bars indicate genes in the dataset that were also found in the previous experiments, with genes previously found to be upregulated on the top in red and genes previously found downregulated on the bottom in blue. Genes are ordered by significance (eBayes t-statistic).

2.12 Illustrator/Affinity Designer

If not stated otherwise, figures were created using Adobe Illustrator version 27.1.1 or Affinity Designer version 1.10.6.

2.13 Statistical Analysis

Typically, three to five independent experimental runs were performed and results depicted as mean ± standard deviation (SD) or mean ± standard error of the mean (SEM). Mean ± SD was generally used for technical replicates. It was further used for experiments with fewer than three biological replicates. In all other cases (experiments with equal to three or more biological replicates), either mean ± SD or mean ± SEM was shown: SD was used to underline the variation in the data, while SEM was used to visualise the variability in the means and thus as a way of quantifying the uncertainty in the estimation of the mean.
Statistical significance was calculated using R as described above (section 2.11) or using a paired t-test. n (in figure legends) represents the number of experimental runs performed.

2.14 Ethics

Human T cells and blood EVs were isolated from blood taken from healthy donors under the Ethikantrag Lfd. Nr. 392/20 “Antrag zur Verwendung von Buffy Coats und Vollblut am Institut für Angeborene Immunität”. All experiments complied with the relevant ethical regulations for animal testing and research.

3 Results

3.1 EV Characterisation

Our lab has extensively characterised the RNA content of EVs derived from THP-1 MΦs (Budden *et al*, 2021). Following up on this, my work aimed to expand this knowledge to the protein content of EVs, as well as to EVs derived from human blood.

EV isolation was performed according to the protocol established by Dr. Christina Budden (Budden *et al*, 2021; Figure 8A). Using an endotoxin quantification assay, she has previously demonstrated that, even though treated with LPS, these isolated EVs are free of LPS (Budden *et al*, 2021).

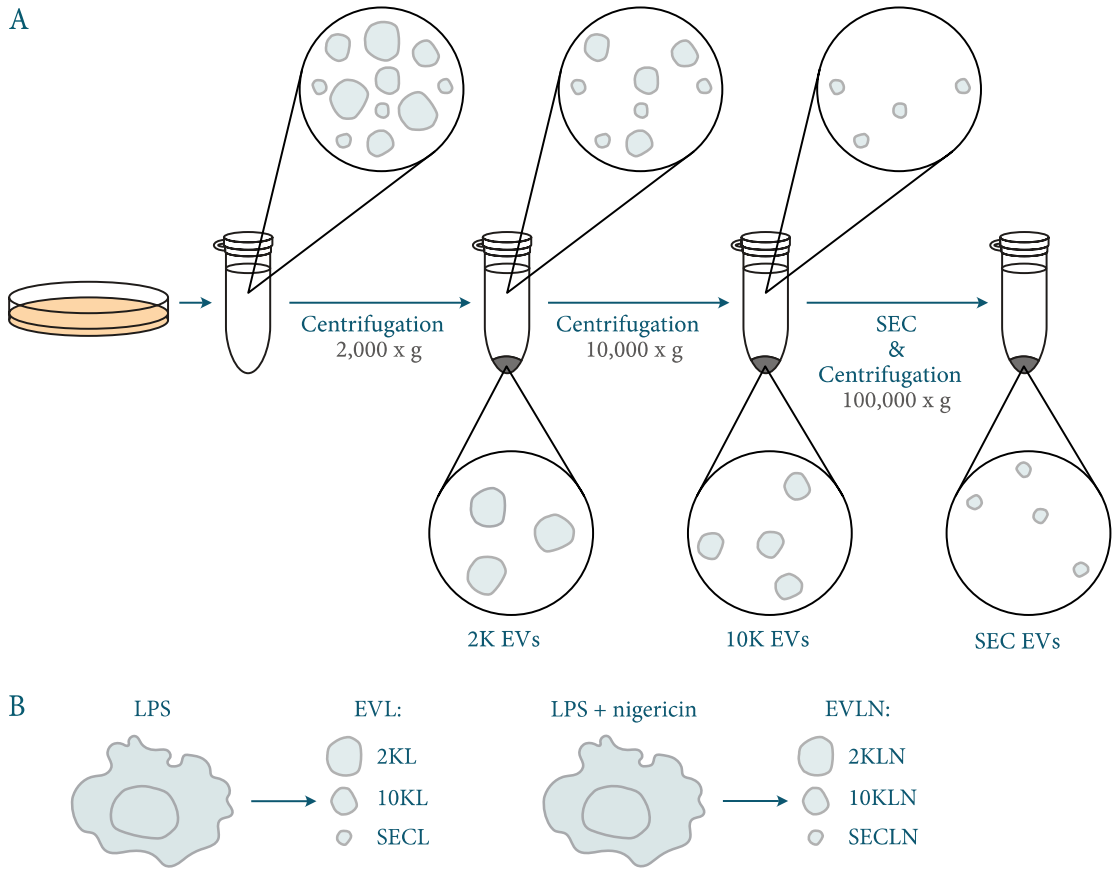

Figure 8: EV isolation from cell culture supernatant. (A) Cell culture supernatant was centrifuged at 340 x g for 10 min to remove any remaining cells. Supernatant was spun at 2,000 x g for 20 min to pellet large 2K EVs and cell debris. Supernatant was transferred to UC tubes and centrifuged at 10,000 x g for 45 min to pellet medium-sized 10K EVs. Supernatant was then filtered

through a 0.22 μm filter and concentrated using a 10K nominal molecular weight limit filter before being transferred onto a Size Exclusion Chromatography (SEC) column. 0.5 mL fractions were collected. For small SEC EVs, fractions seven, eight, and nine were pooled. If needed, SEC EVs were concentrated through centrifugation at 100,000 x g for 90 min. (B) Generally, EVs from cells treated for 2 h with LPS followed by treatment for 90 min with nigericin (inflammasome activation) were compared to EVs from cells treated for 2 h with LPS only. Isolated EV fractions were named according to the isolation method: 2K for EVs isolated at 2,000 x g, 10K for EVs isolated at 10,000 x g, and SEC for EVs isolated using SEC. Additionally, the stimuli used for EV donor cell stimulations were always mentioned. This was done either by writing out the treatment, by referring to the donor cell state, or by combining EV fraction names with abbreviations for the stimuli. 2K, 10K, and SEC EVs from inflammasome-activated cells would thus be referred to either as 2K/10K/SEC EVs from LPS and nigericin treated cells, inflammasome-elicited 2K/10K/SEC EVs or 2KLN, 10KLN, and SECLN EVs.

3.1.1 Inflammasome-Elicited EVs From THP-1 MΦs

In my experiments, I compared EVs from LPS + nigericin-stimulated cells to EVs from LPS only-stimulated cells. EVs from LPS + nigericin-treated cells will be referred to as EVLN or 2KLN/10KLN/SECLN, while EVs from LPS only-treated cells will be referred to as EVL or 2KL/10KL/SECL (Figure 8B).

Firstly, EVs released from THP-1 MΦs were isolated and characterised using NTA (Figure 9). The size and concentration of the SEC, 10K, and 2K fractions were analysed. Three different experimental runs were compared to ensure reproducibility. Each individual experiment consisted of three technical replicates, which are shown for one representative experimental run in Figure 9B. The mean for each experimental run was calculated and plotted in Figure 9C. EV size and concentration measurements were generally reproducible across experiments.
In case of the SEC fractions, undiluted samples fell out of the linear range determined by Dr. Christina Budden (Budden, 2020) and were thus diluted. Dilution reduced the spread of measurements (Figure 9D+E) and was therefore applied in all future experiments when samples were too concentrated.
When EVs were used for transfer experiments, the isolated pellets were washed once using PBS. Figure 9F+G shows how the washing procedure affects EV concentration and particle number measured. It was observed that washing

strongly reduced particle number. This cannot be avoided, as we need a pure EV preparation with as little as possible of the original treatment (nigericin) present, but should be kept in mind for transfer experiments.

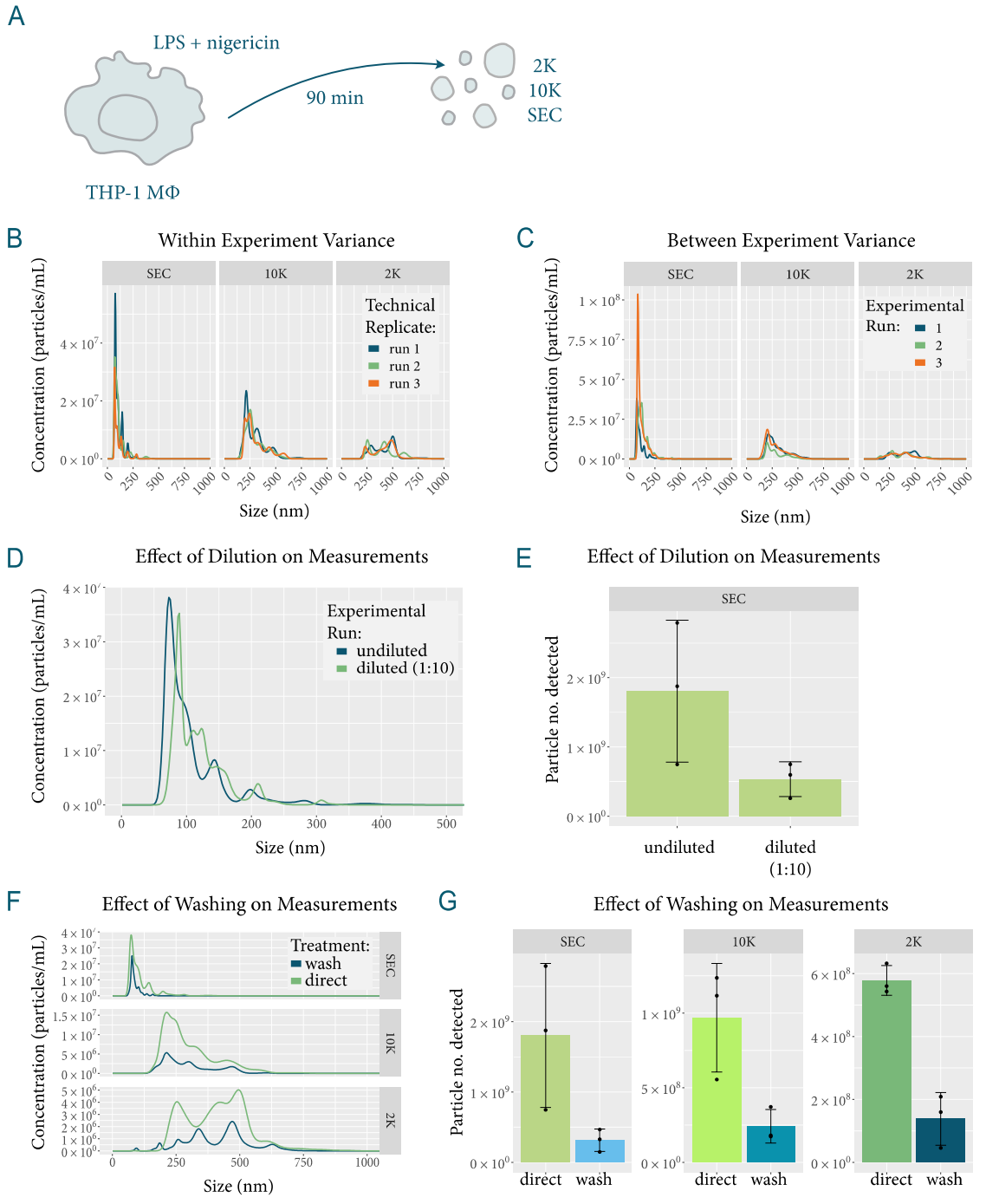

Figure 9: Nanoparticle tracking analysis of THP-1 MΦ-derived vesicles after inflammasome activation. (A) Schematic representation of the experimental plan. THP-1 MΦs were treated with LPS and nigericin to activate the NLRP3 inflammasome and EVs released were isolated. (B) EV concentrations of three technical replicates from one representative experimental run were compared.

(C) EV concentrations of three different experimental runs were compared to one another. The mean of three technical replicates is shown for each experimental run. (D+E) SEC fractions were either diluted 1 in 10 or left undiluted. (D) Concentration of particles in undiluted and diluted samples. The mean of three technical replicates of one representative experimental run is shown. (E) Number of particles detected in undiluted and diluted samples. Mean ± standard deviation (SD) of three experimental runs (mean of technical replicates shown for each run). (F+G) EV pellets were either analysed directly or washed once with PBS. (F) Mean concentration of particles in direct and washed samples of three technical replicates of one representative experimental run. (G) Number of particles detected in direct and washed samples. Mean ± SD of three experimental runs (mean of technical replicates shown for each run). (B–G) Technical replicates = 3, n = 3.

Next, EVs released from THP-1 MΦs after inflammasome activation (LPS + nigericin) were compared to those released after priming only (LPS) (Figure 10A). It was shown that the number of particles released from cells is strongly increased after inflammasome activation with LPS and nigericin, as opposed to cells primed with LPS only (Figure 10B+C). For most of the LPS only samples, EV numbers were indeed so low that detection was hardly possible and was thus performed under sub-optimal levels. Even though the overall number of EVs released after LPS-only stimulation is lower, the size distribution of EVs released after LPS (Figure 10D) is still similar to the size distribution of EVs released after LPS + nigericin stimulation (Figure 10E).

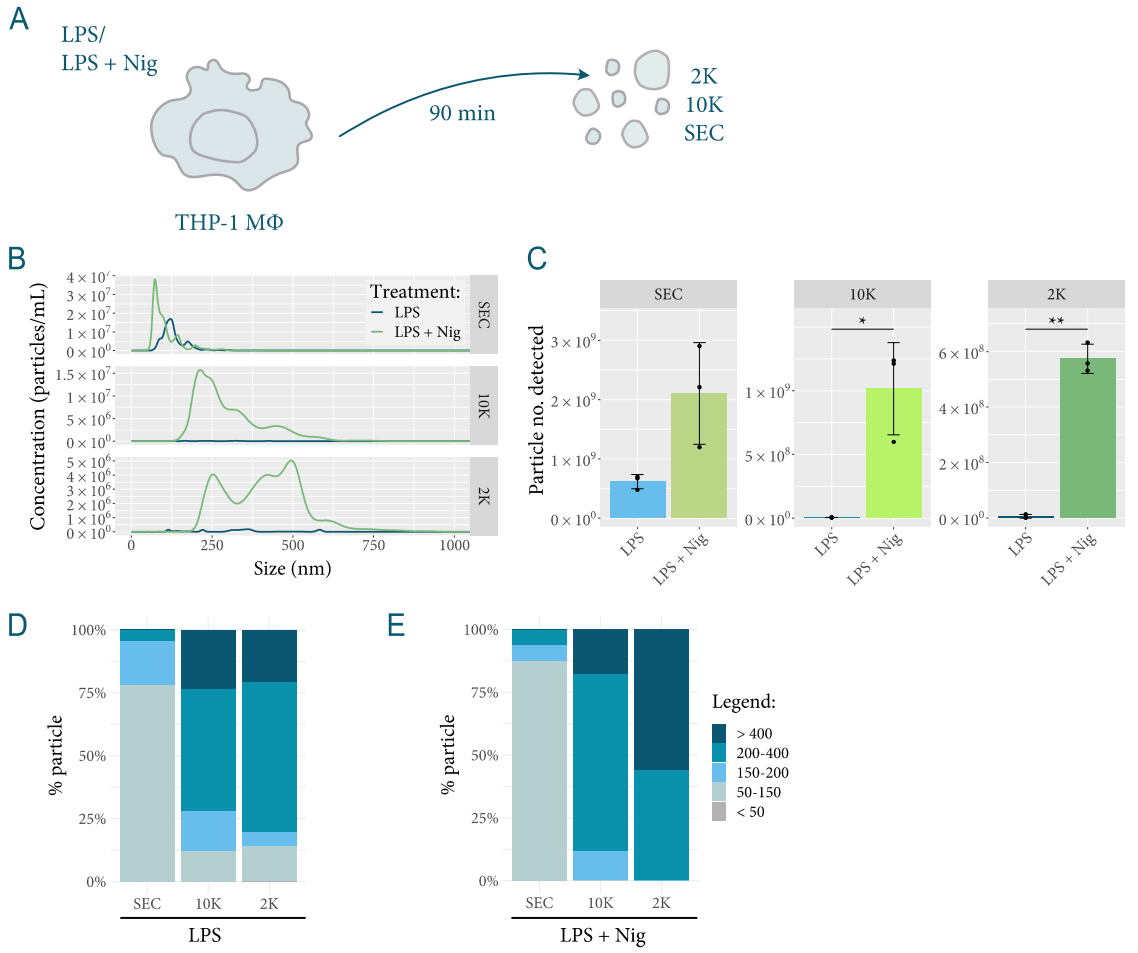

Figure 10: EV release after inflammasome activation compared to release after priming only. (A) Schematic representation of the experimental plan. EVs released from THP-1 MΦs after LPS + nigericin stimulation (inflammasome activation) were compared to those released after LPS stimulation only (priming only). (B) Concentration of particles measured in EV samples from LPS + nigericin-stimulated cells compared to LPS only-stimulated cells. The mean of three technical replicates of one representative experimental run is shown. (C) Total number of particles detected in EV samples from LPS + nigericin stimulated cells and LPS only stimulated cells. Mean ± SD of three experimental runs (Mean of three technical replicates is shown for each run). * p-value < 0.05, ** p-value < 0.005. (D+E) Size distribution (in nm) of particles released after LPS only stimulation (D) and LPS + nigericin stimulation (E). Mean of three technical replicates is shown for one representative experimental run. (B–E) Technical replicates = 3, n = 3.

Besides characterising the number of EVs released and their size profiles, the presence of certain proteins was investigated.

In 2014, the International Society for Extracellular Vesicles (ISEV) published common guidelines termed “Minimal information for studies of extracellular

vesicles 2014 (MISEV2014)" (Lötvall *et al*, 2014). These guidelines were updated in 2018, giving rise to the MISEV2018 guidelines (Théry *et al*, 2018). They comprise recommendations for studies on EVs, amongst them on EV characterisation. According to the MISEV guidelines, it is essential to demonstrate the presence of proteins expected to be present in EVs of interest and proteins not expected to be enriched. To do so, they have established five categories. Category one comprises transmembrane or GPI-anchored proteins associated with the plasma membrane and/or endosomes, e.g., different tetraspanins like CD9, CD63, CD81 or MHC class I. Category two comprises cytosolic proteins recovered in EVs. These can either have lipid or membrane protein-binding ability (e.g., TSG101) or be promiscuously incorporated into EVs (e.g., HSP70). This is necessary to demonstrate that the material analysed contains not solely open membrane fragments. Category three comprises proteins that are major components of non-EV co-isolated structures and thus serves as a purity control. Examples are surfactant in case of EVs isolated from BALF or apolipoprotein A (APOA)1/2 from EVs isolated from blood. Category four comprises transmembrane, lipid-bound and soluble proteins associated with other intracellular compartments than the plasma membrane and endosomes and is used to further characterise the nature of EVs with regard to their cellular origin. Examples are cytochrome C (mitochondria) or CANX (secretory pathway). Finally, category five comprises secreted proteins recovered with EVs, for example cytokines and growth factors like transforming growth factor beta (TGFB)1/2, or IFNG. In this case, the mode of association with EVs needs to be determined. This category also provides further information on the nature and function of EVs. While proving the presence of proteins from categories four and five is optional, the presence of at least one protein from categories one and two, and absence in case of category three must be demonstrated (Théry *et al*, 2018). We mainly focused on the establishment of vesicle markers from categories one to three. For category one, blotting for CD9, CD63 and CD81 was tested. With regard to category two, TSG101 and HSP70 antibodies were used. Category three is especially important for EVs from complex matrices such as whole blood and was not investigated for cell culture derived EVs. Instead, a category three

EV marker was investigated for blood-derived vesicles, where it was checked for the presence or absence of APOA1.

Using Western blotting, Dr. Christina Budden has previously demonstrated the presence of TSG101, CANX, actin beta (ACTB), and histone group H3 (H3) in 2K, 10K, and SEC EVs from untreated THP-1 MΦs left for 48 h in serum-free medium (Figure 11B+C). 30 µg of protein were required per lane in the Western blot. Using whole cell lysates of HEK293T cells instead of EVs from THP-1 MΦs (Figure 11D; as larger amounts of protein could more easily be generated), I tested the antibodies against TSG101 and CANX together with further antibodies to see if, in general, I could replicate these findings and expand blotting to more EV-specific targets. 35 µg of protein were loaded per lane. Blotting for TSG101 and CANX was successful, as was blotting for HSP70 (Figure 11E). However, blotting for the three tetraspanins CD9, CD63, and CD81, other commonly-used EV markers, was unsuccessful using standard Western blotting techniques, even when increasing the protein amount to 100 µg per lane or performing the experiment using non-reducing conditions (Figure 11F).

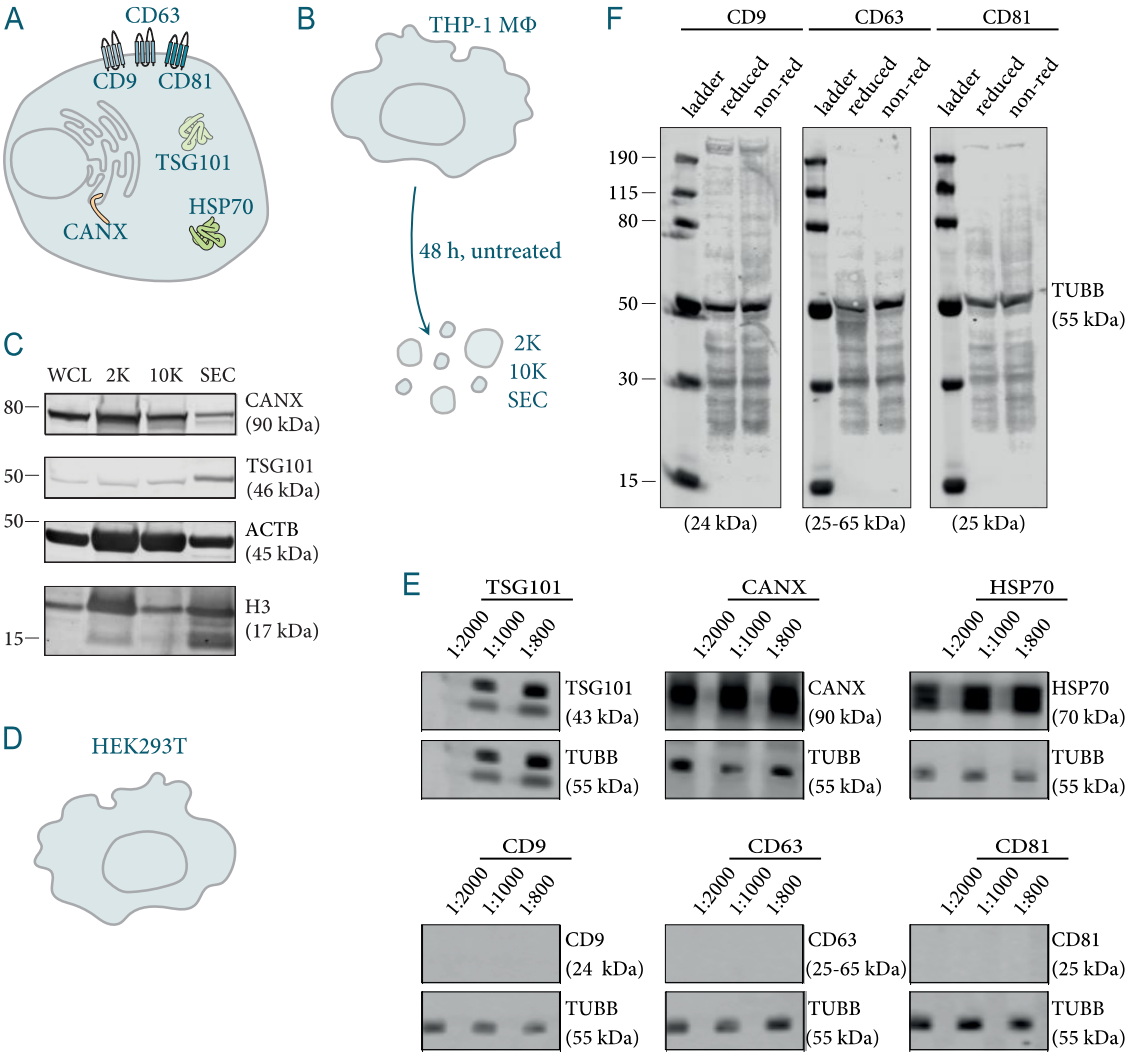

Figure 11: Establishing Western blotting for EV marker proteins. (A+B) Schematic representation of the experimental plan. Whole cell lysates or EV fractions (2K, 10K, SEC) were analysed with regard to common EV marker proteins such as CD9, CD63, CD81, TSG101, and HSP70, as well as the suggested negative exosome marker CANX (A). Markers were either investigated in whole cell lysates (WCLs) or EV fractions isolated from THP-1 MΦs left untreated for 48 h (B). (C) Data obtained by Dr. Christina Budden (Budden, 2020). THP-1 MΦs were left untreated for 48 h in serum-free medium. 2K, 10K, and SEC EVs were isolated. 30 µg of protein (either from each EV fraction or unstimulated WCL) were applied per lane. Immunoblotting for CANX (1:1000 dilution), TSG101 (1:2000), ACTB (1:2000), and H3 (1:2000) was performed. Representative experiment, n = 2. (D) Untreated HEK293T cells were lysed and WCL was used to test different antibodies. (E) 490 µg of protein isolated from HEK293T WCL was applied to a single-lane gel. After running SDS-polyacrylamide gel electrophoresis, blotting was performed. Antibodies against TSG101, CANX, HSP70, CD9, CD63, and CD81 were tested at three concentrations. Blotting for tubulin beta class I (TUBB) acted as a loading control. Representative experiment, n = 2. (F) 100 µg of protein isolated from HEK293T

WCL were applied per lane. Samples were run under reducing and non-reducing conditions. Blotting for CD9, CD63, and CD81 was performed using a 1:800 dilution. TUBB (1:2000) acted as a loading control. n = 1.

Thus, I switched from standard Western blotting to the Simple Western WES technology from ProteinSimple. The advantage of this technology is that it is highly sensitive and allows for a protein input of as little as 0.6 to 1.2 µg per lane. Western blotting using the Simple Western WES technology was performed on EVs isolated from THP-1 MΦs left untreated for 48 h (Figure 12A) using antibodies against CD9, CD63, CD81, TSG101, and HSP70 (Figure 12B). Blotting for CD63 in THP-1 MΦs was not successful (data not shown), while blotting against CD9, CD81, TSG101, and HSP70 was successful. HSP70 is present in whole cell lysates and all EV fractions. It is of note that the molecular weight of HSP70 in SEC samples appears to be a bit lower than for 10K, 2K, and whole cell lysate samples. As standard Western blotting, the Simple Western WES technology only allows determination of the observed molecular weight, as opposed to the predicted molecular weight: while the predicted molecular weight assumes a constant charge-to-mass ratio based on binding of SDS to protein, this is actually not always the case. In reality, the amount of SDS bound to proteins varies and depends on factors such as the pH of the running buffer or whether complete denaturation has taken place (Wiesner et al. 2021). Additionally, sample migration depends on the protein concentration. While protein concentrations were measured and I aimed to load the same amount of protein, there still might be some slight differences that then led to different migration efficiencies. Considering that the different vesicle fractions are isolated using different techniques with especially the SEC fractions having been treated quite differently to the other fractions and resulting in a lower protein amount isolated, a slight change of observed molecular weight can be expected. CD9, CD81, and TSG101 are enriched in SEC EVs (Figure 12C). It can thus be concluded that the isolation of EVs was successful. Although the technique has been described to work with protein concentrations as little as 0.6 to 1.2 µg of protein, slightly higher concentrations (around 3 µg) were required for the detection of CD9 and CD81.

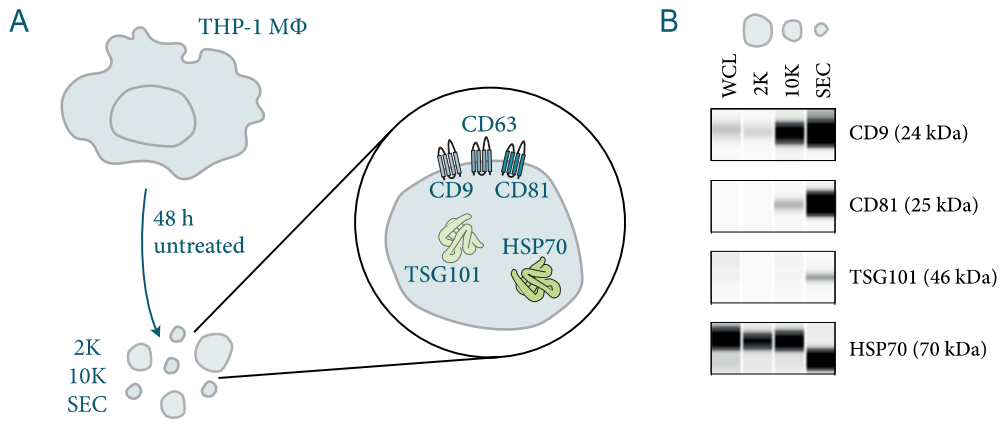

Figure 12: Characterisation of EVs released by THP-1 MΦs using Simple Western WES. (A) Schematic representation of the experimental plan. EVs released from THP-1 MΦs left untreated (UT) for 48 h were characterised for common EV marker proteins such as CD9, CD63, CD81, TSG101, and HSP70. (B) 1.2 x 10^8 THP-MΦs were incubated for 48 h in RPMI medium without FBS. EVs were isolated from supernatants and Western blotting using the Simple Western WES system from ProteinSimple was performed for CD9 (1:20), CD81 (1:20), TSG101 (1:20), and HSP70 (1:100). 3 µg of protein were loaded onto each lane. Representative blot of n = 3.

3.1.2 Presence of GSDMD in Inflammasome-Elicited EVs

Western blotting was not only performed to confirm the successful isolation of EVs, but also to investigate the presence of specific proteins of interest, such as GSDMD. Upon NLRP3 activation, full-length GSDMD is cleaved, and the N-terminal fragment is released from the intramolecular inhibitory action between the N- and C-terminal GSDMD domains. As a result, the N-terminal fragment will insert into the plasma membrane to form GSDMD pores (Broz & Dixit, 2016). Ca^{2+} can then enter the cell's cytoplasm through GSDMD pores, resulting in the recruitment of the ESCRT machinery to GSDMD pores and the subsequent initiation of ESCRT-dependent membrane repair (Rühl *et al*, 2018). During this process, GSDMD pore-containing damaged membrane areas are excluded from the plasma membrane and pinched off into EVs (Rühl *et al*, 2018). Thus, the question arose, if GSDMD or GSDMD pores are found on EVs isolated in our experiments, possibly making EVs leaky, but also potentially acting as a marker for inflammasome activation in clinical settings (Figure 13A). Results are shown for THP-1 MΦs (Figure 13B). The presence of full-length GSDMD protein was

detected in whole cell lysates of unstimulated cells. In all three EV subtypes (2K, 10K, and SEC), the presence of the N-terminal fragment of GSDMD was shown upon NLRP3 activation in EV donor cells, while full-length GSDMD was absent. NLRP3 activation thus took place, resulting in cleavage of GSDMD, GSDMD pore formation, and release of GSDMD N-termini in EVs.

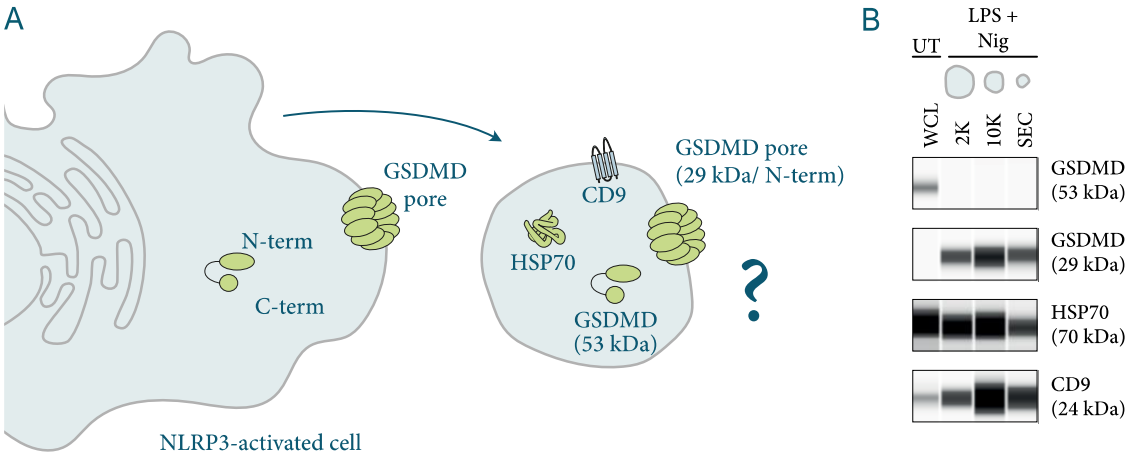

Figure 13: Characterisation of EVs for the presence of GSDMD. (A) Schematic representation of the experimental plan. The presence of GSDMD was assessed in EVs released from THP-1 MΦs stimulated with LPS + nigericin. (B) 1.2 x 10^8 THP-1 MΦs were stimulated with LPS + nigericin. EVs were isolated from supernatants and Western blotting was performed for GSDMD (1:20), HSP70 (1:100), and CD9 (1:20). 3 µg of protein were loaded on each lane. Representative blot of n = 3.

3.1.3 Inflammasome-Elicited EVs From Blood

Besides investigating EVs released from inflammasome-activated THP-1 MΦs, we characterised EVs isolated from human blood with the goal to later isolate EVs from patients and diagnose inflammasome-related diseases. EVs were isolated in a similar way to EVs from cell culture supernatant (Figure 14): first, the blood was centrifuged at 1,000 x g for 15 min without breaks, in order to separate the blood plasma. The plasma was then centrifuged at 340 x g for 10 min to remove any remaining cells and large debris, followed by a centrifugation step at 2,500 x g for 15 min to remove platelets. This also removed 2K EVs, which are similar in size to platelets and were therefore not examined here. Centrifugation at 2,500 x g was repeated to ensure all platelets had been removed, as platelets can be activated by shear forces (Holme *et al*, 1997) and, once activated, have

been shown to secrete EVs (Warren & Vales, 1972; Polasek, 1982; Sims *et al*, 1989; Gemmell *et al*, 1993), thus contaminating the EV fractions isolated. The platelet-free plasma generated in this way was then spun at 10,000 x g for 45 min to pellet 10K EVs. Next, the supernatant was concentrated, run through a SEC column, filtered, and concentrated at 100,000 x g for 90 min.

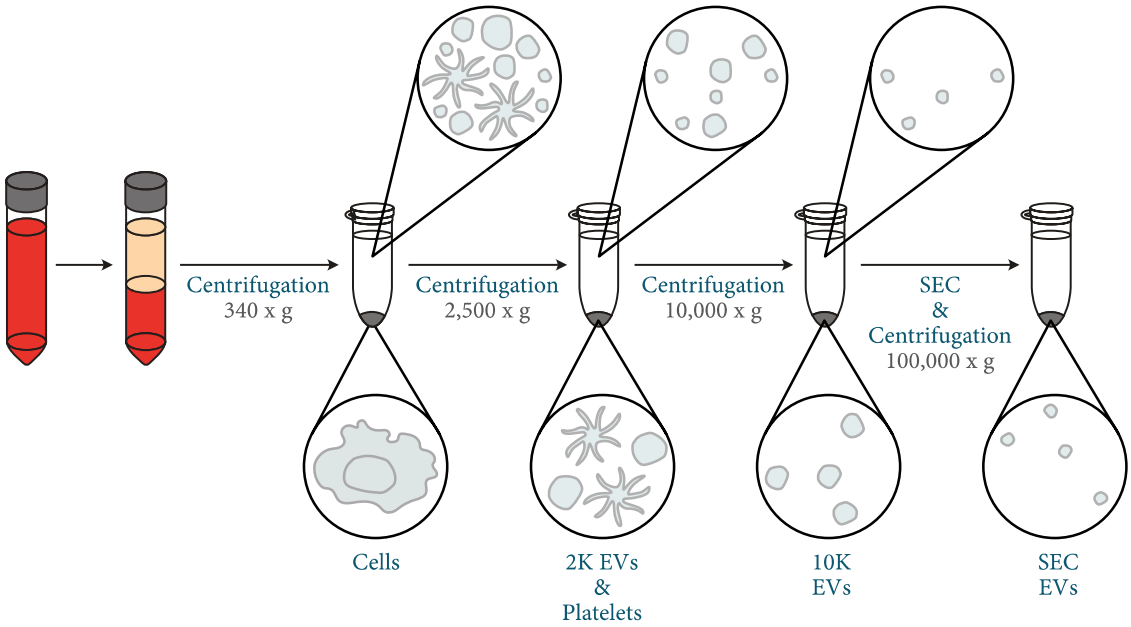

Figure 14: EV isolation from blood. Blood was centrifuged at 1,000 x g to isolate plasma. From that plasma, platelet-free plasma was generated through centrifugation at 340 x g followed by two centrifugations at 2,500 x g. The platelet free plasma was spun at 10,000 x g to pellet the 10K EV fraction, which was washed once with PBS. The 10K supernatant was further processed through concentration, SEC, and filtration to get the SEC fraction, which was concentrated through centrifugation at 100,000 x g.

Healthy donors were used to establish the assay: blood was stimulated with LPS for 23 h to activate the NLRP3 inflammasome and EVs were isolated as described above.

We made use of whole blood assays because they come the closest to patient blood: The same cell populations are found so that EVs are not only secreted from monocytes but also from other cells such as neutrophils which have been shown to contribute to IL-1β in circulation (Mankan *et al*, 2012; Bakele *et al*, 2014; Tran *et al*, 2019). They further allow the consideration of the contribution of effects from soluble plasma factors as well as cellular fractions to the stimulation (Levy *et al*, 2004; Rolfes *et al*, 2020; Busatto *et al*, 2022).

While the 2 h LPS plus 90 min nigericin stimulation used so far leads to the activation of the canonical inflammasome, LPS stimulation for 23 h has been shown to result in both canonical and non-canonical inflammasome activation (Baker *et al*, 2015; Rathinam *et al*, 2019; Tran *et al*, 2019; Viganò *et al*, 2015) and, in human monocytes, in alternative inflammasome activation (section 1.3.3; Gaidt *et al*, 2016). Thus, we expected to have a mix of different inflammasome activation pathways present.

It is important to note that, in essence, the outcome is basically the same as with canonical inflammasome activation: A major difference between the canonical and the non-canonical inflammasome is that the canonical inflammasome (section 1.3.1) leads to activation of caspase-1, while non-canonical inflammasome (section 1.3.2) activation leads to the activation of caspases-4 and -5. However, the functional consequences of canonical and non-canonical inflammasome activation are the same (Downs *et al*, 2020): Both lead to GSDMD pore formation and in the end result in IL-1β and IL-18 release. This is the case as activation of the non-canonical inflammasome leads to GSDMD pore formation, which then triggers the activation of the canonical inflammasome, resulting in the final ability of caspase-1 to cleave pro-IL-1β and pro-IL-18. So while the activation mechanisms themselves might be different, the outcome is very similar and as we are looking at one of the outcomes of inflammasome activation, namely vesicle secretion, our analysis was not much affected by changing the stimulus.

Indeed, previous experiments performed by Dr. Christina Budden have shown that a common inflammasome signature can be observed for the different NLRP3 stimuli and even for the different inflammasomes (NLRP3 and NLRC4), indicating that the content of inflammasome-elicited EVs is not determined by the sensing of the stimulus, but rather by mechanisms mediated downstream of inflammasome activation (Budden *et al*, 2021).

Considering this, a main reason for switching to a long LPS stimulation was the fact that long LPS stimulation is commonly used in whole blood assays and thus we could adapt a protocol established previously and compare our results to the literature.

Another important reason was that vesicle isolation from the blood alone takes so long that, together with the stimulation of whole blood, we would not have been able to fit the experiment into one day.

Two inflammasome inhibitors were used to be able to identify transcripts associated with NLRP3 activation vs TLR stimulation: CRID3 and IFM-2384. CRID3, commonly also referred to as MCC950, was discovered to be an IL-1β processing inhibitor in 2001 (Perregaux *et al*, 2001) and was subsequently shown to inhibit NLRP3 (Coll *et al*, 2015). In 2022, Hochheiser and colleagues showed that CRID3 does so by stabilising the NACHT and LRR domains relative to one another. It ties five NLRP3 subunits together. This leads to the stabilisation of the inactive NLRP3 (Hochheiser *et al*, 2022). IFM-2384, here referred to as IFM, is another NLRP3 inhibitor, kindly donated to us by IFM. IFM-2384 has for example been shown by Friker and colleagues to block NLRP3 induced IL-1β release in microglia (Friker *et al*, 2020). Blood was pre-treated with these inhibitors (or DMSO for controls) for 1 h before LPS was applied for the next 23 h (Figure 15A). TNF-α and IL-1β protein levels in platelet-free plasma were measured to determine how responsive cells were to TLR4 and inflammasome activation respectively (Figure 15B). TNF-α levels for untreated samples varied from around 500 to 1,000 pg/mL. TNF-α levels were roughly between 1,000 pg/mL and 3,000 pg/mL for samples treated with LPS, with the exception of one donor at around 5,000 pg/mL. It can thus be concluded that LPS stimulation was successful. IL-1β levels showed more variation. In unstimulated and inhibited samples, IL-1β levels were at around 200 pg/mL for four donors and around 400 pg/mL for donor one. LPS-stimulated samples showed IL-1β levels of around 400 pg/mL for four donors, and at around 2,000 pg/mL for donor three. This shows that there was quite a bit of donor variation, which has also been reported in literature (Sahdo *et al*, 2013). Particle numbers for 10K and SEC fractions were determined for the different stimuli and no strong differences between different stimuli could be observed (Figure 15C). Particle size distribution was investigated and, as for particle numbers, no strong differences were observed (Figure 15D).

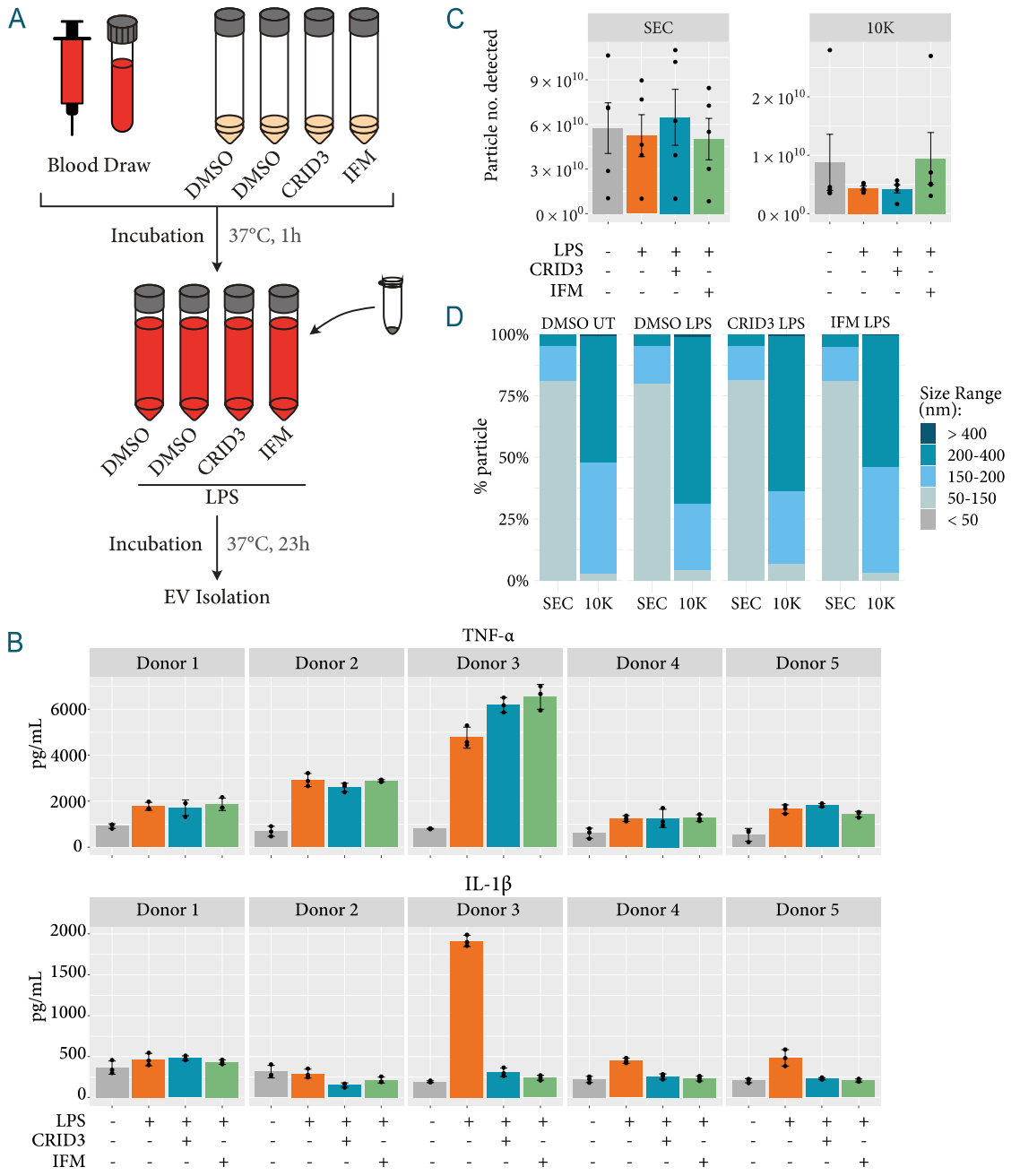

Figure 15: Protein and NanoSight analysis of EVs released from whole blood after inflammasome activation. (A) Schematic representation of experimental plan. Blood was drawn from healthy donors and pre-treated with inflammasome inhibitors (CRID3 or IFM) or DMSO (control). After 1 h of incubation, LPS was added, and samples were incubated for 23 h to activate the NLRP3 inflammasome. EVs were isolated. (B) TNF-α and IL-1β protein levels in platelet-free plasma. Mean ± SD of three technical replicates, n = 5 (C) Total number of particles released. Shown are the means of three technical replicates for five experimental runs. Mean ± SEM. (D) Particle size distribution for different stimuli. Representative plot for one experimental run showing the mean of three technical replicates, n = 5.

Based on previous results with THP-1 MΦs, we expected the particle number to increase in LPS-stimulated samples (DMSO + LPS) compared to untreated samples (DMSO + UT) and inflammasome-inhibited samples (CRID3 + LPS and IFM + LPS). However, this was not the case (Figure 15C). To further investigate this, we looked at each experimental run individually (Figure 16). For each individual run, particle size distributions and total particle numbers released are shown. However, the expected phenotype could still not be observed.

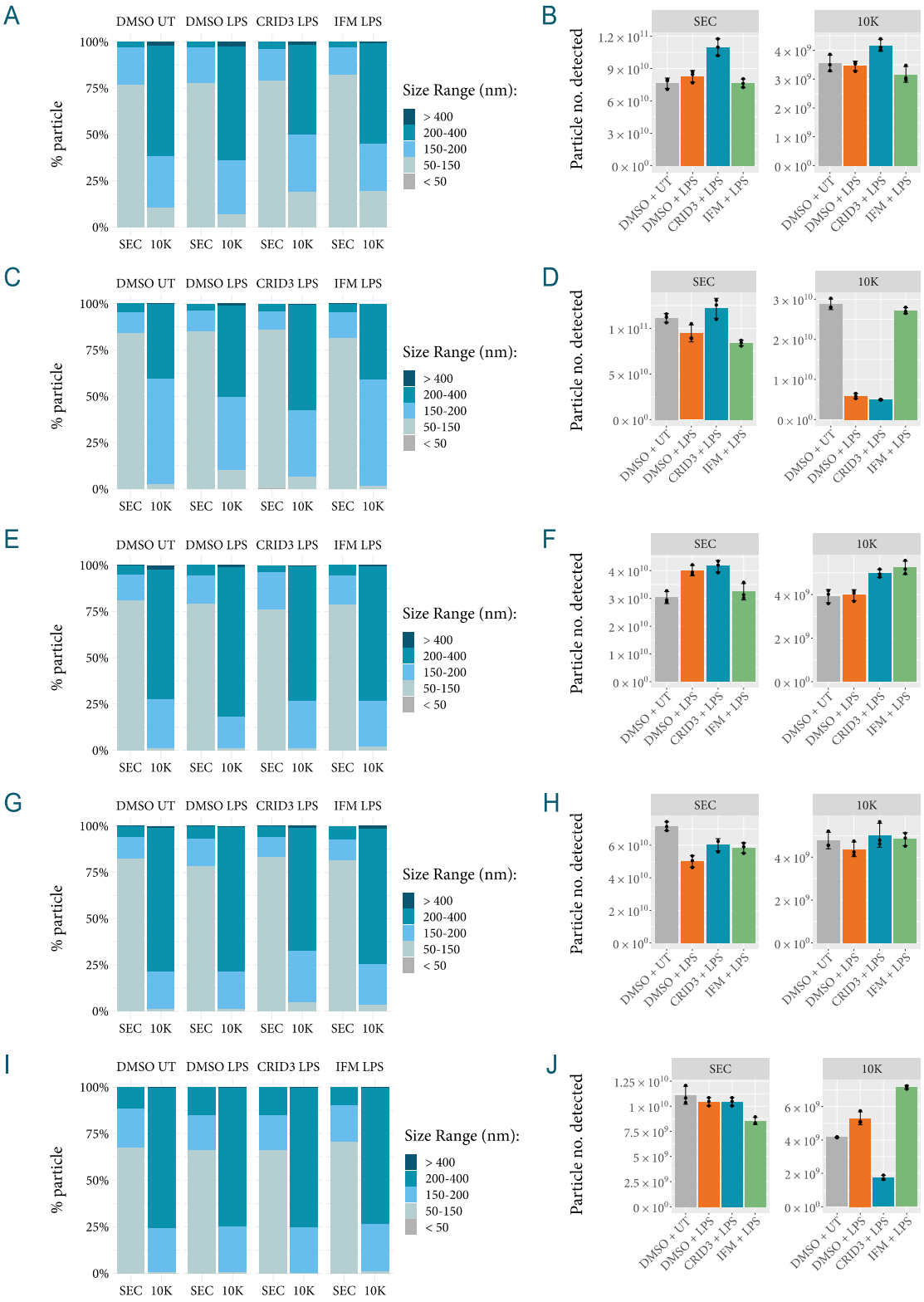

Figure 16: Individual NanoSight analysis of EVs released from whole blood after inflammasome activation. Particle Size distributions and total number of particles released for each experimental run individually. Blood was drawn from healthy donors and pre-treated with inflammasome inhibitors (CRID3 or IFM) or DMSO (control). After 1 h of incubation, LPS was added, and samples were

incubated for 23 h to activate the NLRP3 inflammasome. EVs were isolated. (A, C, E, G, I) Particle size distribution for experimental runs 1, 2, 3, 4, and 5, respectively. Means of three technical replicates are shown. (B, D, F, H, J) Total particles released for experimental runs 1, 2, 3, 4, and 5, respectively. Mean ± SD of three technical replicates.

Since we could not observe the expected increase in particle number after NLRP3 activation compared to inhibited or unstimulated conditions, we investigated possible reasons for this. We first checked if EV isolation from plasma was successful, especially with regard to EV purity. We employed Western blotting for the previously established EV markers (Figure 17). Indeed, we could not show the enrichment of CD9 and TSG101 in EVs, nor could we show the presence of HSP70 (Figure 17B). This led us to suspect that we were co-isolating other particles from human blood, such as lipoproteins and chylomicrons, which diluted the EV fractions so much that blotting for EV proteins became impossible. From the literature, it is known that blood contains about 20- to 100-fold more lipoproteins than EVs and that chylomicrons increase after food intake (Karimi *et al*, 2018; Mathieu *et al*, 2019). We thus performed Western blotting for APOA1, a protein found on chylomicrons and high-density lipoprotein (HDL). We could indeed show the presence of APOA1 (Figure 17C), indicating that the isolated vesicle fractions were contaminated with lipoproteins. To decrease lipoprotein content, we tried to pull down lipoproteins with an antibody against APOB. APOB was chosen as SEC already strongly decreases HDL contamination through separation by size (Karimi *et al*, 2018), thus the idea was to reduce the levels of other lipoproteins (very low density lipoprotein (VLDL), intermediate density lipoprotein (IDL), and LDL), which all contain APOB-100 on their surface, as well as chylomicrons, which expose APOB-48 on their surface (Noels *et al*, 2021). However, enriching EVs with this method was unsuccessful, as seen when comparing Western blots for CD9 and TSG101 for SEC EVs isolated without a pull-down to those for SEC EVs isolated with a pull-down (Figure 17D).

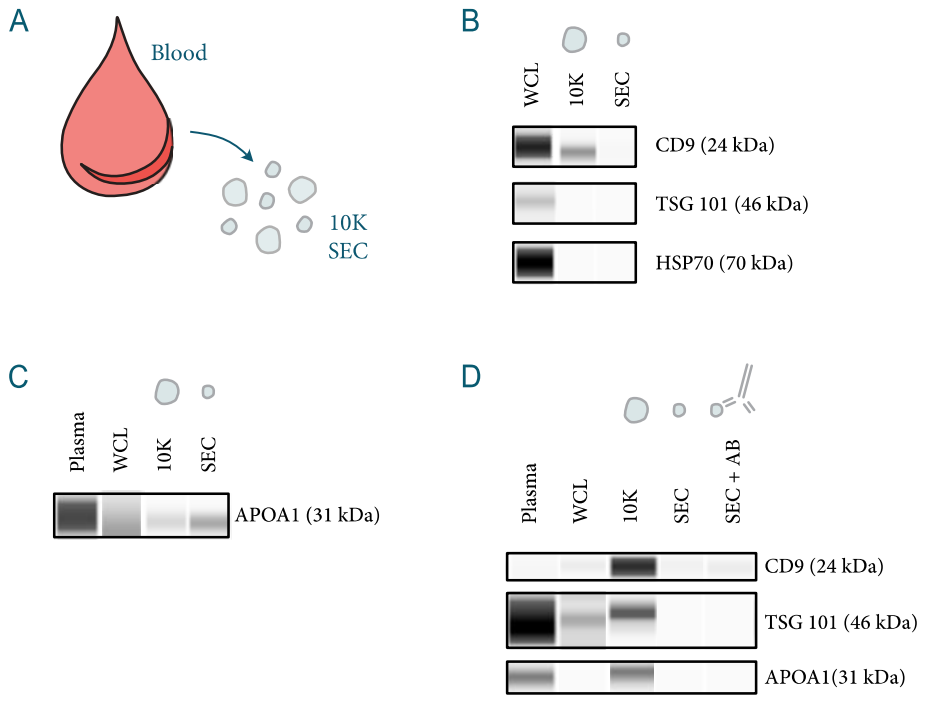

Figure 17: Characterisation of blood-derived EVs using the Simple Western WES system. (A) EVs were isolated from human blood and analysed for the presence of different proteins. (B) 10K and SEC EVs isolated from blood were compared to WCL from THP-1 MΦs for the presence of the EV marker proteins CD9, TSG101, and HSP70. Representative blot of n = 2. (C) 10K and SEC EVs isolated from blood were compared to WCL from THP-1 MΦs, as well as to plasma samples, for the presence of APOA1. n = 1. (D) SEC EVs isolated from blood (either directly or after immune pull-down with antibodies against APOB) were compared to WCL from THP-1 MΦs, as well as to plasma samples and 10K EVs, for the presence of APOA1 and EV markers CD9 and TSG101. Antibody dilutions used: CD9 (1:20), TSG101 (1:20), HSP70 (1:100), APOA1 (1:20). n = 1.

Since the original pull-down of lipoproteins with an antibody against APOB did not work, one could try other methods to enrich the isolated EVs and remove apolipoproteins. However, while the presence of lipoproteins would affect proteomics, the presence of lipoproteins does not have a big effect on transcriptomic analysis, as most lipoproteins do not carry RNA. It should be noted though that HDL has been shown to carry RNA, which therefore might contribute to the RNA analysed (Vickers *et al*, 2011). Keeping this in mind and considering that particle numbers are not informative because lipoproteins are present, we decided to move forward with EV transcriptomics regardless.

We thus progressed to try RNA-seq for blood-derived EVs (Figure 18A). Again, IL-1β levels of platelet-free plasma were determined to investigate the strength of the response to NLRP3 activation (Figure 18B). Indeed, again, there was a lot of variation between different blood donors (Figure 18B). However, we were able to see a good inhibition of NLRP3 inflammasome activation for donors 1, 3, and 4. For donor 2 inflammasome inhibition also seemed to work well; however, here we observed a certain background level of IL-1β. This was also the case for the unstimulated sample of donor 4. In case of donor five, inhibition with CRID3 worked, while inhibition with IFM was not successful (Figure 18B).

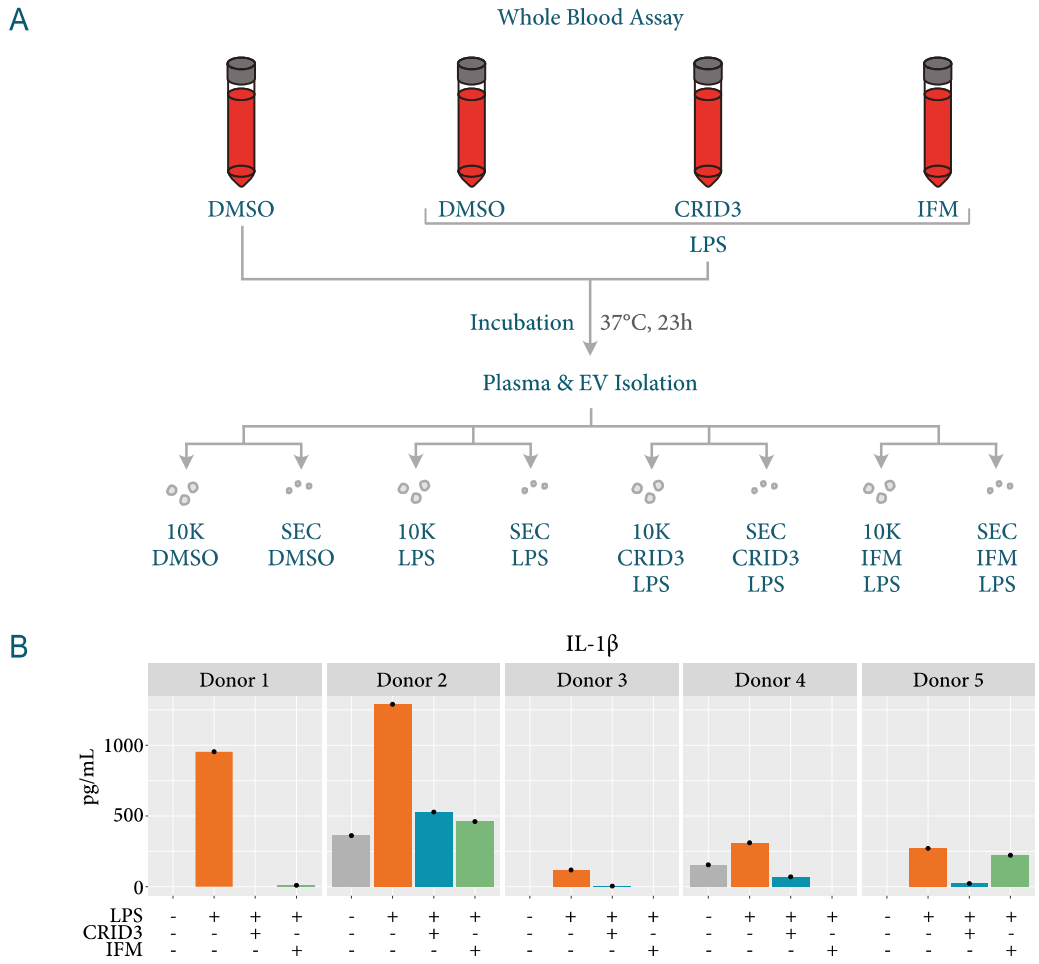

Figure 18: Experimental setup and IL-1β levels for RNA sequencing of blood-derived EVs. (A) Blood was drawn from healthy donors and pre-treated with inflammasome inhibitors (CRID3 or IFM) or DMSO (control). After 1 h of incubation, LPS was added and samples were incubated for 23 h to activate the NLRP3 inflammasome. EVs were isolated. (B) IL-1β protein levels in platelet-free plasma. n = 5.

EVs isolated were sequenced by Marius Jentzsch and Dr. Jonathan Schmid-Burgk. Between 800 and 1.5 x 10^4 genes were detected per sample (Figure 19B), with a high percentage of haemoglobin reads per sample (Figure 19C), which led to a reduction in sequencing depths. For data pre-processing, haemoglobin genes were removed. Library sizes of the different samples were roughly between 1 x 10^3 and 1.7 x 10^5. Samples with library sizes below 1 x 10^4 (dashed line) were removed, which resulted in the exclusion of nine samples from the analysis (Figure 19D). Lowly expressed genes (counts below 2) were removed from the analysis and samples were normalised by the TMM method.

MDS plots were created to examine the distances between the samples based on their gene expression profiles. MDS plots for dimensions one and two, coloured by EV type, are shown before (Figure 20B left) and after removing an observed donor effect (Figure 20B right). Samples clustered according to EV type. Sample data was then split up into 10K and SEC data and further MDS plots were generated (Figure 20C). A clear clustering according to treatment was observed for both 10K and SEC EVs in dimensions one and two (Figure 20C). This is comparable to results obtained previously in our lab (Budden *et al*, 2021).

Even though samples showed clustering according to treatment, the high number of haemoglobin reads caused problems when it came to DE gene calling. To circumvent most of the reads mapping to haemoglobin reads, we tried to use a haemoglobin removal kit. While normally a good option, haemoglobin removal kits are designed for higher amounts of RNA input than can be isolated from EVs under our settings. While we still tried using the haemoglobin removal kit GLOBINclear, too little RNA was left afterwards. We also tried sending EVs off for sequencing to GeneWiz, a company specialising in sequencing. They too were not able to remove the haemoglobin reads and still have enough sample left for sequencing.

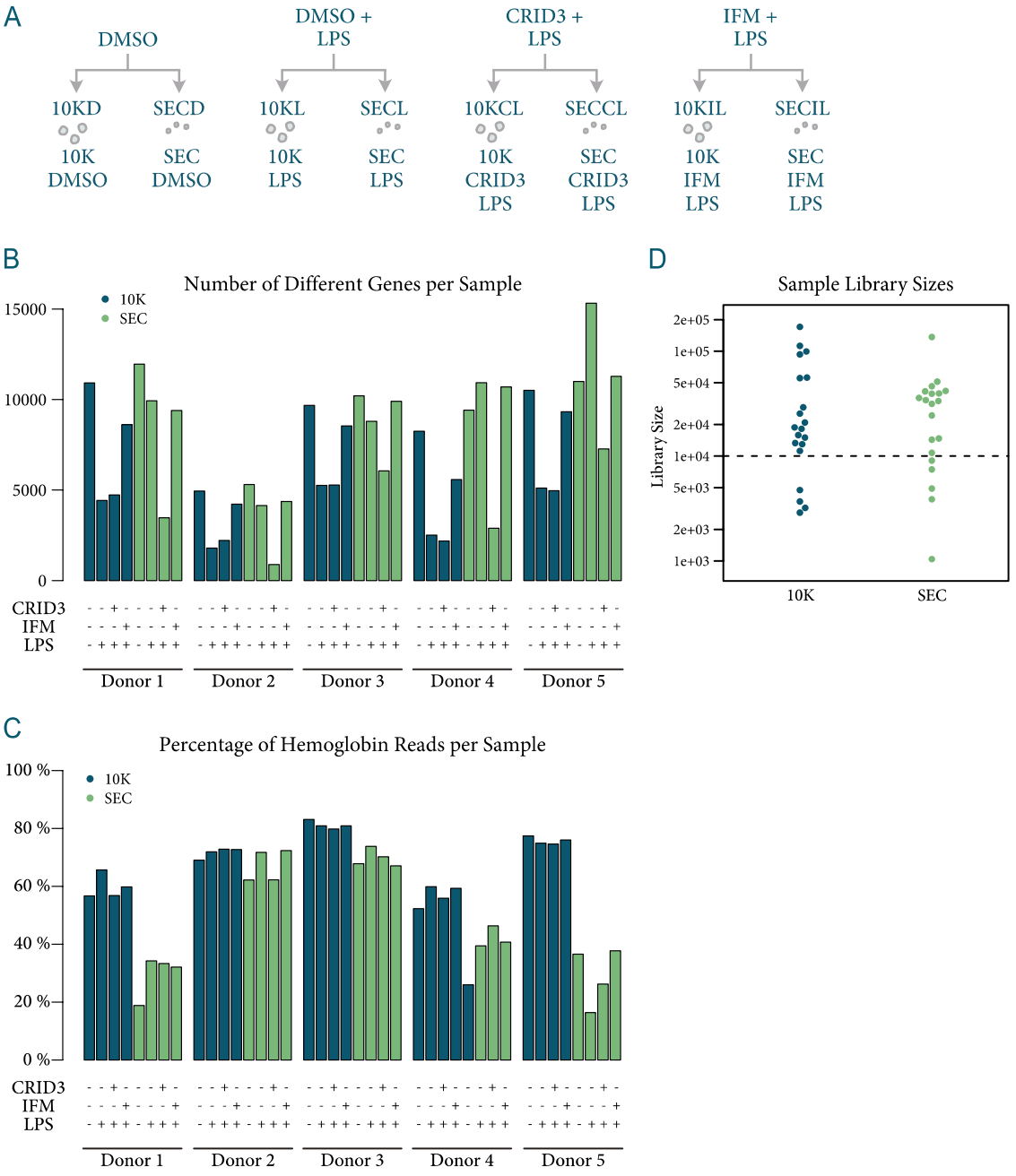

Figure 19: Pre-processing of RNA sequencing results of blood-derived EVs. (A) Schematic of the experiment. EVs were isolated from control (DMSO only) samples, from LPS stimulated (DMSO + LPS) samples, from CRID3 + LPS stimulated samples, and from IFM + LPS stimulated samples. n = 5. (B) Number of genes detected per sample. (C) Percentage of reads mapping to haemoglobin genes per sample. (D) Library sizes of different samples. Samples with library sizes below 1 x 10^4 (dashed line) were excluded from the analysis.

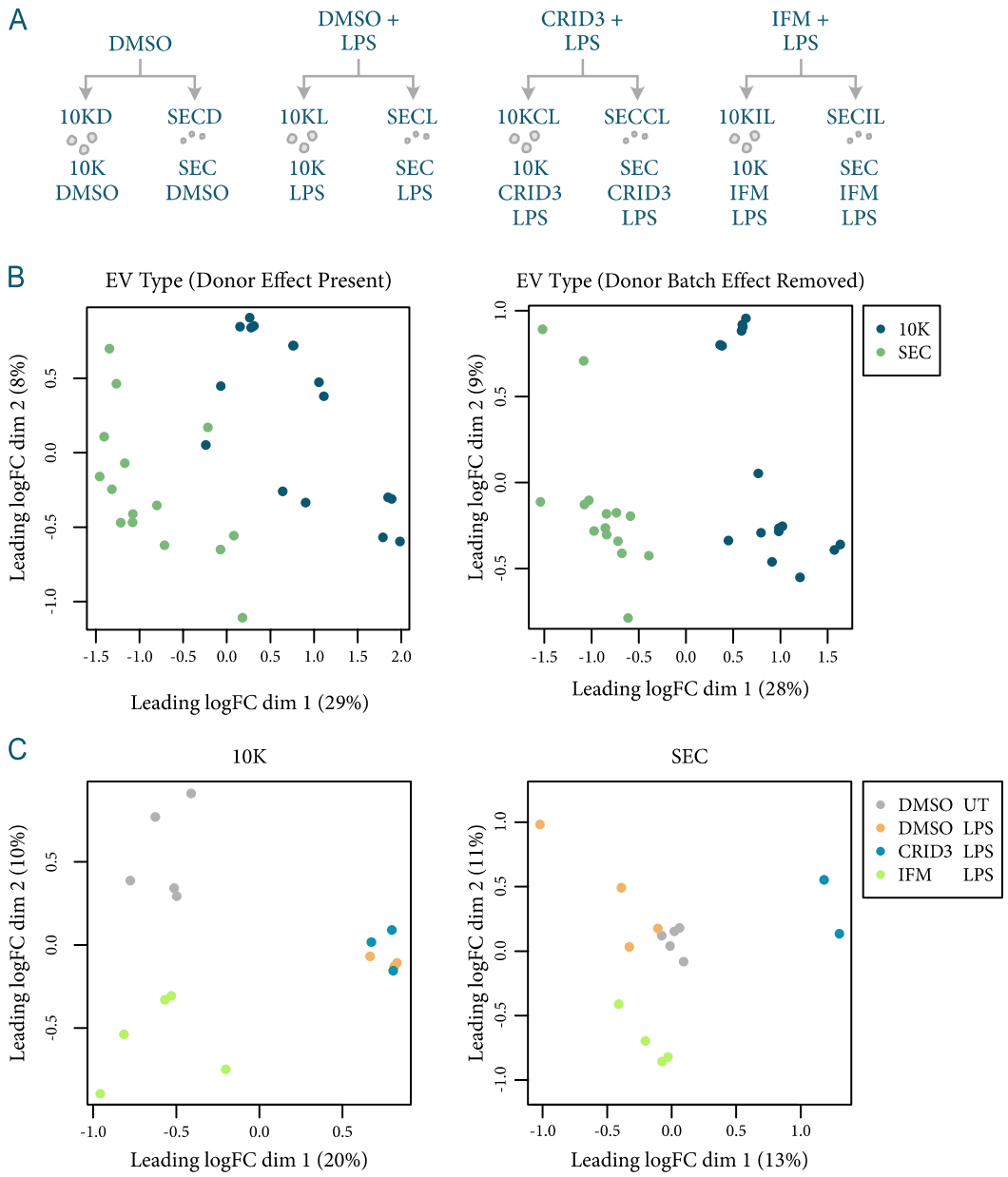

Figure 20: Clustering of blood-derived EV RNA-seq samples. (A) Schematic of the experiment. EVs were isolated from control (DMSO only) samples, from LPS stimulated (DMSO + LPS) samples, from CRID3 + LPS stimulated samples, and from IFM + LPS stimulated samples. n = 5. (B) MDS plot before (left) and after (right) removal of the donor batch effect for dimensions one and two, coloured by EV type. (C) MDS plots with the donor batch effect removed, split up for 10K and SEC EV types for dimensions one and two. Coloured by treatment.

Another way to examine RNA content that would solve the haemoglobin problem would be to use microarrays. In this approach, excess haemoglobin RNA would be washed away, while RNA mapping to genes of interest would hybridise to the microarray. The microarray technique had already been established by Dr.

Christina Budden (Budden, 2020; Budden *et al*, 2021) and the same protocol was followed. Samples were generated and sent for processing to the Gene Expression Affymetrix Facility at the Centre for Molecular Medicine Cologne. Samples were analysed by me with help from Dr. Jamie Gearing.

The same experimental setup was chosen as for the RNA sequencing experiment and new samples were generated: whole blood was stimulated with LPS for 23 h either in the presence of an inflammasome inhibitor (CRID3 or IFM) or without inhibition. After stimulation, plasma was isolated and subsequently EVs were isolated from plasma (Figure 21A). TNF-α and IL-1β levels were measured (Figure 21B+C). TNF-α was increased in all samples stimulated with LPS for 23 h (Figure 21B). IL-1β levels showed a clear increase in donor 2 (Figure 21C). For all other samples, a clear increase in IL-1β levels after LPS treatment and a reduction for samples stimulated with LPS in the presence of an inflammasome inhibitor was not seen (Figure 21C).

Generally, IL-1β level measurements from blood plasma have been quite varied: in the case of the RNA sequencing experiment, HTRF results showed less background IL-1β (except for donor 2), but IL-1β levels after inflammasome activation did not increase to levels above 500 pg/mL for most samples (Figure 18B). When whole blood was stimulated to isolate vesicles for NTA measurements, also only one donor showed a strong IL-1β response, while for all other donors IL-1β levels remained at around 500 pg/mL, with similar background levels (Figure 15). Thus, HTRF results were in line with previous HTRF readouts, although higher IL-1β levels would generally be expected in case of LPS-stimulated samples with no inhibitor present. This raises the questions, whether IL-1β measurements are a good readout for inflammasome activation in whole blood, whether an alternative technique to HTRFs should be used (e.g., flow cytometry), or if the 23 h stimulation with LPS is not suitable. We nevertheless decided to proceed with the microarray analysis of the isolated RNA, mainly as samples previously differed based on the treatment (Figure 20C, even without clear IL-1β HTRF measurements [Figure 18B]) and as variability

between technical replicates was high (Figure 21C), pointing towards an issue with the IL-1β HTRF measurements.

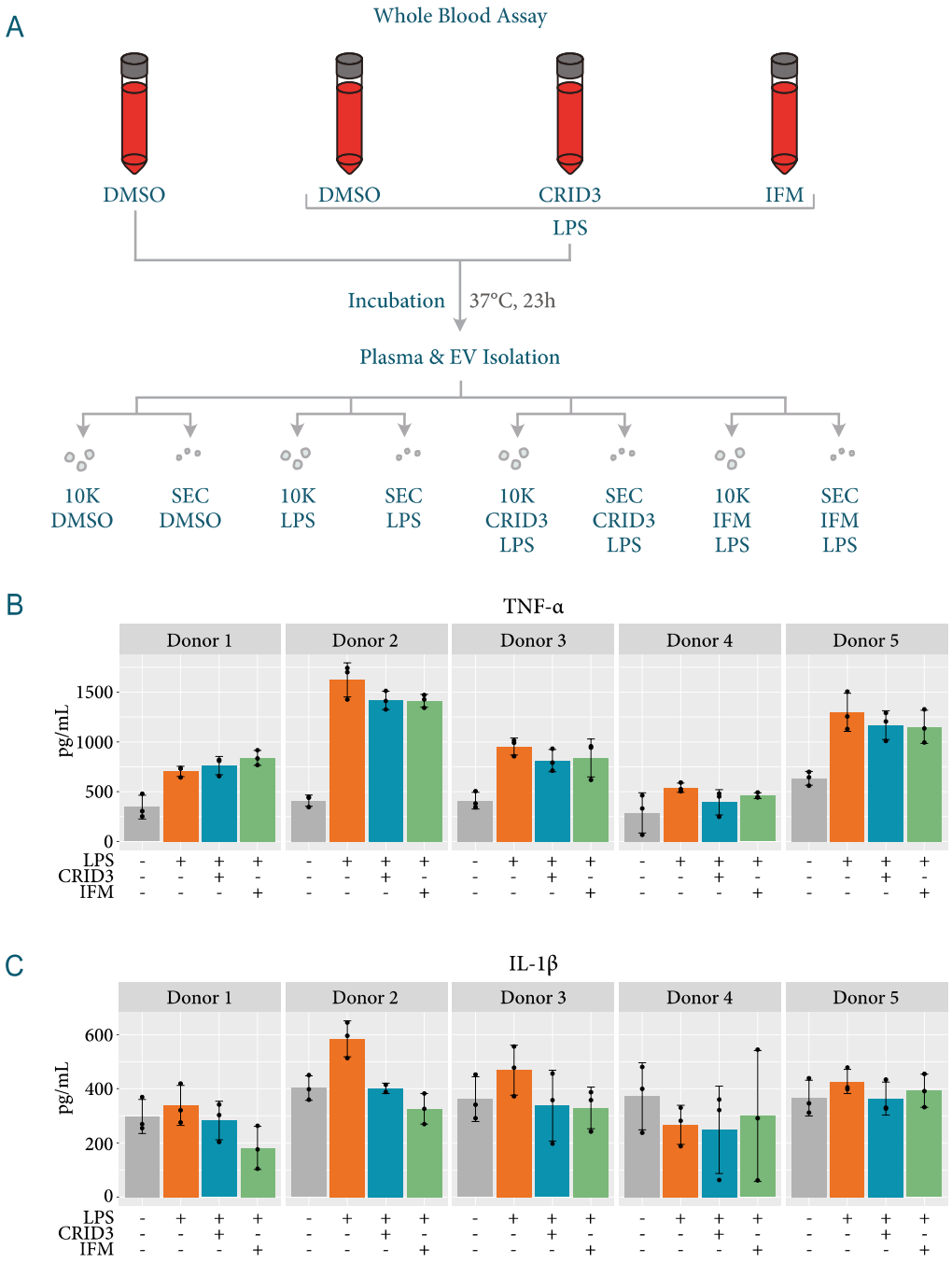

Figure 21: Experimental setup and IL-1β levels for microarray analysis of blood-derived EVs. (A) Blood was drawn from healthy donors and pre-treated with inflammasome inhibitors (CRID3 or IFM) or DMSO (control). After 1 h of incubation, LPS was added and samples were incubated for 23 h to activate the NLRP3 inflammasome. EVs were isolated and RNA was subjected to microarray analysis. n = 5. (B) TNF-α protein levels in platelet-free plasma. (C) IL-1β protein levels in platelet-free plasma. (B+C) Means ± SD of three technical replicates.

Microarray analysis was performed using the Clariom D Pico Chip. Samples were normalised using RMA normalisation and MDS plots were generated. MDS plots show clustering of samples by EV type, with 10K EVs clustering together and SEC EVs building a separate cluster. No clustering according to treatment could be observed in the first two dimensions. The different microarray batches and the different donors led to batch effects (Figure 22B).

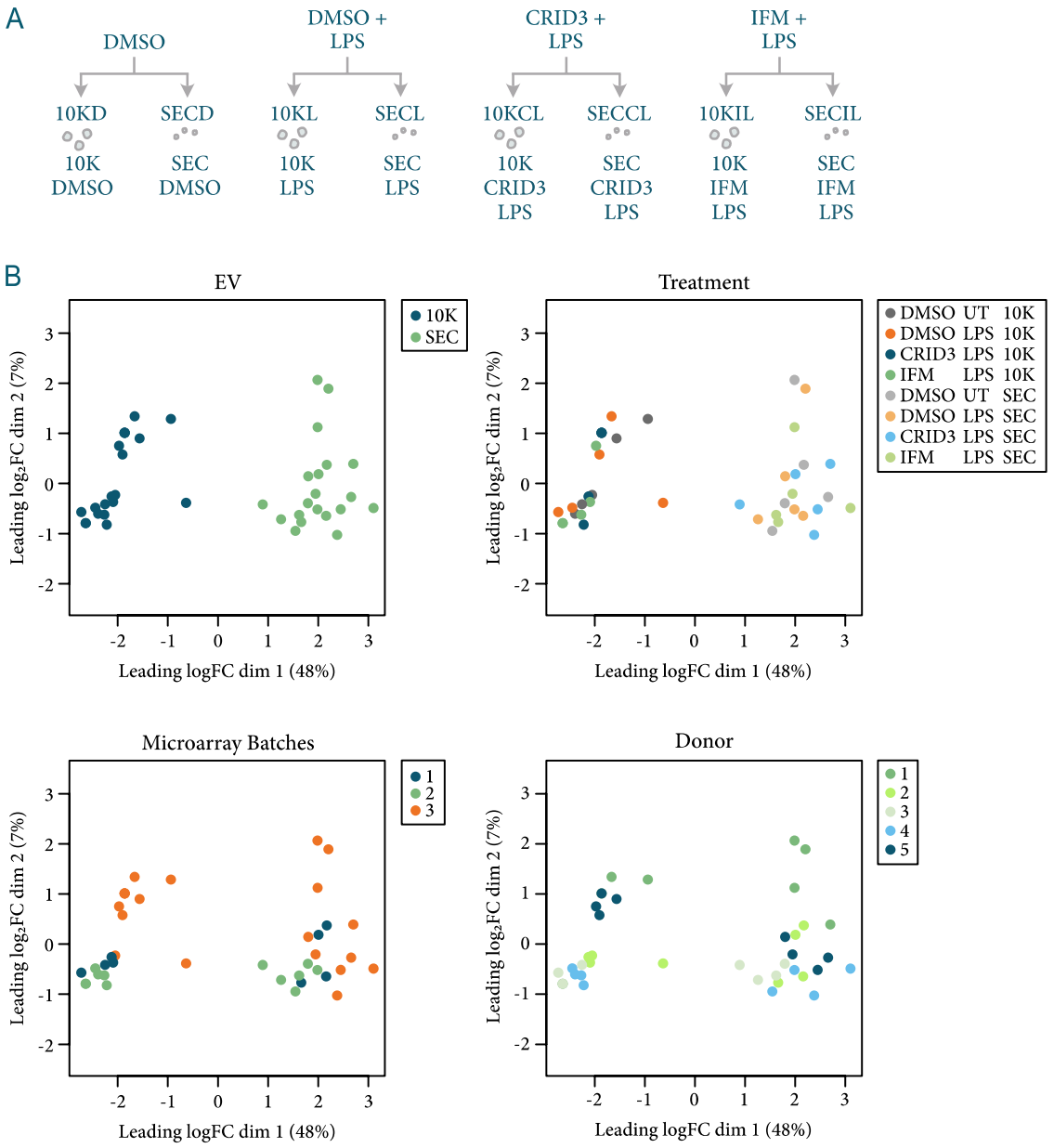

Figure 22: MDS plots of blood-derived EV microarray samples. (A) Schematic of the experiment. EVs were isolated from control (DMSO only) samples, from LPS stimulated (DMSO + LPS) samples, from CRID3 + LPS stimulated samples, and from IFM + LPS stimulated samples. n = 5. (B) MDS

plots for dimensions one and two, coloured according to vesicle type, treatment, microarray batches, and donor.

The microarray and donor batch effects were removed and non-coding and unassigned transcripts were filtered out, leaving coding, multiple-complex (genes that have both coding and non-coding transcripts), precursor microRNA, pseudogenes, ribosomal, and small RNA transcripts. MDS plots of these processed samples show the successful removal of the microarray and donor batch effects and even more pronounced clustering according to EV type (Figure 23).

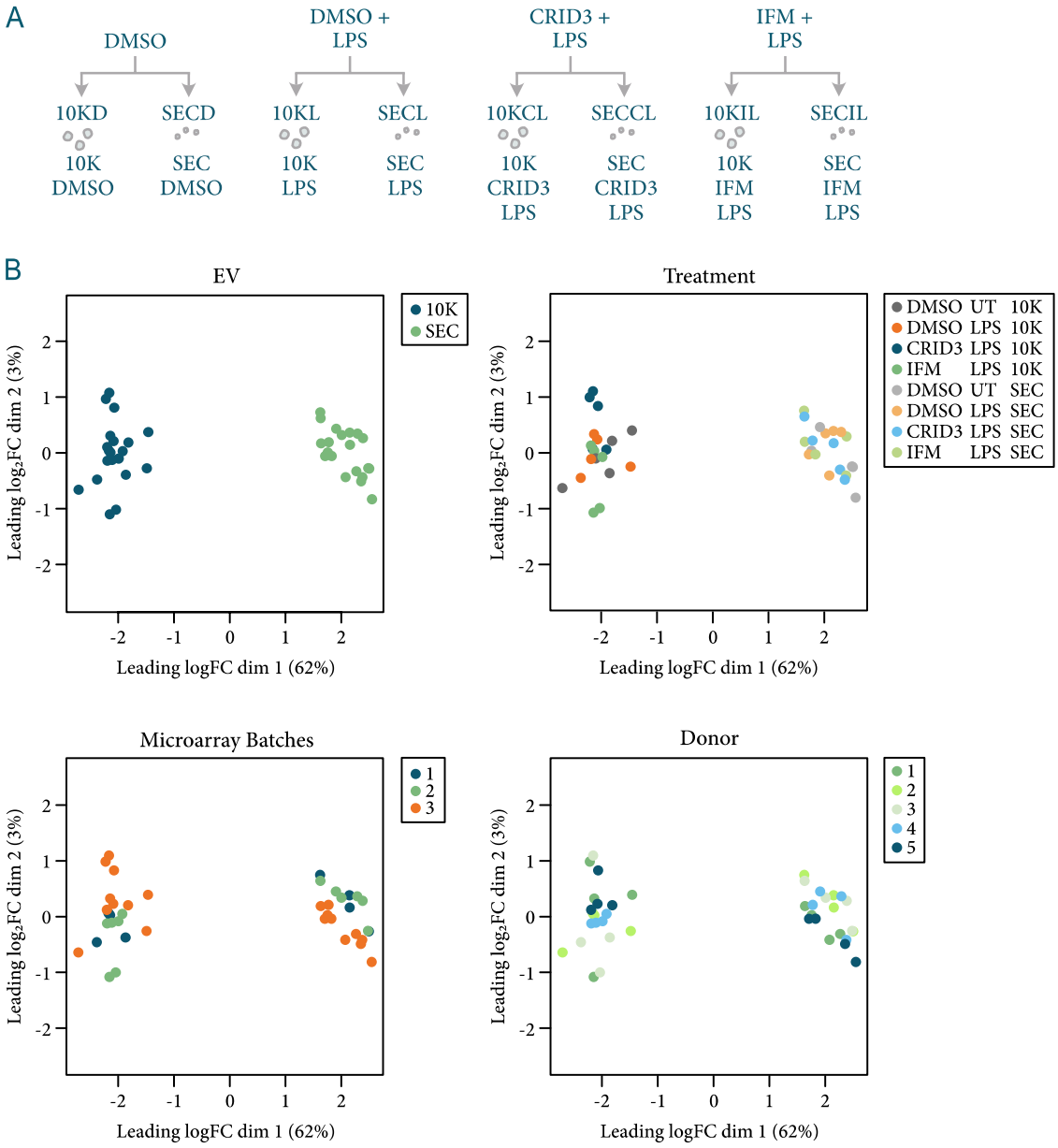

Figure 23: MDS plots of blood-derived EV microarray data after sample pre-processing. (A) Schematic of the experiment. EVs were isolated from control (DMSO only) samples, from LPS stimulated (DMSO + LPS) samples, from CRID3 + LPS stimulated samples, and from IFM + LPS stimulated samples. n = 5. (B) MDS plot for dimensions one and two, after filtering out unassigned and non-coding transcripts and removing microarray and donor batch effects. Samples are coloured according to vesicle type, treatment, microarray batches, and donor.

As was expected, the difference in EV type accounted for most of the sample differences. To investigate the treatment effect further, the data was split into the 10K and the SEC samples. 10K samples showed some clustering according to

treatment, especially in dimensions three and four (Figure 24B). Clustering of SEC samples by treatment could not be observed (Figure 24C).

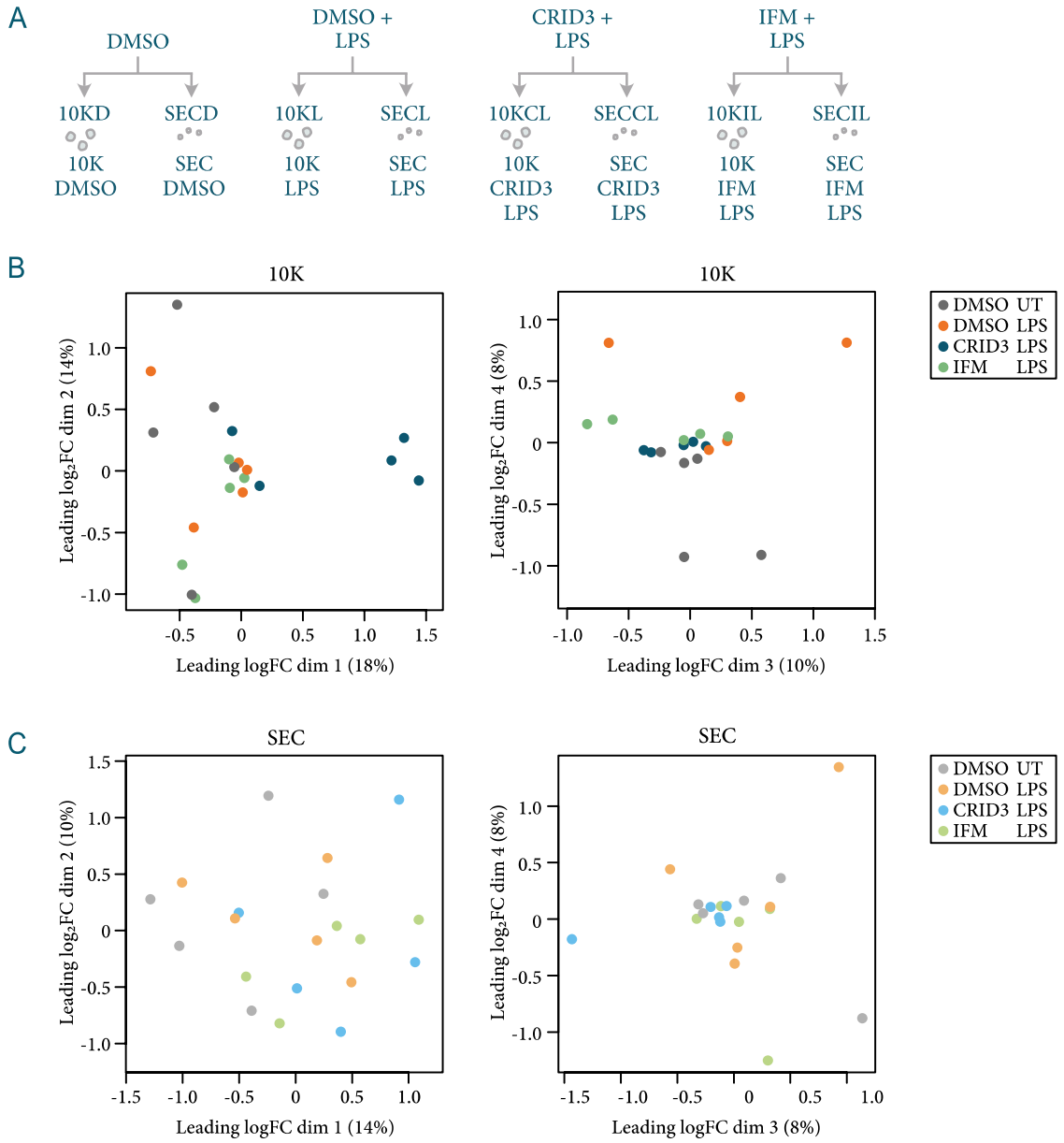

Figure 24: MDS plots of blood-derived 10K and SEC microarray data. (A) Schematic of the experiment. EVs were isolated from control (DMSO only) samples, from LPS stimulated (DMSO + LPS) samples, from CRID3 + LPS stimulated samples, and from IFM + LPS stimulated samples. n = 5. (B+C) MDS plots for dimensions one and two (left) and three and four (right) for 10K samples (B) and SEC samples (C) after filtering out unassigned and non-coding transcripts and removing microarray and donor batch effects. Samples are coloured according to treatment.

After sample pre-processing, linear modelling was performed. A design matrix was set up using the sample group (the combination of treatment and EV type),

the donor, and microarray batches as factors. The donor and microarray batches were included to account for the observed batch effects. Model contrasts were set up for pairwise comparisons between the different stimulations and respective untreated samples and between uninhibited LPS-stimulated samples and respective inhibited samples. Linear modelling was performed on RMA normalised values with the lmFit function, followed by the contrasts.fit function. The lmFit function averages the normalised log_2 expression values in the different groups according to the design matrix. The contrasts.fit function then considers the contrast information to calculate log_2FCs.

Moderated t-tests were performed using either eBayes or treat. Treat was used with a log_2FC threshold of 1.2. The decideTests function was used to determine the number of differentially abundant transcripts (Figure 25B). Since the abundance of RNAs was checked in vesicles and not cells, it cannot be said that transcripts are indeed differentially expressed by EV donor cells, nor can it be said that they are differentially expressed by EVs, as EVs do not actively express DNA to create RNA transcripts. Instead, rather than investigating DE genes, the relative abundance of transcripts in EVs was investigated.

The treat method is more stringent and, in this case, only one transcript was shown to be differentially abundant (in 10K EVs from CRID3 LPS stimulated cells, 10KCL, compared to 10K EVs from untreated cells, 10KD). The same comparison led to the identification of more genes when applying the eBayes method. Here, 139 transcripts with different abundance levels between 10KCL EVs and 10KD EVs could be identified. Comparing 10KL EVs to 10KD EVs, only eight transcripts with different abundance levels were identified, and comparing 10KIL EVs to 10KD EVs, seven transcripts with different abundance were found (Figure 25B).

We would have expected that inflammasome activation has the strongest effect on relative transcript abundance between conditions and thus to find most differently abundant transcripts between 10KL/SECL EVs and 10KD/SECD EVs, respectively. CRID3 and IFM block inflammasome activation. Thus, we expected EVs from these donor cells to be more similar to EVs from unstimulated donor

cells and a decrease in differently abundant transcripts. However, this is not the case for 10KCL EVs (Figure 25B), suggesting that CRID3 may have an even stronger effect on EV content than inflammasome activation.
SEC EVs barely showed any differently abundant transcripts (Figure 25B).

MD plots for 10K EVs from DMSO + LPS-, CRID3 + LPS-, and IFM + LPS-stimulated donor cells, each compared to 10K EVs from unstimulated donor cells were generated (Figure 25C). All eight differentially abundant transcripts identified when comparing 10KL to 10KD EVs are labelled. Six of these transcripts were also differentially abundant in 10KCL EVs compared to 10KD EVs (shown as labelled, intense blue and red differentially abundant transcripts). These include *SPP1*, *IL1B*, *VCAN*, *HM13;MCTS2*, *BAZ1B*, and *CHICH2*. Differentially abundant transcripts found between 10KCL and 10KD EVs that were not identified in 10KL vs 10KD EVs are shown in light blue and light red and were not labelled. Of the eight differentially abundant transcripts identified between 10KL and 10KD EVs, only two were also identified in 10KIL vs 10KD EVs—*SPP1* and *HM13;MCTS2*. They are shown in dark red and are labelled. Other differentially abundant transcripts in this comparison are shown in light blue (Figure 25C).

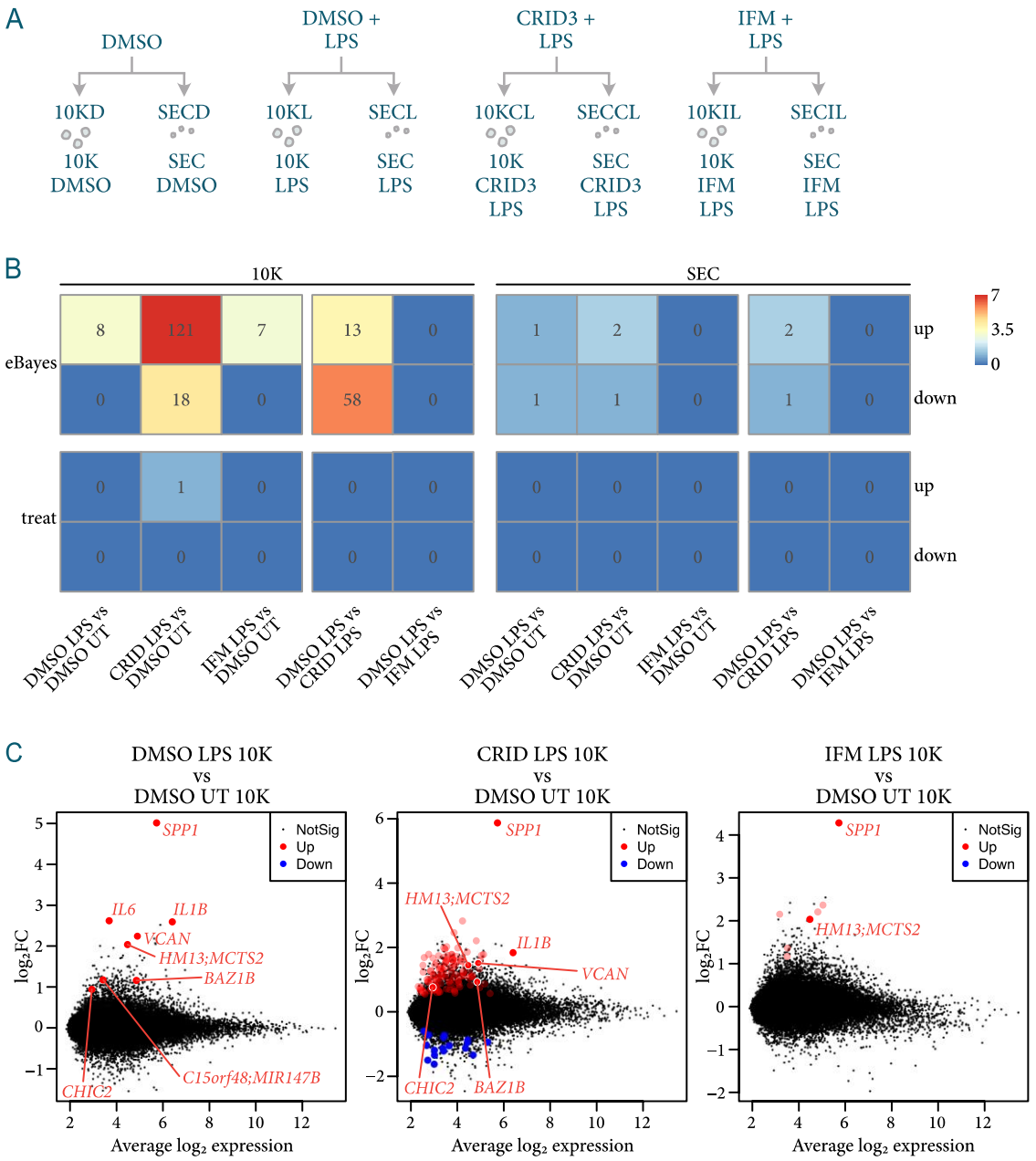

Figure 25: Differentially abundant transcripts. (A) Schematic of the experiment. EVs were isolated from control (DMSO only) samples, from LPS stimulated (DMSO + LPS) samples, from CRID3 + LPS stimulated samples, and from IFM + LPS stimulated samples. n = 5. (B) Significantly differentially abundant transcripts for each comparison are shown. Differentially abundant transcripts were determined either by applying the eBayes function or the treat function with a $\log_2$ fold change threshold of 1.2. The number of differentially abundant transcripts is represented by the colour ($\log_2$ of the number of differentially abundant transcripts + 1) and the actual number of differentially abundant transcripts found is indicated within each square. (B) Mean-difference plots showing transcripts with significantly higher abundance (up, red)- or lower abundance (down, blue) between 10KL and 10KD EVs (left), 10KCL and 10KD EVs (middle), and 10KIL and 10KD EVs (right), using the eBayes method.

Significantly differentially abundant transcripts between 10KL and 10KD EVs are highlighted in all three plots and labelled when (also) identified in the 10KL vs 10KD comparison. Differentially abundant transcripts not found in 10KL and 10KD EVs but only in 10KCL vs 10KD or 10KIL vs 10KD EVs are slightly transparent.

Expression plots for six of the differentially abundant transcripts between 10KL and 10KD EVs are shown (Figure 26). *SPP1* and *HM13;MCTS2* transcripts are more abundant in 10KL, 10KCL, and 10KIL EVs than in other EVs (Figure 26B), suggesting they depend on LPS stimulation, regardless of inflammasome activation, and are in general higher in 10K EVs than SEC EVs. *IL1B* and *VCAN* transcripts were significantly more abundant in 10KL and 10KCL EVs but not in 10KIL EVs (Figure 26C). This might suggest that either CRID3 inhibition did not work as well as IFM inhibition, especially as *VCAN* abundance in 10KCL EVs is slightly lower than in 10KL EVs, or it suggests that the transcripts are not only specific to inflammasome activation. *IL6* and *MIR147B* transcripts are significantly more abundant in 10KL EVs than in all other EVs (Figure 26D), implying that they might be inflammasome specific.

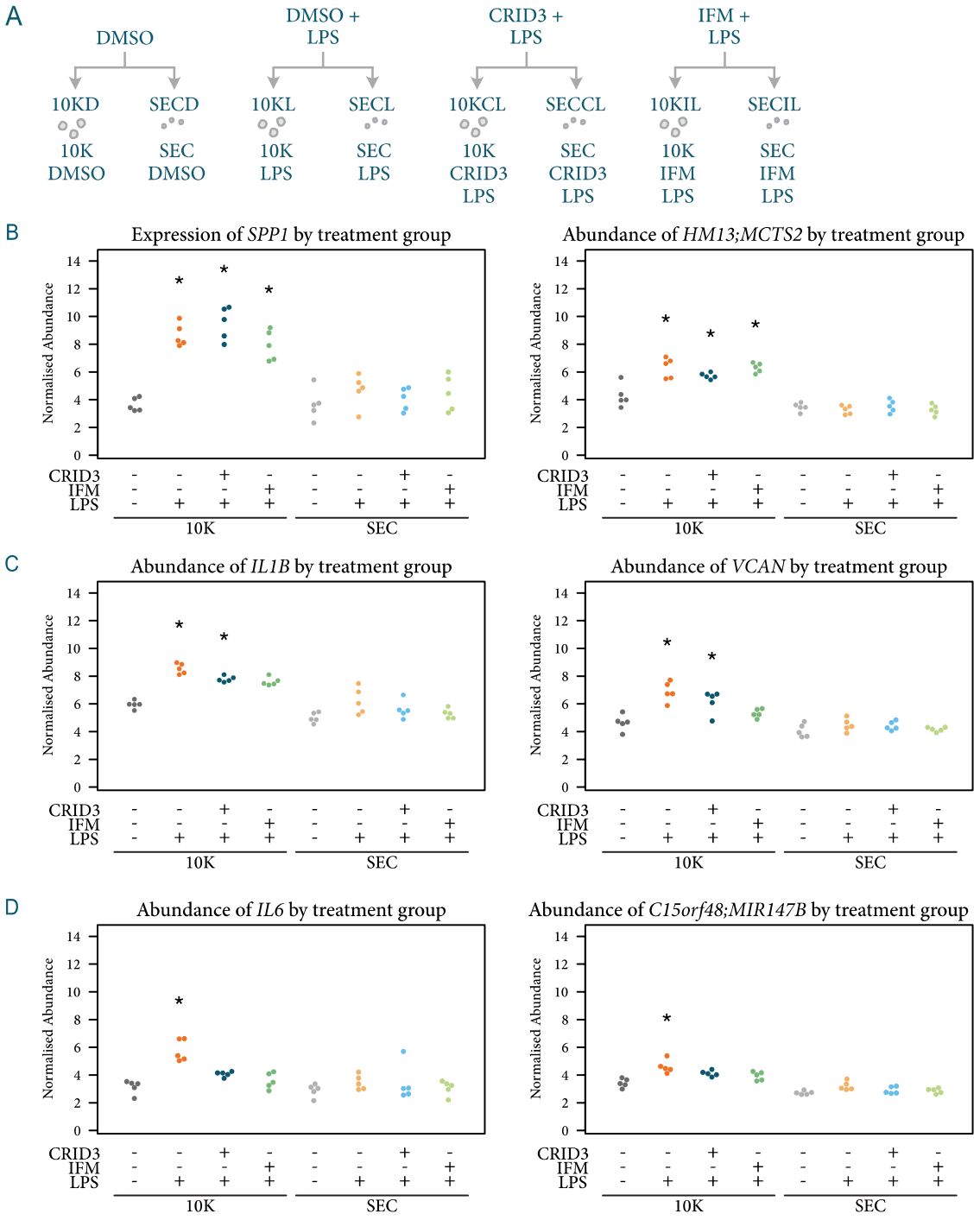

Figure 26: Examples of differentially abundant transcripts. (A) Schematic of the experiment. EVs were isolated from control (DMSO only) samples, from LPS stimulated (DMSO + LPS) samples, from CRID3 + LPS stimulated samples, and from IFM + LPS stimulated samples. n = 5. (B) Normalised Expression after batch correction of *SPP1* and *MCTS2* (B), *IL1B* and *VCAN* (C), and *IL6* and *MIR147B* (D) by treatment group. Asterisks indicate significantly different transcript abundances compared to relevant DMSO-only control, as determined by eBayes.

As mentioned previously, the Clariom D microarray technology had already been established in our lab and had been used with both THP-1 MΦ-derived EVs as well as with whole blood derived EVs. We thus had the opportunity to compare our newly generated data with previously obtained data to investigate how reliable EVs are in terms of repeatedly showing the same signature transcripts.

First, we looked at 10K EVs vs SEC EVs generally: Previous data showed that 10K EVs from THP-1 MΦs treated with various stimuli were enriched in mitochondrially encoded transcripts compared to SEC EVs (Budden *et al*, 2021), as were 10K EVs from unstimulated, whole blood samples (Budden *et al*, 2021), indicating that mitochondrial transcript are a hallmark of 10K EVs. To test if this could be replicated yet again, we checked for the presence of these transcripts in our 10K EVs from stimulated whole blood samples. Indeed, we could show an enrichment of the same mitochondrially encoded transcripts in all our 10K EVs compared to SEC EVs (Figure 27).

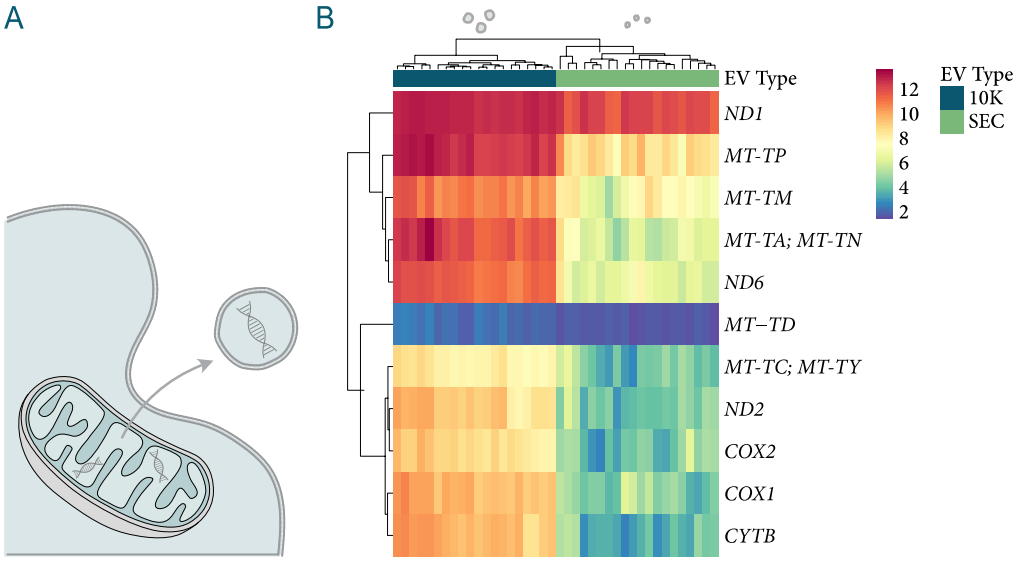

Figure 27: Presence of mitochondrially encoded transcripts in EVs. (A) The presence of mitochondrially encoded transcripts in 10K and SEC EVs across all treatments was investigated. n = 5. (B) Heat map showing normalised log_2 expression values of detected mitochondrially encoded transcripts for 10K (blue) and SEC (green) samples. Multiple transcripts per row indicate transcripts that could not be distinguished with the microarray probe set used. The scale shows the normalised log_2 expression values.

To further confirm the reproducibility of EV microarray experiments, we compared whole blood-derived inflammasome-elicited EVs with THP-1 MΦ-derived inflammasome-elicited EVs: Dr. Christina Budden has previously performed an experiment in which she treated THP-1 MΦs with LPS for 2 h followed by 90 min long nigericin treatment to activate the NLRP3 inflammasome. She then isolated 10K EVs and compared these inflammasome-elicited 10K EVs to control 10K EVs which were isolated from cells solely treated with LPS for 2 h. Instead of using the short-term LPS (2 h) plus nigericin (90 min) stimulation for inflammasome activation, inflammasome-elicited EVs from whole blood were isolated after long-term LPS stimulation (23 h). And instead of comparing them to EVs released after 2 h of LPS stimulation, they were compared to EVs released from DMSO treated whole blood. But while the stimuli appear different, in the end, in both comparisons, inflammasome-elicited 10K EVs were compared to control 10K EVs (Figure 28A).
Indeed, we could see a correlation between the data obtained from whole blood and the THP-1 MΦ data (Figure 28B). Considering that we used a complex biological matrix (whole blood) and compared that to cell culture data, that the inflammasome-elicited EVs in whole blood stem from several different cell types instead of just one, as is the case for THP-1 cell data, and that the inflammasome-activating stimuli were different, the fact that we see a correlation, although not a strong one, is promising. Together with the fact that 10K EVs consistently show an enrichment of mitochondrial transcripts, this shows that EVs indeed hold the potential to be used as biomarkers in the future and that microarray analysis of EV content is a reliable method to do so.

Having shown that the microarray technology allows the characterisation of EV transcript content and having identified some transcripts unique to inflammasome activated EVs (as opposed to LPS activation generally), the next step is to analyse samples from patients suffering from diseases driven by inflammasome activation. This will hopefully allow the confirmation and even further identification of transcripts unique to EVs released after inflammasome activation. Knowing those transcripts would allow the usage of EVs as biomarkers.

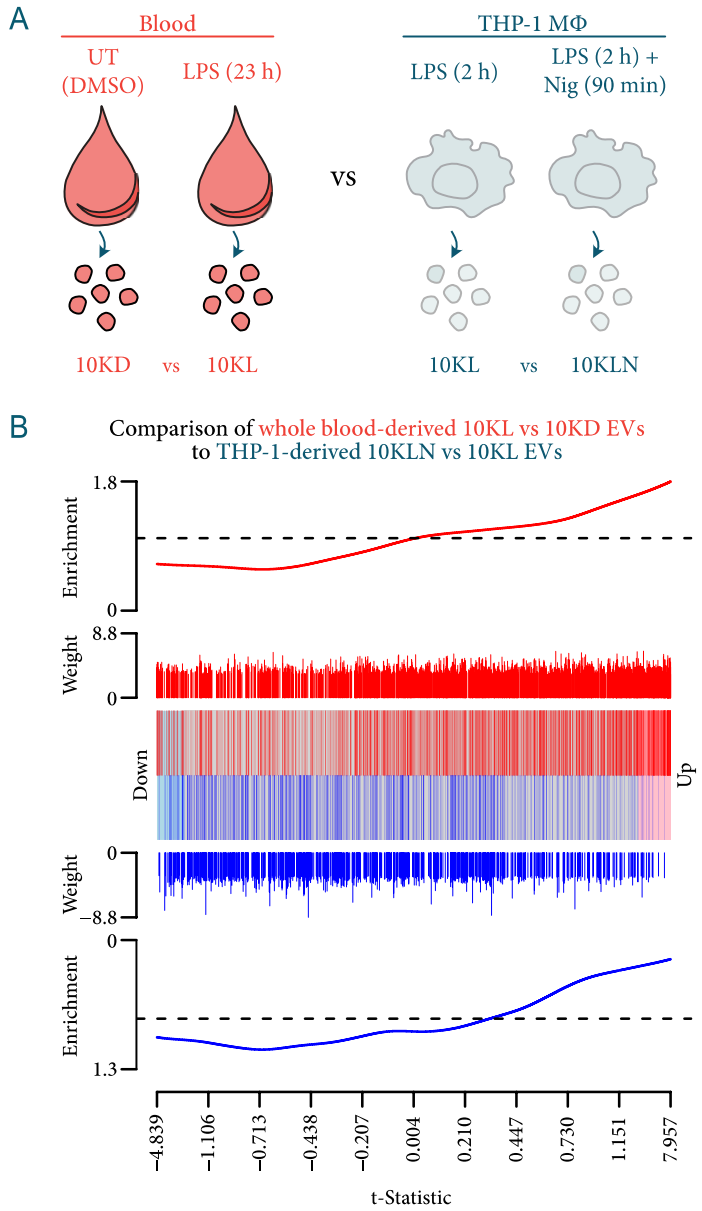

Figure 28: Comparison to previously generated cell line data. (A) Transcripts with higher or lower abundance between THP-1-derived inflammasome-elicited EVs (10KLN) vs control EVs (10KL) were compared to differentially abundant transcripts between whole blood-derived inflammasome-elicited EVs (10KL) vs control EVs (10KD). (B) Barcodeplot showing significantly higher (red vertical lines) or lower (blue vertical lines) abundant transcript from previous data (10KLN vs 10KL). Transcripts are ranked based on their t-statistic in the 10KL vs 10KD comparison. The relative enrichment of the two gene sets is depicted in the form of enrichment worms (the lines above and below the vertical bars). Enrichment worms were calculated to show how the previously identified differentially abundant transcripts are distributed in the current data.

3.2 Uptake Mechanism of Inflammasome-Elicited EVs

3.2.1 Visualisation of EV Uptake

In order to visualise and thus to study EV uptake, different methods of labelling EVs were investigated. Previously, EVs were labelled with CellTrace CFSE in our lab. For this, the standard EV isolation protocol was adapted to be able to include staining steps and remove free dye. To avoid a change of protocol, a different approach was tried: two different fluorescent proteins (EGFP and tdTomato) were coupled to a palmitoylation signal (EGFP-Palmi and tdTomato-Palmi respectively), allowing their recruitment to cell membranes (Figure 29A). Using lentiviral transduction, these constructs were then used to create THP-1 cells that stably express the desired constructs. Live-cell confocal microscopy was performed to confirm the successful generation of these cell lines (Figure 29B). Recruitment of the respective fluorescent protein to the cell membrane was successful for both EGFP-Palmi THP-1 cells and tdTomato-Palmi THP-1 cells (Figure 29B). Fixation of cells using 4% PFA for 10 min at room temperature led to a reduction in the signal, as shown for example for tdTomato-Palmi THP-1 cells (Figure 29C).

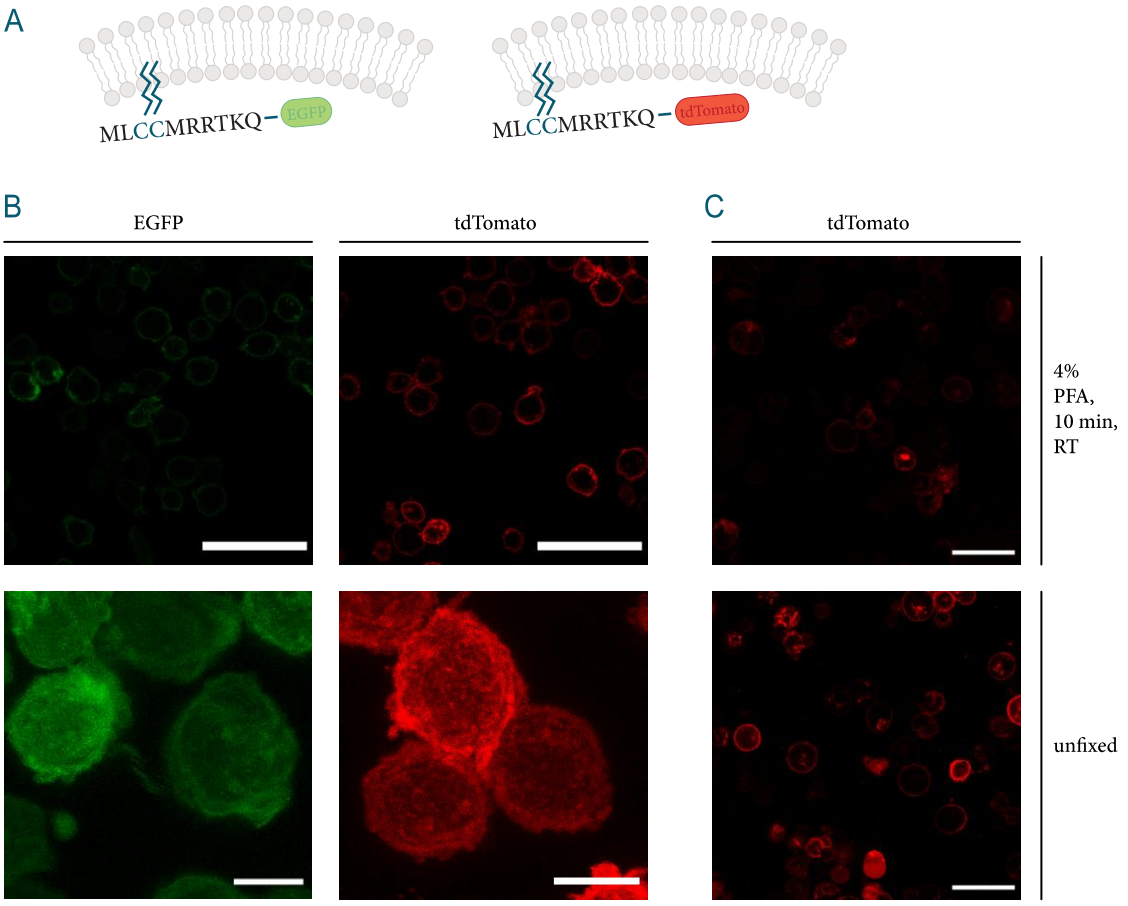

Figure 29: Generation of cell lines stably expressing fluorescent proteins targeted to cell membranes. (A) EGFP and tdTomato were fused to a palmitoylation signal that allows targeting to cell membranes. Using lentiviral transduction THP-1 cells that stably express these constructs were created (EGFP-Palmi THP-1 and tdTomato-Palmi THP-1). Technical replicates = 3, n = 1. (B) Live cell microscopy of undifferentiated THP-1 cells, stably expressing the above-described constructs (EGFP-Palmi THP-1 cells and tdTomato THP-1 cells). Maximum intensity z-projections. Scale bar top images: 50 μm; lower images: 10 μm. Representative images. (C) Effect of fixation on fluorescent proteins in THP-1 cells. tdTomato THP-1 cells were either fixed using 4 % PFA for 10 min at room temperature (upper image) or imaged without previous fixation (lower image). Scale bar: 50 μm. Representative images. (B+C) EGFP-Palmi THP-1 MΦs are shown in green, tdTomato-Palmi THP-1 MΦs are shown in red.

Next, EVs from EGFP-Palmi THP-1 MΦs were isolated as shown in Figure 8 and transferred to tdTomato-Palmi THP-1 MΦs (Figure 30A). After incubation of tdTomato-Palmi THP-1 MΦs with EGFP-Palmi THP-1 MΦ-derived EVs for 15 h, cells were fixed using 4 % PFA for 10 min at room temperature. In these experiments, only a very weak EV signal was observed in case of tdTomato-Palmi THP-1 MΦs treated with EGFP-Palmi THP-1 MΦ-derived 10K EVs and no

signal could be observed in case of tdTomato THP-1 MΦs treated with EGFP-Palmi THP-1 MΦ-derived SEC EVs (Figure 30B).

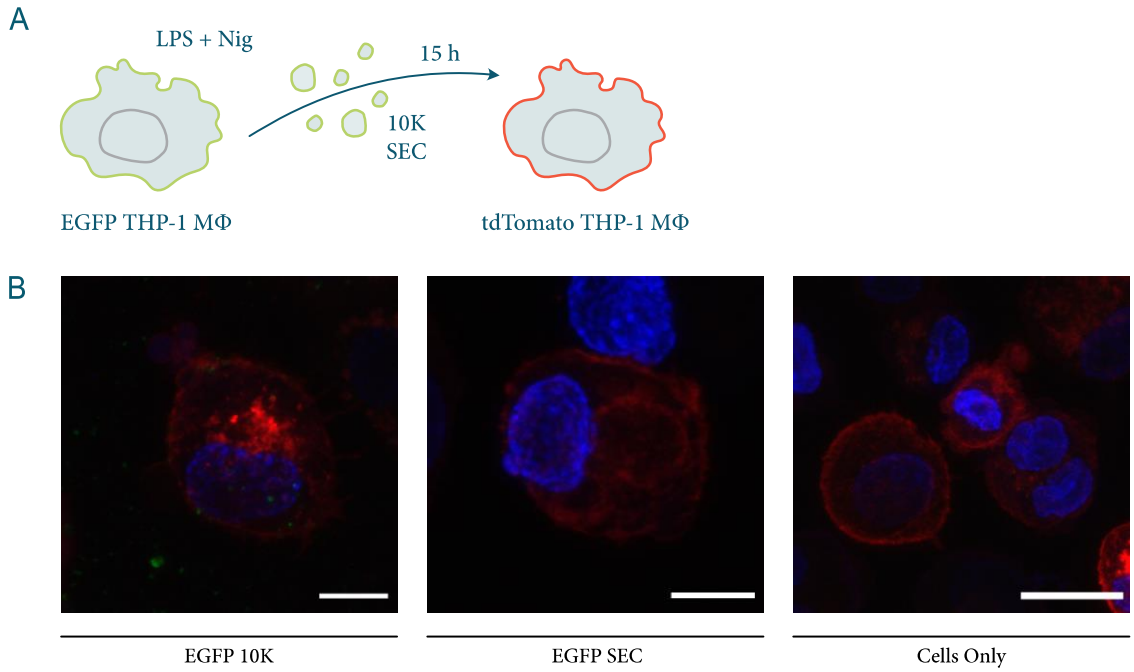

Figure 30: Transfer of EGFP-Palmi THP-1-derived EVs to tdTomato-Palmi THP-1 recipient cells. (A) Schematic representation of experimental plan. EVs were isolated from EGFP-Palmi THP-1 MΦs after inflammasome activation and incubated with recipient tdTomato-Palmi THP-1 MΦs. (E) tdTomato-Palmi THP-1 MΦs after incubation for 15 h with EGFP-Palmi THP-1 MΦ-derived EVs from inflammasome-activated cells. Scale bar: 10 μm. EGFP-Palmi THP-1 MΦ-derived EVs are shown in green, tdTomato-Palmi THP-1 MΦs are shown in red. Nuclei are shown in blue. Representative images of three technical replicates, n = 1.

One idea was that fixation affects the strength of the signal. As can be seen in Figure 29C, this is indeed the case. However, in unfixed samples barely any 10K EVs and no SEC EVs could be observed either (data not shown). Another idea was that the expressed fluorescent proteins that are targeted to all membranes within the cell might affect vesicle production leading to a reduction of overall vesicle release. To ensure that expression of the constructs did not affect EV secretion after inflammasome activation and thus led to a decrease in the number or the size of EVs released, NanoSight measurements of EVs released from EGFP-Palmi and tdTomato-Palmi THP-1 MΦs were performed (Figure 31). These measurements were compared to wild type THP-1 MΦ-derived EVs. The concentration of particles detected (particles/mL) and size distribution of the

detected particles were comparable between wild type, EGFP-Palmi and tdTomato-Palmi THP-1 MΦ-derived EVs (Figure 31B and C). The overall particle number released by EGFP-Palmi and tdTomato-Palmi THP-1 MΦs was even slightly higher than for wild type THP-1 MΦs (Figure 31D).

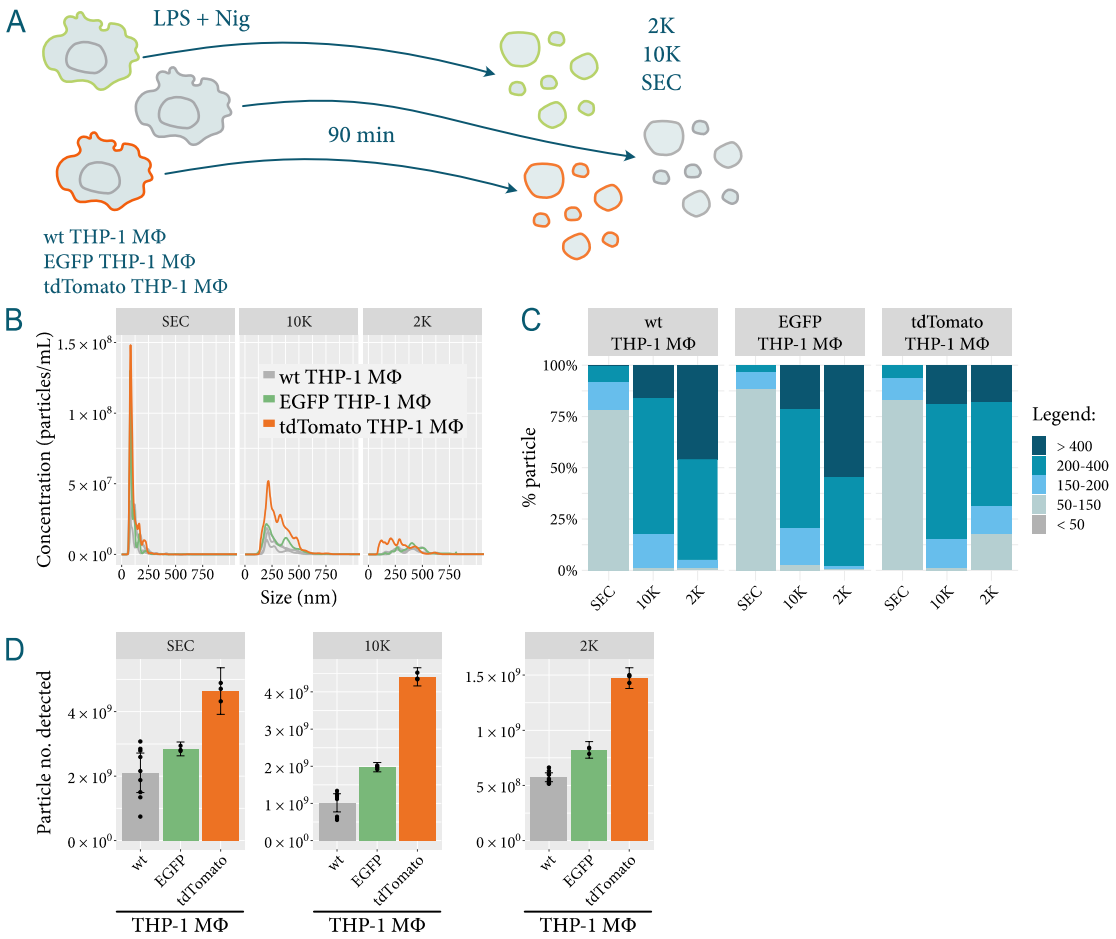

Figure 31: Characterisation of EVs released by EGFP-Palmi and tdTomato-Palmi THP-1 MΦs. (A) Schematic representation of the experimental plan. EVs were isolated from wt, EGFP-Palmi, or tdTomato-Palmi THP-1 MΦs after inflammasome activation with LPS + nigericin and characterised using NanoSight. (B) Concentration (particles/mL) for the three EV fractions (2K, 10K, SEC) for EGFP-Palmi and tdTomato-Palmi THP-1 MΦs compared to wild type (wt) THP-1 MΦs. Means of technical replicates (of one representative experimental run for wt THP-1 MΦs) are shown. (C) (Representative [for wt THP-1 MΦs]) Size distribution of particles released for the three EV fractions (2K, 10K, SEC) for EGFP-Palmi and tdTomato-Palmi THP-1 MΦs compared to wt THP-1 MΦs are shown. Means of technical replicates are shown. (D) Total number of particles detected for EGFP-Palmi and tdTomato-Palmi THP-1 MΦs compared to wt THP-1 MΦs. Mean ± SD. All technical replicates of all experimental runs are shown. n = 1 for EGFP-Palmi and tdTomato-Palmi THP-1 MΦs; n = 3 for wt THP-1 MΦs.

As EVs could not be observed without fixation nor could a reduced number of inflammasome-elicited EVs be observed, it had to be concluded that the technique was unsuitable for the application. Probably not enough fluorescent protein is expressed by the cells or not enough fluorescent protein is loaded into EVs, resulting in the signal being too weak. Thus, we decided to go back to the visualisation of EVs using dyes—even if that meant having to change the EV isolation protocol in parts.

Previously, Dr. Christina Budden had established CFSE staining to visualise EVs. In short, PMA-differentiated THP-1 MΦs were stimulated with LPS and nigericin. Supernatant was collected, centrifuged at 340 x g and 2,000 x g to remove cells and 2K EVs respectively, and then centrifuged at 10,000 x g to pellet the 10K fraction. 10K EVs were then stained with 20 μM CFSE for 30 min. After incubation, unbound dye was removed through centrifugation at 10,000 x g. To stain SEC EVs, 10K supernatant was spun at 100,000 x g to pellet SEC EVs. SEC EVs were then stained with 20 μM CFSE for 30 min. After incubation, unbound dye was removed through SEC. Stained EVs were pelleted through centrifugation at 100,000 x g.
I employed this staining method to stain 10K and SEC EVs isolated from LPS and nigericin stimulated THP-1 MΦs. These EVs were then transferred to THP-1 MΦs as well as to the epithelial cells A549 and BEAS-2B (Figure 32A). While staining of 10K EVs with CFSE worked well (Figure 32B), staining SEC EVs with CFSE did not work in my hands (Figure 32B).

Additionally, I wanted to test different methods to quantify EV uptake in an unbiased manner that would work for different cell lines/types and could differentiate between EVs just bound to the cell membrane versus those that were actually taken up by cells. I set out to achieve this using a combination of Fiji/ImageJ, the machine learning software ilastik, and the Cell Profiler software. I tested three different quantification methods that all differentiated between 10K EVs found close to the centre of the cell (Centre EVs) and those closer to the cell membrane and thus not necessarily taken up by the cell (Peripheral EVs) (Figure

32C–E). The first quantification method divided the number of EVs per image by the number of cells present in the given image, giving an average number of EVs per recipient cell (Figure 32C). A second approach was to identify recipient cells and then count the number of EVs for every recipient cell individually (Figure 32D). Finally, EV uptake was quantified by determining the overall EV fluorescence and dividing this number by the number of recipient cells counted; this gives the average fluorescence per cell (Figure 32E). All three methods lead to roughly the same results and thus could all be used in future analyses.

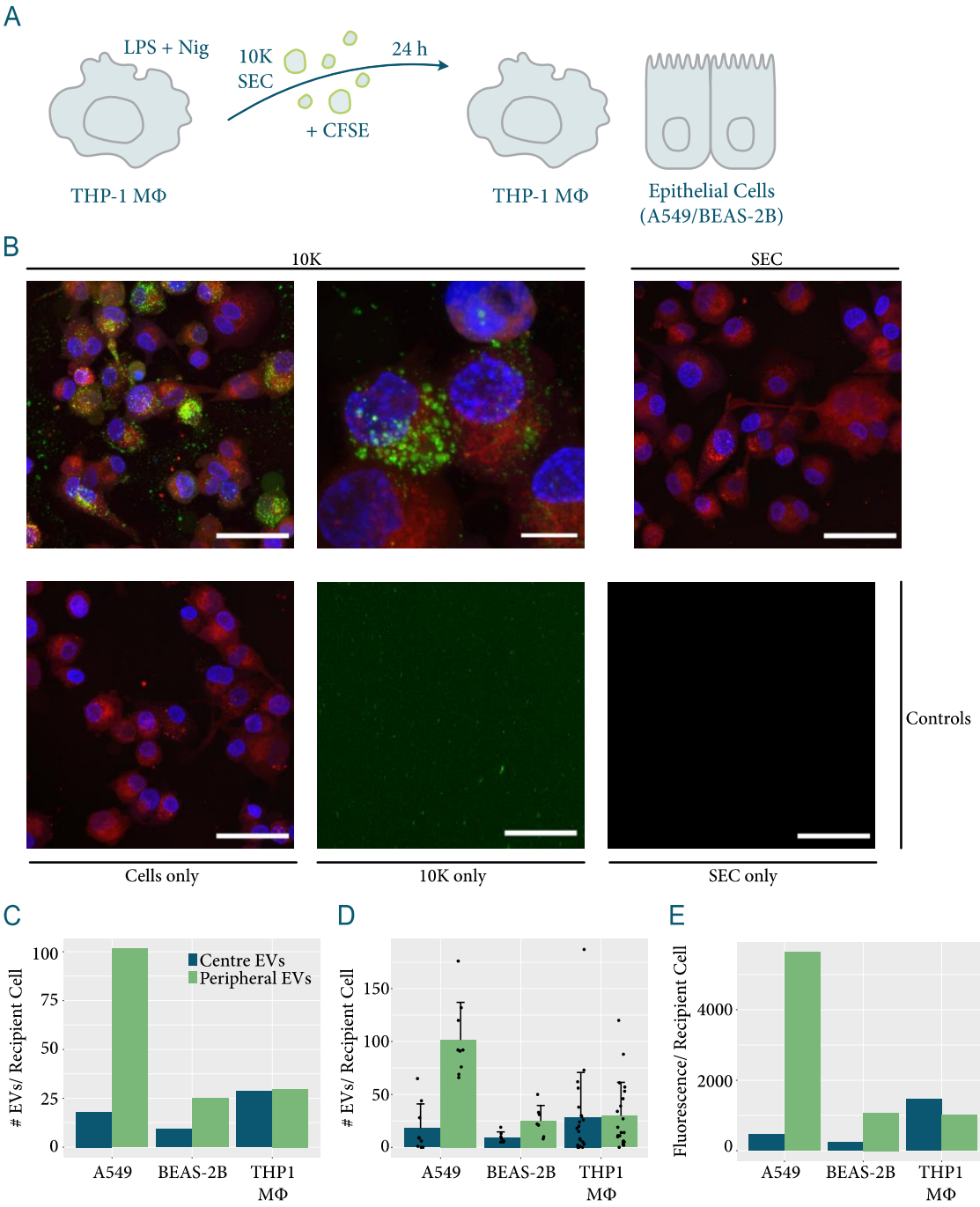

Figure 32: Characterisation of EV uptake using CFSE. (A) Schematic representation of the experimental plan. EVs were isolated from inflammasome-activated THP-1 MΦs, stained with CFSE, and incubated for 24 h with recipient THP-1 MΦs or epithelial cells (A549 and BEAS-2B cells) stained with Cell Tracer Far Red. Nuclei were stained with DAPI. n = 1. (B) Microscopy images showing EVs taken up by THP-1 MΦs. Recipient cells are shown in red, EVs in green, and nuclei in blue. Representative images of three technical replicates. Maximum intensity z-projections. Scale bars top row (from left to right): 50 μm, 10 μm, 50 μm. Scale bars bottom row: 50 μm. (C–E) Different ways of quantifying 10K EV uptake shown for three different recipient cells (THP-1 MΦs, A549 cells, and

BEAS-2B cells). (C) Average number of EVs per recipient cell. (D) Number of EVs per recipient cell with mean + SD. (E) Fluorescence per recipient cell (arbitrary units).

Since the CFSE staining did not work for the SEC fraction (Figure 32B), a different dye was tried. R18 is a self-quenching dye that is commonly used to investigate virus uptake. Since SEC EVs are about the same size as viruses, the dye has been found to be useful for EVs as well (Parolini *et al*, 2009; Montecalvo *et al*, 2012). THP-1 MΦs were stimulated with LPS and nigericin to activate the NLRP3 inflammasome and EVs were isolated. The staining protocol described above was used but instead of labelling EVs with CFSE, EVs were stained with R18. Stained EVs were then transferred to A549 or BEAS-2B recipient cells and incubated for 15 h (Figure 33A). Results are shown in Figure 33B. Both 10K and SEC EV uptake could be demonstrated. As expected, no signal was detected in cells only controls (Figure 33B). The SEC EV only control shows that the R18 dye self-quenches when used on these small EVs. This was expected, as SEC EVs are comparable in size to viruses. On the other hand, the 10K EV only control shows a clear signal, indicating that 10K vesicles are big enough that the dye, at the used concentration, can no longer self-quench (Figure 33B). Nevertheless, it is still suitable to study EV uptake.

As was shown above for the CFSE staining, EV uptake can be quantified. While it was possible to count the number of vesicles and relate this to the individual recipient cells in the CFSE staining experiments, this is not possible for the R18 staining due to its nature: it is especially useful to study membrane fusion as, at least in case of the SEC EVs, it only fluoresces when diluted. For example, this is the case when EVs fuse with the cell membrane or any other membrane within the cell. While this gives a strong signal, it no longer allows to enumerate EVs. Thus, as a measure of EV uptake, the overall fluorescence was quantified and related to the number of recipient cells (Figure 33C).

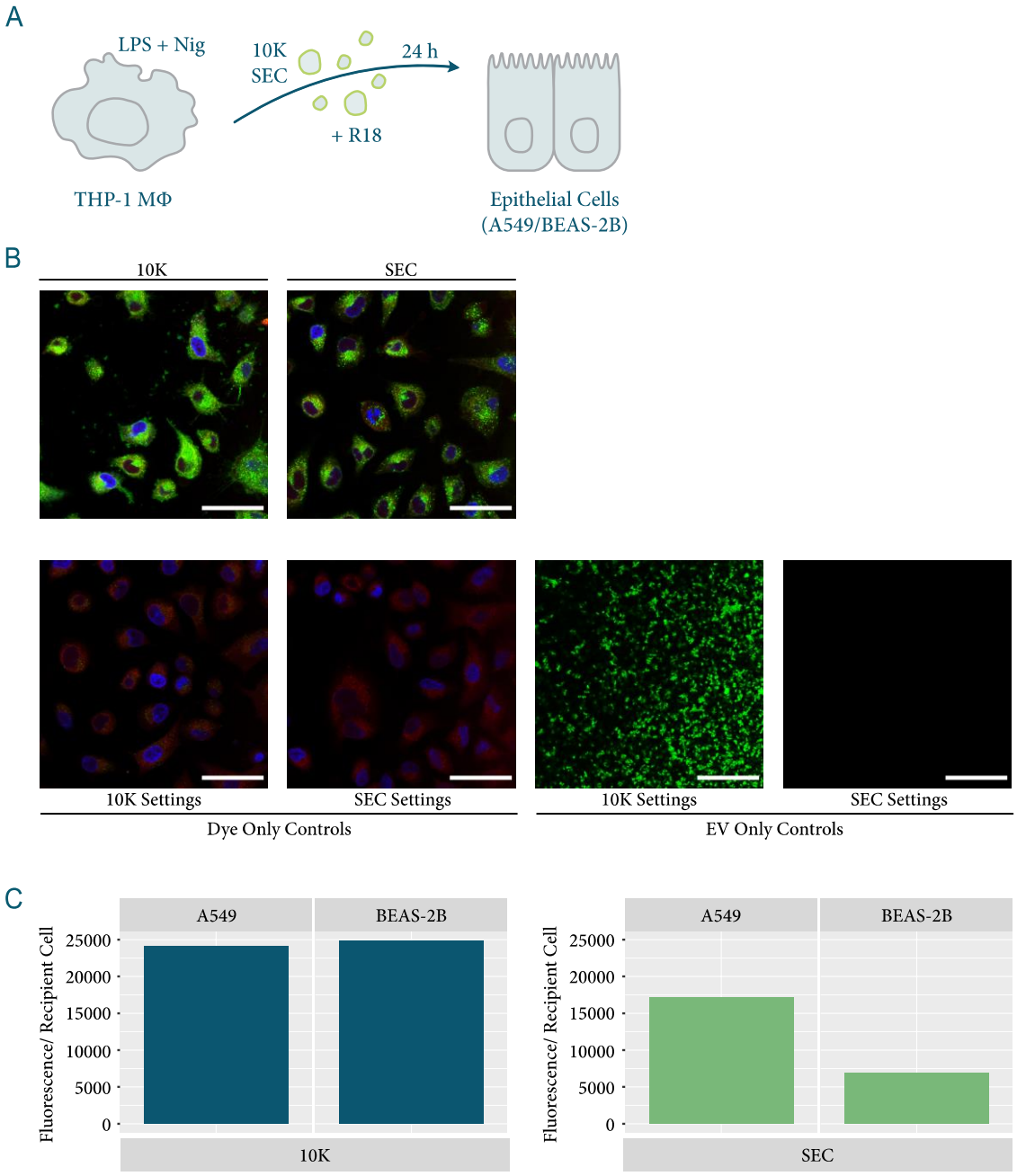

Figure 33: Characterisation of EV uptake using R18. (A) Schematic representation of the experimental plan. EVs were isolated from THP-1 MΦs, stained with R18 and incubated for 24 h with recipient epithelial cells (A549 or BEAS-2B cells) stained with Cell Tracer Far Red. Nuclei were stained with Hoechst 34580. n = 1. (B) Microscopy images showing EV uptake by A549 cells. Recipient cells are shown in red, EVs in green, and nuclei in blue. Representative Images of three technical replicates. Scale bars: 50 μm. (C) Quantification of EV uptake shown for A549 and BEAS-2B cells. Fluorescence per recipient cell (arbitrary units).

3.2.2 Uptake Mechanism

After establishing a way of visualising EVs in microscopy experiments, EV uptake was studied in a time-dependent manner and for different recipient cells.

We wanted to gain an understanding of EV uptake in different cell types to understand which cells might possibly interact with inflammasome-elicited EVs *in vivo*. To do so, in addition to using THP-1 MΦs, we made use of the two human lung cell lines A549 and BEAS-2B.

The A549 cell line is derived from a lung tumour explant of a 58-year-old male (Lieber *et al*, 1976) and is similar to alveolar epithelial cells (AEC)2 cells in its characteristics. Together with AEC1 cells, AEC2 cells make up the alveolar epithelium. While the flat AEC1 cells are involved in the gas exchange between the alveoli and the blood, the cuboidal AEC2 cells are responsible for the production and secretion of surfactant. AEC2 cells further act as progenitor cells for AEC1 cells (Hiemstra *et al*, 2018). A549 cells possess lamellar bodies and microvilli, they express cystic fibrosis transmembrane conductance regulator (CFTR), surfactant protein(SP)-A, SP-C, SP-D, mucin(MUC)1 and several other receptors common in AEC2 cells. They synthesise lecithin and high levels of unsaturated fatty acids (Bhowmick & Gappa-Fahlenkamp, 2016). These cells can be cultured in monolayers, both anchored and suspended, at air liquid interfaces and in 3D culture systems (Bhowmick & Gappa-Fahlenkamp, 2016). For simplicity, A549 cells were grown in monolayers in this study. A549 cells are commonly used as a model for alveolar epithelial cells.

In contrast to the alveolar epithelium, the airway epithelium consists of more than just two cell types, including goblet cells, ciliated cells, non-ciliate club cells, neuro-endocrine cells, and basal cells. Basal cells are progenitor cells for various cell types of the airway epithelium (Hiemstra *et al*, 2018). A representative for airway epithelial cells is the BEAS-2B cell line. BEAS-2B cells are immortalised human bronchial epithelial cells, generated with the SV40 virus from a cancer-

free individual (Reddel *et al*, 1988). While they resemble both airway and bronchial epithelial cells, they do not differentiate nor do they form a strong barrier (Stewart *et al*, 2012; Bhowmick & Gappa-Fahlenkamp, 2016). BEAS-2B cells express club cell secretory protein and produce mucin only when grown on collagen (Bhowmick & Gappa-Fahlenkamp, 2016). They can be grown in monolayers, both submerged and at air liquid interface (Bhowmick & Gappa-Fahlenkamp, 2016).

A first experiment was conducted to determine if, in general, a longer (48 h) or a shorter (24 h) timepoint would be needed. EVs were isolated from inflammasome-activated THP-1 MΦs, stained with CFSE and incubated with A549 cells, BEAS-2B cells, and THP-1 MΦs for 24 h and 48 h (Figure 34A). While 10K EVs were heavily taken up by THP-1 cells, A549 cells primarily bound EVs on their membrane and only internalised a few (Figure 34B). BEAS-2B cells also bound EVs on their membrane, but to a lesser extent, and only took up a few EVs (Figure 34B). Representative images are shown for the 24 h incubation timepoint (Figure 34B). Images looked similar after 48 h of incubation (data not shown). The above-described pipeline, employing Fiji/ImageJ, Ilastik and Cell Profiler, was used to calculate the average number of EVs per recipient cell (Figure 34C). Overall, it can be concluded that, for the longer time point, EV numbers were already decreasing, particularly for A549 cells, suggesting that an earlier time point should be the focus of this study.

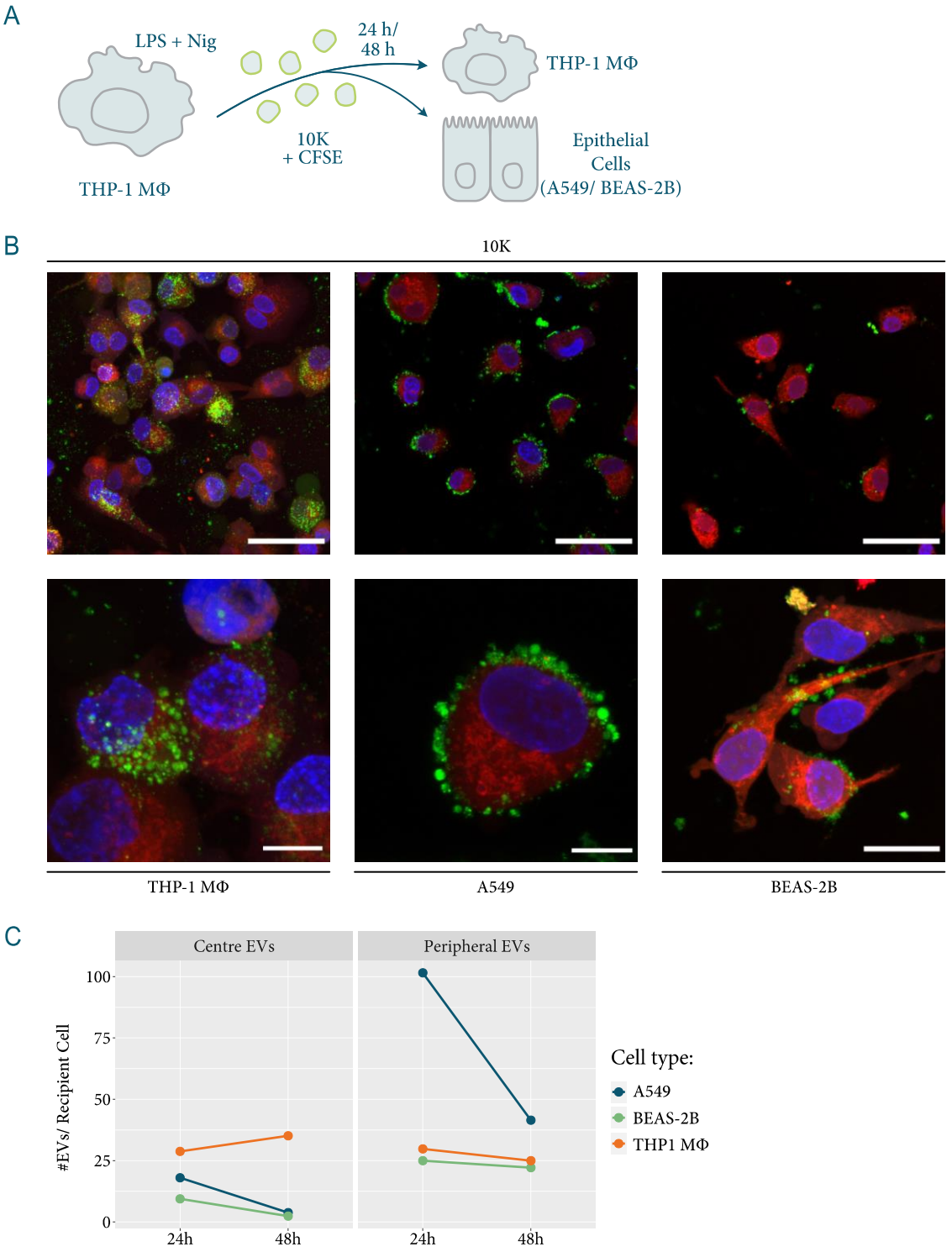

Figure 34: Uptake of EVs by A549, BEAS-2B, and THP-1 MΦs in a time-dependent manner. (A) Schematic representation of the experimental plan. EVs were isolated from inflammasome-activated THP-1 MΦs, stained with CFSE, and incubated for 24 h and 48 h with recipient A549, BEAS-2B, and THP-1 MΦs stained with Cell Tracer Far Red. Nuclei were stained with DAPI. n = 1. (B) EV uptake by A549, BEAS-2B, and THP-1 MΦs after 24 h. Recipient cells are shown

in red, EVs in green, and nuclei in blue. Maximum intensity z-projections. Scale bars top row: 10 μm, bottom row: 50 μm. Representative images of three technical replicates. (C) Quantification of EV uptake. Average number of EVs per recipient cell is shown for centre EVs and peripheral EVs after 24 h and 48 h incubation with A549 cells, BEAS-2B cells, and THP-1 MΦs.

The results shown in Figure 34 indicate that interaction between EVs and recipient cells can be quite diverse: while THP-1 MΦs readily take up many EVs, A549 cells appear to mainly just bind EVs and BEAS-2B cells generally do not interact much with EVs. Regardless of whether cells take up or bind EVs, both forms are likely to influence the recipient cell: in case of EV uptake, signalling molecules and interfering RNAs might directly be delivered to the cell's cytosol. In case of EV binding to the cell's membrane, signalling probably plays a more significant role—surface EV proteins could bind membrane receptors and initiate signalling cascades. It is of interest that even though both A549 and BEAS-2B cells are epithelial cell lines, they show such distinctly different uptake behaviour. This could be an artefact of immortalising cells or be caused by the cancerous phenotype of A549 cells; however, it could also be caused by the subtle difference between alveolar and bronchial epithelial cells.

Having studied EV uptake at a 24 h and a 48 h timepoint, EV uptake at shorter timepoints was investigated. THP-1 MΦ-derived EVs were isolated after inflammasome activation and stained with CFSE or R18. CFSE was chosen for 10K EVs, as it allowed better quantification of 10K EVs than R18 (Figure 32, Figure 33). R18 was chosen for SEC EVs as CFSE staining of SEC EVs did not work (Figure 32) and R18 resulted in a strong, clear signal (Figure 33). Stained EVs were transferred to THP-1 MΦs (Figure 35), A549 cells (Figure 36), and BEAS-2B cells (Figure 37) and incubated for 1 h, 3 h, 7 h, 15 h, or 24 h.

The above-described pipeline for EV uptake quantification relied on recipient cell staining with Cell Tracer Far Red. As the following experiments were quite labour intensive and as I only aimed for a broad overview of changes in EV uptake, like overall uptake trends, I opted for a simpler EV quantification method that would eliminate too many washing and staining steps and keep experiments as simple as possible. Thus, recipient cells were no longer stained with Cell Tracer Far Red.

Instead, cell numbers were determined through counting stained cell nuclei. As only the CFSE staining allows EV counting, the overall EV fluorescence instead of EV number was used for uptake quantification and then related to the recipient cell number, giving the average fluorescence per recipient cell (Figure 35C, Figure 36C, Figure 37C).

Uptake of 10K EVs by THP-1 MΦs was observed after 1–3 h and from then on increased until the highest levels were reached after about 15 h (Figure 35B). SEC EV uptake by THP-1 MΦs was first observed after 7 h and then increased over time (Figure 35B). The same trend was observed for A549 cells (Figure 36). In case of BEAS-2B cells, 10K EV uptake was observed after 1 h, but then remained relatively stable (Figure 37), instead of further increasing and then decreasing, as observed in case of THP-1 MΦs and A549 cells. SEC uptake by BEAS-2B cells was again similar to SEC uptake of THP-1 MΦs and A549 cells, with uptake starting after around 7 h and increasing over time (Figure 37).

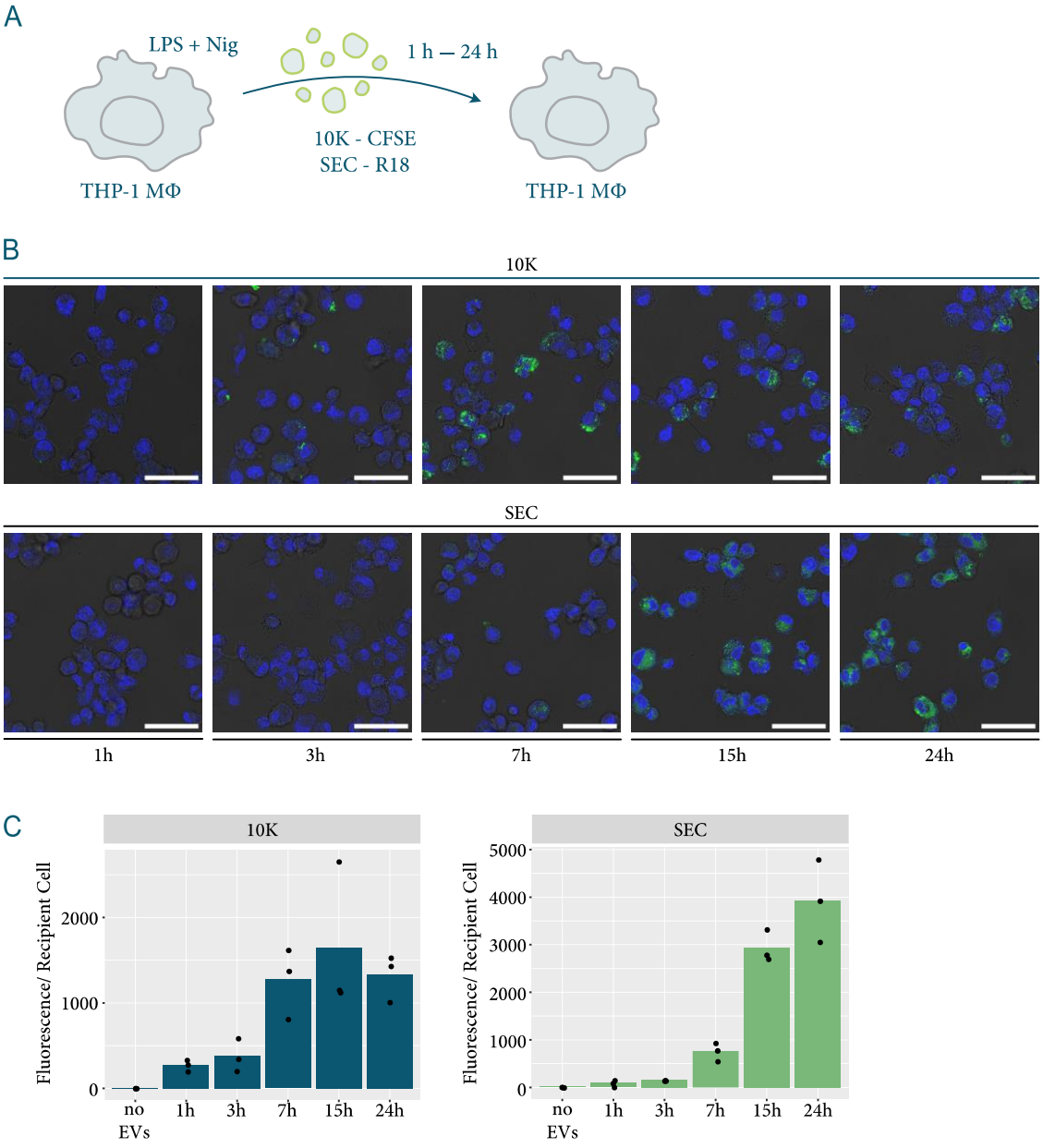

Figure 35: Uptake of EVs by THP-1 MΦs in a time-dependent manner. (A) Schematic representation of the experimental plan. EVs were isolated from THP-1 MΦs after inflammasome activation, stained with CFSE (10K) or R18 (SEC), and incubated with recipient THP-1 MΦs for 1 h, 3 h, 7 h, 15 h, and 24 h. Nuclei were stained with DRAQ5. (B) Uptake of 10K (upper row) and SEC (lower row) EVs by THP-1 MΦs over 24 h. Nuclei are shown in blue, EVs in green. Scale bars: 50 µm. Representative images. (C) Fluorescence per recipient cell for one representative experimental run showing all technical replicates. (B+C) Trend was the same across all experimental runs. Technical replicates = 3. n = 3.

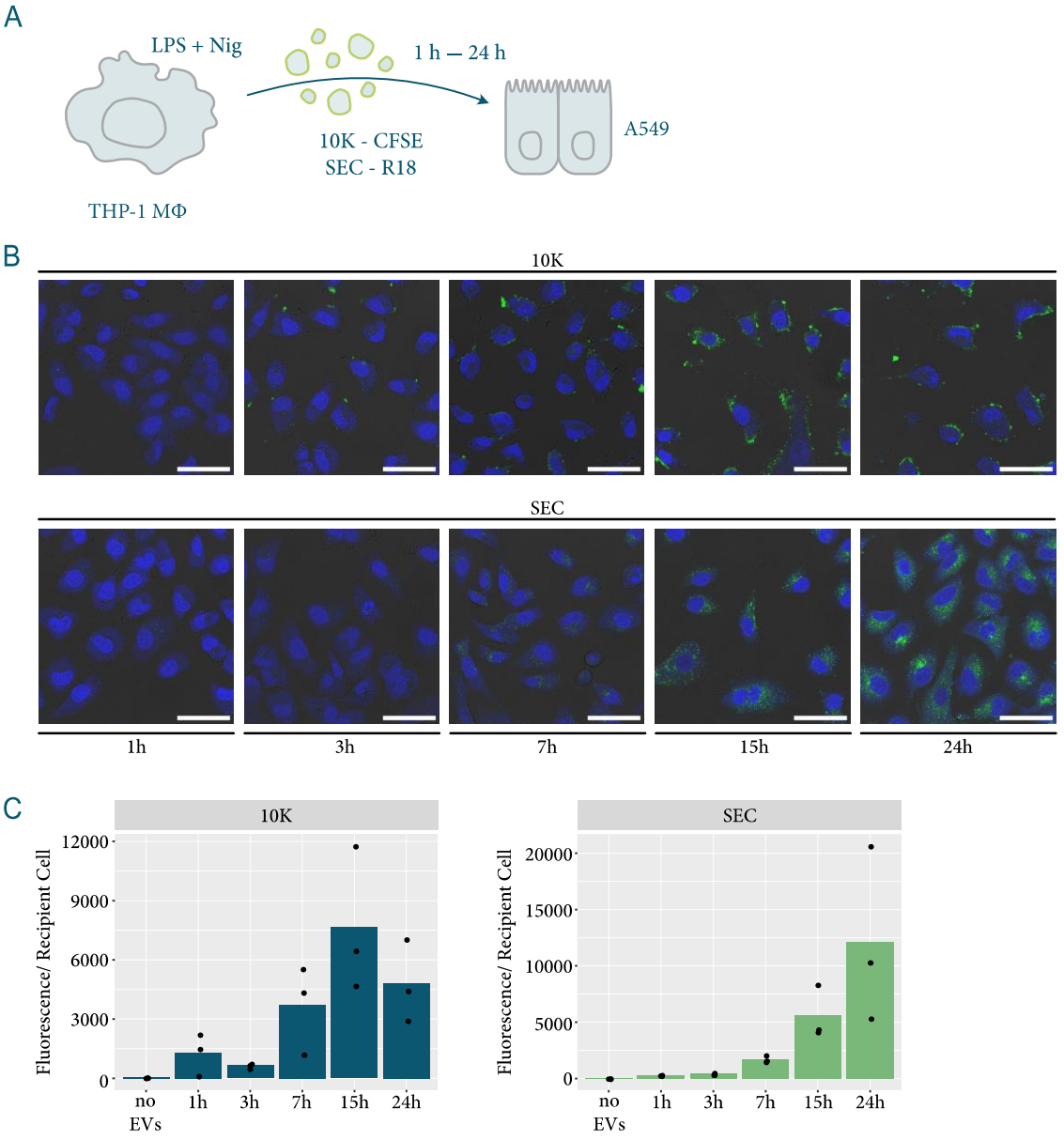

Figure 36: Uptake of EVs by A549 cells in a time-dependent manner. (A) Schematic representation of the experimental plan. EVs were isolated from THP-1 MΦs after inflammasome activation, stained with CFSE (10K) or R18 (SEC), and incubated with recipient A549 cells for 1 h, 3 h, 7 h, 15 h, and 24 h. Nuclei were stained with DRAQ5. (B) Uptake of 10K (upper row) and SEC (lower row) EVs by A549 cells over 24 h. Nuclei are shown in blue, EVs in green. Scale bars: 50 μm. Representative images. (C) Fluorescence per recipient cell for one representative experimental run showing all technical replicates. (B+C) Trend was the same across all experimental runs. Technical replicates = 3. n = 3.

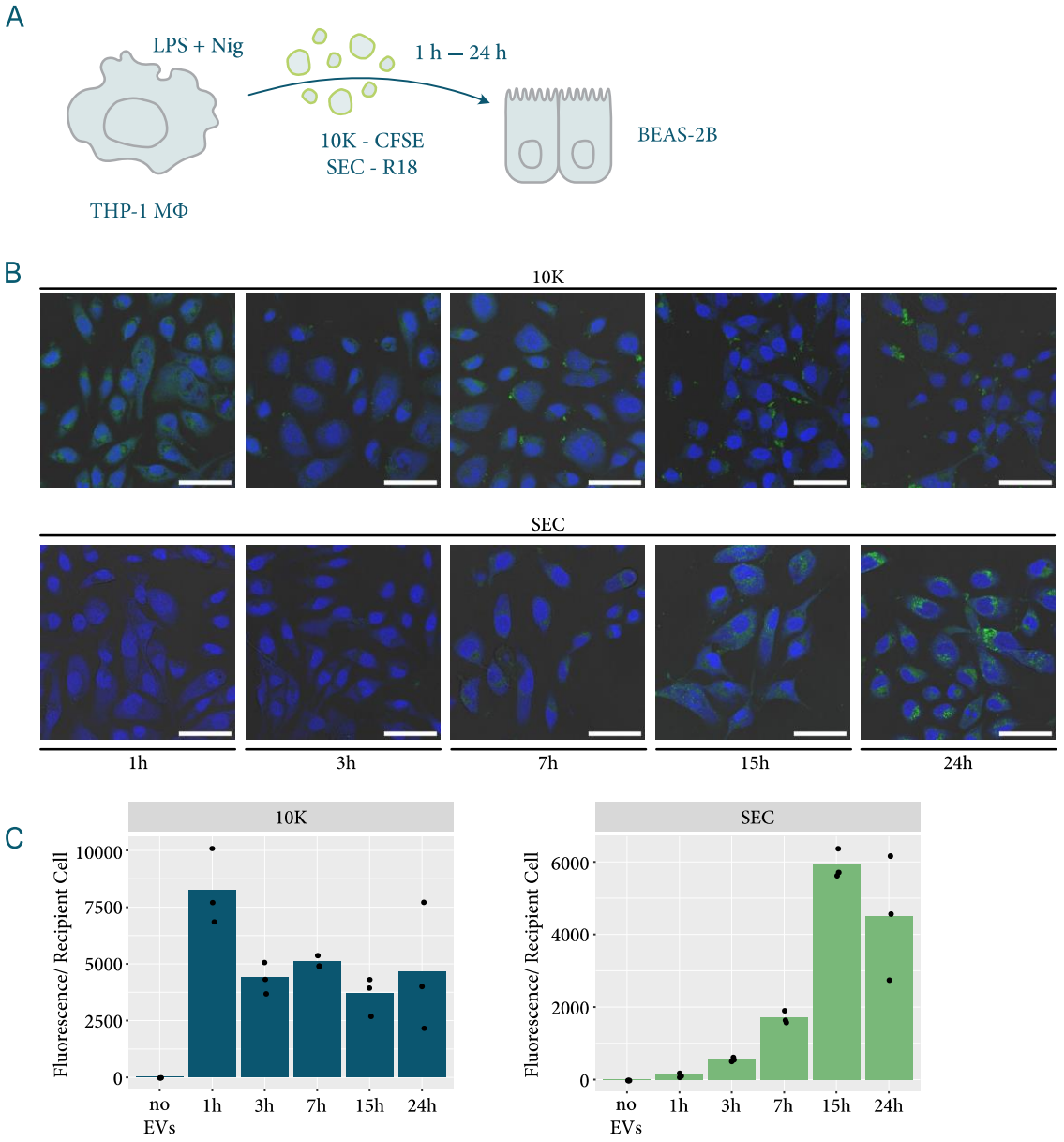

Figure 37: Uptake of EVs by BEAS-2B cells in a time dependent manner. (A) Schematic representation of the experimental plan. EVs were isolated from THP-1 MΦs after inflammasome activation, stained with CFSE (10K) or R18 (SEC) and incubated with recipient BEAS-2B cells for 1 h, 3 h, 7 h, 15 h, and 24 h. Nuclei were stained with DRAQ5. (B) Uptake of 10K (upper row) and SEC (lower row) EVs by BEAS-2B cells over 24 h. Nuclei are shown in blue, EVs in green. Scale bars: 50 μm. Representative images. (C) Fluorescence per recipient cell for one representative experimental run showing all technical replicates. (B+C) Trend was the same across all experimental runs. Technical replicates = 3. n = 3.

Having demonstrated that EV uptake is time dependent, it was investigated whether EV uptake is mediated by a specific process, excluding a significant contribution of transfer of free dye to the fluorescent signal. To do so, unstained inflammasome-elicited EVs were incubated with different amounts of stained inflammasome-elicited EVs, thus leaving the overall EV concentration the same while increasing the concentration of stained EVs. Recipient THP-1 MΦs were either incubated with no EVs, with 10% stained EVs (90% unstained), 50% stained EVs (50% unstained), or 100% stained EVs (no unstained EVs) (Figure 38). The more stained EVs, the higher the fluorescent signal that was observed for both 10K EVs (Figure 38B+D) and SEC EVs (Figure 38C+E). Additionally, I kept the concentration of stained EVs the same, while increasing the concentration of unstained EV and thus the overall EV concentration (Figure 39). Adding an excess of unstained EVs reduced the signal observed for both 10K and SEC EVs. Thus, it can be concluded that EVs are taken up by a specific process and that transfer of free dye does not markedly contribute to the signal observed.

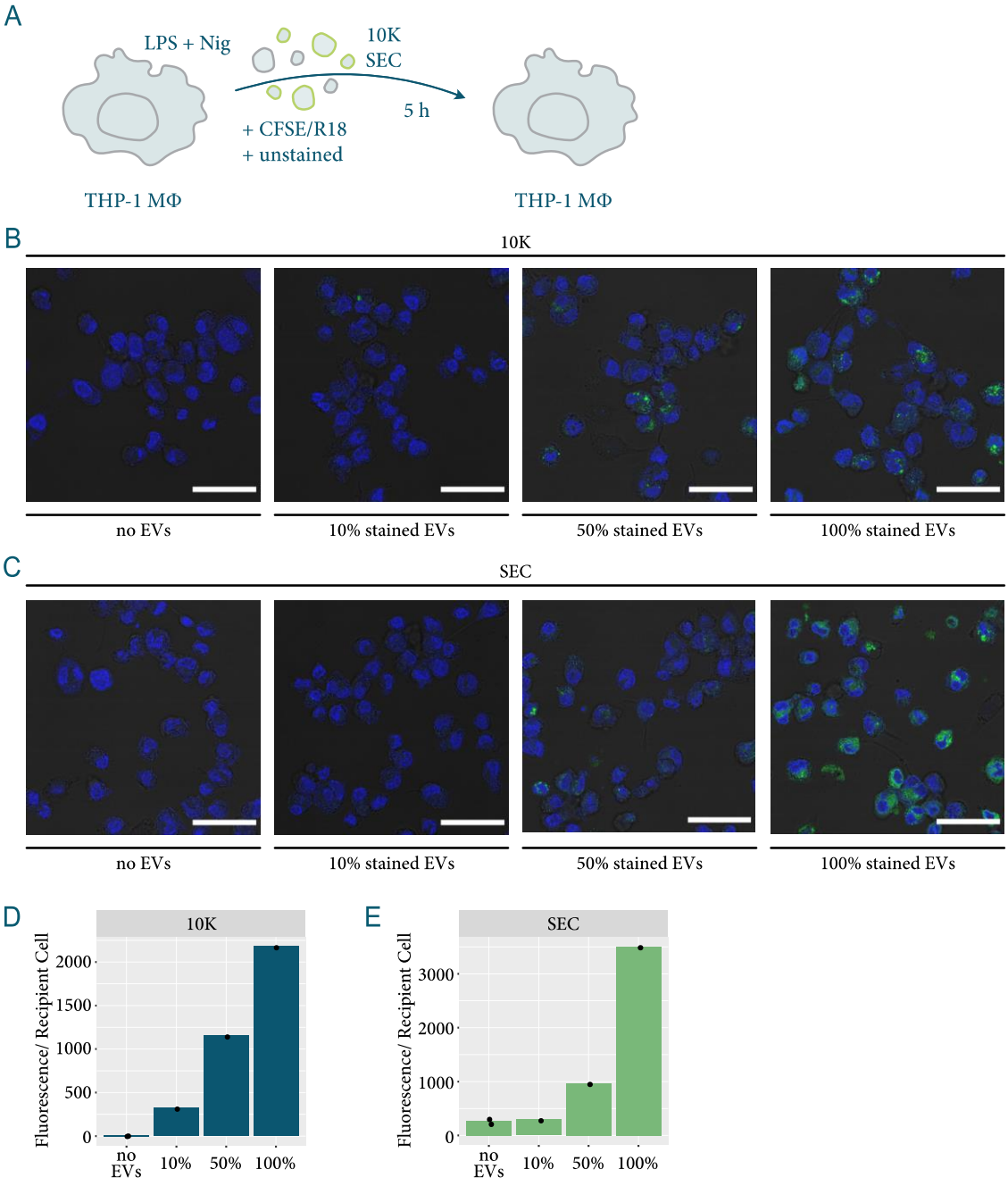

Figure 38: Uptake of increasing amounts of stained EVs in the presence of unstained EVs. (A) Schematic representation of experimental plan. EVs were isolated from inflammasome-stimulated THP-1 MΦs and either stained with CFSE/R18 or left unstained. EVs were then transferred in different proportions to recipient THP-1 MΦs. Nuclei were stained using DRAG5. (B–E) Uptake of stained 10K EVs (B+D) or SEC EVs (C+E) in the presence of different amounts of unstained EVs. Overall EV concentration was kept constant. Nuclei are shown in blue, EVs in green. Scale bars: 50 μm. Representative images. (D+E) Quantification of EV uptake. Technical replicates of one representative experimental run are shown. (B–D) Technical replicates = 3, n = 3.

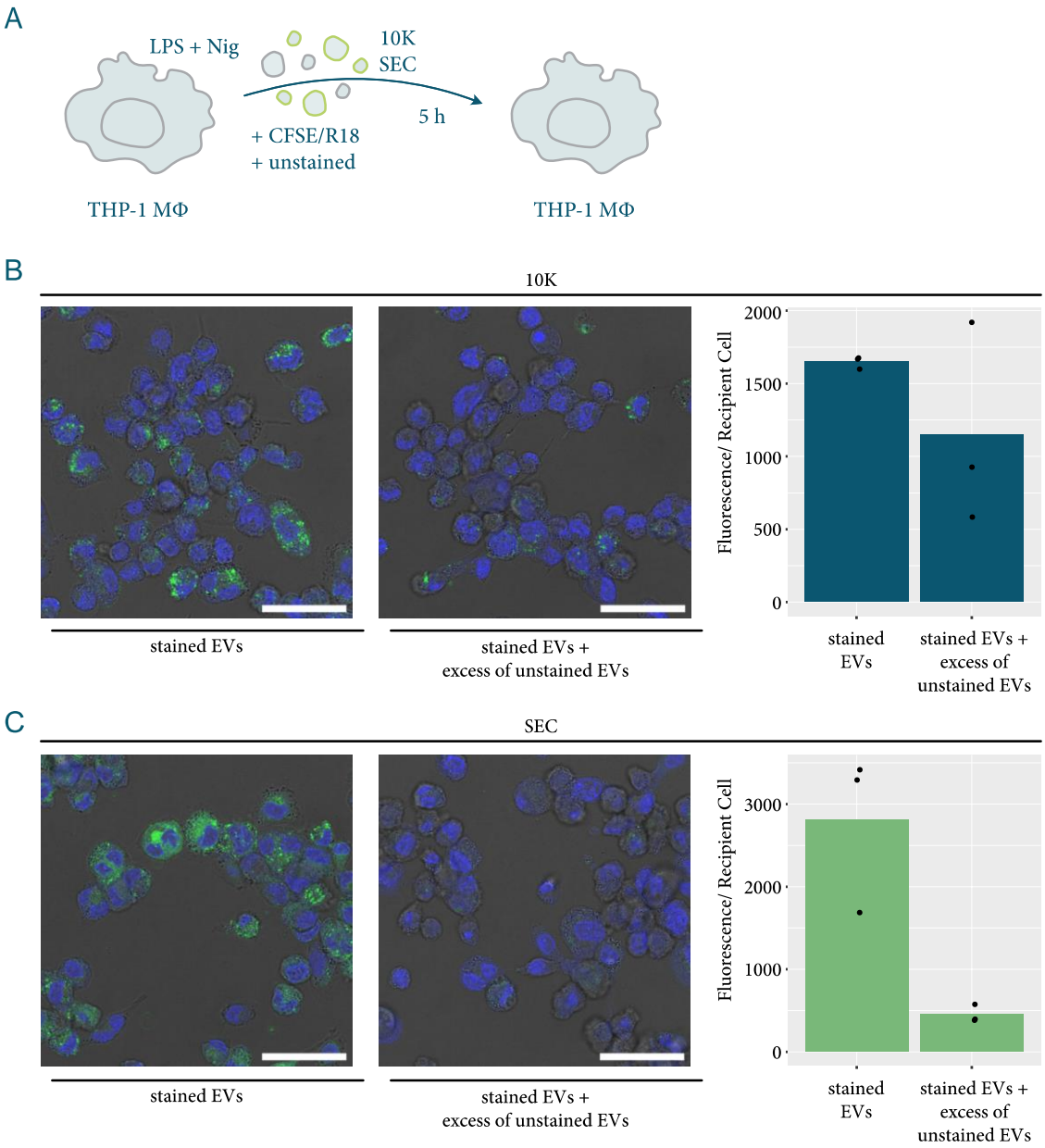

Figure 39: Uptake of stained EVs in the presence of an excess of unstained EVs. (A) Schematic representation of experimental plan. EVs were isolated from inflammasome-stimulated THP-1 MΦs and isolated EVs were either stained with CFSE/R18 or left unstained. EVs were then transferred in different proportions to recipient THP-1 MΦs and cells were incubated for 5 h. Nuclei were stained using DRAQ5. (B+C) Uptake of stained 10K EVs (B) and stained SEC EVs (C) in the presence of an excess of unstained EVs (keeping the concentration of stained EVs constant while increasing the overall EV concentration). Nuclei are shown in blue, EVs are shown in green. Scale bars: 50 μm. Representative images. Graphs show quantifications of all technical replicates for one representative experimental run. (B+C) Technical replicates = 3, n = 3.

Next, EV uptake was investigated at different temperatures to differentiate between active and passive uptake. This was done as endocytosis, which can be inhibited by incubation at 4 °C, has been reported to be a major EV uptake route. Thus, THP-1 MΦs were stimulated with LPS and nigericin and released EVs were isolated and stained. Stained EVs were then co-incubated for 5 h with recipient THP-1 MΦs at either 37 °C or at 4 °C (Figure 40A). A timepoint of 5 h was chosen as longer time points led to too much cell death in the case of cells incubated at 4 °C. In one of the three experimental runs, a low amount of 10K EV uptake was observed at 4 °C with an increased 10K EV uptake at 37 °C (Figure 40B+D). This, however, could not be observed in the two following runs. On the contrary, now a decrease in 10K signal at 37 °C compared to at 4 °C was observed (Figure 40E). Investigating this phenotype further by looking at the microscopy EV channel images (Figure 40F), it became clear that, while the signal, as quantified by Fiji/ImageJ and Cell Profiler, does not show a difference, the phenotype at 4 °C is quite distinct from the one at 37 °C: while there is just a diffuse signal at 4 °C, the signal at 37 °C is more punctuate and the individual puncti show a strong signal. This would suggest, for example, an uptake by phagocytosis at 37 °C and maybe just some dye diffusion at 4°C, which might cause a problem for the automatic quantification of EV uptake. Uptake of SEC EVs could not be demonstrated at 4°C at all, but only at 37°C (Figure 40C). Quantifying SEC EV uptake, it could be shown in all three experimental runs (two are shown in Figure 40D+E) that the majority of SEC EVs were only taken up at 37 °C. The major uptake of inflammasome-elicited EVs thus seems to be an active process.

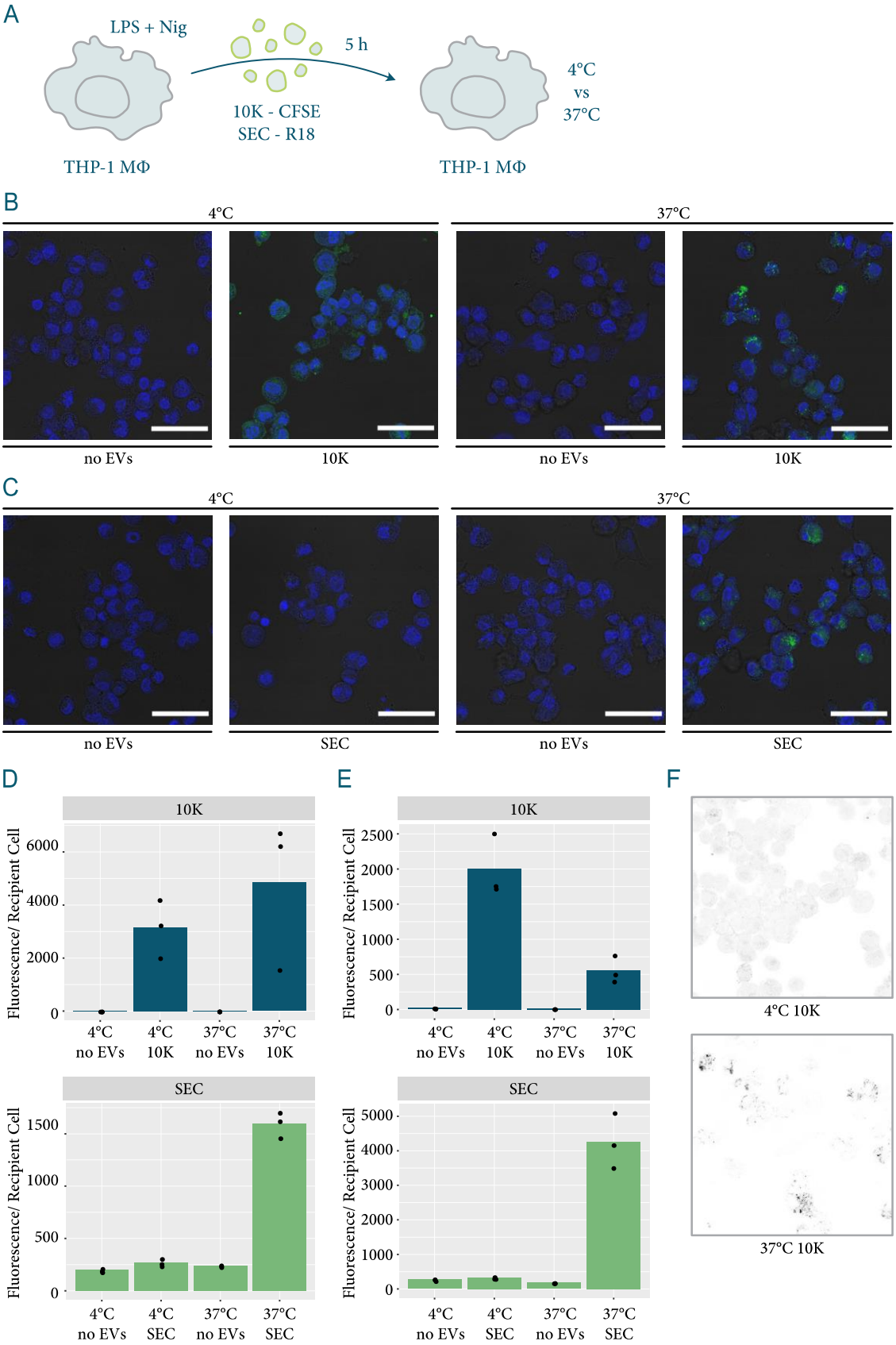
A
LPS + Nig
5 h
10K - CFSE
SEC - R18
4°C
vs
37°C
THP-1 MΦ
THP-1 MΦ
B
4°C
37°C
no EVs
10K
no EVs
10K
C
4°C
37°C
no EVs
SEC
no EVs
SEC
D
10K
SEC
Fluorescence/ Recipient Cell
4°C no EVs
4°C 10K
37°C no EVs
37°C 10K
4°C no EVs
4°C SEC
37°C no EVs
37°C SEC
E
10K
SEC
Fluorescence/ Recipient Cell
4°C no EVs
4°C 10K
37°C no EVs
37°C 10K
4°C no EVs
4°C SEC
37°C no EVs
37°C SEC
F
4°C 10K
37°C 10K

Figure 40: Temperature dependency of EV uptake. (A) Schematic representation of the experimental plan. EVs were isolated from inflammasome-stimulated THP-1 MΦs and stained with CFSE (10K) or R18 (SEC). Stained EVs were transferred to recipient THP-1 MΦs and incubated for 5 h at either 4 °C or 37 °C. Nuclei were stained with DRAG5. Technical replicates = 3, n = 3. (B) Uptake of 10K EVs at 4 °C (left) and 37 °C (right) for the first experimental run. (C) Uptake of SEC EVs at 4 °C (left) and 37 °C (right) for the first experimental run. (B+C) Nuclei are shown in blue, EV in green. Scale bars: 50 μm. Representative images. (D+E) Quantification of 10K (top) and SEC (bottom) EV uptake (Fluorescence/Recipient cell) for two different experimental runs (D and E respectively). D shows quantification of the first experimental run (the one shown in B and C), while E shows quantification of the second experimental run. Mean of technical replicates. (F) Representative images of one technical replicate of the second experimental run showing the 10K EV channel at 4 °C (top) and 37 °C (bottom).

Cytochalasin D is a very broad inhibitor of multiple uptake mechanisms, through the inhibition of actin polymerisation. Thus, to check whether EV uptake is actin dependent, Cytochalasin D was used in transfer experiments (Figure 41). THP-1 MΦs were stimulated with LPS and nigericin and EVs were isolated and stained with CFSE/R18, which were then incubated with recipient THP-1 MΦs that were left untreated or were pre-treated with Cytochalasin D (2 μM) (Figure 41A). In order to verify that Cytochalasin D was working, Bodipy-labelled LDL was used as a control (Figure 41B). Uptake of Bodipy-labelled LDL, 10K, and SEC EVs was quantified as described before. Results are shown for two of the three experimental runs (Figure 41C). For both Bodipy-labelled LDL and SEC EVs, a decrease of EV uptake in the presence of Cytochalasin D was observed (Figure 41B+C). In case of 10K EVs, no clear decrease was observed when quantifying results (Figure 41C). Again, this might be a problem of the quantification pipeline, since 10K EV uptake showed the same qualitative differences that were observed when comparing uptake at 37 °C and 4 °C (distinct puncti under untreated conditions versus diffuse signal under Cytochalasin D treatment; Figure 41B); this underlines the importance of not only relying on quantification, but also studying microscopy images. While (SEC) EV uptake is reduced in the presence of Cytochalasin D, it is not completely blocked. This could be either because actin polymerisation is not completely blocked (which is probably the case to some extent, as LDL uptake was also not completely blocked in Cytochalasin D pre-

treated cells) or because there are also actin-independent EV uptake processes taking place.

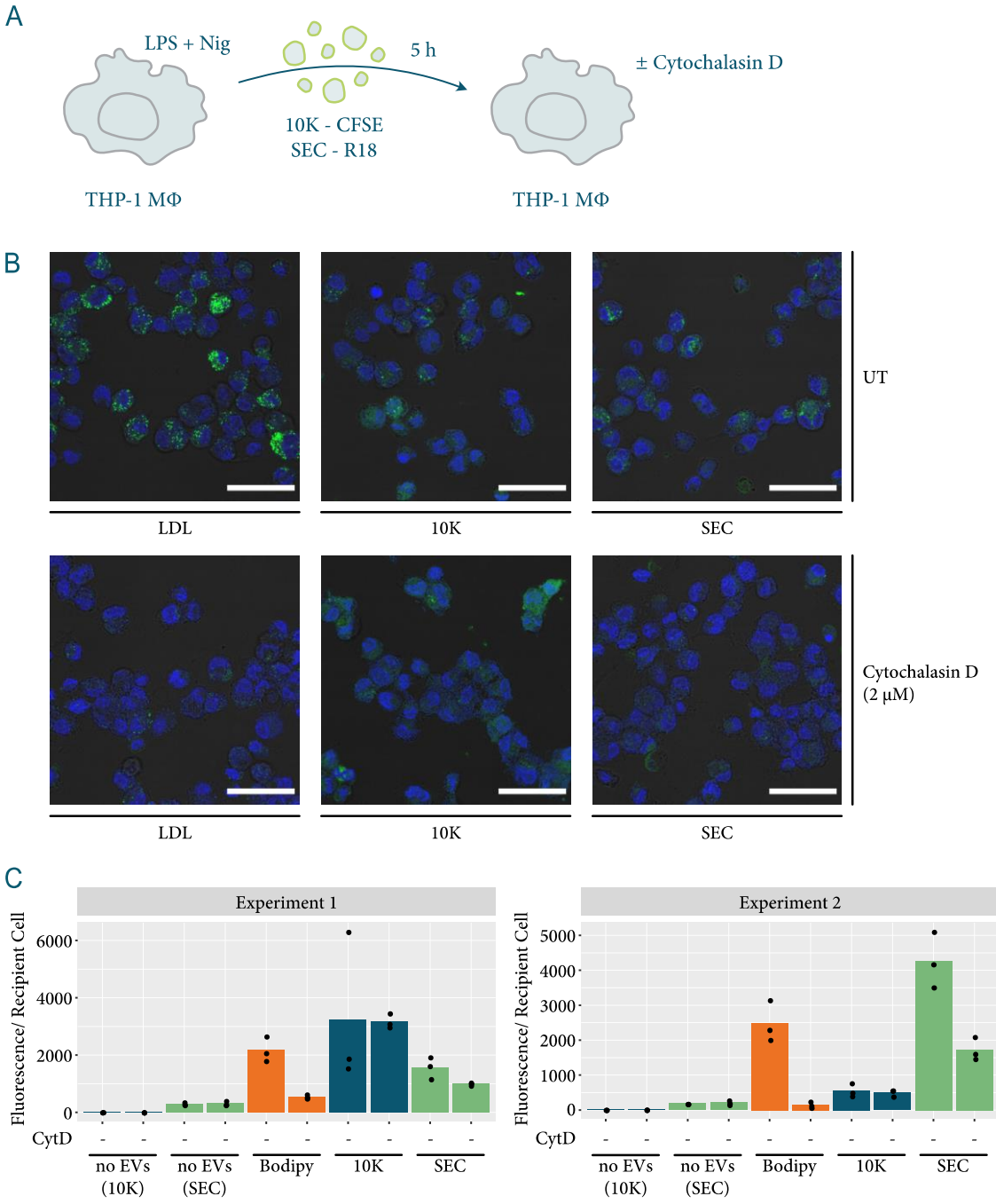

Figure 41: Uptake of EVs in the presence of Cytochalasin D. (A) Schematic representation of the experimental plan. EVs were isolated from inflammasome-stimulated THP-1 MΦs and either stained with CFSE (10K) or R18 (SEC). Stained EVs were transferred to recipient THP-1 MΦs and incubated for 5 h either in the presence or absence of Cytochalasin D. Nuclei were stained with DRAQ5. Technical replicates = 3, n = 3. (B) Uptake of 10K EVs, SEC EVs, or Bodipy-labelled LDL (positive control) with or without Cytochalasin D pre-treatment of

recipient cells. Nuclei are shown in blue, EVs and LDL in green. Scale bars: 50 μm. Representative images. (C) Quantification of EV uptake (Fluorescence/Recipient cell) for two of the three experimental runs (mean of three technical replicates shown).

3.2.3 EV Content Release

EV uptake by recipient cells does not directly imply that intraluminal EV contents end up in the recipient cell's cytosol. To investigate if EVs not only interact with recipient cells through surface-surface interaction but also deliver proteins (and possibly RNA) to recipient cells' cytosol, THP-1 cells that stably express NLuc-tagged HSP70 were generated (Figure 42A). HSP70 is an intraluminal-associated EV marker and has been shown to be bulk loaded into EVs (Bonsergent *et al*, 2021). Additionally, CD63, a membrane-associated EV marker that is enriched in EVs (Escola *et al*, 1998; Bonsergent *et al*, 2021), was tagged with NLuc and introduced into THP-1 cells (Figure 42A). NLuc allows high sensitivity detection and is thus highly useful when working with small amounts of samples and therefore in case of EVs (Gupta *et al*, 2020).

I have generated four different THP-1 cell lines: the two described above and two additional controls that express HSP70 or CD63 respectively, but without the NLuc tag (Figure 42B). Expression of these constructs was tested using an assay for in-gel luciferase activity of cell lysates. Cell lysates were prepared as if used in a normal Western blot. They were then loaded onto an SDS-polyacrylamide gel and gel electrophoresis was performed. After running the gel, it was washed in 25 % isopropanol to remove the SDS, allowing the NLuc to refold spontaneously. Finally, the gel was covered in NLuc detection reagent and luciferase activity was measured with a chemiluminescent imager. Measuring in-gel luciferase activity thus allowed me to test whether NLuc is expressed and functional and, additionally, whether coupling to HSP70/CD63 had been successful. NLuc activity could be observed for NLuc-CD63 THP-1 MΦs as well as for NLuc-HSP70 THP-1 MΦs. In case of NLuc-CD63 THP-1 MΦs, NLuc signal was observed in the range of roughly 30–60 kDa (Figure 42C). Usually, the observed molecular weight of CD63 lies between 28 and 35 kDa. NLuc has a

molecular weight of 19 kDa. The observed NLuc signal therefore suggests successful tagging of CD63. In the case of NLuc-HSP70 THP-1 MΦs, NLuc signal was observed at around 70 and 80 kDa (Figure 42C). HSP70 has a molecular weight of 70 kDa. Thus, one of the two bands seems to be NLuc-HSP70. The nature of the second band is less clear. The faint upper and lower bands in case of both NLuc-tagged THP-1 MΦs are probably due to sample that has not passed through the gel and NLuc that was no longer coupled to HSP70 or CD63. In addition to performing in-gel luciferase activity assays, luciferase activity can be measured in solution. Cell lysates were mixed with luciferase substrate and luciferase activity was directly measured. Results are shown in Figure 42D. While a strong signal could be observed for NLuc-HSP70 THP-1 MΦ and NLuc-CD63 THP-1 MΦ lysates, little to no signal was observed in case of control cell lysates (Figure 42D). The signal decreased over time, probably resulting from the growing depletion of available luciferase substrate.

Knowing that the cells expressed NLuc coupled to CD63/HSP70, I set out to investigate whether the tagged proteins are incorporated into inflammasome-elicited EVs and, if so, whether the signal is strong enough to be measured. Thus NLuc-CD63 THP-1 MΦs and NLuc-HSP70 THP-1 MΦs were stimulated with LPS and nigericin and EVs were isolated. NLuc activity was then measured in all three EV fractions (2K, 10K, and SEC), as well as in whole cell lysates. Whole cell lysates from wt, CD63, and HSP70 THP-1 MΦs, and PBS were used as controls. All three EV fractions isolated from NLuc-CD63 THP-1 MΦs showed measurable NLuc activity (Figure 42E). In case of NLuc-HSP70 THP-1 MΦs-derived EVs, only 10K EVs showed a strong measurable signal, while 2K and SEC EV NLuc activity was relatively low (although still detectable) (Figure 42E). Controls showed little to no NLuc activity (Figure 42E). Considering that HSP70 is only bulk loaded into EVs and not enriched, as CD63, these results were expected.

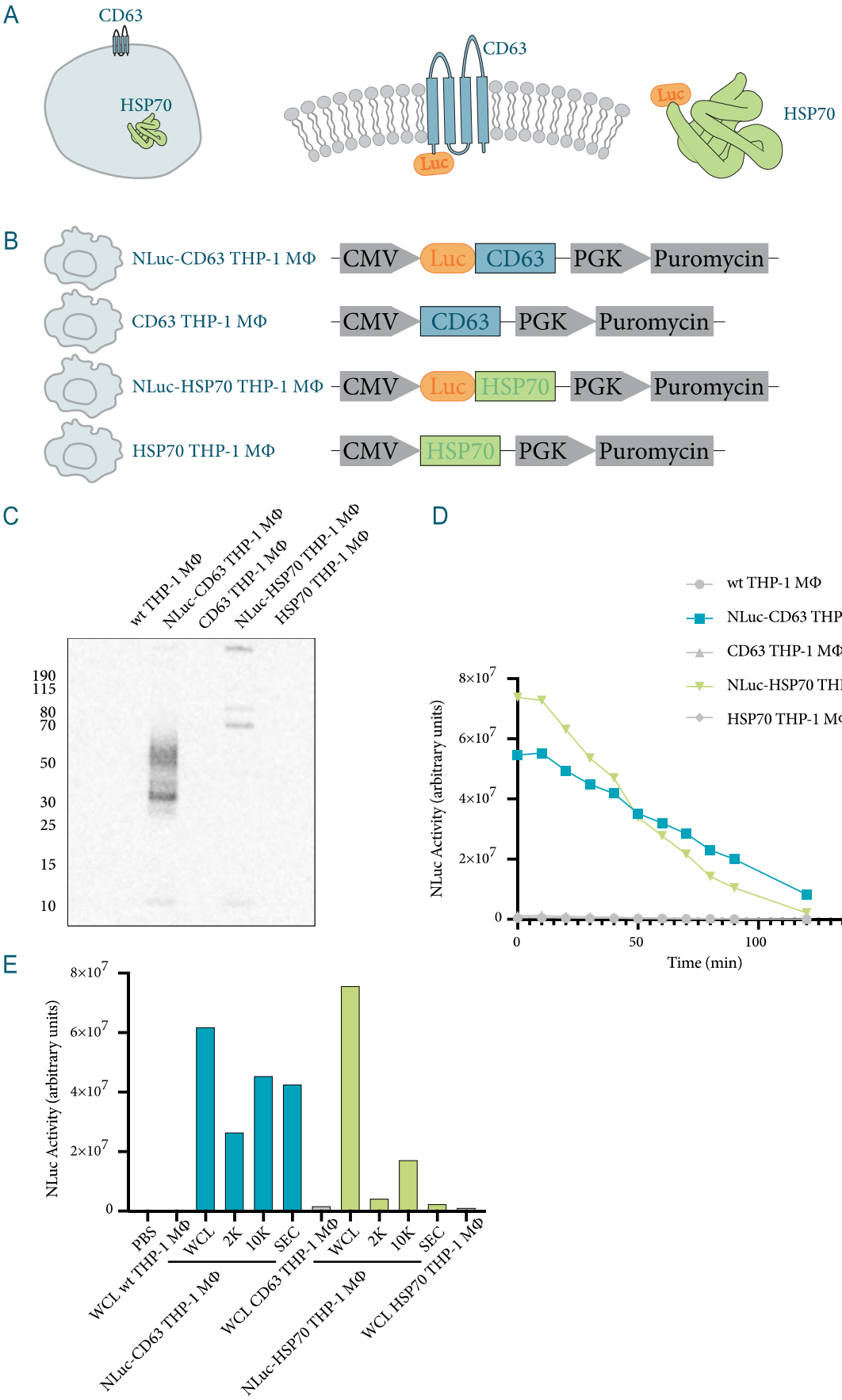
A
CD63
HSP70
CD63
Luc
Luc
HSP70
B
NLuc-CD63 THP-1 MΦ
CMV
Luc
CD63
PGK
Puromycin
CD63 THP-1 MΦ
CMV
CD63
PGK
Puromycin
NLuc-HSP70 THP-1 MΦ
CMV
Luc
HSP70
PGK
Puromycin
HSP70 THP-1 MΦ
CMV
HSP70
PGK
Puromycin
C
wt THP-1 MΦ
NLuc-CD63 THP-1 MΦ
CD63 THP-1 MΦ
NLuc-HSP70 THP-1 MΦ
HSP70 THP-1 MΦ
190
115
80
70
50
30
25
15
10
D
wt THP-1 MΦ
NLuc-CD63 THP-1 MΦ
CD63 THP-1 MΦ
NLuc-HSP70 THP-1 MΦ
HSP70 THP-1 MΦ
NLuc Activity (arbitrary units)
8×10^7
6×10^7
4×10^7
2×10^7
0
0
50
100
150
Time (min)
E
NLuc Activity (arbitrary units)
8×10^7
6×10^7
4×10^7
2×10^7
0
PBS
WCL wt THP-1 MΦ
WCL
2K
10K
SEC
NLuc-CD63 THP-1 MΦ
WCL CD63 THP-1 MΦ
WCL
2K
10K
SEC
NLuc-HSP70 THP-1 MΦ
WCL HSP70 THP-1 MΦ

Figure 42: Generation of NLuc-tagged HSP70/CD63-expressing THP-1 cell lines. (A) HSP70 and CD63 are EV marker proteins. While HSP70 is found in the EV lumen, CD63 is associated with EV membranes. Both proteins were tagged with NLuc, a highly sensitive nano luciferase. (B) Different THP-1 cell lines stably expressing the indicated constructs. (NLuc-tagged) EV markers are under control of a CMV promoter. Puromycin is under control of a phosphoglycerate kinase (PGK) promoter and used for selection. (C) In-gel luciferase activity assay. Whole cell lysates of NLuc-CD63-, CD63-, NLuc-HSP70-, HSP70-, and wt THP-1 MΦs were run on a SDS polyacrylamide gel. The gel was washed to allow refolding of nano luciferase and chemiluminescence was measured. (D) Cell lysates of the above-described cell lines were generated, and nano luciferase activity was measured in cell lysates over time. Nano luciferase activity is given in arbitrary units. (E) Inflammasome-elicited EVs (2K, 10K, SEC) were isolated from NLuc-CD63 THP-1 MΦs and NLuc-HSP70 THP-1 MΦs and luciferase activity of EVs and WCLs was measured. WCLs of wt, CD63, and HSP70 THP-1 MΦs, as well as PBS, acted as controls. (C) n = 1. (D+E) representative figures with n = 2.

Having generated the above-mentioned cell-lines and having determined they work as expected, EVs from inflammasome-activated NLuc-CD63 THP-1 MΦs and NLuc-HSP70 THP-1 MΦs (10K and SEC) were isolated and transferred to recipient wild type THP-1 MΦs. After incubation for 15 h, cells were washed to remove any remaining EVs and then lysed (Figure 43A). NLuc activity was measured in recipient cells' whole cell lysates (Figure 43B). Recipient cells treated with NLuc-CD63 THP-1 MΦ-derived EVs showed strong NLuc activity for both 10K and SEC EVs. NLuc activity for recipient cells treated with NLuc-HSP70 THP-1 MΦ-derived 10K and SEC EVs showed no NLuc activity but only background (roughly the same as controls) signal (Figure 43B).

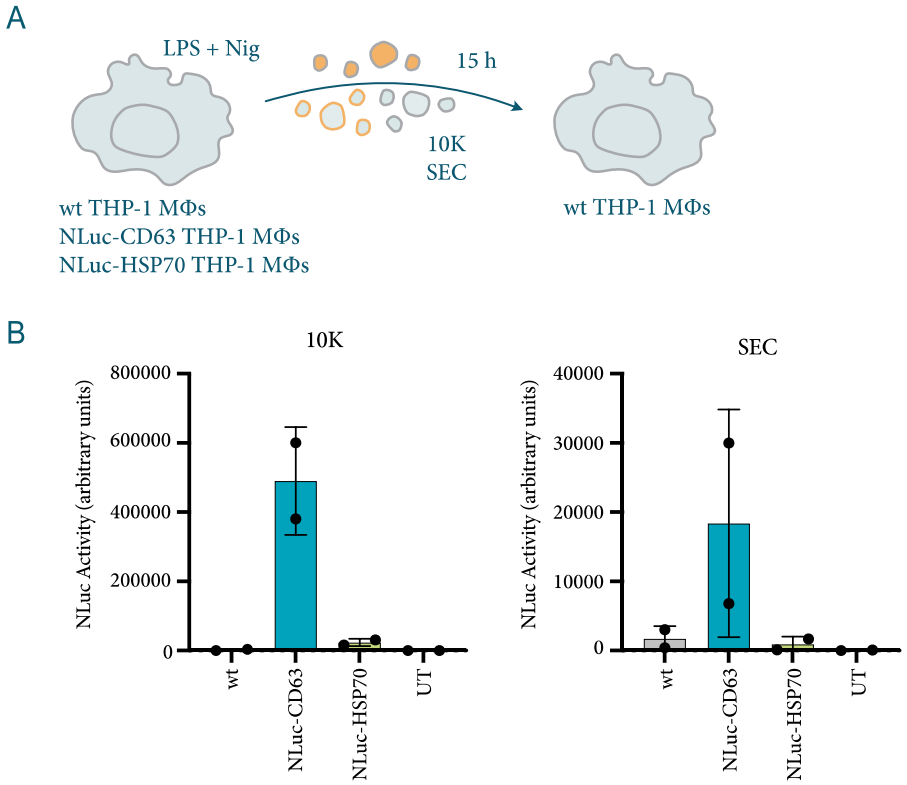

Figure 43: Transfer of NLuc-tagged HSP70/CD63 to recipient THP-1 MΦs. (A) EVs were isolated from inflammasome-activated wt, NLuc-CD63, and NLuc-HSP70 THP-1 MΦs and transferred to recipient wt THP-1 MΦs. After 15 h of incubation, cells were lysed and NLuc activity was measured. (B) NLuc activity (in arbitrary units) in whole cell lysates of wt THP-1 MΦs treated with inflammasome-elicited 10K EVs (left) and SEC EVs (right) from wt, NLuc-CD63, and NLuc-HSP70 THP-1 MΦs. Mean ± SD, n = 2.

After showing that EVs from NLuc-CD63 and NLuc-HSP70 THP-1 MΦs transfer NLuc tagged HSP70/CD63 to recipient cells, I investigated, whether EVs are just taken up by recipient cells or if their cytosolic content is released. As HSP70 is an intraluminal protein, it should end up in the recipient cell's cytoplasm, if EV content is released. Thus, after performing detergent-free cell fractionation of recipient cells, it would be expected in the cytosolic fraction. On the other hand, if EVs are shuttled to lysosomes for degradation, it would be expected in the membrane fraction. By contrast, CD63, an EV transmembrane protein, would be expected to end up in the membrane fraction. Thus, to test EV content release, EVs were isolated from inflammasome-activated NLuc-CD63 and NLuc-HSP70 THP-1 MΦs and transferred to recipient wild type THP-1 MΦs. After 15 h of incubation, recipient wild type THP-1 MΦs were then fractionated using a Dounce

homogeniser (Figure 44A). Centrifugation at 340 x g was performed to separate intact cells from the membrane and cytosolic fractions. Centrifugation at 100,000 x g was then performed to pellet membranes (including intact organelles, such as lysosomes) and separate the membrane fraction from the cytosolic fraction (Figure 44A). The cytosolic fraction was expected to contain NLuc tagged HSP70, while the membrane fraction was expected to contain NLuc tagged CD63 and HSP70 that was not released into the cytosol.

Successful detergent-free cell fractionation was tested by performing Western blotting for CANX (Figure 44B). CANX is a transmembrane ER protein and, as such, should be absent from cytosolic fractions and present in membrane fractions. This was indeed the case in samples after detergent-free cell fractionation (Figure 44B). As a control, 1 % Triton X-100 was added to samples. Triton X-100 is a detergent and was used to disrupt membranes. After membrane disruption, CANX was expected in the cytosolic fraction, which was the case in the above-described experiment (Figure 44B). Thus, it was concluded that the chosen method for detergent-free cell fractionation was suitable and worked well.

Finally, recipient wild type THP-1 MΦs, after incubation with inflammasome-elicited EVs (10K and SEC) from NLuc-CD63 and NLuc-HSP70 THP-1 MΦs, were fractioned and NLuc activity was measured in membrane and cytosolic fractions. Strong NLuc activity was measured in membrane fractions of recipient wild type THP-1 MΦs treated with 10K and SEC EVs from NLuc-CD63 THP-1 MΦs (Figure 44C). Some signal was detected in cytosolic fractions of recipient wild type THP-1 MΦs treated with 10K and SEC EVs from NLuc-CD63 THP-1 MΦs (Figure 44C), probably due to some membrane disruption and thus leakage of CD63 to the cytoplasmic fraction. Membrane fractions of recipient wild type THP-1 MΦs treated with 10K and SEC EVs from NLuc-HSP70 THP-1 MΦs showed some NLuc signal (Figure 44C). This might be due to the lack of a washing step in the protocol and thus some cytosolic components still being present in the membrane fraction. A washing step was purposely excluded, as it would further reduce the amount of sample remaining and work was already

conducted with little material. Cytosolic fractions of recipient wild type THP-1 MΦs treated with 10K and SEC EVs from NLuc-HSP70 THP-1 MΦs did not show any NLuc activity (Figure 44C). This might be due to the NLuc signal already being weak in case of EV lysates (Figure 43B), which, in turn, is probably due to HSP70 being bulk-loaded into EVs, while CD63 is enriched. Using more EVs, using a transwell luciferase assay to allow signal from constant EV released to accumulate over time, trying other incubation periods, varying the Dounce homogeniser step to get higher cell rupture, or using a smaller volume for cell fractionation and therefore having more concentrated cytosolic fractions are just some ideas to try and improve the experiment in the future.

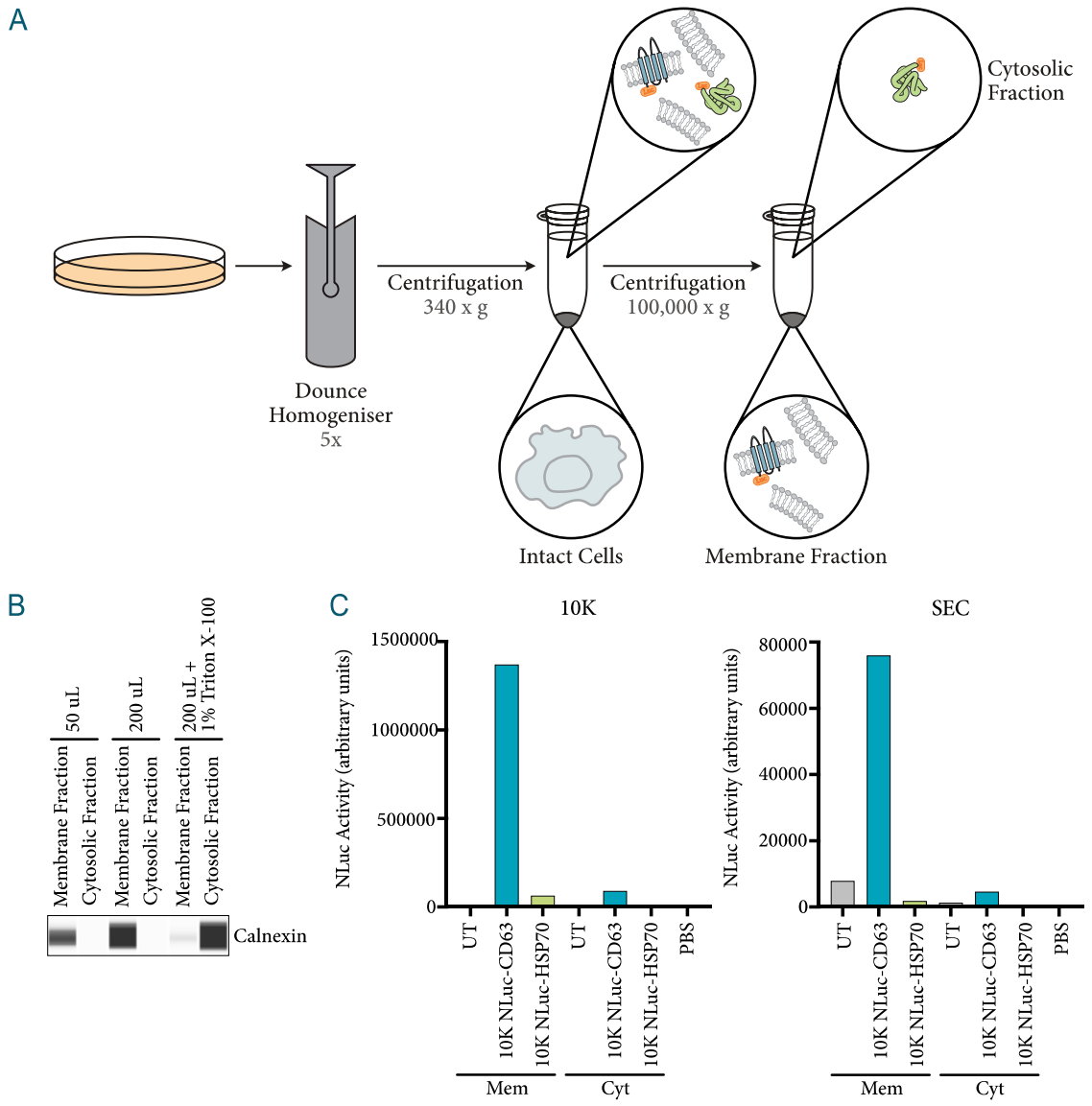

Figure 44: Detergent-free cell fractionation to investigate EV content release in recipient THP-1 MΦs after transfer of EVs carrying NLuc-tagged HSP70/CD63. (A) EVs were isolated from inflammasome-activated NLuc-CD63 and NLuc-HSP70 THP-1 MΦs and transferred to recipient wt THP-1 MΦs. After 15 h of incubation, cells were resuspended in PBS. Detergent-free cell fractionation was performed using a Dounce homogeniser five times. Afterwards, samples were centrifuged at 340 x g to remove intact cells, followed by centrifugation at 100,000 x g to separate the membrane from the cytosolic fraction. (B) Western blotting for the transmembrane ER protein CANX. Two different volumes (50 µL and 200 µL) were used for cell fractionation and resulting membrane and cytosolic fractions were used for Simple Western WES. As a control, samples were treated with detergent (1 % Triton X-100) to rupture membranes. (C) Nano luciferase activity given in arbitrary units for membrane (Mem) and cytosolic (Cyt) fractions of recipient wt THP-1 MΦs either untreated or treated with inflammasome-elicited 10K EVs (left) and SEC EVs (right) from wt, NLuc-CD63, and NLuc-HSP70 THP-1 MΦs. (B+C) n = 1.

3.3 THP-1 MΦ-Derived EVs and their Effect on Different Human Cells

Next, primary human cells were used. These cells have a limited ability to replicate and have a shorter lifespan and as such were only used once experimental conditions had been established. For every primary cell type, EV uptake was investigated through confocal microscopy. While time courses were performed for cell lines, primary cells were just investigated at a limited number of time points to see if they, as their cell line counterparts, took up vesicles and if uptake was roughly comparable.

As introduced previously, inflammasome-elicited EVs from THP-1 MΦs affect recipient THP-1 MΦs in various ways. To expand this knowledge and to gain a better understanding of the role of NLRP3-elicited EVs in the spread of inflammation, THP-1 MΦ-derived EVs were transferred to different human primary cells: NHBECs, HUVECs, NHLFs, and T cells (naïve and activated) isolated from human blood. To keep results comparable to experiments performed with THP-1 MΦ-derived EVs, experimental conditions were not altered, where possible. Therefore, the same EV concentration was applied to recipient cells using FBS-free medium (as the standard FBS used in tissue culture contains bovine EVs (Driedonks *et al*, 2019) and thus would bias results) and the incubation time was kept at 15 h.

3.3.1 Uptake of Inflammasome-Elicited EVs by Different Human Cells

MΦs are phagocytic cells and, as such, are known to take up EVs rapidly. Above, I have shown that THP-1 MΦs took up 10K EVs after 1–3 h (Figure 35). From then on, the mean EV count per cell increased until reaching the highest levels after about 15 h. This was followed by a decrease in EV levels (Figure 35). Uptake of SEC EVs by THP-1 MΦs took longer. After 7 h SEC EVs started to accumulate in recipient THP-1 MΦs. The mean EV count per cell constantly increased from this time point up to 24 h (Figure 35). To keep the incubation time

consistent for both 10K and SEC EVs, an incubation time of 15 h was chosen in previous studies (Budden, 2020).

Experiments with the epithelial cell lines A549 and BEAS-2B showed a similar trend (Figure 36, Figure 37), thus I expected that the incubation time of 15 h might also be suitable for the different primary cell types. However, to make sure that there was indeed interaction/uptake of EVs after 15 h and to study how different recipient cells interact with inflammasome-elicited EVs, I performed microscopy experiments with fluorescently labelled EVs for all five recipient cells.

3.3.1.1 Epithelial Cells

NHBECs are cells isolated from the epithelial lining of airways above bifurcation of the lungs. NHBECs were purchased from LONZA. They were first expanded for 3–7 days in a submerged culture in culture flasks. After expansion, cells were transferred to a transwell insert where they were further expanded for 2–4 days until having reached a confluent monolayer. Once this confluency was reached, the medium in the apical chamber of transwell inserts was removed, exposing the NHBECs on their apical side to air (Figure 45B). This procedure is called “airlift”. The cells were then cultivated for at least 21 days in these ALI cultures to allow differentiation, resulting in a pseudostratified epithelium consisting of basal cells, secretory cells (goblet cells), and ciliated cells (Figure 45A+C). Mucous production can be observed by looking at cells through a standard wide field microscope. The same microscope also allows observation of ciliary beating. To confirm this observation, ALI cultures were cryo-embedded and antibody staining against acetyl-alpha tubulin, a ciliary protein, was performed (Figure 45D). The expression of cilia could be confirmed, as well as the successful establishment of a pseudostratified epithelium (Figure 45D).

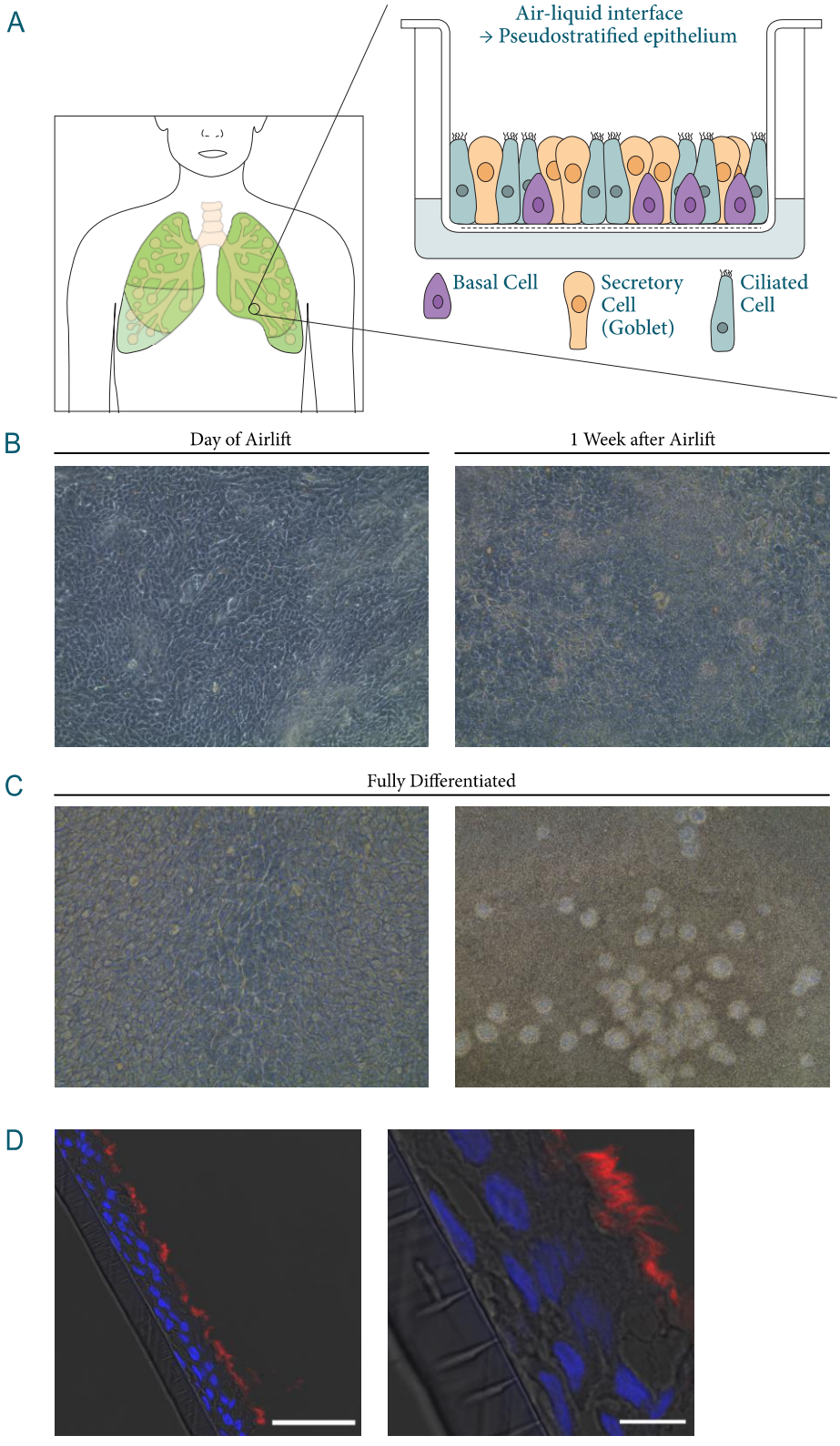

Figure 45: Culture of lung epithelial cells. (A) NHBECs are cells isolated from the epithelial lining of airways. They were purchased from LONZA and cultured in air-liquid interface (ALI) cultures on transwell plates until differentiated to a pseudostratified epithelium consisting of basal cells, secretory cells (goblet cells),

and ciliated cells. (B+C) Light microscopy images of ALI cultures. (B) Cells on the day of airlift, right after removal of apical chamber medium (left) and one week after airlift (right). (C) Two different fields of view of fully differentiated ALI cultures. (D) ALI cultures were cryo-embedded, sliced, and stained for acetyl-alpha tubulin to visualise cilia (red). Hoechst 34580 was used to stain nuclei (blue). Scale bar top image: 50 μm; lower image: 10 μm. (B–D) Representative images, n = 6.

After establishing NHBEC cultures, EV transfer experiments were performed to check for interaction/uptake of EVs after 15 h of incubation. EVs were isolated from THP-1 MΦs after inflammasome activation, stained with R18, and transferred to NHBEC cultures (applied on the apical (top) side). Incubation was performed for 15 h after which cells were fixed, cryo-embedded, and used for immunostainings (Figure 46A). EV uptake was shown for 10K and SEC EVs (Figure 46B).

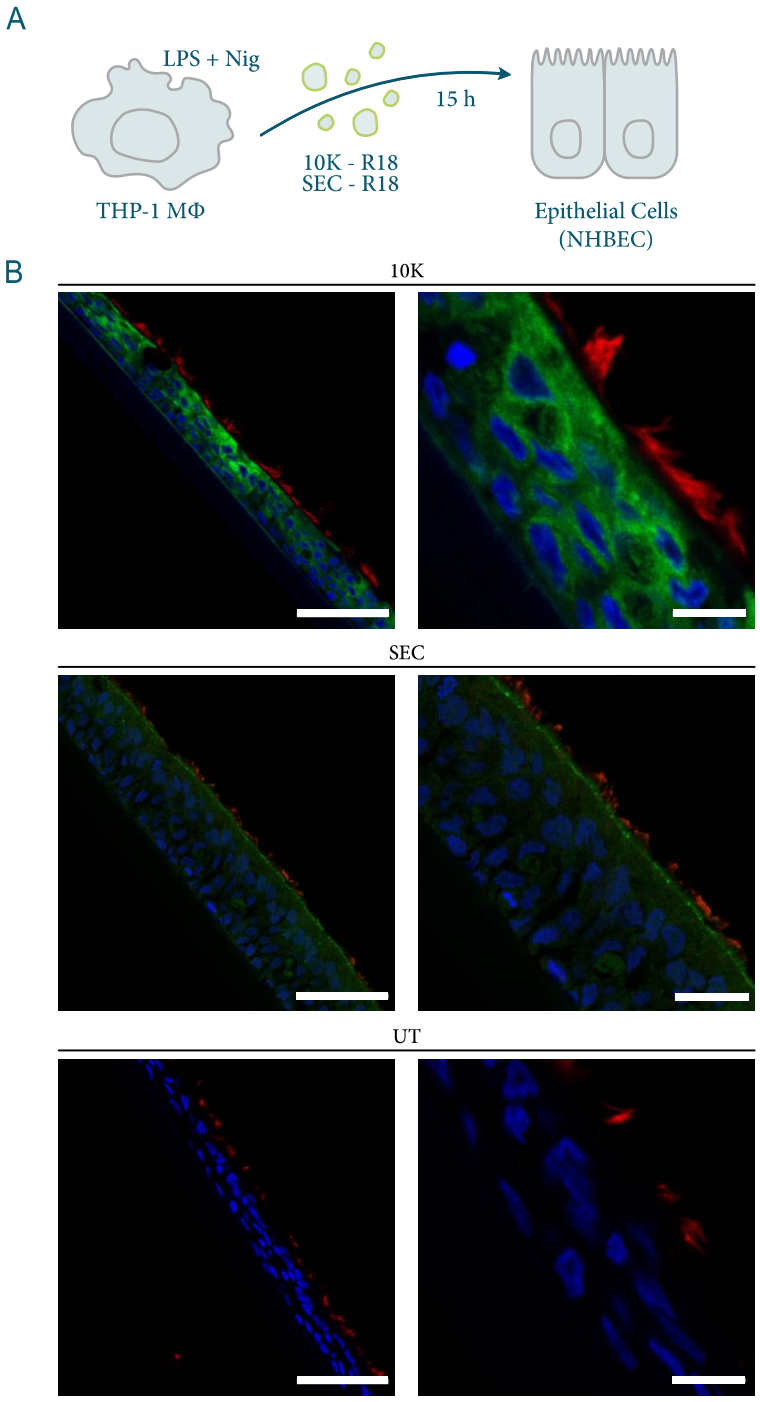

Figure 46: EV uptake by lung epithelial cells after 15 h. (A) Schematic representation of the experimental plan. 10K and SEC EVs were isolated from THP- MΦs after inflammasome activation and stained with R18. Incubation with epithelial cells was performed for 15 h, after which cells were fixed, cryo-embedded, and immunostained. (B) Uptake of 10K and SEC EVs (shown in green). Nuclei were stained using Hoechst 34580 (shown in blue), cilia were stained for acetyl-alpha tubulin (shown in red). Scale bars top row left to right: 50 μm, 10 μm, 50 μm, 10 μm; bottom row left to right: 50 μm, 10 μm. Representative images, technical replicates = 3, n = 1.

3.3.1.2 Endothelial Cells

As a model for endothelial cells, HUVECs were cultured. There are different methods to culture HUVECs, resulting in different phenotypic representation of the endothelium. The simplest method is to culture HUVECs directly on a culture surface. A simple modification is to pre-treat this culture surface with fibronectin. A more advanced culture system would be to culture HUVECs on transwell inserts (Figure 47A). All three culture systems were tested before using HUVECs in transfer experiments. To do so, inflammasome-elicited EVs from THP-1 MΦs were isolated and stained with R18. Stained EVs were then transferred to HUVECs either grown on uncoated or fibronectin-coated culture surfaces (Figure 48A). Cells were stained with acti-stain 488 phalloidin to assess polarisation (Figure 47B–D). Acti-stain 488 phalloidin binds to F-actin only (Wulf *et al*, 1979). It is a peptide toxin from the mushroom *Amanita phalloides* (Wieland *et al*, 2008). Using acti-stain 488 phalloidin allows the identification of pronounced circumferential actin filaments, which are found parallel to the junction to neighbouring cells in resting endothelium, as well as stress fibres, which are a sign of activated endothelial cells (Schnittler *et al*, 2014).

First, it was investigated whether coating with fibronectin makes a difference. Investigating the actin stain, both circumferential actin filaments and stress fibres could be observed in HUVEC cultures (Figure 47). More cell death was observed under uncoated conditions, as well as the presence of more stress fibres (Figure 47B+C), indicating that coating culture surfaces with fibronectin might be advantageous.

Next, transwell cultures of HUVECs were investigated. HUVECs were seeded on fibronectin-coated transwells with the same medium in the upper and lower chambers and grown until confluent (about 3 days). They were then allowed to rest for a further 3 days to allow the formation of tight junctions between cells. Cells looked healthier than HUVECs directly grown on either uncoated or coated culture surfaces and only a few apoptotic cells were observed (Figure 47D).

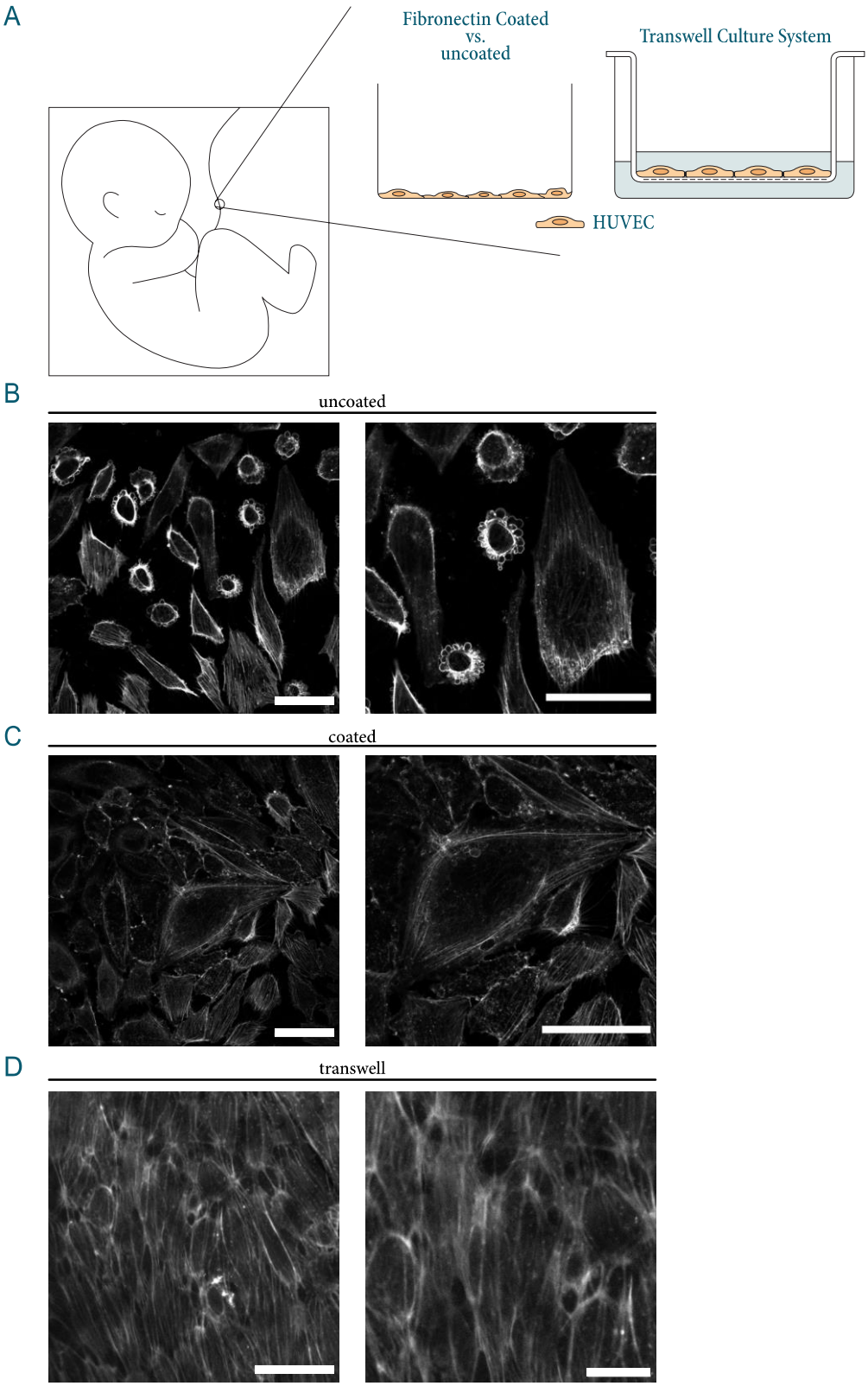

Figure 47: Establishment of HUVEC culture. (A) HUVECs are isolated from human umbilical cords. They can be grown either directly on culture surfaces, on fibronectin pre-treated culture surfaces, or in transwell systems, amongst other methods. (B–D) F-actin in HUVECs grown either on uncoated (B), on fibronectin-

coated (C) culture surfaces, or on a fibronectin-coated transwell surface (D). (B+C) Scale bars: 50 µm. (D) Scale bars: 50 µm (left), 20 µm (right). (B–D) Representative images, technical replicates = 3, n = 1.

Next, it was investigated whether the difference in HUVEC culture and thus the state of HUVECs might also affect EV uptake. When comparing HUVECs grown on culture surfaces with fibronectin coating to those without coating, HUVECs grown on fibronectin coated culture surfaces seemed to have taken up more EVs (Figure 48B+C).

Microscopy of transwell cultures is not as straightforward as imaging cells directly grown on coated or uncoated surfaces. The laser power needed to be increased a lot to be able to detect a signal and, even then, the signal was not very strong. Thus, EV uptake could not directly be compared to cells grown on culture dishes. However, it can be observed that EV uptake takes place (Figure 48D).

Thus, it was decided to use transwell plates for HUVEC culture in transfer experiments.

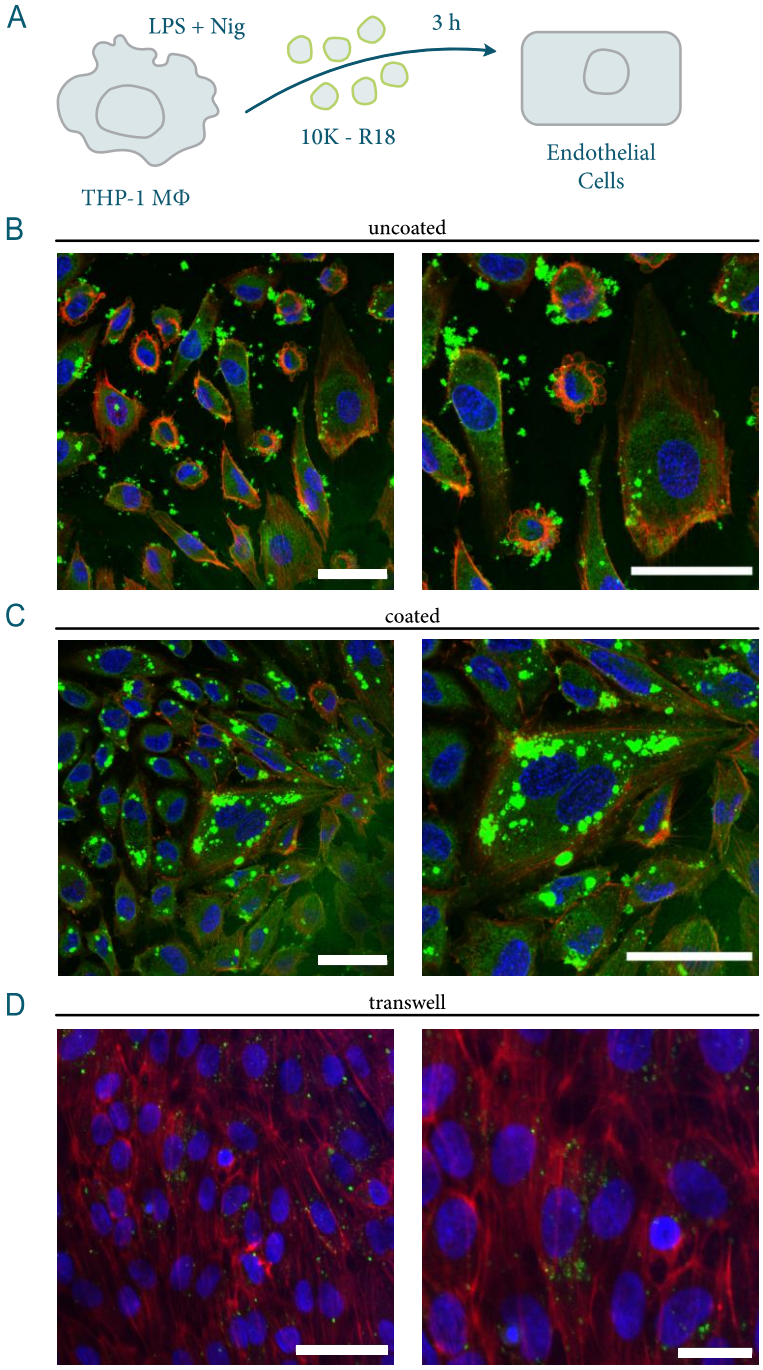

Figure 48: Influence of cell culture conditions on EV uptake. (A) Scheme of the experiment: 10K EVs were isolated from inflammasome-activated THP-1 MΦs and stained with R18 before transfer to HUVECs and incubation for 3 h. F-actin was stained using acti-stain 488 Phalloidin, nuclei were stained using DRAQ5. (B+C) EV uptake by HUVECs cultured on uncoated (B) and fibronectin-coated (C) culture surfaces. Scale bars: 50 μm. (D) EV uptake by HUVECs cultured on fibronectin-coated transwells. Scale bars: 50 μm (left), 20 μm (right). (B–D) F-actin is shown in red, nuclei in blue, EVs in green. (B–D) Representative images, technical replicates = 3, n = 1.

While I decided to use HUVEC transwell cultures for future transfer experiments, I still wanted to investigate the effect culture conditions might have on inflammasome-elicited EV uptake. Leaving out the transwell conditions as different laser powers needed to be used for microscopy, thus making these samples quantitatively incomparable, I compared EV uptake for HUVECs cultured on coated versus uncoated surfaces (Figure 49A). Inflammasome-elicited EVs from THP-1 MΦs were isolated and stained with CFSE (10K) or R18 (SEC). Stained EVs were transferred to HUVECs grown on fibronectin-coated and uncoated culture surfaces (Figure 49B). EV uptake was determined using the previously described analysis pipeline. Indeed, as suspected, HUVECs grown on fibronectin-coated surfaces, within a 3 h time course, take up more 10K and SEC EVs than HUVECs directly grown on uncoated culture surfaces (Figure 49C). This finding is especially important as it underlines the importance of carefully finding a suitable culture system for cells used in transfer experiments instead of just defaulting to the simplest culture system.

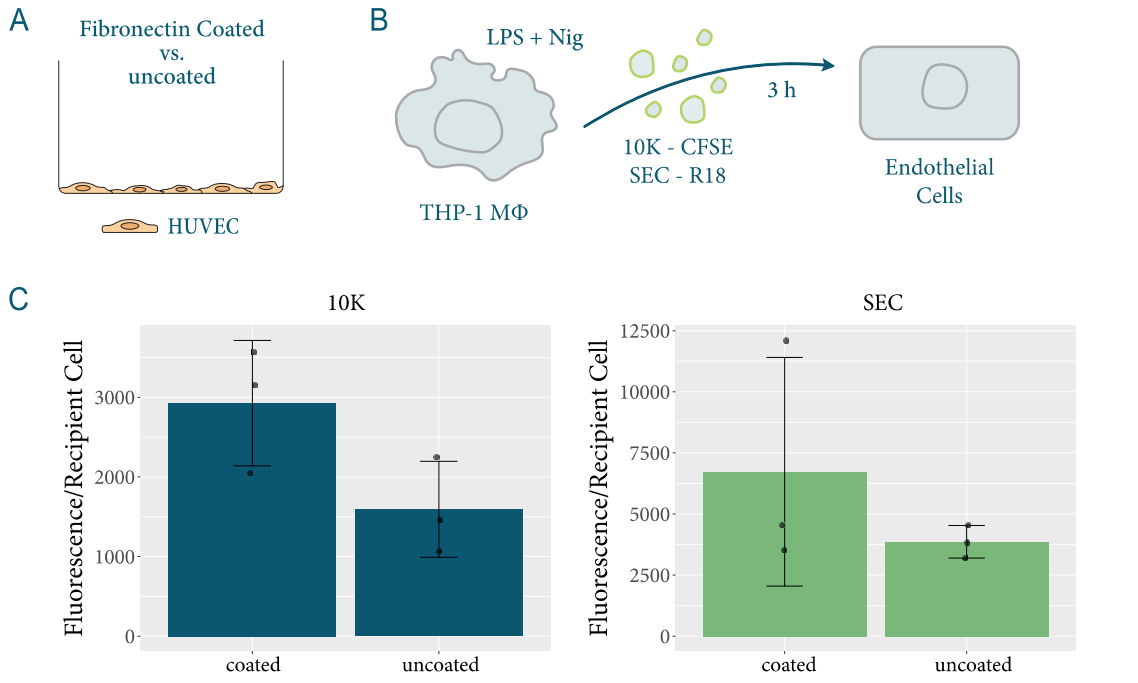

Figure 49: Quantification of the influence of cell culture conditions on EV uptake. (A) HUVECs were grown either directly on culture surfaces or on fibronectin pre-treated culture surfaces. (B) 10K EVs were isolated from inflammasome-activated THP-1 MΦs and stained with CFSE (10K) or R18 (SEC) before being transferred to HUVECs and incubated for 3 h. Nuclei were stained using DRAQ5. (C) 10K and SEC EV uptake by HUVECs cultured on uncoated

and fibronectin-coated culture surfaces. Representative figure showing the mean ± SD of technical replicates of one experimental run. Technical replicates = 3, n = 2.

After investigating different culture systems for HUVECs, I checked whether they interact with or take up EVs after 15 h of co-incubation, the timepoint used for later RNA-seq experiments. EVs were isolated from inflammasome-activated THP-1 MΦs and stained with CFSE (10K) and R18 (SEC). Co-incubation was performed for 15 h with HUVECs grown on fibronectin-coated culture surfaces (Figure 50A). Note that while the transwell culture system was chosen for the RNA-seq transfer experiment, EV uptake after 15 h was assessed using the fibronectin-coated culture system to be able to properly visualise EVs. Uptake of both 10K and SEC EVs was observed (Figure 50B+C).

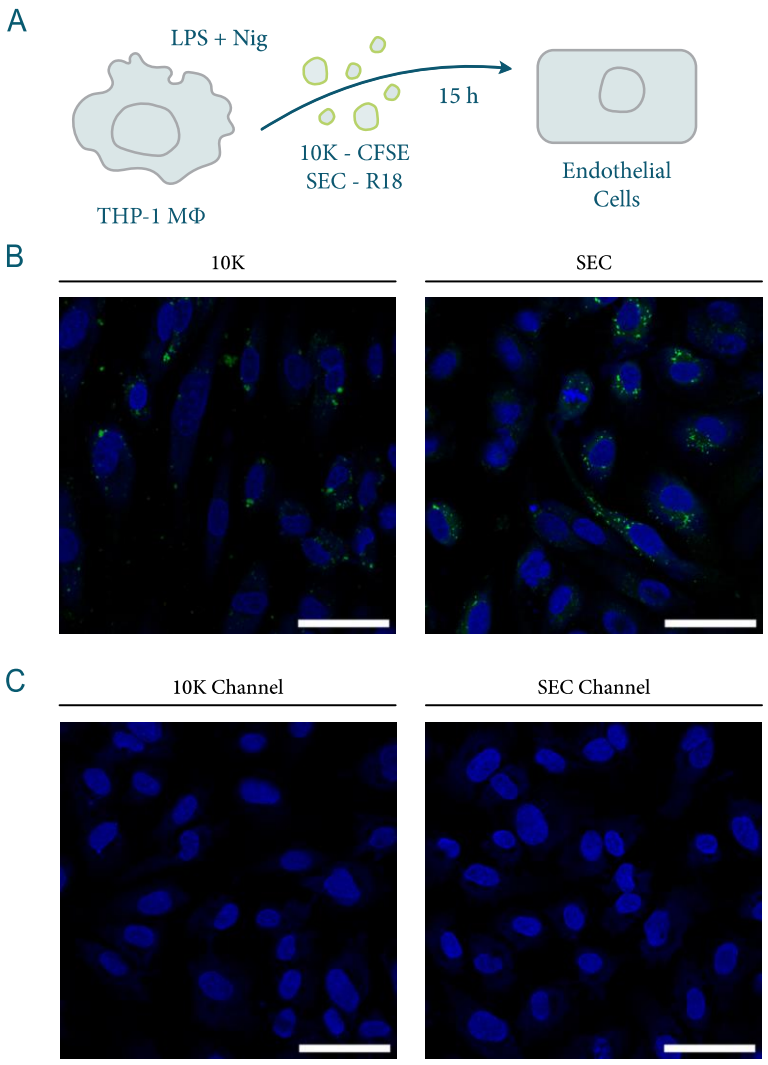

Figure 50: EV uptake by endothelial cells after 15 h. (A) Schematic representation of experimental plan. THP-1 MΦ-derived inflammasome-elicited EVs were isolated and stained with CFSE (10K) and R18 (SEC) before being transferred to HUVECs grown on fibronectin-coated culture surfaces. Nuclei were stained using DRAQ5. (B) 10K and SEC uptake after 15 h incubation with CFSE/R18-stained EVs. (C) Cell-only controls imaged with 10K microscopy settings and SEC settings. (B+C) Nuclei are shown in blue, EVs in green. Scale bars: 50 μm. Representative images, technical replicates = 3, n = 2.

3.3.1.3 Fibroblasts

While culture conditions for HUVECs and especially for NHBECs are more complex, fibroblasts can be cultured directly on culture surfaces commonly used in cell culture. After finding a suitable cell density, EV uptake was thus directly studied. THP-1 MΦs were stimulated with LPS and nigericin to induce inflammasome activation and EVs were isolated and stained with CFSE (10K) or

R18 (SEC). Stained EVs were transferred to recipient fibroblasts and cells were incubated for 15 h (Figure 51A). Successful EV uptake was visualised for both 10K and SEC EVs (Figure 51B+C).

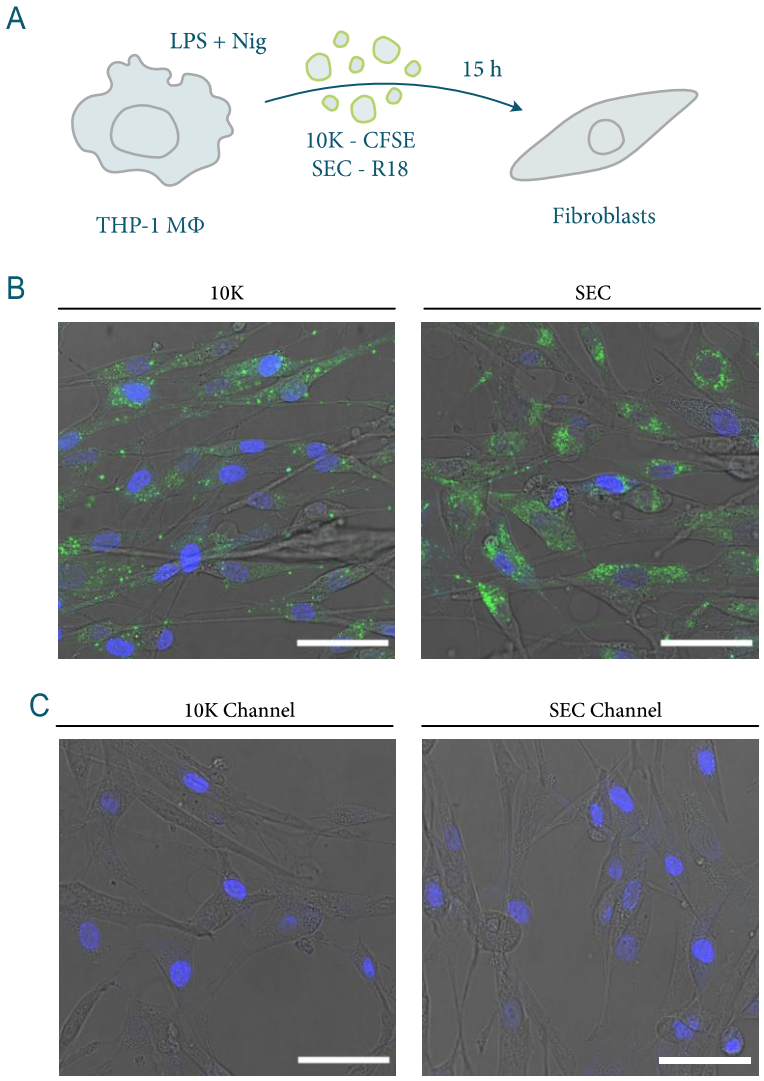

Figure 51: EV uptake by fibroblasts after 15 h. (A) Schematic representation of experimental plan. THP-1 MΦ-derived inflammasome-elicited EVs were isolated and stained with CFSE (10K) or R18 (SEC) before being transferred to fibroblasts grown on standard culture surfaces. (B) 10K and SEC uptake after 15 h co-incubation with CFSE/R18-stained EVs. (C) Cell-only controls imaged with 10K microscopy settings and with SEC settings. (B+C) Nuclei are shown in blue, EVs are shown in green. Scale bars: 50 μm. Representative images, technical replicates = 3, n = 3.

3.3.1.4 T cells

NHBECs, HUVECs and NHLFs were all purchased. T cells on the other hand were directly isolated from human blood. Firstly, PBMCs were purified using Ficoll. T cells were then isolated using the StemCell EasySep Human T cell isolation kit according to the manufacturer's instructions. This kit employs negative selection of T cells. T cell purity was checked using flow cytometry (Figure 52). Naïve T cells were then directly used for transfer experiments. To activate T cells, 96-well plates were coated with CD3 and CD28 antibodies and cells were grown on these plates for 7 days. T cells were cultured in the presence of IL-2.

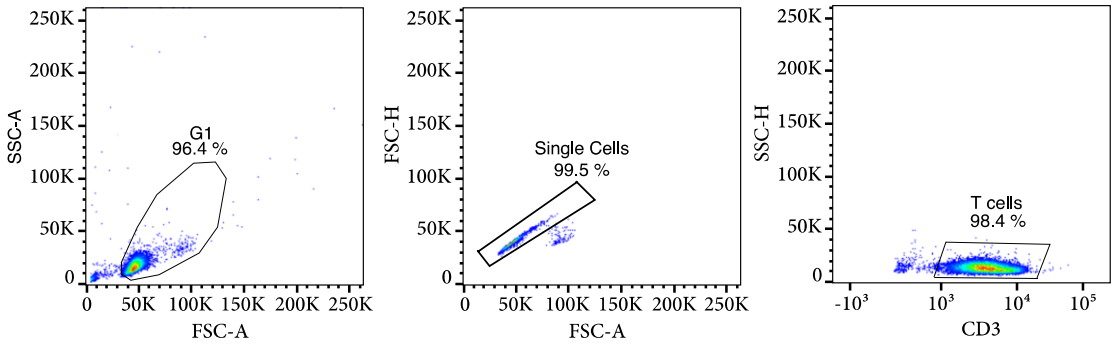

Figure 52: Isolation of T cells from human blood. Flow cytometry gating to determine T cell purity. T cells were stained for CD3. Data obtained by Lea Jenster. Representative of n = 2.

Both activated and naïve T cells were used for transfer experiments. Inflammasome-elicited EVs were isolated and stained with CFSE (10K) or R18 (SEC) and incubated with naïve and activated T cells for 15 h (Figure 53A). EV uptake was visualised under the microscope. While NHBECs, HUVECs and NHLFs are adherent cells, T cells are suspension cells. In case of adherent cells, EVs that had not bound to recipient cells nor had been taken up by recipient cells were washed away with PBS before fixation. This was not possible in case of T cells. Instead, PFA was directly added to the wells (together with DRAQ5 to stain nuclei). Thus, it had to be ensured that EVs are really inside cells. This was achieved through z-stacks and by looking at cell size in bright field images. This is of course suboptimal, but it nevertheless gives an impression of whether or not T cells take up inflammasome-elicited EVs. Results are shown in Figure 53B.

Uptake of 10K EVs was not observed in case of naïve T cells, but could be demonstrated for activated T cells, although only a few EVs were taken up and only by a few cells (Figure 53B). SEC EV uptake was observed for a few naïve T cells and for most activated T cells (Figure 53B).

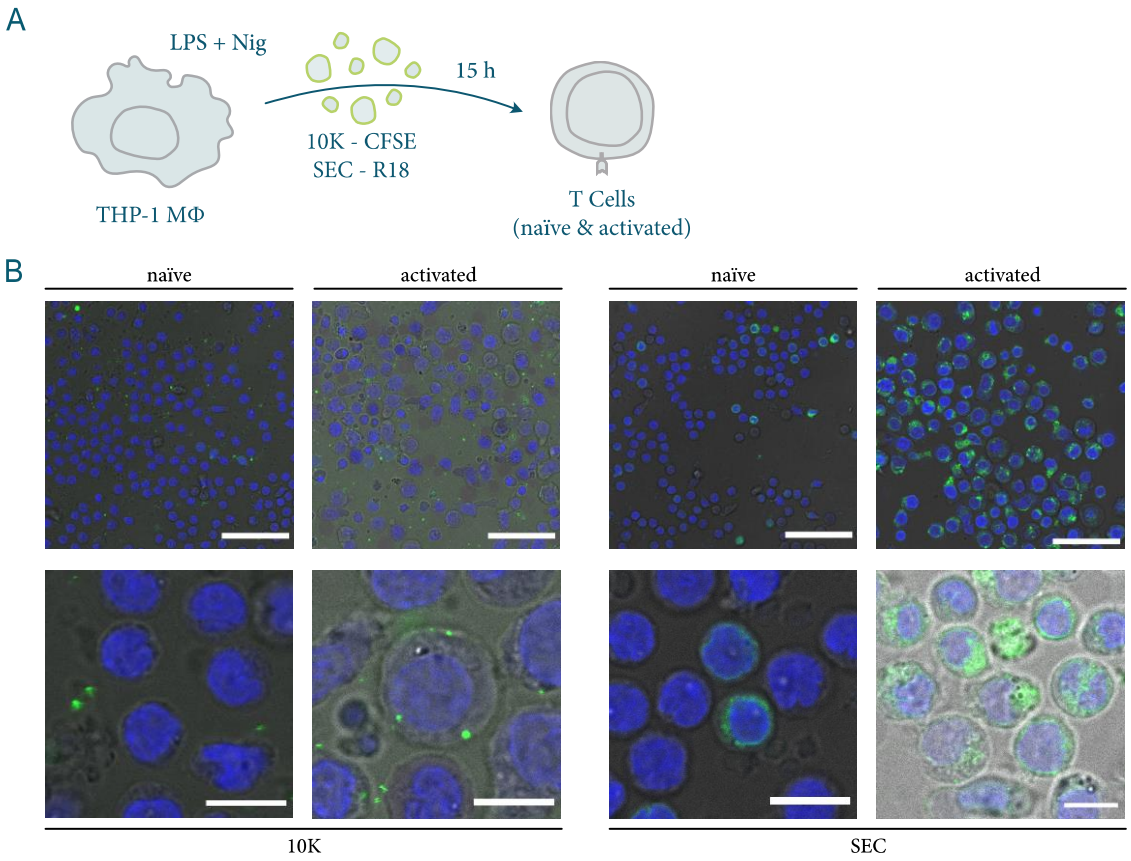

Figure 53: EV uptake by naïve and activated T cells after 15 h. (A) Schematic representation of the experimental plan. THP-1 MΦ-derived inflammasome-elicited EVs were isolated and stained with CFSE (10K) or R18 (SEC) before being transferred to naïve or activated T cells. Nuclei were stained using DRAQ5. (B) 10K and SEC uptake after 15 h incubation with CFSE/R18-stained EVs. Nuclei are shown in blue, EVs in green. Scale bars top row: 50 μm, bottom row: 10 μm. Representative images, technical replicates = 3, n = 3.

3.3.2 Transcriptomic Changes in Recipient Cells After Transfer of Inflammasome-Elicited EVs

Having established suitable culture conditions for the different recipient cells and having studied how they interact with EVs, the effect of inflammasome-elicited EVs on these cells was studied using RNA sequencing. While the EV isolation, transfer of EVs to the different recipient cells, and cell lysis was performed in our

lab, we collaborated with Dr. Jonathan Schmid-Burgk and Marius Jentzsch for the library preparation and sequencing. They have established a library preparation protocol that reduces the pipetting steps of a classical library preparation and skips the step of RNA isolation from cell lysates. Instead, lysates can directly be used.

To test whether this procedure is also suitable for our application and, if so, which conditions to use, we first tested the protocol in two pilot experiments (Figure 54). In the first pilot experiment, sequencing conditions for EVs were tested (Figure 54A). EVs were either directly lysed with RLT buffer and RNA was isolated using RNeasy plus micro kits or a dry EV pellet was frozen. Both samples were stored at −80°C before processing. Additionally, EVs were directly lysed after isolation using different amounts of buffer. Samples were then processed in Dr. Jonathan Schmid-Burgk's lab by Marius Jentzsch. He either directly used lysates or first purified the RNA using a bead-based RNA purification approach. After performing whole transcriptome amplification (WTA), gels were run to determine fragment sizes. Direct lysis of EVs in 10 μL of lysis buffer led to the best results (Figure 54A).

Having established good sequencing conditions for EVs, conditions for the different recipient cells were established in a second pilot experiment (Figure 54B). Cells were lysed in either 100 μL or 200 μL lysis buffer and directly used for WTA or lysed in 100 μL followed by bead-based RNA purification before WTA was performed. Best results were achieved using 100 μL lysis buffer (Figure 54B).

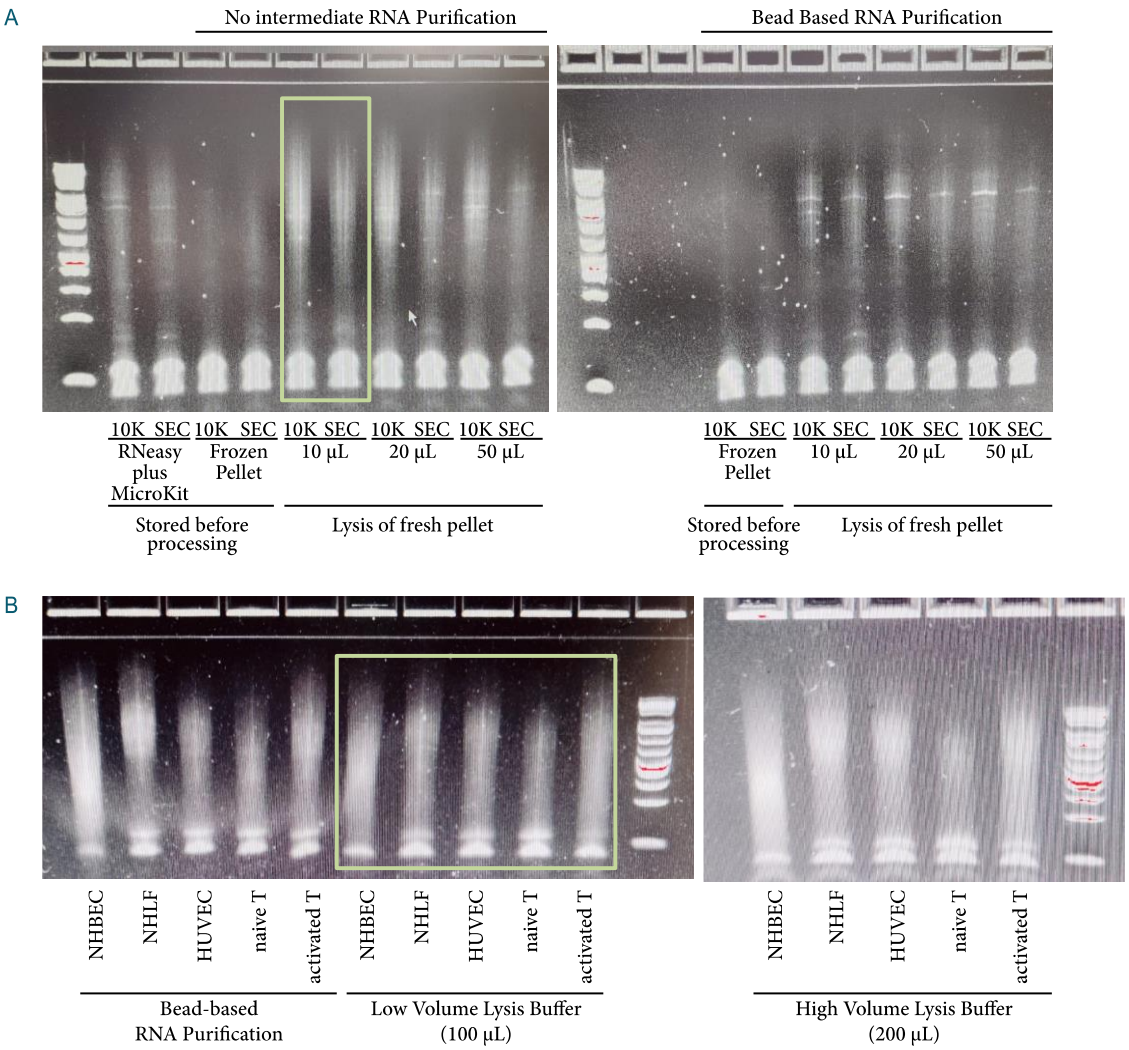

Figure 54: Establishment of sequencing conditions. (A) Different sequencing conditions for isolated EVs were tested. EVs were isolated and either lysed in RLT buffer followed by RNA isolation with the RNeasy plus micro kit or the isolated EV pellet was directly frozen. Both samples were stored at −80°C before further processing. Alternatively, EVs were isolated and freshly lysed in different volumes of lysis buffer. WTA was performed either on direct lysates or on RNA purified by bead-based isolation. (B) The different recipient cells were lysed in either 100 µL or 200 µL lysis buffer and directly used for WTA. Alternatively, cells were lysed in 100 µL lysis buffer and bead-based RNA purification was performed before lysis. Data obtained by Marius Jentzsch. n = 1.

Additionally, Dr. Jonathan Schmid-Burgk and Marius Jentzsch sequenced and analysed the above-mentioned samples and confirmed that library preparation and sequencing conditions were suitable for the different cell- and vesicle types (data not shown).

After establishing cell culture conditions, checking for EV uptake/interaction after 15 h, and finding suitable sequencing conditions, the actual transfer experiment was performed. THP-1 MΦs were stimulated with LPS and nigericin to activate the NLRP3 inflammasome or just with LPS (control). 10K and SEC EVs from both conditions were isolated and transferred to NHBECs, HUVECs, NHLFs, naïve T cells and activated T cells and incubated for 15 h. As controls, the different recipient cells were stimulated with LPS (2 h), Nigericin (1.5 h), or left untreated. All different recipient cells, as well as part of the transferred vesicles, were lysed and RNA-seq was performed (Figure 55).

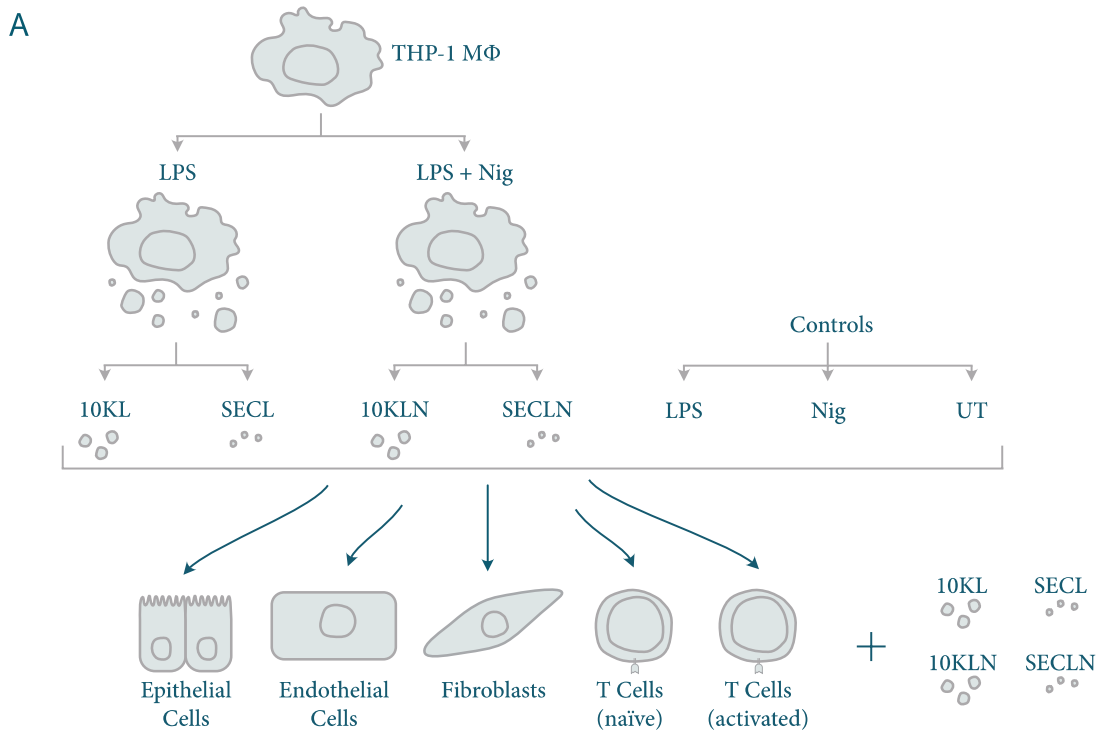

Figure 55: The effect of inflammasome-elicited THP-1 MΦs on different recipient cells. (A) Schematic representation of experimental plan. THP-1 MΦs were stimulated with either LPS only (control) or LPS + nigericin. 10K and SEC EVs were isolated from both conditions and transferred to different recipient cells: NHBECs, HUVECs, NHLFs, naïve and activated T cells. Recipient cells were also directly stimulated with LPS (2 h), nigericin (1.5 h), or left untreated. Recipient cell supernatant was taken directly before lysis. Cells, as well as part of the transferred vesicles, were lysed and used for RNA-seq. n = 5.

Supernatants were taken directly before cell lysis and TNF-α and IL-1β protein levels were determined (Figure 56B). The highest TNF-α levels were observed for naïve (~1800 pg/mL) and activated T cells (~2500 pg/mL) after transfer of 10K

EVs from inflammasome activated cells (Figure 56B). The highest IL-1β levels were observed after transfer of 10K EVs from inflammasome activated cells to HUVECs (~750 pg/mL), NHLFs (~1250 pg/mL), naïve (~500 pg/mL) and activated T cells (~500 pg/mL). NHBECs showed little TNF-α and IL-1β secretion (Figure 56B). As TNF-α levels are different between cell types, it is probably an induction of these cytokines instead of just a transfer through 10K vesicles. If it were just a transfer, the same levels should be observed for all cell types—with the exception of NHBECs: here EVs and stimuli were applied on the apical side (upper) and supernatants were taken from the basal side (lower) as there was no medium in the upper chamber (which was exposed to air). In the case of IL-1β, it cannot be ruled out that the IL-1β is transferred through the 10K EVs.

Figure 56: Cytokine secretion after inflammasome-elicited EV transfer to different recipient cells. (A) Schematic representation of the experimental plan. The effect of EVs on epithelial cells (NHBECs), endothelial cells (HUVECs), fibroblasts (NHLFs), and T cells (naïve and activated) was studied. (B) TNF-α and IL-1β protein levels after stimulation of NHBECs, HUVECs, NHLFs, and naïve and activated T cells with 10K and SEC EVs from either LPS or LPS + Nig stimulated THP-1 MΦs. Mean ± SEM. n = 5.

Cell and EV lysates were given to Marius Jentzsch for library preparation and sequencing using the NextSeq 2000 Illumina sequencer. Even though sequencing of EVs themselves worked in the pilot experiment, it was not successful for this experiment. Thus, only the effect on recipient cells could be analysed (Figure 56A). Additionally, sequencing depth for recipient cells, especially for NHBEC and naïve T cells, was very low. It was thus decided to re-sequence the whole library to increase sequencing depths. One problem of the library preparation approach used is that RNA input levels for different samples differ as, without direct RNA isolation, there is no RNA quantification step. This led to HUVEC, NHLF, and activated T cell samples being overrepresented and NHBEC and naïve T cell samples being underrepresented (Figure 57B). We therefore decided, in addition to the re-sequencing of the whole library, to prepare a separate library for NHBEC and naïve T samples. However, after trying to do so, Marius Jentzsch reported that this was no longer possible, as samples were already too degraded. As a result, the sequencing analysis had its limits and could only detect major transcriptomic changes, mainly for HUVEC cells, NHLFs, and activated T cells.

Read alignment and data analysis was performed by me with the help of Dr. Jamie Gearing. Reads were aligned to the human genome using the Rsubread package. Genes were annotated and raw counts were converted to $\log_2$CPM. MDS plots of the raw data showed a dependence on library size (Figure 57A); thus, filtering was performed to remove samples with library sizes less than or equal to 1×10^4. While this is still a very small library size, we wanted to try to perform at least some comparisons in the NHBEC and naïve T cells, and thus decided for this cut-off. It led to the exclusion of 32 samples with library sizes ranging from 14 to ~9.9×10^3 with a mean of ~4.0×10^3 reads and leaving samples with library sizes ranging from ~1.2×10^4 up to ~2.6×10^7 with a mean of 2.9×10^6 (Figure 57B). Filtering for larger library sizes removed many of the NHBEC and naïve T cell samples, thus decreasing group sizes for these cell types (Table 1).

Cell Type	10KL	10KLN	SECL	SECLN	LPS	Nig	UT
NHBEC	1	4	2	2	3	3	3
HUVEC	5	5	5	5	5	5	5
NHLF	5	5	5	5	5	5	5
Naïve T cell	4	3	3	3	3	2	2
Activated T cell	5	5	5	5	5	5	5

Table 1: Group sizes. The number of samples remaining per group after removing samples with library sizes smaller than 1×10^4. Group sizes are represented by colour.

Next, lowly expressed genes were removed, leaving ~3.9×10^4 genes in the analysis, and normalisation was performed. After sample pre-processing, samples clustered (in the first two dimensions) according to cell type (Figure 57C), but not stimulation (Figure 57D).

For the differential expression analysis, linear modelling was performed. A design matrix was set up using the sample group (cell type and treatment) and, for each cell type, pairwise comparisons were made between the different stimulations and untreated samples. Linear modelling was performed on $\log_2$CPM values with accommodated mean-variance relationships using precision weights calculated using the voom method with the voomLmFit function (Figure 58A). Moderated t-tests were performed using either eBayes or treat. Treat was used with a $\log_2$ fold change threshold of 1. The number of significantly up- or downregulated genes for each comparison is shown in Figure 58B determined by either the eBayes function (left) or the treat function with a $\log_2$ fold change threshold of 1 (right). Most DE genes are found in NHLFs, followed by HUVECs. The eBayes function is less stringent, since it does not apply a $\log_2$ fold change threshold, and thus more DE genes are found. In case of HUVECs, most DE genes are found upon treatment with 10K EVs from inflammasome-activated cells, both using eBayes and treat. In the case of NHLFs, the most DE genes are found upon treatment with 10K EVs from LPS-only stimulated cells (eBayes) or 10K EVs from inflammasome-activated cells (treat). In NHLFs, SEC EVs also seem to have an influence on cells (Figure 58B).

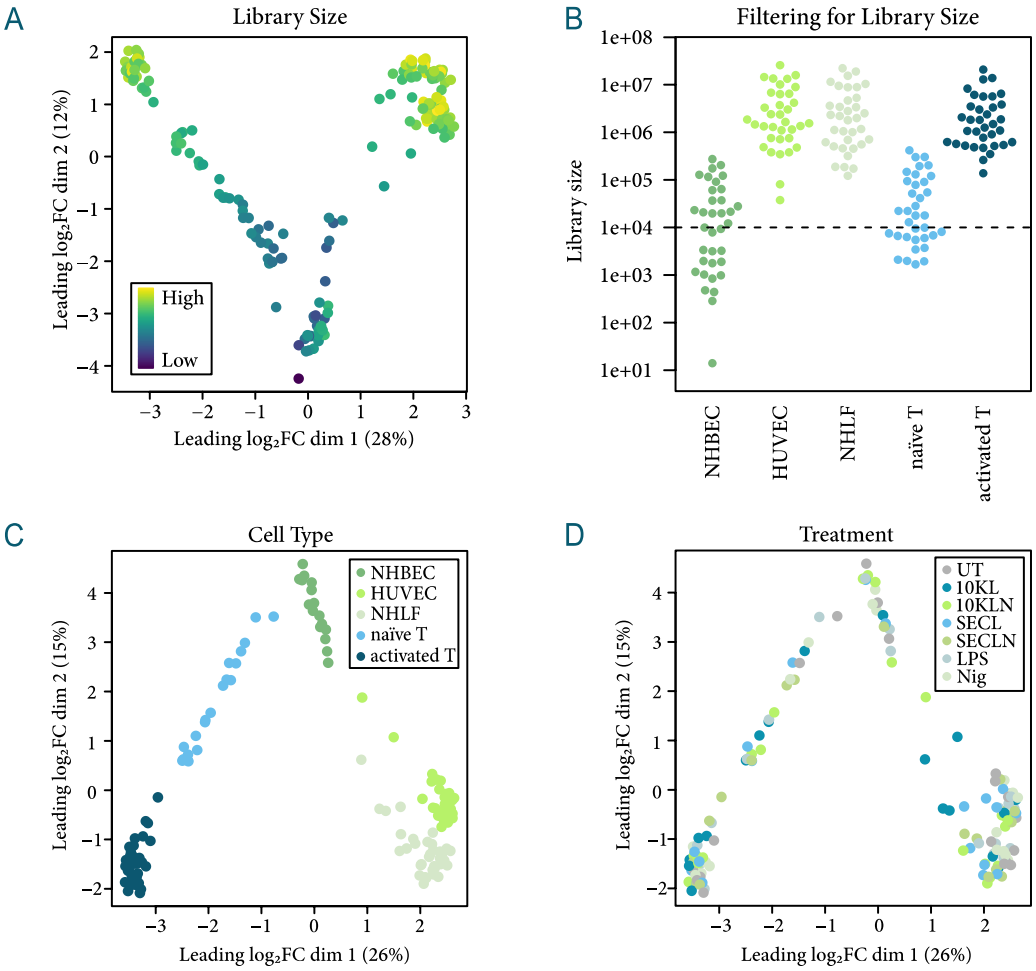

Figure 57: Overview of the effect of THP-1 MΦ inflammasome-elicited EVs on different recipient cells. (A) MDS plot showing sample relationships, coloured by library size. (B) Plot showing the library sizes for the different samples, coloured by cell type. Dashed line indicates the filtering cut-off at 1 x 10^4. Samples below this cut-off were removed from the analysis. (C+D) MDS plots showing sample relationships, coloured by cell type (C) or stimulation (D). (A-D) n = 5.

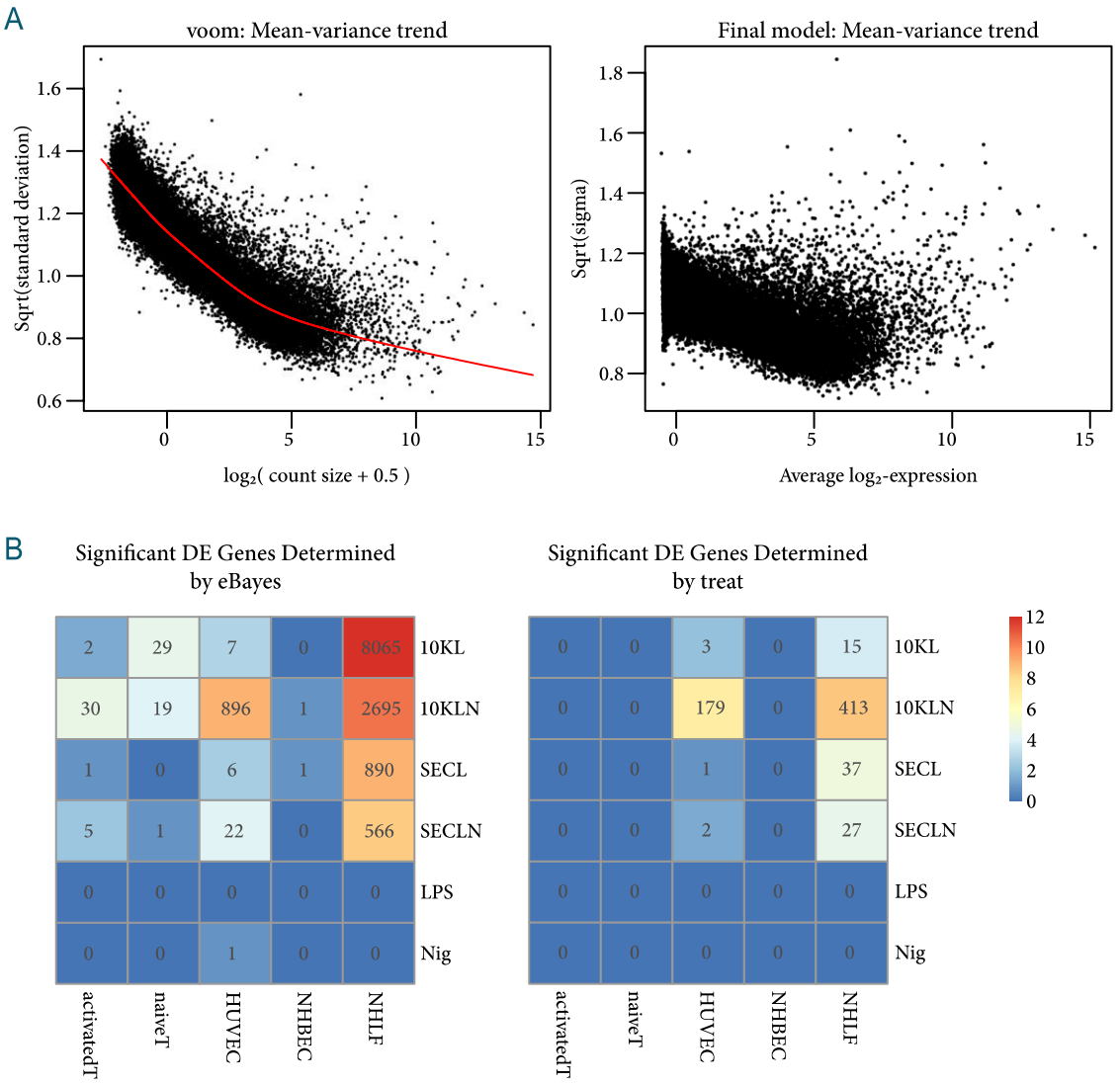

Figure 58: Linear modelling to determine significantly differentially expressed genes. (A) Means (log_2(count size + 0.5) on the left and mean log_2CPM values on the right) of each gene are shown on the x-axis with corresponding variances (square-root of standard deviations on the left and residual standard deviations on the right) on the y-axis, showing the dependency between genes and variances before applying the voom function (left) and once it has been applied and the trend removed through the application of voom precision weights (right). The red line indicates the estimated mean-variance trend used to compute the voom precision weights. (B) Heat maps showing the numbers of significantly differentially expressed genes (either up- or downregulated) for each cell type for each comparison (all stimuli compared to untreated). DE genes were determined either by applying the eBayes function or the treat function with a log_2 fold change threshold of 1. The number of DE genes is represented by the colour (log_2 of the number of DE genes + 1) and the actual number of DE genes found is indicated within each square. (A+B) n = 5.

3.3.2.1 Epithelial Cells

After investigating the distances between all samples from all cell types, MDS plots were generated separately for every cell type. In the case of NHBECs, neither dimensions one and two nor three and four showed clustering of samples according to treatment (Figure 59B). Only two DE genes were found: *PCM1* was found to be downregulated upon treatment of NHBECs with 10KLN EVs compared to the untreated condition (Figure 59C). *OASL* was found to be upregulated upon treatment of NHBECs with SEC EVs from LPS-only stimulated cells (Figure 59C). NHBEC library sizes were quite small compared to library sizes of other cell types (Figure 56D) and Marius Jentzsch reported a lot of problems when preparing the library and sequencing these cells.

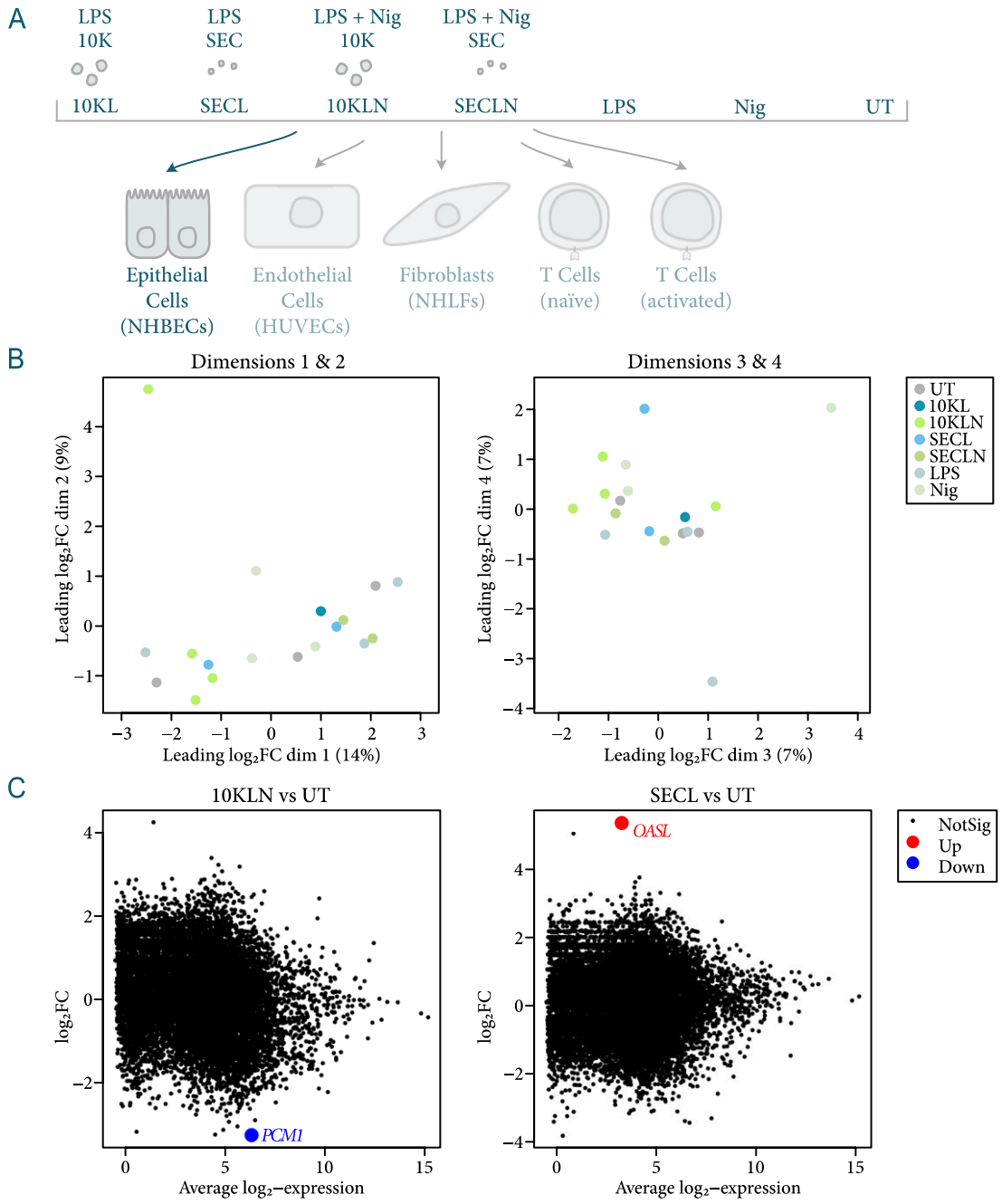

Figure 59: Effect of inflammasome-elicited EVs on epithelial cells. (A) NHBECs were treated with 10K and SEC EVs from LPS-stimulated THP-1 MΦs, 10K and SEC EVs from LPS + nigericin-stimulated THP-1 MΦs, as well as with LPS, nigericin, or they were left untreated. n = 5. (B) MDS plots of leading log_2FC (average (root-mean-square) log_2FC for the 500 genes most different between samples) over dimensions one and two (left) and three and four (right), coloured by stimulations. (C) Mean-difference plot showing significantly up (red)- or down (blue)-regulated genes in NHBECs stimulated with 10KLN EVs (left) or SECL EVs (right) compared to untreated. *PCM1*: Pericentriolar Material 1. *OASL*: 2'-5'-Oligoadenylate Synthetase-Like.

One reason for not seeing many DE genes in NHBEC samples could be that the library preparation or sequencing of these cells failed, resulting in small library sizes and, for half of the stimulations, only one or two samples. This makes it very hard to detect statistically significant changes, especially when the effect is subtle.

Another reason could be that these cells are not very reactive. In addition to analysing the effect of inflammasome-elicited EVs on the transcriptome of epithelial cells through RNA-sequencing, qPCR was performed. While RNA-sequencing allows a broad, unbiased analysis, qPCR requires the preselection of targets. Based on our previous results that showed that inflammasome-elicited 10K EVs induce interferon-stimulated gene (ISG) expression in recipient MΦs, we checked for some common ISGs. In addition of treating NHBECs with different EVs, we used IFN-β as a control (10KLN, SECLN, and IFN-β were applied on top of cells, except for one condition where 10KLN and SECLN were combined and applied to the bottom chamber; Figure 60A). While we expected to see upregulation of the selected ISGs, we barely saw any reaction to IFN-β (Figure 60B). NHBECs also showed little to no changes in ISG gene expression after EV treatment (Figure 60B). 10KLN stimulation did, however, lead to the upregulation of TNF-α (Figure 60B). In the RNA-seq data, TNF-α was not detected, probably because of the extremely small library sizes that did not allow the detection of genes with low baseline expression. And even if there would have been a strong induction, it might have still ended up below the limit of detection. While the qPCR data hints that NHBECs might not respond much to IFN-β stimulation, they might of course still respond to other stimuli. Additionally, the experiment was only performed once and a rather long timepoint for IFN-β stimulation of 15 h was chosen (a shorter timepoint would have been better with regards to a maximal response), so results have to be interpreted with caution.

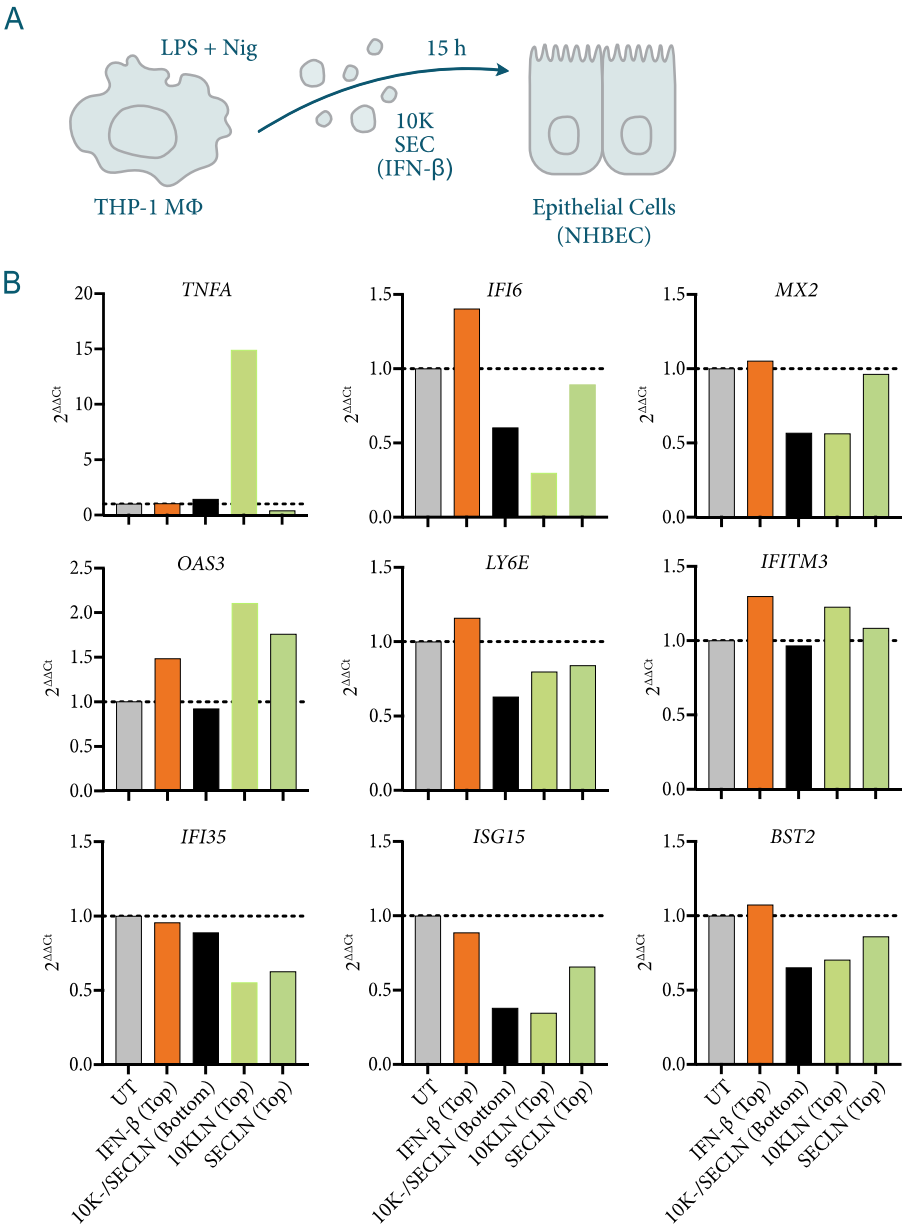

Figure 60: Effect of inflammasome-elicited EVs on ISG expression in epithelial cells. (A) NHBECs were treated with 10K and SEC EVs from LPS + nigericin stimulated THP-1 MΦs, as well as with IFN-β, or they were left untreated. 10KLN, SECLN, and IFN-β were applied to the top chamber of ALI cultures, while a mixture of 10KLN and SECLN EVs was applied to the bottom chamber. All stimuli were applied for 15 h. (B) RNA was isolated from NHBECs and qRT-PCR was performed. n = 1.

3.3.2.2 Endothelial Cells

Library preparation and sequencing of HUVEC samples was more successful, which was reflected in the number of DE genes found (Figure 58). MD plots of samples for dimensions one and two and for dimensions three and four show clustering of samples treated with 10KLN EVs (especially in dimensions three and four; Figure 61B). Figure 61C shows significantly up- or downregulated genes for these samples compared to UT samples. The top 20 DE genes for 10KLN compared to untreated samples are shown in Figure 61D. *AQP1*, *NTN4*, and *ADGRG6* were downregulated in HUVECs treated with 10KLN EVs. Other genes such as selectin E (*SELE)*, colony stimulating factor (*CSF)3*, C-C Motif Chemokine Ligand (*CCL)2*, *CCL20*, C-X-C Motif Chemokine Ligand (*CXCL)2*, *TLR2*, or superoxide dismutase 2 (*SOD2)* and matrix metalloproteinase (*MMP)10* were upregulated (Figure 61D).

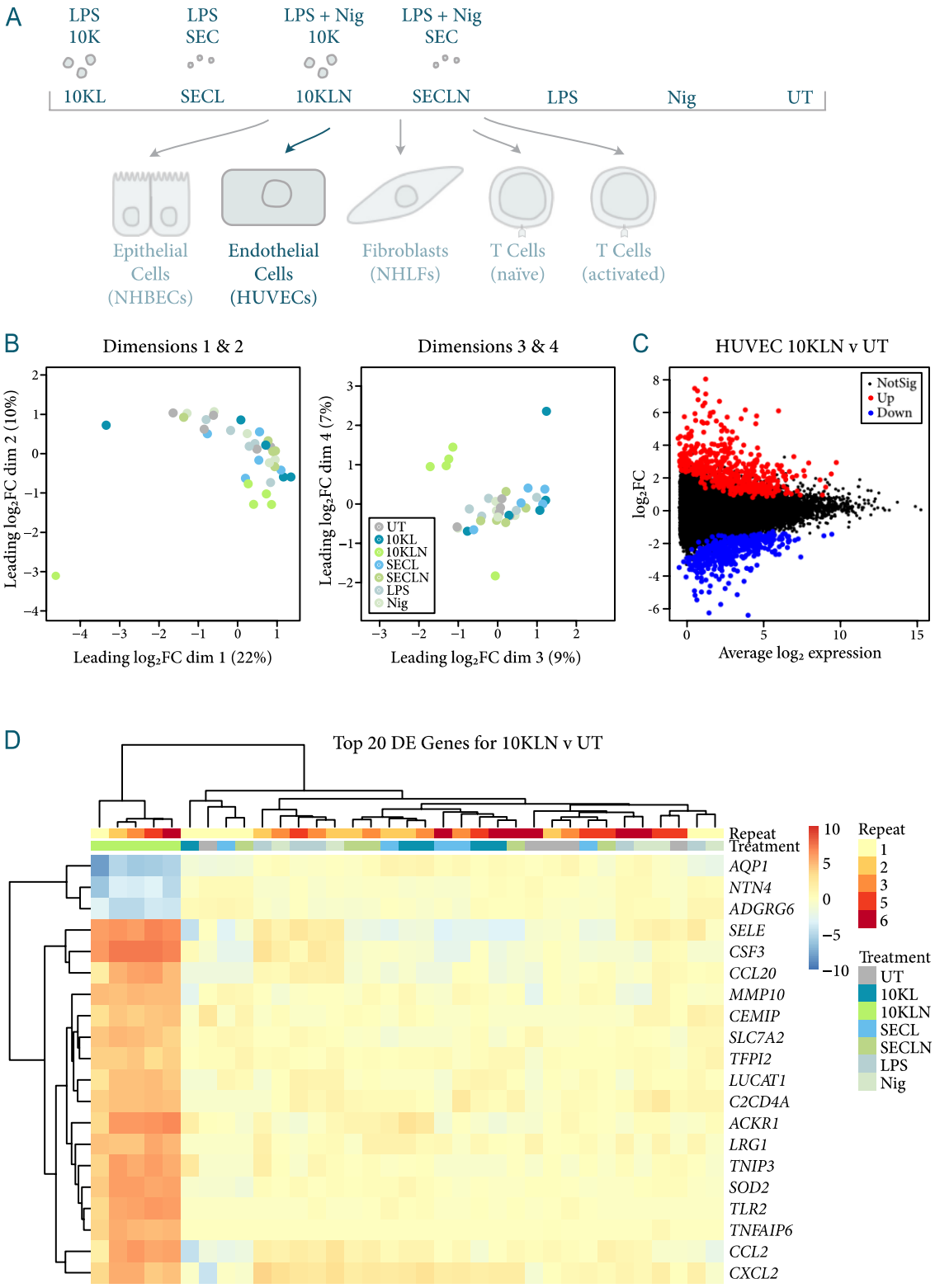

Figure 61: Effect of inflammasome-elicited EVs on endothelial cells. (A) HUVECs were treated with 10K and SEC EVs from LPS-stimulated THP-1 MΦs, 10K and SEC EVs from LPS + nigericin-stimulated THP-1 MΦs, as well as with LPS, nigericin, or they were left untreated.) n = 5. (B) MDS plot of leading log_2FC (average (root-mean-square) log_2FC for the 500 genes most different between

samples) over dimensions one and two (left) and three and four (right) coloured by stimulations. (C) Mean-difference plot showing significantly up (red)- or down (blue)-regulated genes in HUVECs stimulated with 10KLN EVs compared to untreated. (D) Heat map showing the top 20 DE genes (ranked by p-value) for 10KLN treated HUVECs compared to untreated HUVECs. The scale shows the relative log_2CPM values (log_2CPM values were normalised to the respective untreated condition).

Gene set testing for MSigDB hallmark gene sets reflects that most change is observed when comparing 10KLN-treated samples to untreated and points toward an involvement of TNF-α-, IFN-α/γ -, and IL-6 signalling (Figure 62B, Table 2). Knowing that inflammatory signalling in endothelial cells can lead to the activation of the endothelium (Szmitko *et al*, 2003; Zhang, 2022), it was checked if some of the upregulated genes are markers of activated epithelium (e.g., *SELE*, *CCL2*, *IL6*, intercellular adhesion molecule 1 (*ICAM1)*, and *MMP1*), which was indeed the case (Figure 62C).

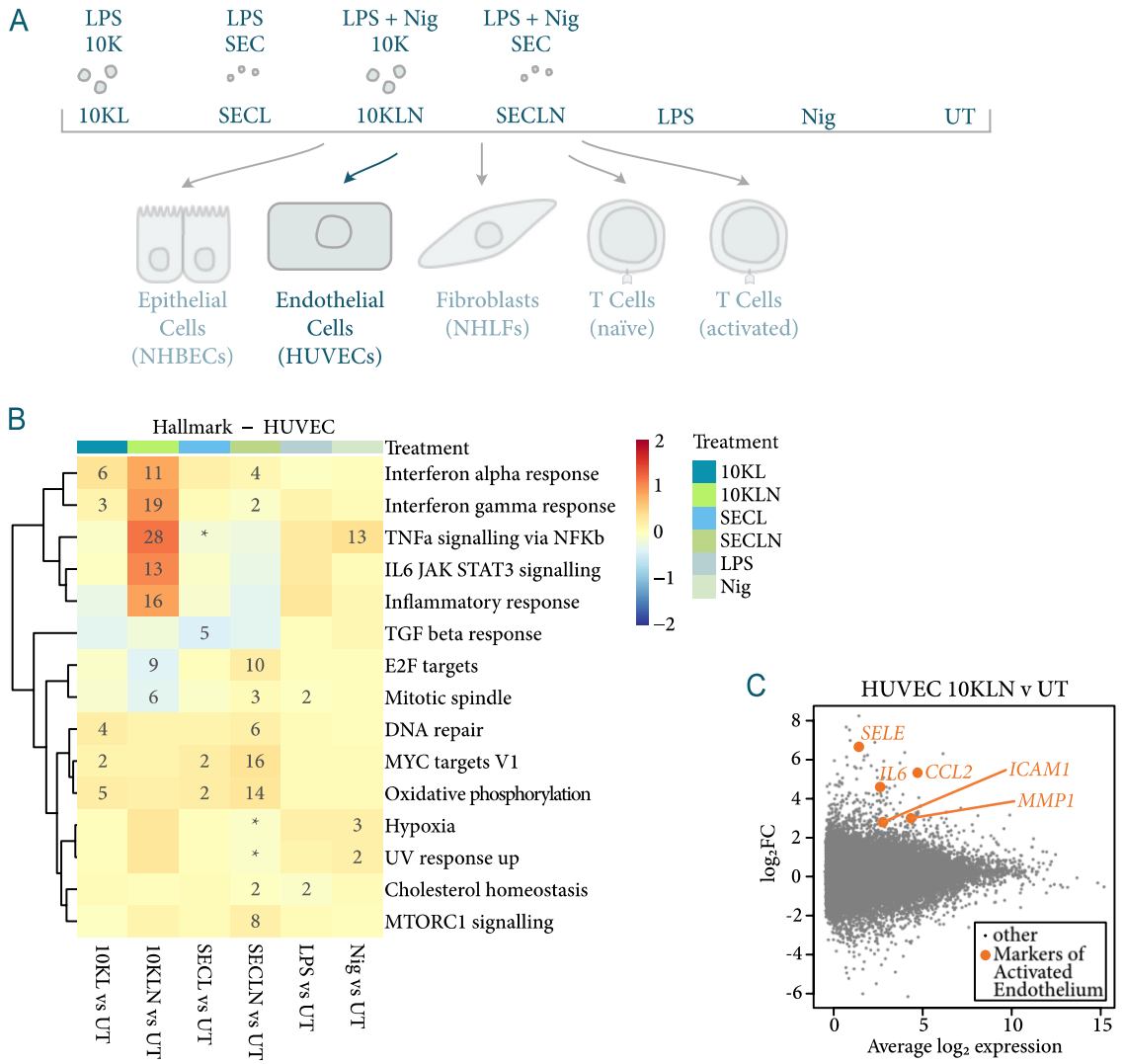

Figure 62: Effect of inflammasome-elicited EVs on endothelial cell activation. (A) HUVECs were treated with 10K and SEC EVs from LPS-stimulated THP-1 MΦs, 10K and SEC EVs from LPS + nigericin-stimulated THP-1 MΦs, as well as with LPS, nigericin, or they were left untreated. n = 5. (B) Gene set testing was performed using the cameraPR function from the limma package. The heat map shows the top MSigDB hallmark gene sets for the different treatments vs untreated cells. The scale shows the average $\log_2$ fold change of the genes in each set. Annotation indicates significance ($-\log_{10}$ adjusted p-value; * $p < 0.1$, 2: $p < 0.01$, 3: $p < 0.001$, …). (C) Mean-difference plot of transcripts in HUVECs stimulated with 10KLN compared to untreated HUVEC cells. Genes commonly found on activated endothelium are highlighted.

	Number of Genes	Direction	p-value	FDR-adj. p-value	Average log_2FC	Top significant genes
TNFa signalling via NFKb	199	Up	3.07e-31	1.50e-29	1.124	*TLR2; TNFAIP6; CCL20; CCL2; CXCL2; NAMPT; CXCL6; PTGS2; LIF; CXCL3; TNFAIP3; F3; CSF2; MSC; IL6; CXCL1; CSF1; TNFAIP2; DNAJB4; TNFAIP8; SAT1; BCL6; ICAM1; SLC2A6; IL7R; ID2; TNIP1; ACKR3; IL1B; TRAF1; ZFP36; GCH1; PTGER4; NFKBIA; TNC; CD69; NR4A3; CCL4; CEBPD; SDC4; JUNB; ZC3H12A; CCN1; SERPINE1; DUSP5; ICOSLG; NFKB1; PLPP3; NFKBIE; FOS; TGIF1; EGR1; IRS2; CCRL2; IER3; SOCS3; CLCF1; LAMB3; TRIB1; AREG; PANX1; NFKB2; SPSB1; BCL2A1; CXCL10; JUN*
Interferon gamma response	198	Up	1.17e-21	2.93e-20	0.917	*TNFAIP6; CCL2; NAMPT; PTGS2; C1R; TNFAIP3; IL6; MT2A; TNFAIP2; C1S; ISG20; CFB; ICAM1; SOCS1; VCAM1; IRF9; PLA2G4A; CCL7; PNP; GCH1; NFKBIA; HLA-B; CD69; IFI27; OAS2; CSF2RB; PSME2; MX1; XAF1; PARP14; NFKB1; IL4R; SPPL2A; SOCS3; OAS3; ARL4A; APOL6; HLA-A; CXCL10*
Inflammatory response	198	Up	4.53e-18	7.55e-17	0.879	*SELE; CSF3; TLR2; SLC7A2; TNFAIP6; CCL20; CCL2; NAMPT; CXCL6; CXCL8; LIF; CX3CL1; F3; IL6; CSF1; EBI3; LPAR1; ICAM1; TIMP1; IRAK2; IL7R; CCL7; IL1B; IL18R1; GCH1; PTGER4; NFKBIA; CD69; AXL; SERPINE1; ICOSLG; ITGB8; APLNR; NFKB1; ADM; CCRL2; IL4R; IFNAR1; KCNJ2; CXCL10; TPBG*
IL6 JAK STAT3 signalling	83	Up	8.04e-16	1.00e-14	1.008	*TLR2; CXCL3; CSF2; IL6; CXCL1; CSF1; EBI3; SOCS1; IRF9; CCL7; IL1B; IL18R1; LTB; CSF2RB; IL4R; IFNAR1; SOCS3; CD36; CXCL10; JUN; PDGFC*
Interferon alpha response	97	Up	1.47e-13	1.47e-12	0.820	*CSF1; C1S; ISG20; IRF9; HLA-C; IFI27; PSME2; MX1; PROCR; PARP14; NCOA7; CCRL2; IL4R; TENT5A; CXCL10; GBP2*
E2F targets	200	Down	6.31e-11	5.26e-10	-0.393	*TOP2A; AURKA; CDCA8; CDC20; DEPDC1; MKI67; H2AX; HMMR; BUB1B; CENPE; MMS22L; CDCA3; E2F8; CKS1B; UBE2S*

Table 2: Hallmark gene sets of 10KLN vs UT HUVEC samples. Hallmark gene sets whose genes were highly ranked in terms of differential expression relative to genes that are not in the set in the comparison of 10KLN samples versus untreated samples in HUVECs. Names of gene sets, number of genes included in each set, directionality (up- or down), p-value, FDR-adj. p-value, average log_2FC, and genes from the sets that were significantly differentially regulated are shown.

3.3.2.3 Fibroblasts

In the case of NHLFs, MDS plots of samples showed a distinct clustering of NHLFs treated with 10K EVs from inflammasome-activated THP-1 MΦs (Figure 63B). Significant genes for NHLFs treated with these 10KLN EVs compared to untreated NHLFs were identified and sorted by FDR-adjusted p-value. The six genes with the lowest FDR-adjusted p-values were *SOD2*, *PTGS2, CXCL8*, *IL6*, *TNFAIP6*, and *TFPI2* (Table 3). The top 20 DE genes for 10KLN compared to untreated samples are shown in Figure 63C.

Gene Name	log_2FC	Average Expression	FDR-adjusted p-value
SOD2	6.23	6.13	3.02×10^{-32}
PTGS2	9.03	2.79	9.91×10^{-31}
CXCL8	10.28	4.66	9.91×10^{-31}
IL6	9.66	2.61	9.91×10^{-31}
TNFAIP6	8.98	0.89	1.45×10^{-27}
TFPI2	7.58	3.13	3.98×10^{-27}

Table 3: DE genes between 10KLN and untreated NHLFs. DE genes with the lowest adjusted p-values according to eBayes are shown. Gene names, log_2FC, average expression and FDR-adjusted p-values are shown.

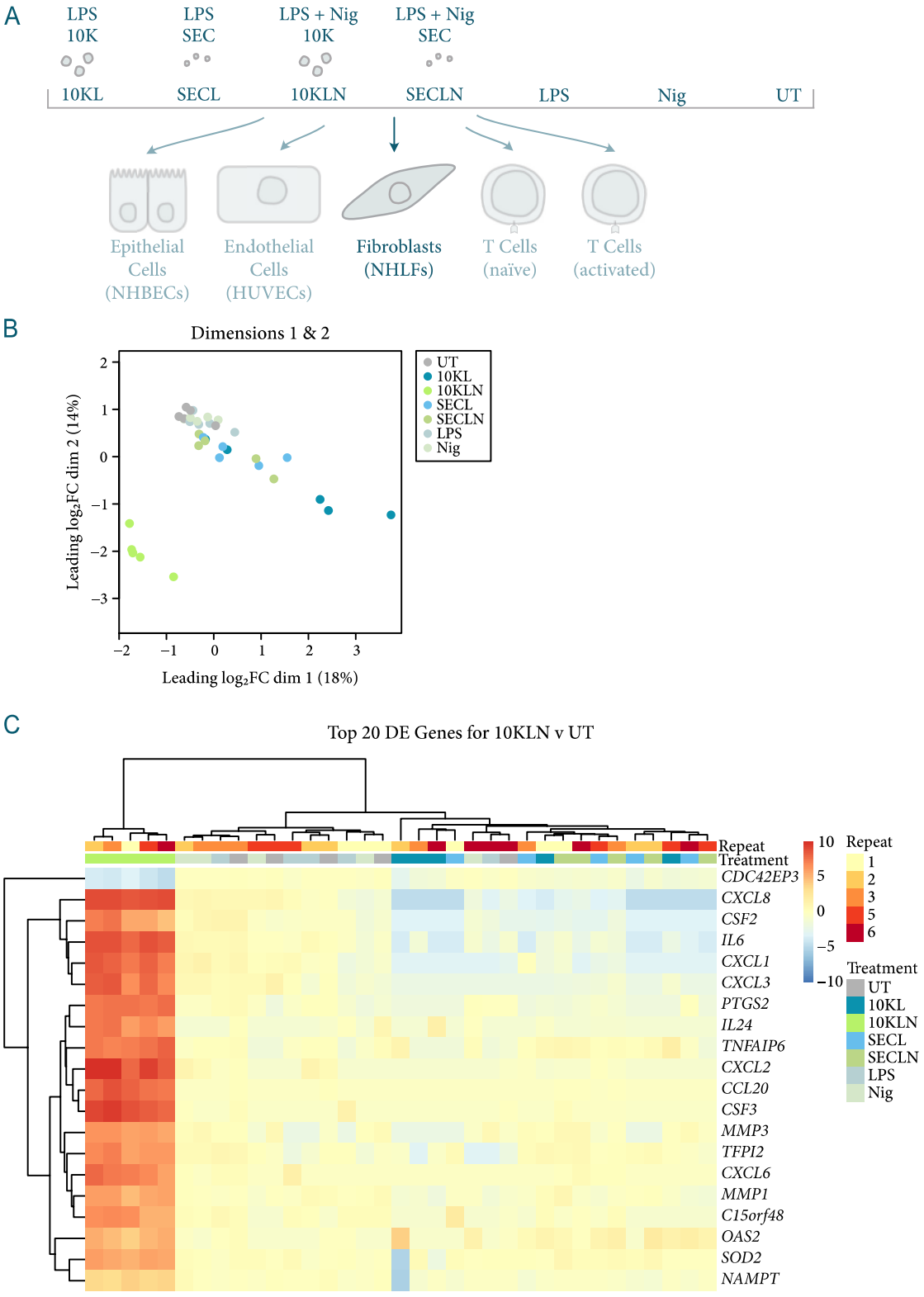

Figure 63: Effect of inflammasome-elicited EVs on fibroblasts. (A) NHLFs were treated with 10K and SEC EVs from LPS-stimulated THP-1 MΦs, 10K and SEC EVs from LPS + nigericin-stimulated THP-1 MΦs, as well as with LPS, nigericin, or they were left untreated. n = 5. (B) MDS plot of leading log_2FC (average (root-mean-square) log_2FC for the 500 genes most different between

samples) over dimensions one and two shows clustering of NHLFs treated with 10KLN EVs. (C) Heat map showing the top 20 DE genes (ranked by p-value) for 10KLN treated NHLFs compared to untreated NHLFs. The scale shows the relative log_2CPM values (log_2CPM values were normalised to the respective untreated condition).

Performing gene set testing for MSigDB hallmark gene sets pointed towards the involvement of IFN-α/γ -, TNF-α-, and IL-6 signalling (Figure 64B) upon 10KLN exposure of endothelial cells. Gene set testing for Reactome gene sets further pointed towards the involvement of IL-10 signalling (Figure 64C). A list of Reactome genes sets shown in Figure 64C with corresponding statistics and significant DE genes from the dataset found in these gene sets is shown in Table 4.

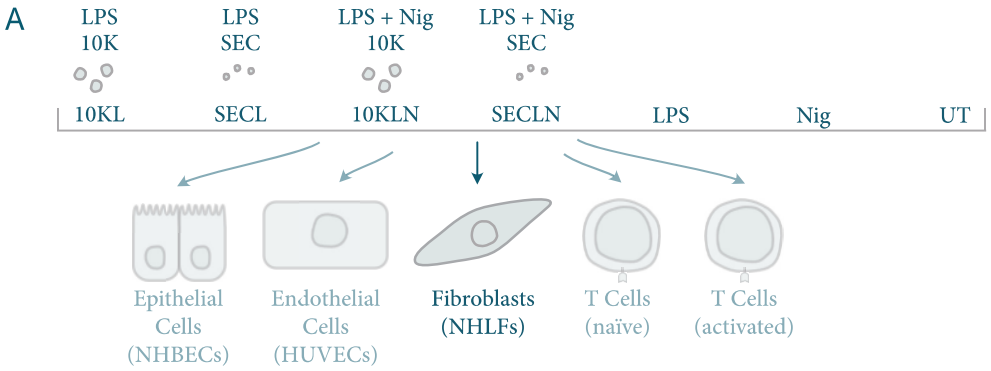
A
LPS
10K
LPS
SEC
LPS + Nig
10K
LPS + Nig
SEC
10KL
SECL
10KLN
SECLN
LPS
Nig
UT
Epithelial Cells (NHBECs)
Endothelial Cells (HUVECs)
Fibroblasts (NHLFs)
T Cells (naïve)
T Cells (activated)

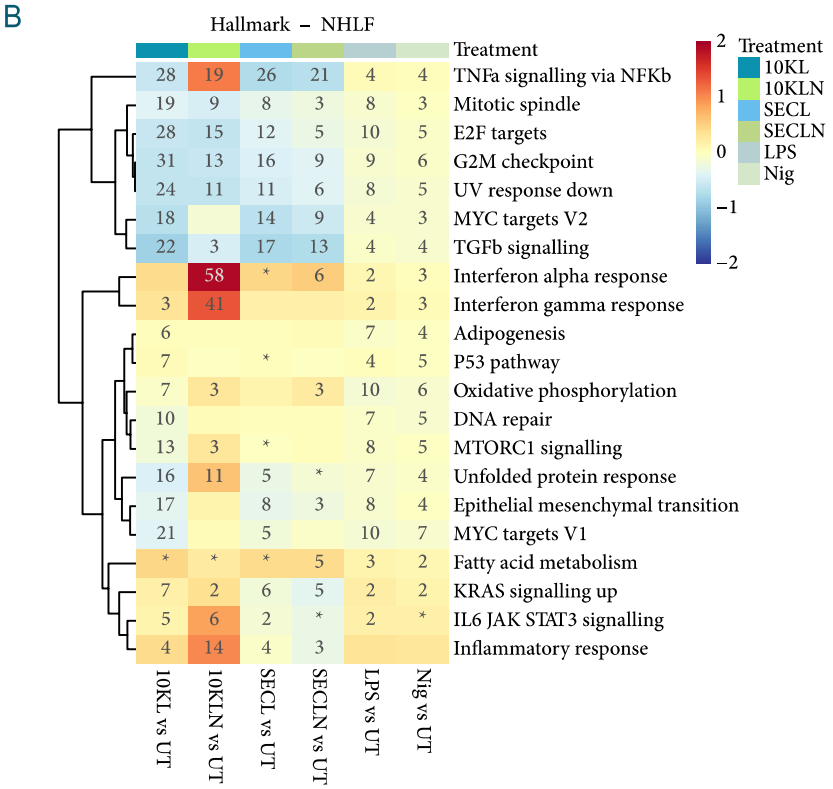
B
Hallmark – NHLF
Treatment
10KL
10KLN
SECL
SECLN
LPS
Nig
2
1
0
−1
−2
TNFa signalling via NFKb
Mitotic spindle
E2F targets
G2M checkpoint
UV response down
MYC targets V2
TGFb signalling
Interferon alpha response
Interferon gamma response
Adipogenesis
P53 pathway
Oxidative phosphorylation
DNA repair
MTORC1 signalling
Unfolded protein response
Epithelial mesenchymal transition
MYC targets V1
Fatty acid metabolism
KRAS signalling up
IL6 JAK STAT3 signalling
Inflammatory response
10KL vs UT
10KLN vs UT
SECL vs UT
SECLN vs UT
LPS vs UT
Nig vs UT

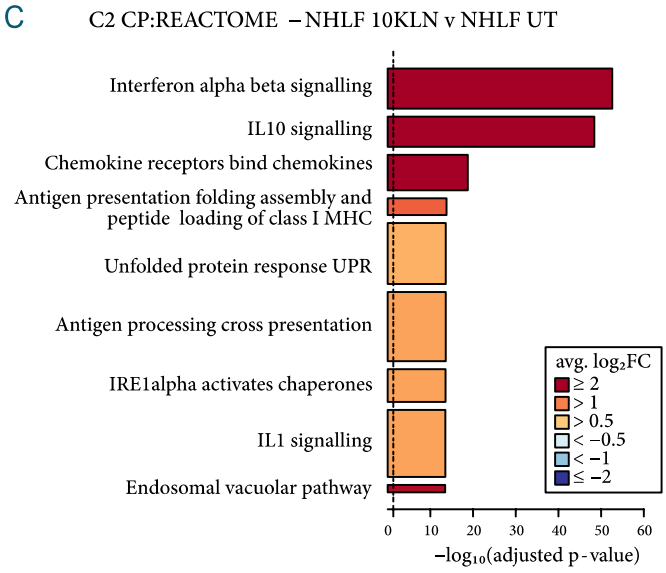
C
C2 CP:REACTOME – NHLF 10KLN v NHLF UT
Interferon alpha beta signalling
IL10 signalling
Chemokine receptors bind chemokines
Antigen presentation folding assembly and peptide loading of class I MHC
Unfolded protein response UPR
Antigen processing cross presentation
IRE1alpha activates chaperones
IL1 signalling
Endosomal vacuolar pathway
avg. log2FC
≥ 2
> 1
> 0.5
< −0.5
< −1
≤ −2
0
10
20
30
40
50
60
−log10(adjusted p-value)

Figure 64: Effect of inflammasome-elicited EVs on fibroblasts—pathway enrichment analysis. (A) NHLFs were treated with 10K and SEC EVs from LPS-stimulated THP-1 MΦs, 10K and SEC EVs from LPS + nigericin-stimulated THP-1 MΦs, as well as with LPS, nigericin, or they were left untreated. (B+C) Gene set testing was performed using the cameraPR function from the limma package. n = 5. (B) The heat map shows the top MSigDB hallmark gene sets for the different treatments vs untreated cells. The scale shows the average $\log_2$FC. Annotation indicates significance ($-\log_{10}$ adjusted p-value; * $p < 0.1$, 2: $p < 0.01$, 3: $p < 0.001$, …). (C) The bar plot shows the top Reactome gene sets for NHLFs treated with 10KLN EVs vs untreated NHLFs. Bars are coloured by average log fold change. Bar lengths represent $-\log_{10}$ adjusted p-values and widths represent relative gene set size.

In addition to analysing the effect of inflammasome-elicited EVs on the transcriptome of fibroblasts through RNA-sequencing, qPCR was performed on A549 cells. While RNA-sequencing allows a broad, unbiased analysis, qPCR requires the preselection of targets. Based on some studies linking inflammation to fibrosis (Wynn, 2011; Crystal *et al*, 2012) we checked for three genes commonly associated with fibrosis: vimentin (*VIM), TGFB1*, and *MMP7*. While these three genes were not differentially regulated (*VIM* had a $\log_2$FC of -0.28 and a FDR-adjusted p-value of 0.96, *TGFB1* had a $\log_2$FC of 1.18 and a FDR-adjusted p-value of 0.94, and *MMP7* had a $\log_2$FC of 0.40 and a FDR-adjusted p-value of 0.99) and *MMP7* was not really detected in the RNA-seq experiment (average expression of 0.03), one of them, *MMP7*, was upregulated upon 10KLN treatment and slightly increased upon SECLN treatment (Figure 65B). For *VIM* and *TGFB1*, no changes in gene expression were observed (Figure 65B). This finding, taken together with the RNA-sequencing results described above (Figure 63, Figure 64), suggests that while 10KLN EVs induce inflammatory signalling (mainly IFN, TNF-α and IL-10 based), they do not induce genes associated with fibrosis—at least not at a 15 h time point; it is of course still possible that a constant activation of inflammatory signalling mediated through 10KLN EVs leads to fibrosis at some point.

	Number of Genes	Direction	p-value	FDR-adj. p-value	Average log_2FC	Top significant genes
Interferon alpha beta signalling	60	Up	1.45e-56	2.35e-53	2.198	*OAS2; MX1; RSAD2; IFI6; ISG15; OAS1; IFI27; MX2; IFIT1; OAS3; IFITM1; IRF7; BST2; IFIT3; GBP2; HLA-F; OASL; ISG20; IFI35; XAF1; IFITM3; STAT2; USP18; SAMHD1; STAT1; HLA-E; IRF9; IFIT2; HLA-B; IFNA13; HLA-C; ADAR; HLA-H; HLA-G; IFNA1; HLA-A*
IL10 signalling	45	Up	4.68e-52	3.78e-49	3.027	*PTGS2; CXCL8; IL6; CXCL1; CXCL2; CCL20; CSF3; CSF2; IL1B; CXCL10; ICAM1; CCL3L3; TIMP1; LIF; CCL3; CCL2; CCL4; IL1A; IL1RN*
Chemokine receptors bind chemokines	53	Up	2.95e-22	1.59e-19	2.025	*CXCL8; CXCL1; CXCL2; CCL20; CXCL3; CXCL6; CXCL5; CXCL10; CCL3L3; CXCL11; CCL3; CCL2; CXCL12; CCL4; CXCR4*
Antigen presentation folding assembly and peptide loading of class I MHC	25	Up	3.99e-17	1.61e-14	1.221	*HSPA5; HLA-F; SEC13; HLA-E; HLA-B; PDIA3; B2M; TAP1; HLA-C; SEC24A; HLA-G; HLA-A*
Unfolded protein response UPR	91	Up	7.89e-17	2.36e-14	0.790	*CXCL8; HERPUD1; HSPA5; XBP1; DNAJB9; SRPRB; SERP1; WIPI1; HYOU1; HSP90B1; DNAJB11; CREB3; KDELR3; GFPT1; YIF1A; CCL2; LMNA; DNAJC3; FKBP14; MYDGF; ARFGAP1; ATF4; EIF2AK3; CEBPB; SRPRA; DDIT3; ADD1; GOSR2; PDIA6; TSPYL2; NFYB; PREB; EXOSC1; ATF3*
Antigen processing cross presentation	103	Up	8.80e-17	2.36e-14	0.804	*CTSS; HLA-F; PSMC4; UBB; PSMA6; PSMA5; CTSL; HLA-E; UBC; PSME2; PSMB7; HLA-B; SEC61G; PDIA3; B2M; PSMB4; PSME1; SEC22B; PSMC2; PSMB9; TAP1; HLA-C; PSMB3; PSMD4; PSMA3; PSMD7; PSMB5; PSMD14; HLA-G; PSMD6; HLA-A; SEC61B*
IRE1alpha activates chaperones	49	Up	1.16e-16	2.68e-14	0.874	*HSPA5; XBP1; DNAJB9; SRPRB; SERP1; WIPI1; HYOU1; DNAJB11; KDELR3; GFPT1; YIF1A; LMNA; DNAJC3; FKBP14; MYDGF; ARFGAP1; SRPRA; ADD1; GOSR2; PDIA6; TSPYL2; PREB*
IL1 signalling	100	Up	1.52e-16	3.07e-14	0.879	*IL1B; IRAK3; NFKBIA; RIPK2; IRAK2; SQSTM1; PSMC4; UBB; PSMA6; NFKB2; PSMA5; UBC; NFKB1; PSME2; PSMB7; PSMB4; PSME1; IRAK1; PSMC2; PSMB9; PSMB3; IL1A; PSMD4; PSMA3; MAP3K8; PSMD7; PSMB5; IL1RN; PSMD14; NFKBIB; PSMD6*
Endosomal vacuolar pathway	11	Up	1.83e-16	3.28e-14	1.880	*CTSS; HLA-F; CTSL; HLA-E; HLA-B; B2M; HLA-C; HLA-G; HLA-A*

Table 4: Reactome gene sets of 10KLN vs UT NHLF samples. Reactome gene sets whose genes were highly ranked in terms of differential expression relative to genes that are not in the set in the comparison of 10KLN samples versus untreated samples in NHLFs. Names of gene sets, number of genes included in each set, directionality (up- or down), p-value, FDR-adj. p-value, average log_2FC, and significantly regulated genes from the dataset part of the gene set are shown.

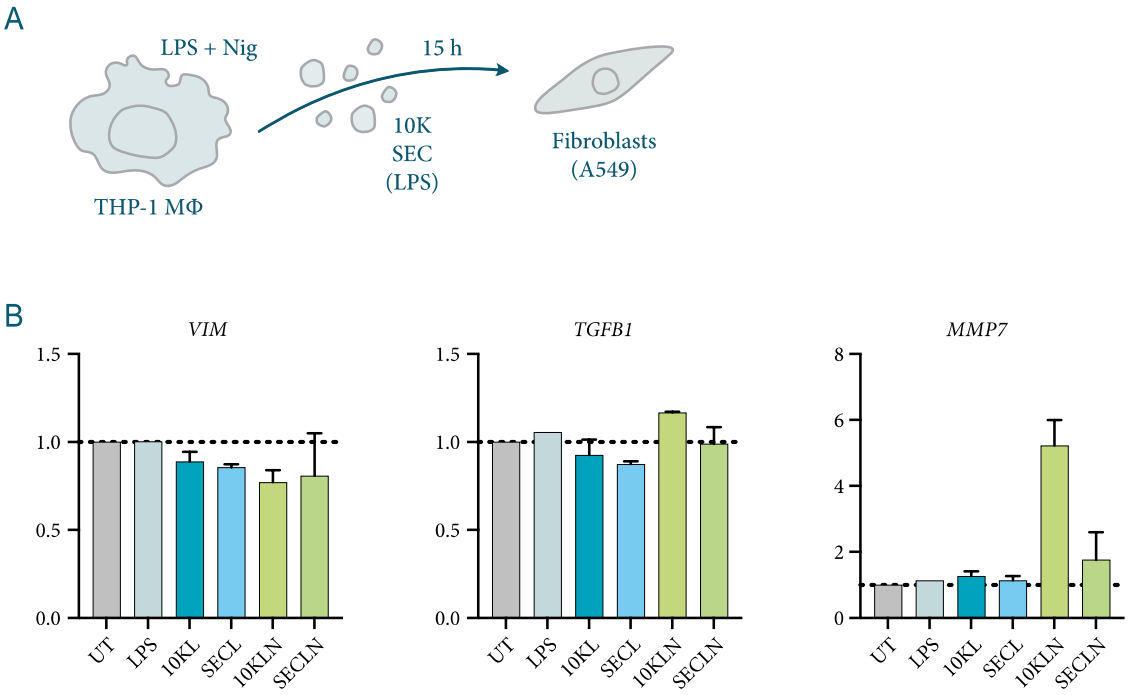

Figure 65: Effect of inflammasome-elicited EVs on fibroblasts with regards to fibrosis. (A) A549 cells were treated for 15 h with 10K and SEC EVs from LPS-stimulated THP-1 MΦs, 10K and SEC EVs from LPS + nigericin-stimulated THP-1 MΦs, as well as with LPS, or they were left untreated. (B) RNA was isolated from A549 cells and qRT-PCR was performed. Mean ± SD, n = 2 (n = 1 for LPS treated samples).

3.3.2.4 T cells

In the case of naïve T cells, clustering of 10KLN EVs was observed in MDS plots (Figure 66B). The top 20 DE genes for 10KLN treated versus untreated naïve T cells are shown in Figure 66C.

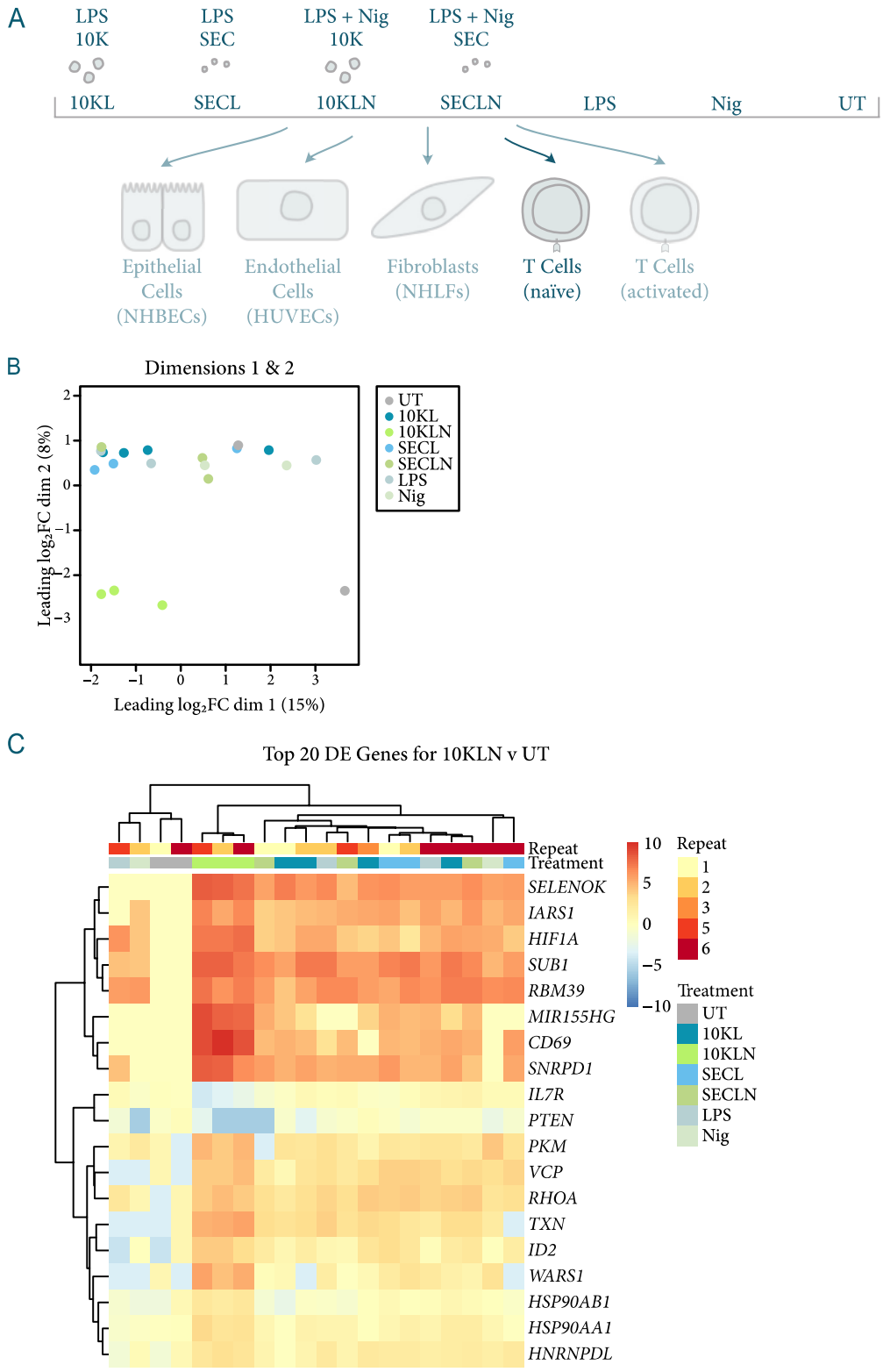

Figure 66: Effect of inflammasome-elicited EVs on naïve T cells. (A) naïve T cells were treated with 10K and SEC EVs from LPS-stimulated THP-1 MΦs, 10K and SEC EVs from LPS + nigericin-stimulated THP-1 MΦs, as well as with LPS, nigericin, or they were left untreated. n = 5. (B) MDS plot of leading log_2FC (average (root-mean-square) log_2FC for the 500 genes most different between

samples) over dimensions one and two, coloured by treatment. (C) Heat map showing the top 20 DE genes (ranked by p-value) for 10KLN treated naïve T cells compared to untreated naïve T cells. The scale shows the relative log_2CPM values (log_2CPM values were normalised to the respective untreated condition)

Gene set testing for MSigDB hallmark gene sets pointed towards an effect of 10KLN EVs on MYC targets (version 1 and 2, Figure 67B) and thus towards an effect on proliferation (Bishop *et al*, 2021). Indeed, when looking at bright field images after transfer of 10KLN EVs to naïve T cells vs untreated naïve T cells, cell proliferation was observed (Figure 68), although this has not yet been quantified. This is supported by the enrichment of genes involved in oxidative phosphorylation, as well as in mechanistic target of rapamycin complex 1 (mTORC1) signalling (Figure 67B): oxidative phosphorylation (along with glycolysis) is shown to be increased in proliferating T cells (Bishop *et al*, 2021); mTOR promotes cell growth (Bishop *et al*, 2021). Additionally, 10KLN EVs seem to induce some inflammatory signalling: gene set testing points towards the upregulation of TNF-α and IFN-α/γ signalling (Figure 67B). Interestingly, while 10KLN EVs seem to lead to the upregulation of TNF-α signalling, the opposite (although more subtle) is seen for the other stimuli (Figure 67B). Table 5 shows the different hallmark gene sets and their statistics, as well as the significant genes from the dataset that are part of these pathways.

	Number of Genes	Direction	p-value	FDR-adj. p-value	Average log_2FC	Top significant genes
MYC TARGETS V1	199	Up	2.56e-107	1.28e-105	1.404	*SNRPD1; HSP90AB1; IARS1*
OXIDATIVE PHOSPHORYLATION	200	Up	2.36e-56	5.91e-55	0.911	
UNFOLDED PROTEIN RESPONSE	113	Up	4.27e-39	7.11e-38	0.710	*IARS1*
MTORC1 SIGNALING	200	Up	6.04e-38	7.55e-37	0.578	*WARS1*
INTERFERON GAMMA RESPONSE	198	Up	2.63e-37	2.63e-36	0.568	*CD69; WARS1; HIF1A*
MYC TARGETS V2	57	Up	8.33e-33	6.94e-32	0.982	
INTERFERON ALPHA RESPONSE	97	Up	3.08e-31	2.20e-30	0.692	*WARS1*
TNFA SIGNALING VIA NFKB	199	Up	7.66e-25	4.78e-24	0.313	*CD69; IL7R; ID2*

Table 5: Hallmark gene sets of 10KLN vs UT naïve T cell samples. Hallmark gene sets whose genes were highly ranked in terms of differential expression relative to genes that are not in the set in the comparison of 10KLN samples versus untreated samples in naïve T cells. Names of gene sets, number of genes included in each set, directionality (up- or down), p-value, FDR-adj. p-value, average log_2FC, and significantly regulated genes from the dataset part of the gene set are shown.

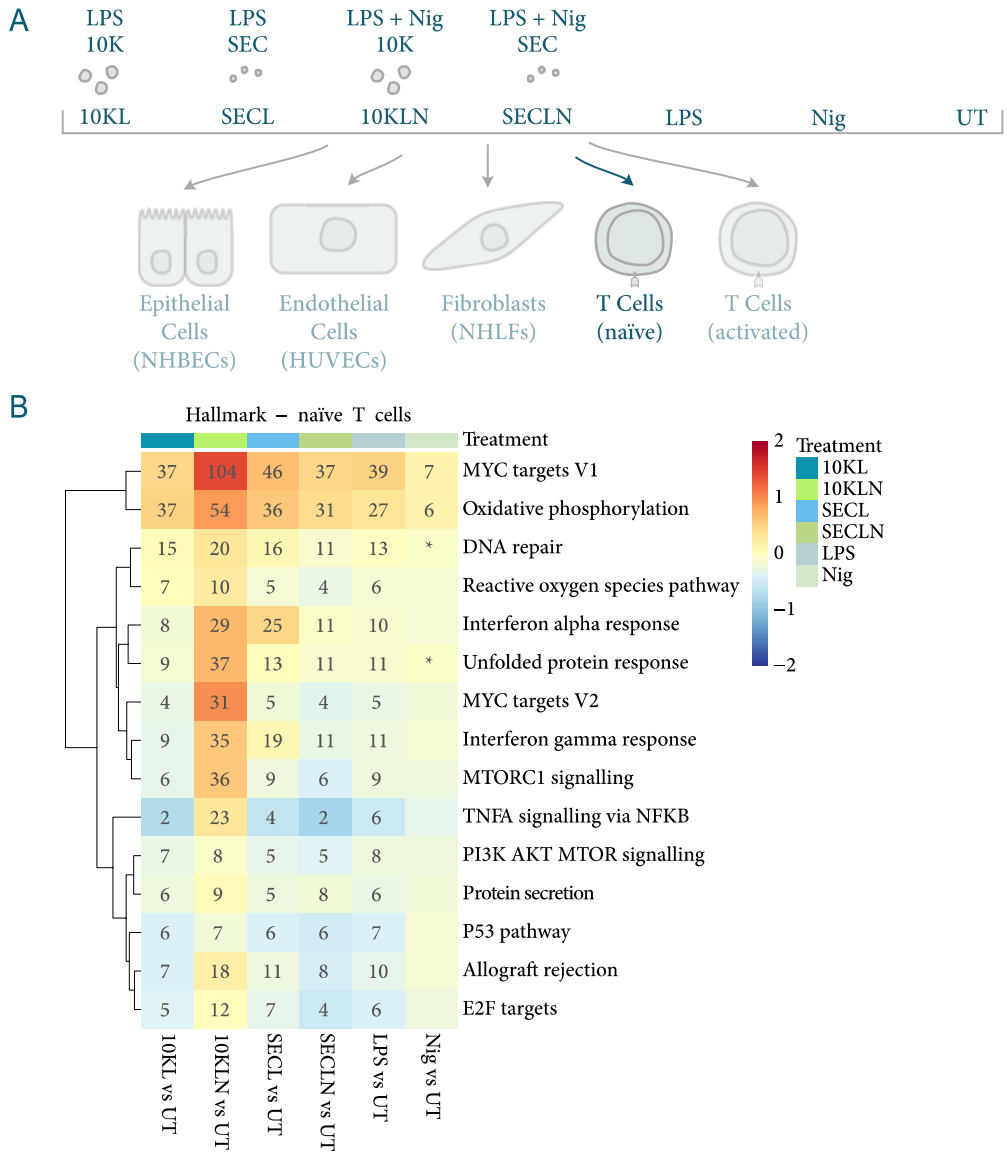

Figure 67: Effect of inflammasome-elicited EVs on naïve T cells—pathway enrichment analysis. (A) naïve T cells were treated with 10K and SEC EVs from LPS-stimulated THP-1 MΦs, 10K and SEC EVs from LPS + nigericin-stimulated THP-1 MΦs, as well as with LPS, nigericin, or they were left untreated. (B) Gene set testing was performed using the cameraPR function from the limma package. The heat map shows the top MSigDB hallmark gene sets for the different treatments vs untreated cells. The scale shows the average log_2 fold change.

Annotation indicates significance ($-\log_{10}$ adjusted p-value; * $p < 0.1$, 2: $p < 0.01$, 3: $p < 0.001$, …). n = 5.

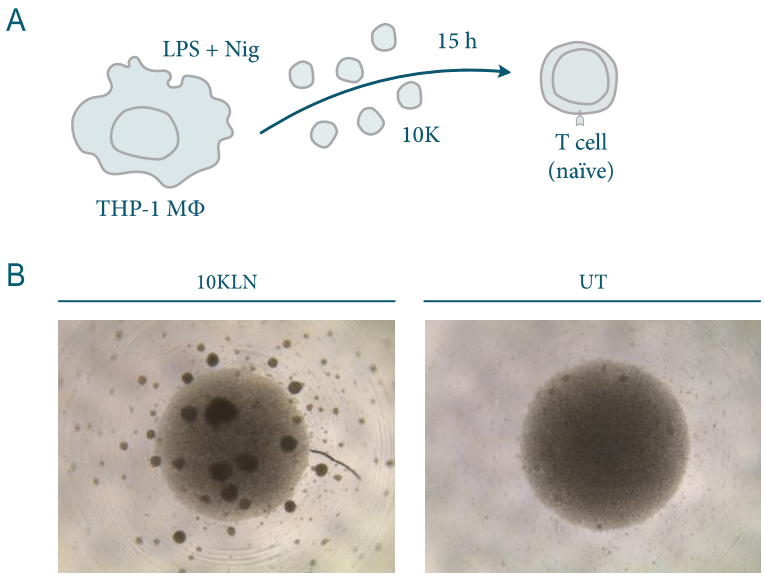

Figure 68: Effect of inflammasome-elicited EVs on naïve T cells with regards to cell proliferation. (A) naïve T cells were treated with 10K and SEC EVs from LPS-stimulated THP-1 MΦs, 10K and SEC EVs from LPS + nigericin-stimulated THP-1 MΦs, as well as with LPS, or they were left untreated. (B) Bright field images of naïve T cells. n = 1.

No DE genes were found for activated T cells and no clustering of samples by stimulation was observed (Figure 69B). It is of interest that a stronger effect of inflammasome-elicited EVs was found for naïve T cells, especially as library preparation and sequencing worked better in case of activated rather than naïve T cells and activated T cells took up more EVs than naïve T cells (Figure 53). Actually, naïve T cells could not be shown to take up 10KLN EVs, but only took up SECLN EVs in a subset of cells. Nevertheless, the 10KLN EV fraction had the strongest effect on naïve T cells. This is then probably induced through surface-surface interactions, rather than EV uptake.

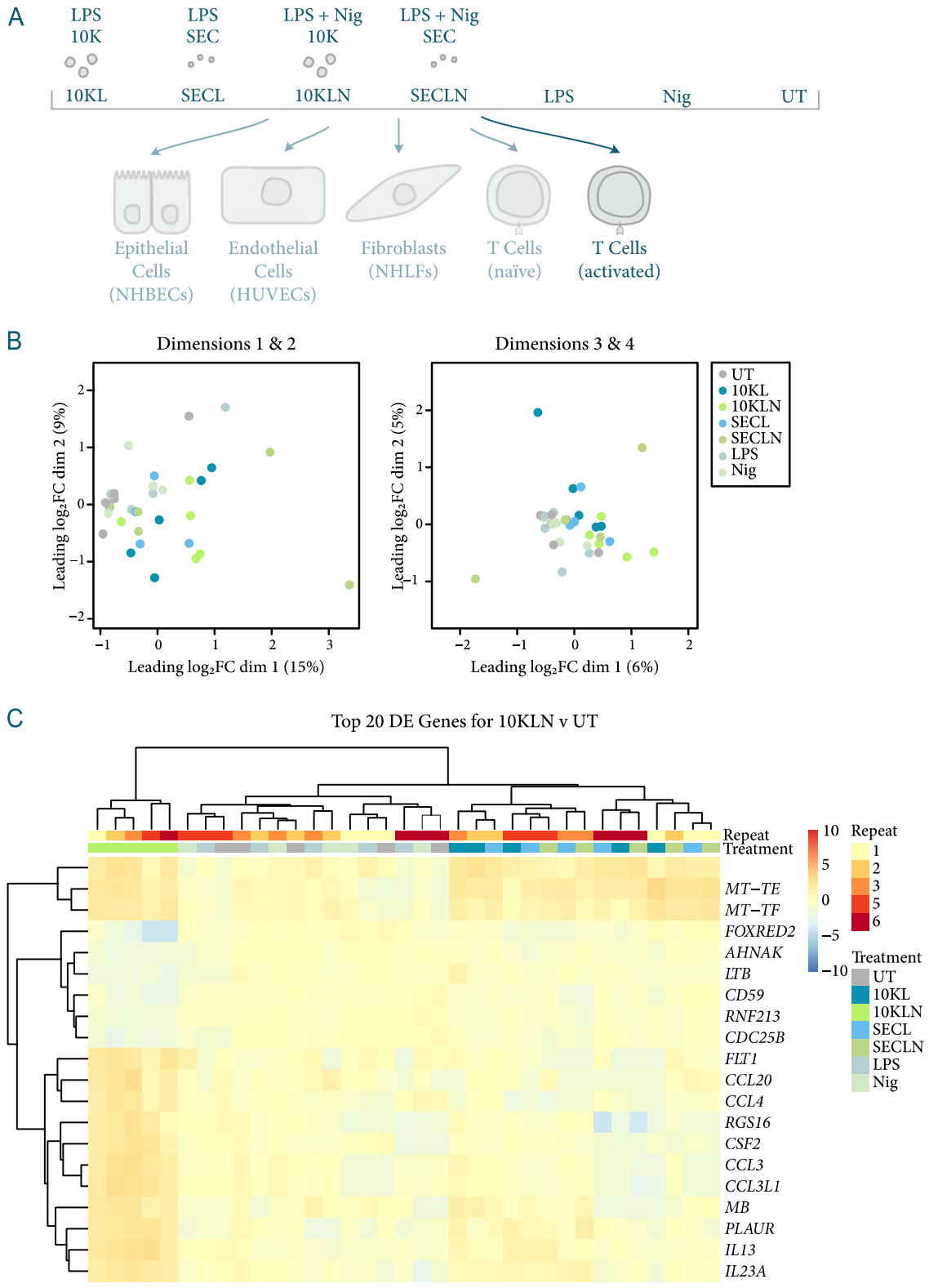

Figure 69: Effect of inflammasome-elicited EVs on activated T cells. (A) Activated T cells were treated with 10K and SEC EVs from LPS-stimulated THP-1 MΦs, 10K and SEC EVs from LPS + nigericin-stimulated THP-1 MΦs, as well as with LPS, nigericin, or they were left untreated. n = 5. (B) MDS plot of

leading log_2FC (average (root-mean-square) log_2FC for the 500 genes most different between samples) over dimensions one and two (left) and three and four (right) coloured by treatments. (C) Heat map showing the top 20 DE genes (ranked by p-value) for 10KLN treated activated T cells compared to untreated activated T cells. The scale shows the relative log_2CPM values (log_2CPM values were normalised to the respective untreated condition).

4 Discussion

4.1 EVs as Biomarkers for Inflammasome-Related Diseases

An important aim of our study was to investigate whether inflammasome-elicited EVs might be suitable biomarkers for NLRP3-elicited diseases. Thus, we characterised inflammasome-elicited EVs with regard to the presence of certain proteins and their RNA content.

We could show that EV release is increased upon inflammasome activation (Figure 9), confirming what had already been shown by Dr. Christina Budden (Budden *et al*, 2021) and various other researchers (MacKenzie *et al*, 2001; Pizzirani *et al*, 2007; Lipinski *et al*, 2019). This is likely due to NLRP3 stimuli leading to changes in Ca^{2+} flux (Swanson *et al*, 2019), since from the literature, it has been shown that an increased Ca^{2+} flux leads to an increase in EV release (Sidhu *et al*, 2004; Bianco *et al*, 2005; Pizzirani *et al*, 2007).
This increase in EV release is promising for their role as biomarkers, as the resulting increase in their concentration in the body would make their detection easier.

4.1.1 The Need for New Biomarkers

But why would we even need new biomarkers for inflammasome-related diseases? Previous studies have taught us that, often years before a disease is at the point of causing symptoms and thus being diagnosed, NLRP3 already drives a subclinical inflammatory state (Coll *et al*, 2022). It is of utmost importance to identify this state early enough and to narrow down the pathways involved.

Currently, this can be done by measuring IL-1β levels. However, measuring IL-1β levels has its limitations. Many cytokines, including IL-1β, show high individual-to-individual (Roth-Isigkeit *et al*, 2001; Li *et al*, 2016a, 2016b; Wu *et al*, 2017; van Deuren *et al*, 2021) as well as day-to-day variability (Scheiermann *et al*, 2013;

Cermakian *et al*, 2014; Labrecque & Cermakian, 2015) in baseline levels, thus making it hard to define certain standard cytokine levels.
In addition, increases in IL-1β are not necessarily caused by inflammasome activation. Besides being cleaved by inflammasome-associated caspases, cleavage of IL-1β has also been demonstrated for other proteases (Netea *et al*, 2015): For example, for several neutrophil- and MΦ-derived neutral serine proteases (Netea *et al*, 2015) such as for proteinase 3 (Coeshott *et al*, 1999; Joosten *et al*, 2009), for the metalloproteinase meprin A (Herzog *et al*, 2009), or by invading microorganism-derived proteases (Netea *et al*, 2010). As a result, detecting high levels of IL-1β in patient plasma is not necessarily a sign of inflammasome activation.

Another cytokine cleaved by caspase-1 during inflammasome activation is IL-18. One could therefore also consider measuring IL-18 levels in patients to detect inflammasome activation. However, as is the case for IL-1β, IL-18 release is not just caspase dependent: cleavage of IL-18 has been demonstrated for proteinase 3 (Sugawara *et al*, 2001), for mast cell-derived chymase (Omoto *et al*, 2006), for NK cell-derived granzyme B (Banerjee & Bond, 2008; Omoto *et al*, 2010), and for meprins A and B (Banerjee & Bond, 2008). Thus, IL-18 would not be a suitable alternative to definitely detect inflammasome activation.

Alternatively, one can measure C-reactive protein (CRP), which is a routine clinical parameter to assess immune activation—for example, in sepsis (Pierrakos *et al*, 2020), rheumatoid arthritis (Pope & Choy, 2021), or atherosclerotic disease (Ridker *et al*, 2017; Grebe *et al*, 2018). CRP is induced by a range of inflammatory cytokines (mainly IL-6) as a result of various immune activators (Sproston & Ashworth, 2018), and thus acts as a good marker for general assessment of immune activation, but is rather unspecific when it comes to determining the exact cause.
Thus, there is a clear need for a better biomarker and EVs might be the solution.

4.1.2 The RNA Content of Inflammasome-Elicited EVs

Previously, the RNA content of THP-1 MΦ-derived inflammasome-elicited EVs was extensively studied in our lab (Budden *et al*, 2021). 10K and SEC EVs released from THP-1 MΦs treated with several different inflammasome stimuli were compared to one another, as well as to EVs from TLR-stimulated cells. The biggest differences between EVs were seen when comparing 10K to SEC EVs, regardless of the stimulus, with 10K EVs from all stimuli (inflammasome and TLR alike) being enriched in mitochondrial genes compared to SEC EVs. This was confirmed when analysing 10K EVs from blood plasma of healthy human donors (Budden *et al*, 2021).

We have now built on this data and further analysed the RNA content of EVs derived from blood plasma. Again, using blood from healthy human donors, we now performed whole blood inflammasome-stimulation assays to model EV release in patients with inflammasome-related diseases. As seen in the THP-1 MΦ data, the biggest differences were observed between 10K and SEC EVs, with samples clustering primarily by EV subtype (Figure 23). Furthermore, we could confirm the enrichment of mitochondrial transcripts in 10K EVs compared to SEC EVs (Figure 27)—something that has also been shown in the literature (Kowal *et al*, 2016).

We were further able to correlate our whole blood assay inflammasome-elicited EV results to the previously obtained THP-1 MΦ inflammasome-elicited EV results (Figure 28). Considering such big differences in experimental setup (primary cells vs cell line, mix of cell types vs one single cell type, non-canonical vs canonical inflammasome-activation), it is remarkable that the results correlated, further supporting the ability to reproduce inflammasome-elicited EV data and thus the suitability of EVs as biomarkers.

Looking for differentially abundant transcripts in our blood-derived EVs, we could identify most differences in the case of CRID3 + LPS-treated samples compared to untreated samples (Figure 25). This would suggest that CRID3 either has a specific (off-target) effect on one of the cell types in the whole blood cell mix, or

the treatment of cells with CRID3 has an even bigger effect on a cell's EV content than inflammasome-activation, which would be quite unexpected as, so far, CRID3 has been shown to barely have any off-target effects (Primiano *et al*, 2016; Kennedy *et al*, 2021). While CRID3 was discovered to block IL-1β release (Perregaux *et al*, 2001) through inhibition of NLRP3 in 2015 (Coll *et al*, 2015), the exact mechanism of NLPR3 inhibition has only recently been demonstrated: Hochheiser and colleagues showed that CRID3 inhibits NLRP3 by stabilising the NACHT and LRR domains relative to one another. It ties five NLRP3 subunits together, which leads to the stabilisation of the inactive NLRP3 (Hochheiser *et al*, 2022). However, using a photoaffinity-based probe for CRID3, Kennedy and colleagues have shown CRID3 to additionally interact with carbonic anhydrase 2 (CA2), which suggests possible off-target effects. This was confirmed using biochemical assays, which showed inhibition of CA2 activity (Kennedy *et al*, 2021).

Carbonic anhydrases catalyse the dissociation of carbon dioxide (CO_2) into bicarbonate (HCO_3^-) and H^+. This leads to the acidification of the surrounding environment (Lindskog & Coleman, 1973). CA2 is found in the cytoplasm and is especially expressed at high levels in phagocytic immune cells, such as PBMC-derived MΦs and THP-1 cells (Strowitzki *et al*, 2022). Strowitzki and colleagues have studied the role of CA2 in immune cells, in particular in THP-1 cells, and shown that increased CO_2 levels led to a decrease in monocyte migration and to the attenuation of LPS-induced MΦ activation. Furthermore, knockdown of CA2 in THP-1 monocytes led to a significant reduction in the rate of cytosolic pH changes when cells were exposed to high CO_2 concentrations, indicating that CA2 plays a role in conferring sensitivity to CO_2 in MΦs (Strowitzki *et al*, 2022). With CRID3 having been shown to inhibit CA2 activity (Kennedy *et al*, 2021), one could speculate that this leads to the disruption of the cell's pH. Since pH has been shown to influence EV-related processes including EV release (Logozzi *et al*, 2018; Nakase *et al*, 2021; Riazanski *et al*, 2022; Parolini *et al*, 2009), this might be the reason for the observed strong effects of CRID3 on EVs. Interestingly, at least in MΦs, it seems to change only transcript loading into EVs and not EV release, as CRID3 inhibition has been previously shown to reverse the NLRP3-

induced increase in EV secretion (Budden *et al*, 2021). Of course, this is all highly speculative and would have to be proven experimentally.

While CRID3 + LPS treatment showed the biggest effect on 10K EV RNA content, IFM + LPS-treated samples and DMSO + LPS-treated samples showed roughly the same number of differentially abundant transcripts compared to controls (DMSO) (Figure 25).

Two of the differentially abundant transcripts were in common between EVs derived from uninhibited LPS-stimulated, CRID3 + LPS-stimulated, and IFM + LPS stimulated samples, all compared to control samples, with *SPP1* showing by far the strongest fold change for all three comparisons (Figure 25C). *SPP1* encodes the protein osteopontin (OPN) (Rittling, 2011). OPN is a secreted protein that has been implicated in the recruitment of monocytes and MΦs and in the regulation of cytokine production in MΦs, DCs, and T cells (Suzuki *et al*, 2009). It has been found to play a role in several inflammatory and cardiovascular diseases, as well as in cancer (Icer & Gezmen-Karadag, 2018). *SPP1* expression levels are low in monocytes but increase upon differentiation of monocytes to MΦs, which has been shown in THP-1 cells upon differentiation using PMA treatment (Oyama *et al*, 2000, 2002; Suzuki *et al*, 2009). It has also been shown to be induced by IL-1β, IFN-γ, TNF-α, and IL-10 (Denhardt & Guo, 1993; Miyazaki *et al*, 1995; Mazzali *et al*, 2002; Li *et al*, 2003b; Konno *et al*, 2006).

Some transcripts were differentially abundant after DMSO + LPS and CRID3 + LPS treatment. These included *IL1B* and *VCAN* (Figure 25C).
While *IL1B* was significant in these comparisons, it was not significant in the comparison between IFM + LPS and DMSO treated samples (Figure 25C). However, looking at the individual abundance plots (Figure 26) we still see an increase of *IL1B* abundance (FDR-adjusted p-value = 0.170, $\log_2$FC = 1.543). This was to be expected, as both CRID3 (Perregaux *et al*, 2001; Coll *et al*, 2015; Hochheiser *et al*, 2022) and IFM (Friker *et al*, 2020) block the NLRP3 inflammasome, but not signalling of LPS through TLR4, which induces *IL1B*

transcription (Bauernfeind *et al*, 2009; Latz *et al*, 2013; Franchi *et al*, 2009). However, since the strong increase in EV release is only seen upon inflammasome activation (Figure 9), we would expect fewer EVs being released in case of the inhibited samples—resulting in a lower abundance of *IL1B* transcripts being detected in the microarray analysis.

VCAN is an extracellular matrix (ECM) protein that has been shown to be increased in several inflammatory diseases, including in cardiovascular diseases and lung disease (Wight *et al*, 2020). Immune cells are recruited from the bloodstream, and once having entered the ECM in tissues, they interact with VCAN with their surface receptors. These include CD44, PSGL-1, and TLRs (Wight *et al*, 2020). Interaction of immune cells with VCAN not only affects their trafficking and migration—it also affects cell differentiation and survival, proliferation, and cytokine expression and activity (Wight *et al*, 2020).

Many different cell types have been shown to synthesise VCAN in response to proinflammatory cytokines, as well as to growth factors. Amongst them are epithelial cells, endothelial cells, stromal cells, and monocytes upon differentiation to MΦs under inflammatory conditions (Wight *et al*, 2014). For example, it has been shown that TLR4 stimulation, through LPS treatment, leads to an increase in VCAN expression in mouse MΦs (Chang *et al*, 2017). Thus, in the case of VCAN, we might have the same situation, in which the decrease in EV release caused by the blockage of NLRP3 leads to a decrease in signal intensity in the microarray analysis.

Finally, there were some significant transcripts unique to inflammasome-activated samples. Those were *IL6* and the multiple complex transcript *C15orf48;miRNA147B* (Figure 25C). “Multiple complex” is a term used by Thermo Fisher Scientific Inc. for some of the probes on the Clariom D Microarray. It means that for the respective microarray probe, both coding and non-coding transcripts were identified. In this case this was C15orf48 and the miRNA *miR-147b*.

Recently, *C15orf48* was identified as a mito-SEP termed modulator of cytochrome C oxidase during inflammation (MOCCI; Lee *et al*, 2021). Mito-SEPs are small open reading frame (sORF)-encoded peptides that are, by definition,

smaller than 100 residues and localise to the mitochondria (Zhang *et al*, 2020). They function in mitochondrial processes, such as in calcium homeostasis, lipid metabolism, or electron transport. In the case of MOCCI, it was shown to be a paralogue of the NDUFA4 subunit of complex IV, also known as cytochrome c oxidase: it replaces NDUFA4 during inflammation, thus leading to a reduction in mitochondrial ROS production, as well as to a lower mitochondrial membrane potential. MOCCI additionally leads to the suppression of the interferon response. As a result, the immune response is dampened. This dampening of the immune response is further achieved through the second transcript encoded by the same locus: *miR-147b*. This miRNA targets *NDUFA4* mRNA, thus working in union with MOCCI; together they have been shown to lead to the suppression of IL-6 and MCP-1 secretion (Lee *et al*, 2021).

However, *miR-147b* has an additional function: it enhances viral immunity mediated through RIG-I/MDA-5 signalling, leading to the induction of interferon signalling (Lee *et al*, 2021). Therefore, while MOCCI solely leads to a dampening of immune responses, including viral immunity and thus allows a certain degree of viral replication—probably to create a cytoprotetctive effect—*miR-147b* is also immunosuppressive but anti-viral at the same time (Lee *et al*, 2021).

Transcription of *C15orf48*, leading to the upregulation of the MOCCI mito-SEP and *miR-147b*, has been shown to be upregulated through IL-1β stimulation and viral infection (Lee *et al*, 2021). This is further supported by a study by van Scheppingen and colleagues, who have also shown that *miR-147b* is induced upon IL-1β stimulation and that it leads to the reduced expression of pro-inflammatory cytokines such as IL-6 (van Scheppingen *et al*, 2018).

Considering these results, it would be of interest to study the *C15orf48* locus in the context of NLRP3 or other inflammasome knockout models to see if inflammasomes are directly involved in the upregulation of MOCCI and *miR-147b* or if this is a general phenomenon also observed in the absence of inflammasome activation.

This transcript from the *C15orf48;miRNA147B* locus that we identified in 10KLN EVs, might potentially be processed by the RNAi machinery in recipients cells to the mature *miR-147b*. Additionally, it might also be possible that the actual mature

miRNA hairpin itself is present in inflammasome-elicited EVs as miRNAs with a certain motif that is also found in miR-147b, have been shown to be released in EVs from inflammasome-activated cells: Wozniak and colleagues have shown that miRNAs are selectively loaded into exosomes after inflammasome activation. They showed that caspase-1 activation, as a result of inflammasome activation, enables the cleavage of RILP by caspase-1. RILP is a trafficking adaptor protein that, once cleaved, plays a role in the relocation of MVBs to the cell periphery. It further induces the selective loading of certain miRNA exosomal cargo. Specificity for certain miRNAs is given by a short sequence motif in miRNAs that allows miRNAs to be loaded into exosomes by the ESCRT machinery (Wozniak *et al*, 2020).

The transcriptional upregulation of *IL6* is generally not inflammasome-specific, but seen in response to various inflammatory stimuli (Wight *et al*, 2014; Murphy *et al*, 2017; Chang *et al*, 2017; Wight *et al*, 2020). Nevertheless, *IL6* release in EVs in the absence of inflammasome activation seems to be very low, so that it is not significantly differentially abundant in EVs isolated under these conditions. Only the combination of its transcriptional upregulation and the increase in EV release allowed it to be detected. Thus, while many stimuli lead to the upregulation of *IL6*, only inflammasome-activation leads to its detection in EVs, therefore making its detection inflammasome-specific in this context.

One way to possibly identify more differentially abundant transcripts in the future would be to use a different stimulus to achieve inflammasome activation. While we chose to use 23 h LPS stimulation for the reasons outlined above (section 3.1.3), this stimulation led to highly variable IL-1β release in different donors (Figure 15, Figure 18, Figure 21). As discussed in 3.1.3, this could be due to donor variations in IL-1β release previously reported (Sahdo *et al*, 2013) or due to problems with the HTRF measurements, it could also suggest that inflammasome activation using long-term LPS stimulation was not successful in all donors. This high variation in donor responsiveness to long-term LPS stimulation would of course make it harder to identify significantly abundant

transcripts. Thus, it would be useful to try an alternative inflammasome activator that leads to more consistent IL-1β release in different donors and, as a result, possibly allows the identification of more significantly differential transcripts.

4.1.3 N-Terminal GSDMD as a Possible Biomarker

An alternative to identifying an RNA signature for biomarker development, may be to focus on N-terminal GSDMD, which we could identify in inflammasome-elicited EVs.

So far, we have only demonstrated the presence of N-terminal GSDMD in EV fractions (Figure 13). We have not yet characterised if it is present in EV membranes, or in the EV lumen. However, taking the current literature on GSDMD pore formation during pyroptosis into account, we would expect N-terminal GSDMD to be part of EV membranes.

As mentioned in the introduction (section 1.2), caspase-1,4,5, and 11 activation leads to a GSDMD-mediated form of cell death called pyroptosis. GSDMD is cleaved into its C- and N-terminal parts. While full length GSDMD does not bind to lipids (Liu *et al*, 2016; Chen *et al*, 2016a), once GSDMD is cleaved, the N-terminal part is able to bind to lipids and as such translocates to the plasma membrane (Sborgi *et al*, 2016; Chen *et al*, 2016a). This recruitment of N-terminal GSDMD seems to be quite strong, as studies have shown that N-terminal GSDMD is only found in the membrane fraction (Liu *et al*, 2016; Aglietti *et al*, 2016). Furthermore, this enrichment of GSDMD N-terminus on the plasma membrane has already been shown at early stages of pyroptosis and persists throughout pyroptosis and, once the cell has died from pyroptosis, N-terminal GSDMD is still found to be associated with the dead cell's plasma membrane (Chen *et al*, 2016a).

Besides pore formation, Hu and colleagues have found that N-terminal GSDMD can act as a negative feedback loop during inflammasome activation by binding to and inhibiting caspase-1 (Hu *et al*, 2022).

On the other hand, GSDMD C-terminus is absent from dead cells, suggesting it is released during lytic cell death and does not associate with cell membranes.

This agrees with the finding that C-terminal GSDMD has been found to not interact with lipids (Chen *et al*, 2016a).
Thus, this points to N-terminal GSDMD being within EV membranes as opposed to being inside the EV lumen.

In addition to being able to bind to lipids, N-terminal GSDMD can form oligomers with itself (Chen *et al*, 2016a), allowing GSDMD pore formation in the cell membrane. In our Western blots, we have demonstrated the presence of N-terminal GSDMD in 2K, 10K, and SEC EVs (Figure 13), but we have not performed an experiment to differentiate between N-terminal GSDMD monomers and pores. From the literature, we would expect it to be present in the form of GSDMD pores: on the one hand, because the structure of GSDMD-pores has been investigated in liposomes, in which it has been shown to exist in ring-like structures (Aglietti *et al*, 2016; Sborgi *et al*, 2016); since liposomes are similar to EVs, we would expect the situation in EVs to be similar. On the other hand, because GSDMD pores have been shown to be expelled from cells through microvesicle release, as a way to save cells from pyroptosis. This would indicate that most of our EVs actually contained pre-formed GSDMD pores and that pores would not just form in EVs.
To confirm this, one of the next steps would be to employ cryo-electron and atomic force microscopy on EVs stained for N-terminal GSDMD. Furthermore, one could look at N-terminal GSDMD in vesicles in WES during non-reducing conditions: Liu and colleagues have shown that, in Western blots of whole cell lysates, GSDMD is present either as a monomer (around 30 kDa) or as a multimer of ≥250 kDa. Under reducing conditions, however, the multimeric N-terminal GSDMD is lost, suggesting that GSDMD pore formation requires disulfide-cross-linking (Liu *et al*, 2016). Thus, if we performed Western blotting of EV lysates under non-reducing conditions for N-terminal GSDMD, we might find multimeric N-terminal GSDMD, suggesting the presence of GSDMD pores in EVs.

Considering that GSDMD is likely to be present in the form of GSDMD pores in EVs, the question arises if inflammasome-elicited EVs might be leaky. Cryo-

electron microscopy has recently revealed that GSDMD assembles pores with 31-fold to 34-fold symmetry with the 33-subunit GSDMD pore having an outer diameter of around 310 angstroms (Å) and an inner diameter of around 215 Å (Xia *et al*, 2021). These pores have been shown to allow the passage of small, neutrally charged dextrans, but not large ones. This was demonstrated through the generation of liposomes containing fluorescent dextrans. When the size of the dextrans used (4 kDa and 20 kDa, hydrodynamic radius smaller than 4 nm) was smaller than that of the GSDMD pore, dextran passage through pores was observed. On the other hand, dextrans with a hydrodynamic radius of 27 nm (2000 kDa) were retained (Evavold *et al*, 2018). While these neutrally charged dextrans were able to pass the GSDMD pore, acidic cargo has been shown to be repelled by pores (Xia *et al*, 2021). Indeed, it was shown that both neutral and basic cargo preferentially pass GSDMD pores over acidic cargo (Xia *et al*, 2021), thus explaining why it has been shown that Rac-1 (Heilig *et al*, 2018), HMGB1 (Davis *et al*, 2019) and cytochrome c (Rogers *et al*, 2019), being non-acidic, are rapidly released through GSDMD pores. It also explains why IL-1β and IL-18 are primarily released when in their mature form: In their pro-forms, they contain an acidic domain. However, during maturation the acidic domain is removed through caspase-1 cleavage, resulting in a basic, mature form that is preferentially released (Xia *et al*, 2021).

This alone would allow preferential secretion through GSDMD pores, especially as IL-1β and IL-18 are much smaller in size than GSDMD pores. However, additionally, the basic charge of mature IL-1β has been shown to lead to its accumulation on phosphatidylinositol 4,5-bisphosphate (PIP2) membrane ruffles (Monteleone *et al*, 2018), so it is even targeted to the plasma membrane.

Considering that RNA is acidic, RNA would probably not be released through GSDMD pores. In cells, pyroptosis ultimately occurs as a result of GSDMD pore formation, which would lead to RNA secretion; however, in vesicles, we might only have the presence of GSDMD pores without pyroptosis and, in that case, we would not expect RNA to leak.

Another interesting study that has implications for the use of GSDMD N-terminal-positive EVs as possible biomarkers was published by Rühl and colleagues: they showed that the release of microvesicles is a way for cells to restrict pyroptosis by repairing their membrane through the release of GSDMD pores (Rühl *et al*, 2018). Mechanistically, they have shown that inflammasome-induced GSDMD pore formation leads to calcium influx through GSDMD pores, which then recruits the ESCRT machinery and results in the release of vesicles (Rühl *et al*, 2018).
Interestingly, this release mechanism of GSDMD pores would be in line with experiments previously performed in our lab, which demonstrated that vesicle release is downstream of NLRP3, caspase-1, and GSDMD (Budden *et al*, 2021). This makes sense, if GSDMD is required for pore formation and calcium influx, triggering ESCRT recruitment and vesicle release. A way to test if this is indeed the case would be to quantify inflammasome-elicited EV release in the presence of a calcium-chelating agent.
Considering this mechanism of GSDMD pore-containing microvesicle release upon inflammasome activation, we would expect to not only have a high increase in EV release upon inflammasome activation (which we have demonstrated before), but to also have an enrichment of GSDMD pore-positive microvesicles: since calcium influx takes place through GSDMD pores and the ESCRT machinery is recruited to the sites of calcium influx, vesicle release is thought to take place at the very site of GSDMD pore formation. As a result, we would expect to see large numbers of vesicles with GSDMD pores present.

To summarise, we have shown that inflammasome-activation leads to an increase in EV release. These inflammasome-elicited EVs are distinct from other EVs. They carry N-terminal GSDMD and show a distinct RNA signature. While their RNA content has the potential to elucidate how these inflammasome-elicited EVs affect recipient cells and thus spread inflammation throughout the body, it is especially the presence of GSDMD N-terminal in these EVs that might in the end allow inflammasome-elicited EVs to be used as a biomarker.

4.2 Interaction of Inflammasome-Elicited EVs With Recipient Cells

Besides analysing the content of inflammasome-elicited EVs, we set out to study the effect of EVs on different recipient cells.

4.2.1 Suitability of Different Labelling Approaches

In order to study EV uptake, we used different EV labelling approaches. One approach was to target the fluorescent proteins mCherry and EGFP to the cell membrane (Figure 29A). This approach would have had the advantage that we could have directly isolated labelled EVs, without the need to change the EV isolation protocol and it has been shown to work well before (Lai *et al*, 2015). However, the fluorescent signal was not strong enough to look at EV uptake in our hands (Figure 30). In agreement with this, a review focusing on different microscopy approaches further states that the usage of plasma membrane-anchored GFP or RFP proteins is an inefficient labelling technique for EVs (Colombo *et al*, 2021). Thus, we had to switch to labelling EVs with different dyes. The main disadvantage was that the EV isolation protocol needed to be adapted to include staining and removal of dye, thus changing it from the standard EV isolation protocol used for all other experiments. This might have had an influence on the exact EV composition; however, we believe it was within reason, especially as the same centrifugation spins and SEC columns were used. Another disadvantage of some dyes, in particular lipid-based dyes such as PKH dyes, is their ability to form micelles in aqueous solution, thus leading to false positives (Colombo *et al*, 2021). Such micelles or dye aggregates might appear as EVs (Russell *et al*, 2019). Additionally, PKH dyes have been shown to lead to an increase in EV size (Dehghani *et al*, 2020). We thus avoided lipid-based dyes and opted for CFSE and R18.

CFSE is the fluorescent derivative of Carboxy-Fluorescein Diacetate Succinimidyl Ester (CFDA-SE). Upon entry of CFDA-SE into EVs, it is cleaved by esterases, leading to CFSE. CFSE covalently binds to amine groups and thus can no longer cross the membrane. Instead, it stays permanently inside the EV

lumen (Colombo *et al*, 2021). CFSE by itself was shown not to aggregate (Morales-Kastresana *et al*, 2017).
R18 is a lipid-labelling dye that is incorporated into the lipid bilayer through its alkyl tails (Hoekstra *et al*, 1984). At high enough concentrations it self-quenches. Only upon fusion with membranes does it start to distribute, leading to its dequenching and an increase in fluorescence (Montecalvo *et al*, 2012).
While these two dyes are not known to cause dye aggregates, unspecific transfer of dye might occur. To a small extent, this might indeed be the case in our experiments, as even at incubation of EVs with recipient cells at 4 °C there was some signal (Figure 40). Both endocytosis and membrane fusion are active processes (Ohki *et al*, 1998; McNew *et al*, 2000; Martens & McMahon, 2008; Montecalvo *et al*, 2012) and as such are affected by temperature (Ohki *et al*, 1998; Morelli *et al*, 2004; Escrevente *et al*, 2011; Montecalvo *et al*, 2012; Espósito *et al*, 2015). Thus, when we still see a signal for R18-stained SEC EVs and CFSE-stained 10K EVs after incubation at 4 °C, this might be due to passive dye transfer. This, however, is commonly observed in EV uptake studies performed at 4 °C (Morelli *et al*, 2004; Temchura *et al*, 2008; Tian *et al*, 2010; Escrevente *et al*, 2011; Montecalvo *et al*, 2012; Christianson *et al*, 2013; Delenclos *et al*, 2017) and might also be explained by the fact that the metabolism of cells is just decreased through incubation at 4 °C, yet not completely blocked.

An alternative to using dyes or generic targeting of proteins to membranes, would be to couple EGFP to CD63 or other EV marker proteins and use this to study uptake. This is commonly done in the EV field (Jurgielewicz *et al*, 2020). However, it limits the analysis to certain subtypes of EVs—to those that contain said EV marker proteins. In our case, performing Western blotting, we got a strong signal for CD9, CD81, and HSP70 (Figure 12), so these could be candidates for coupling to EGFP.
We used HSP70 and CD63 when studying EV content release: we tagged both CD63 and HSP70 to NLuc to see if EV content (membrane proteins in case of CD63 and EV lumen content in case of HSP70) ends up in the recipient cell cytoplasm (Figure 42). While we could detect CD63 in recipient cells, so far we

were not able to show the presence HSP70 in recipient cells (Figure 43). This mainly seemed to depend on the fact that CD63 was enriched in vesicles (Escola *et al*, 1998; Bonsergent *et al*, 2021), while HSP70 is bulk loaded into EVs (Bonsergent *et al*, 2021). Thus, HSP70 might not be as suitable as CD63 to be coupled to EGFP to monitor EV uptake. A possible alternative for HSP70 in case of inflammasome-elicited EVs might be IL-1β as its presence has been demonstrated in inflammasome-elicited EVs (section 1.9.2) and as its targeting to PIP2 membrane regions (section 4.1.3) might lead to its enrichment in inflammasome-elicited EVs.

Further pointing towards the suitability of CD9 and CD63 is the fact that these have been identified in multiple EVs (Kowal *et al*, 2016) and the technique has been used in studies before (Chivet *et al*, 2014; Joshi *et al*, 2020). While we would still not be able to exclude the possibility that they are not present in all EVs, they may allow us to look at the majority of inflammasome-elicited EVs and thus may be an alternative to classical dyes.

4.2.2 How do Recipient Cells Take up Inflammasome-Elicited EVs?

While tagging of CD9 or CD63 with EGFP may be a good alternative to EV dyes, the dyes generally worked well and, with the appropriate controls, we were able to study the uptake of inflammasome-elicited EVs by recipient cells (mainly THP-1 MΦs).

As mentioned before (section 4.2.1), CFSE attaches to amine groups inside the EV lumen and permanently stays attached to these EV proteins. R18, on the other hand, is a self-quenching membrane dye that only fluoresces when it becomes distributed in the recipient cell's membranes. Thus, when it came to EV quantification, we could count single dots, representing single EVs or EV aggregates for 10K EVs stained with CFSE, but not for SEC EVs stained with R18. Instead, for R18 we opted to measure the overall increase in fluorescence in recipient cells.

In the case of membrane fusion taking place, we would expect to see the plasma membrane of recipient cells to be fluorescent when transferring R18-stained EVs. In the case of vesicle uptake through endocytosis followed by fusion with

endosomal membranes, we would expect a dot-like appearance of the fluorescence. Indeed, upon treatment of cells with R18 stained EVs we did see distinct puncti, indicating that R18-stained SEC EVs were taken up through endocytic processes and then fused with endosomal membranes after internalisation. Along these lines, in the field of virology, it has been reported that the targeting of viruses to the endosomal compartment is a prerequisite for viral content delivery, due to it being controlled by the acidic pH within the endo-lysosomal system (White & Whittaker, 2016). Studies with EVs further support this dependency of EV content release on the pH (Parolini *et al*, 2009; Bonsergent & Lavieu, 2019; Joshi *et al*, 2020; Bonsergent *et al*, 2021), demonstrating that content release is dependent on endosomal acidification leading to membrane fusion (Joshi *et al*, 2020; Bonsergent *et al*, 2021).

To test if EVs might indeed be taken up by an endocytic process, we performed several kinetic and inhibitory experiments.

First, we showed that the process was time dependent, with 10K uptake in THP-1 MΦs starting at around 1-3 h and peaking after around 15 h (Figure 35). SEC uptake was first observed after around 7 h and from then on increased over time (Figure 35). The same trend was observed in the human lung epithelial cell lines A549 and BEAS-2B (Figure 36, Figure 37). Similar timepoints have been shown by others. For example, Jurgielewicz and colleagues have performed time courses of transfers of HEK293T cell-derived EVs to HEK293T recipient cells. They showed EV uptake at around 2 h. Uptake peaked at 12 h and declined thereafter. They used EVs with a diameter roughly in between 50 nm and 300 nm (Jurgielewicz *et al*, 2020), thus we can roughly compare them in size to our SEC and 10K EVs. Perez *et al.* (2022) showed that in the case of mouse fibroblasts and RAW MΦs, EV uptake peaked at 24 h (Perez *et al*, 2022). This is similar to the steady increase we have seen in case of SEC EVs in our experiments. Finally, it is of note that in an ISEV position paper, it was published that there is consensus within the field of EV research that EV transfer experiments are time dependent (Russell *et al*, 2019).

Next, we investigated the specificity of inflammasome-elicited EV uptake. We could show that it was indeed a specific process and not just random fusion or uptake of dye, as demonstrated through competition experiments with non-labelled EVs, which were able to compete for possible receptor engagement with labelled EVs and thus lead to a decrease in detected fluorescent signal (Figure 38, Figure 39). This was in agreement with published literature on EV uptake (Svensson *et al*, 2013; Costa Verdera *et al*, 2017).

Subsequently, with incubation at 4 °C, we investigated if the uptake was of an active, energy requiring nature. Cell culture at 4 °C leads to an arrest of cell growth and to the inhibition of active processes (Hunt *et al*, 2005). As such, it inhibits active forms of EV uptake. Numerous studies have so far shown that EV uptake is reduced at 4 °C and hence energy dependent (Morelli *et al*, 2004; Temchura *et al*, 2008; Tian *et al*, 2010; Escrevente *et al*, 2011; Montecalvo *et al*, 2012; Christianson *et al*, 2013; Delenclos *et al*, 2017). This was also the case in our experiments (Figure 40), thus agreeing with the previously published literature.

Using Cytochalasin D to disrupt actin polymerisation and thus cytoskeletal remodelling, we showed that the uptake process was mainly an endocytic one; however, membrane fusion might also play a role, as Cytochalasin D did not completely block uptake (Figure 41). This incomplete blocking of EV uptake could also be attributed to the inhibition by Cytochalasin D not being 100 % efficient. A significant reduction, but not complete prevention of EV uptake, through Cytochalasin D inhibition has also been shown in various other studies with several different recipient cells (Morelli *et al*, 2004; Hao *et al*, 2007; Obregon *et al*, 2009; Feng *et al*, 2010; Escrevente *et al*, 2011; Fitzner *et al*, 2011; Montecalvo *et al*, 2012; Svensson *et al*, 2013). Cytochalasin D leads to the depolymerisation of F-actin (Brenner & Korn, 1979) and has been intended to be an inhibitor of macropinocytosis and phagocytosis. However, its interference with actin polymerisation affects multiple pathways (Fujimoto *et al*, 2000), basically including all other forms of endocytic uptake mechanisms (Rennick *et al*, 2021).

Since those are just off-target effects, they might not be 100 % blocked. Together this suggests that many different endocytic pathways might be involved in the uptake of inflammasome-elicited EVs.

Above, we have focused on the possibility of EVs being taken up through endocytosis and then fusing with the endosomal membrane. Alternatively, EVs might be able to fuse with the plasma membrane of recipient cells. However, there is only little evidence suggesting this to be the case. One of the few papers that suggest this was published by Montecalvo and colleagues. While they also showed endocytosis to take place, as determined through the use of pHrodo-exosomes in the presence or absence of Cytochalasin D or incubation at 4 °C, they argued that, additionally, plasma membrane fusion and subsequent exosomal content release takes place. Using spectrofluorimetry, immune-electron microscopy, and fluorescent time-lapse microscopy with R18-stained exosomes, they showed exosomal fusion with the plasma membrane (Montecalvo *et al*, 2012). Plasma membrane fusion and as a result the dequenching of R18 was shown to be dependent on the temperature—fusion decreased drastically when recipient cells were incubated with exosomes at 4 °C (Montecalvo *et al*, 2012).
However, the majority of other studies argues that endocytosis takes place and is then followed by plasma membrane fusion of vesicles with the endosomal membrane. Considering that most viruses are also taken up through this latter route, with only a few showing plasma membrane fusion (Pelkmans & Helenius, 2003; Kalia & Jameel, 2011; Yamauchi & Helenius, 2013; Ripa *et al*, 2021), and taking into account the evidence that has demonstrated fusion to be favoured at low pH conditions (Martens & McMahon, 2008; Parolini *et al*, 2009; Espósito *et al*, 2015; Bonsergent & Lavieu, 2019; Joshi *et al*, 2020; Bonsergent *et al*, 2021), it seems more likely that inflammasome-elicited EVs are first taken up in an endocytic process and only later fuse with internal cell membranes.

In the end, EV uptake is probably mediated through several mechanisms at the same time. This has for example been demonstrated by Escrevente and

colleagues, who showed that exosomes derived from an ovarian carcinoma cell line are taken up by recipient cells through clathrin-mediated endocytosis, phagocytosis, and macropinocytosis (Escrevente *et al*, 2011). Verdera and colleagues have also shown that it is not only one uptake route, but that several routes can contribute to EV uptake: they demonstrated EV uptake through macropinocytosis and several subclasses of clathrin-independent endocytosis pathways (caveolae-, flotillin-1-, and Rho-A-dependent; Costa Verdera *et al*, 2017).

4.2.3 EV Binding Versus Internalisation

Furthermore, not only internalisation of EVs but also plasma membrane binding may affect recipient cells. In experiments with the epithelial cell lines A549 and BEAS-2B compared to THP-1 MΦs, we observed that, while THP-1 MΦs take up large numbers of EVs, A549 cells bound EVs to the plasma membrane. Both A549 and BEAS-2B cells only took up small numbers of EVs. This is in line with a study by (Feng *et al*, 2010) that reported that exosomes from leukaemia cell lines (K562 or MT4) are taken up by phagocytic cells, but only slightly by non-phagocytic cells. In case of non-phagocytic cells, attachment of EVs to the plasma membrane was observed. (Feng *et al*, 2010).
However, other studies show the opposite: some cancer cell lines have a mutation of the KRAS gene, leading to the upregulation of macropinocytosis (Commisso *et al*, 2013, 201; Ha *et al*, 2016). A549 is such a cancer cell line (Yoon *et al*, 2010). Thus, we expected the A549 cells to take up EVs. This was supported by studies showing that EVs were rapidly taken up by A549 cells (Ismail *et al*, 2013).

There are also many studies that looked at the interaction of A549 cells with EVs without analysing EV uptake at all. While this is a major drawback of these studies, it is of note that they all showed an effect of EVs on A549 cells (Neri *et al*, 2011; Cordazzo *et al*, 2014; Zhu *et al*, 2017). Thus, while A549 cells might not necessarily take up many EVs, they do seem to respond to EVs.

To determine if the effects mediated by inflammasome-elicited EVs on the various chosen recipient cells are mediated through uptake or surface protein interaction, it would be of interest to block EV uptake and compare this condition to unblocked uptake conditions. If the same effect is still mediated, uptake is not essential for the observed effect.
Something similar has been shown by Atay and colleagues, who blocked uptake of trophoblast-derived exosomes using Cytochalasin D and investigated the effect of EVs on IL-1β release. Even when blocking uptake, IL-1β was still induced, pointing towards the role of surface protein interaction instead of uptake to be important for this particular effect (Atay *et al*, 2011). Of course, it has to be kept in mind here that Cytochalasin D not only changes the uptake behaviour of cells, but all other mechanisms involving actin as well.

4.2.4 EV Uptake by Different Cell Types

While all of the above insights were gained using THP-1 MΦs, and occasionally human airway epithelial cells A549 and BEAS-2B, we wanted to gain a broader understanding of inflammasome-elicited EV interaction with different cells of the body. Thus, we looked at EV interaction and uptake in epithelial and endothelial cells, fibroblasts, and naïve and activated T cells. Doing so, it became clear that uptake levels depend on the different bystander cells.

When comparing THP-1 cells to A549 and BEAS-2B cells, we observed that THP-1 MΦs showed the strongest uptake. This might be due to them being professional phagocytes, but additionally, the fact that we are investigating THP-1 MΦ-derived EVs might have further contributed to this: it has been shown in several studies that EVs favour their donor cells when it comes to their uptake: for example, MSC-derived EVs have been shown to be taken up by MSCs, instead of by monocytes (Sancho-Albero *et al*, 2019). Similarly, Jurgielewicz and colleagues have shown that HEK293T cell-derived EVs are preferentially taken up by HEK293T cells compared to other recipient cell types (Jurgielewicz *et al*, 2020). However, EVs have also been shown to be taken up by different cell types

regardless of the cell type they originated from (Alvarez-Erviti *et al*, 2011; Zech *et al*, 2012; Svensson *et al*, 2013).

In our experiments, THP-1 MΦ-derived inflammasome-elicited EVs were taken up by THP-1 MΦs themselves, NHLFs, HUVECs, and some T cells, thus confirming that they are not specific to the cell type they originated from. These results are in agreement with previous studies, which have shown these cells to be able to take up EVs (Nolte-'t Hoen *et al*, 2009; Wang *et al*, 2011; Ismail *et al*, 2013; Dörsam *et al*, 2018; Kadota *et al*, 2021).

Interestingly, in the case of HUVECs, we observed differences in EV uptake for different culture conditions: HUVECs took up more EVs when grown to confluency, when grown on a transwell rather than when grown on a standard culture plate, and when grown on fibronectin-coated culture surfaces as opposed to uncoated surfaces, thus indicating that the state of cells might further play a role in EV uptake. Furthermore, naïve T cells did not take up 10K EVs and only some took up SEC EVs. Activated T cells took up 10K EVs and showed strong SEC uptake. This would imply that the differentiation status of cells might influence their EV uptake behaviour, which has been shown in studies before (Morelli *et al*, 2004; Pegtel *et al*, 2010; Czernek *et al*, 2015; Jurgielewicz *et al*, 2020). One study has for example shown that the differentiation status of neurons influences EV uptake as human neuronal stem cells took up higher numbers of HEK293T cell-derived EVs than mature neurons. The authors hypothesised that the neuronal stem cells, due to them being highly proliferative under culture conditions, may internalise nutrients as well as EVs in a rather non-specific way, thus explaining the higher EV uptake levels in these cells (Jurgielewicz *et al*, 2020). Along these lines, another study has found that MΦs and mature DCs take up more EVs than monocytes and immature DCs (Czernek *et al*, 2015). This could be due to the phagocytotic activity of MΦs and mature DCs. With regards to T cells, it has been shown that DC-derived exosomes were not targeted to naïve T cells, but only to activated T cells. And while DC-derived exosomes interacted with activated T cells, most of them stayed bound to the plasma

membrane and were neither taken up by recipient cells nor showed fusion with the plasma membrane (Nolte-'t Hoen *et al*, 2009). This interaction between DC exosomes and activated T cells is thought to be due to LFA-1 on T cells. The authors argue that LFA-1 interacts with ICAM-1 found on DC exosomes. As LFA-1 is only upregulated during T cell activation, no interaction was seen with naïve T cells (Nolte-'t Hoen *et al*, 2009). A similar study by Segura and colleagues showed that indeed DCs display ICAM-1 and that this ICAM-1 is required for the binding of those EVs by recipient DCs (Segura *et al*, 2005).

Considering that only some naïve T cells took up SEC EVs the T cell type might also play a role when it comes to EV uptake. Along these lines, studies have previously shown that different T cell subsets are differentially affected by EVs (Muller *et al*, 2016; Ye *et al*, 2016) and that while $CD8^+$ T cells don't take up small EVs, $CD4^+$ and especially Treg cells show small EV uptake (although lower uptake than B cells, monocytes, and NK cells; Muller *et al*, 2017). Employing negative selection, we have isolated the total T cell pool from donor blood, including both $CD4^+$ and $CD8^+$ T cells. It would thus be of interest to analyse whether for example just $CD4^+$ T cells interacted with SEC EVs.

4.2.5 The Possible Influence of Serum on EV Uptake

All the above-described experiments to investigate inflammasome-elicited EV uptake were performed using either serum-free medium or, in case serum (in the form of FBS) was normally added to the respective cell culture medium, EV-depleted medium. This EV depletion was performed through ultracentrifugation of medium at 100,000 x g for 18 h.

Most studies performed on EVs agree with this approach and, as such, most studies have been performed using EV-depleted medium or serum-free medium (Delenclos *et al*, 2017; Emam *et al*, 2018; Tang *et al*, 2018; Casella *et al*, 2018; Gonda *et al*, 2018; Xu *et al*, 2019; Toribio *et al*, 2019, 2019; Joshi *et al*, 2020; Jurgielewicz *et al*, 2020). The idea behind it is that FBS contains bovine-derived EVs (Driedonks *et al*, 2019) as well as lipoproteins (Théry *et al*, 2018), which might interfere with the uptake and effect of EVs of interest. It is indeed such a

standard in the field, that even the MISEV guidelines suggest to use EV-depleted FBS when performing experiments with EVs (Théry *et al*, 2018).
However, in a recent commentary Busatto and colleagues state that this might not always be a good approach (Busatto *et al*, 2022): The authors mention that EVs in serum-free medium are devoid of what is called a biomolecular corona. Biomolecular coronas form *in vivo* upon contact of proteins with other blood components (Tóth *et al*, 2021) and include proteins such as ApoA1, ApoB, ApoC3, ApoE, complement factors 3 and 4B, fibrinogen α-chain, and immunoglobulin heavy constant γ2 and γ4 chains. The corona has been shown to play a substantial role in the function and uptake of synthetic nanoparticles (Tóth *et al*, 2021) and may play a similar role when it comes to EVs (Busatto *et al*, 2022).
In the case of EV-depleted serum (as opposed to serum-free medium), there might be a similar problem, as ultracentrifugation (used in our case) or polymer-based precipitation (another EV-depletion method) have been shown to lead to the removal of lipoproteins, which might also have an influence on EV function (Busatto *et al*, 2022).
When performing experiments in the future to confirm results obtained in experiments shown here, or in general, it would thus be good practice to include a serum-containing condition and compare the outcomes.

To summarise, we could show that recipient MΦs mainly take up inflammasome-elicited EVs through a specific, energy-requiring process involving cytoskeletal remodelling. Considering the above-described literature and taking all our observations together, we believe that inflammasome-elicited EVs are mainly taken up through various endocytic processes. Once in the endosomal compartment, some EVs might fuse with the endosomal membrane and as a result, release their content into the recipient cell's cytoplasm. However, inflammasome-elicited EVs might also influence recipient cells through surface protein interaction at the plasma membrane or inside the endosomal compartment.

While recipient MΦs rapidly take up inflammasome-elicited EVs, uptake of these EVs seems to vary depending on different cell types and cell states. While MΦs, fibroblasts, and endothelial cells took up many inflammasome-elicited EVs, EV uptake by T cells varied. Generally, not only the cell type, but also culture conditions and differentiation states of cells seem to play an important role, with naïve T cells barely taking up EVs while activated T cells took up more, and endothelial cells being more likely to take up EVs when grown at confluency and on a suitable substrate.

4.3 Effect of Inflammasome-Elicited EVs on Recipient Cells

The main question we asked ourselves after having investigated EV interaction with various recipient cells was if EVs are able to spread NLRP3-elicited inflammation and thus contribute to local and systemic inflammation.
To a great extent, our initial hypothesis was based on findings by Brydges and colleagues who showed that in the absence of IL-1β and IL-18 signalling, lethal inflammation still develops (Brydges *et al*, 2013, 2009). We hypothesised that this could be explained by the release of EVs upon inflammasome activation.
In initial experiments, Dr. Christina Budden demonstrated that inflammasome-activation lead to a strong increase in EV secretion. She showed that this increase in EV release was dependent on NLRP3, caspase-1, and GSDMD. This further supported our initial hypothesis, as while IL-1β and IL-18 were shown to be only partially responsible for the lethal inflammation caused by inflammasome activation, caspase-1 and GSDMD were fully required for the systemic, lethal inflammation observed in this mouse model (Xiao *et al*, 2018).
Indeed, our lab has shown that inflammasome-elicited MΦ 10K EVs carry IFN-β and can induce an interferon signature in recipient cells (Budden *et al*, 2021).

We then went on to further characterise the effect of inflammasome-elicited EVs by expanding our analysis from THP-1 MΦ recipient cells to epithelial cells, endothelial cells, T cells, and fibroblasts. Doing so, we were able to show that 10K EVs also have a significant impact on these cells. Additionally, in some of

those recipient cells, as previously seen for MΦ recipient cells, 10KLN EVs led to the induction of an interferon signature. 10KLN EVs further seemed to induce the proliferation of naïve T cells (possibly of a certain T cell type), the upregulation of endothelial activation markers, and generally of inflammatory signalling pathways in endothelial cells and fibroblasts.

We chose to investigate the effects of THP-1 MΦ-derived EVs on various primary human cell types. Primary human cells were chosen to stay as close to the *in vivo* phenotype as possible. THP-1 MΦs were chosen as EV donor cells, as large amounts of vesicles were needed. Such large amounts would not have been possible with primary MΦs. As mentioned before, we decided to focus on CVDs and lung diseases. As such, an alternative to THP-1 MΦ donor cells would have been PBMC-derived MΦs or lung MΦs. In the future, we will thus try to confirm results at a smaller scale using lung or PBMC-derived MΦs.

As briefly mentioned (section 3.1), our lab has previously demonstrated that, using our isolation method, the EVs isolated after LPS and nigericin stimulation are free of LPS (Budden *et al*, 2021). We thus know that the observed effects are due to the transfer of EVs and not induced by LPS. LPS-free EV preparations were achieved by washing donor cells three times with PBS after initial priming with LPS. Only after these washing steps did we apply nigericin to induce inflammasome activation (section 2.4). After nigericin treatment, a washing step is no longer possible, as EVs are directly secreted into the supernatant. However, each EV fraction was later washed once with PBS before being transferred to the different recipient cells. In the case of SEC samples, size exclusion chromatography further separates EVs from contaminants (section 2.6.1). Through including these washing steps, we aimed to purify EVs as much as possible in order to study the effects of EVs only and not nigericin on recipient cells. Although we never quantified the remaining nigericin in EV preparations, we did include a nigericin-only control. The only shortcoming of this control is that this stimulus was only applied for 90 min, while EVs were applied for 15 h. The

90 min timepoint was chosen as nigericin is routinely applied for 90 min when activating the NLRP3 inflammasome.

Taken together, we can therefore assume that most of the effects on recipient cells are due to inflammasome-elicited EVs, but we cannot exclude completely that nigericin might contribute to some of the observed effects, for example by increasing autophagy in recipient cells (Zhang *et al*, 2007; Shi *et al*, 2012; Nabar *et al*, 2017, 201). One possible experimental setup to exclude the effect of nigericin completely would be to switch to a cleaner system, e.g., use ATP as a stimulus and treat samples subsequently with apyrase to degrade ATP prior to EV isolation. Additionally, one could employ different NLRP3 stimuli, transfer EVs, and investigate if the effects differ based on the activator. If the effects remain the same, we would be able to deduce that they are due to inflammasome-elicited EVs and not nigericin or any other stimulus that might still contaminate the isolated EV fraction.

4.3.1 EV Biodistribution

Another important question to consider when studying the systemic effects of inflammasome-elicited EVs, is how long the EVs would actually stay in the circulation and where they would end up once they have left the circulation.

There have been quite a few studies looking at the biodistribution of EVs in mice. Most of these studies investigated the fate of small EVs after IV administration to the tail of mice. They showed that most small EVs leave the circulation within the first few minutes, with only about 30 % of EVs remaining in the circulation after 2 min and ~1.8–3.3 % remaining after 5–30 min. After 1 h or even longer, only 0–1.4 % of EVs were still detected in the blood. They were then found primarily in the liver and in the lung (Kang *et al*, 2021). For example, in one study, luciferase was coupled to lactadherin and this fusion protein was then expressed in murine melanoma cells. Released exosomes were isolated and injected intravenously into mice. The exosomes showed a half-life of 2 min in blood. After 4 h, only very limited luciferase activity could be detected in serum. *In vivo* imaging showed that

the exosomes were distributed first to the liver and subsequently to the lung (Takahashi *et al*, 2013).

There have been fewer studies looking at the biodistribution of large EVs. Most of these studies show large EVs being distributed to the lung and to a lesser extent to the liver within the first hour. Later, large EV levels were found to be higher in the liver than the lung, although still high in the lung as well (Kang *et al*, 2021).

In a recent study by Perez and colleagues the biodistribution of small, medium, and large mammary carcinoma cell-derived EVs was investigated in mice. They injected EVs retro-orbitally or intraperitoneally into healthy mice. Using a reporter system, they showed that EVs were distributed throughout the body within a time frame of 5 min after retro-orbital injection. Taking plasma samples at time points between 5 min and 24 h, they showed that the highest signal in plasma was present at the earliest, 5 min timepoint. In the case of intraperitoneal administration of EVs, the highest signal was present only after 2 h. Regardless of the injection type, EVs localised to the lung. This was of particular importance as, thereafter, these mice developed metastatic foci in the lung (Perez *et al*, 2022).

While all of the above-mentioned biodistribution studies investigated EV uptake in murine models, a recent study analysed small EV (isolated through SEC) pharmacokinetics and biodistributions in a non-human primate model—the pig-tailed macaque (Driedonks *et al*, 2022). In an *in* vitro assay, they showed that the EVs were stable in macaque serum for up to 24 h (Driedonks *et al*, 2022). Next, the authors looked at the organ distribution of EVs after intravenous injection in macaque. They observed the strongest signal in liver and spleen with some uptake in lung (Driedonks *et al*, 2022), thus recapitulating the findings from murine studies (Kang *et al*, 2021). Additionally, they showed limited uptake of EVs by the kidney, heart, colon, and brain. Factors that possibly affect where EVs end up might depend on their surface proteins, their donor cell, or the disease status of different tissues: MSC-derived EV uptake in the kidney was increased

in acute kidney injury as opposed to healthy kidneys (Grange *et al*, 2014; Han *et al*, 2021).

Taking a closer look at EV uptake by the spleen, Driedonks and colleagues narrowed down uptake of EVs by mainly B cells and additionally by monocytes and $CD3^+$ lymphocytes (Driedonks *et al*, 2022). In plasma, EVs associated with PBMCs within 1 min after injection. In particular, they detected an EV signal in 80.8 % of $CD20^+$ B cells, 14.1 % of granulocytes, 13.8 % of monocytes, and 6.7 % of $CD3^+$ lymphocytes—both $CD4^+$ and $CD8^+$ equally (Driedonks *et al*, 2022). While we have not looked at B cells and investigated MΦs as opposed to monocytes, we also observed a higher uptake of EVs by MΦs than T cells. The general high uptake of EVs by B cells in the Driedonks *et al.* study was rather unusual, with other studies showing uptake of most EVs by monocytes and MΦs (Imai *et al*, 2015; Watson *et al*, 2016; Eitan *et al*, 2017). This might for example be explained by different EV donor cells, different EV subtypes such as size, density, etc., or differences in the EV recipients such as species, immune status, or age.

In addition to PBMCs, endothelial cells seem to play a prominent role in EV uptake from the circulation. For example, Verweij *et al.* have shown uptake of EVs from zebrafish embryo circulation by both MΦs and endothelial cells. (Verweij *et al*, 2019). In agreement, Imai *et al.* have shown that clearance of injected exosomes from the circulation took place through MΦ uptake in the liver and spleen and endothelial cell uptake in the lung (Imai *et al*, 2015).

Considering all these results, the circulatory system as well as the lung seemed indeed of particular interest, in that we expect inflammasome-elicited EVs to travel there. However, EV homing to organs like the lung and uptake in the vascular system or lung through e.g., MΦs or endothelial cells, does not mean that the EVs actually exert an effect on these recipient cells. It could just mean that the recipient cells take up the EVs, degrade them in the lysosome, and benefit from EV-derived nutrients.

As shown previously in our lab, this is not the sole fate of EVs in MΦs. While EVs might still end up in MΦ lysosomes, maybe even the majority (Van Niel *et al*,

2018), they nevertheless have been shown to influence MΦ phenotype (Budden *et al*, 2021). This showed that inflammasome-elicited EVs generally have the capability of inducing effects in recipient cells and pushed us to investigate their effects in additional cells.

4.3.2 Effect of Inflammasome-Elicited EVs on Endothelial Cells

We have shown TNF-α signalling via NF-κB, IL-6-JAK- signal transducer and activator of transcription (STAT)3 signalling and IFN-α and IFN-γ response pathways to be enriched in HUVECs treated with 10KLN EVs performing gene set testing (Figure 62). Some of the top DE genes after 10KLN treatment of HUVECs were known markers of activated endothelium such as *SELE*, *IL6*, *CCL2*, *ICAM1*, and *MMP1* (Figure 62).

In 10KLN-treated THP-1 MΦs, our lab has previously shown a similar response. Here also, the IFN-α and IFN-γ pathways as well as TNF-α signalling showed enrichment when performing gene set testing. In these MΦs, ISG induction was caused by IFN-β shown to be present in 10KLN EVs. IFN-β signalled through the IFN-α/β receptor (IFNAR; Budden *et al*, 2021). IFN-β binding to IFNAR has so far only been described to occur at the plasma membrane. After receptor engagement, IFNAR is endocytosed through clathrin-mediated endocytosis and localises to the endosome (Zanin *et al*, 2023). While this was originally thought to be a mechanism to control IFN signalling through subunit availability at the plasma membrane (Ivashkiv & Donlin, 2014), it has now been shown to be essential in the regulation of signalling output (Altman *et al*, 2020; Zanin *et al*, 2023, 2021). Considering that most studies have shown endocytosis to be the main mechanism of EV uptake (Escrevente *et al*, 2011; Fitzner *et al*, 2011; Svensson *et al*, 2013; Heusermann *et al*, 2016), EV-derived IFN-β might engage IFNAR in the endosome. It remains to be investigated though, if IFNAR translocation to the endosome can take place in the absence of IFN binding at the plasma membrane.

This engagement of the IFNAR receptor through IFN-β contained in 10KLN EVs could of course also be mediating the effects observed here in HUVEC cells.

However, there are further mechanisms than can lead to ISG induction. Besides vesicular IFN-β inducing ISGs in recipient cells, IL-1β can also induce ISGs (Orzalli *et al*, 2018; Aarreberg *et al*, 2019), which could be another way for inflammasome-elicited EVs to possibly induce ISG expression in recipient cells. Another route of ISG induction has been shown by Puhm *et al.* in HUVECs. EVs (isolated through centrifugation at 18,000 x g) from THP-1 monocytes stimulated with LPS for 16 h, could induce ISGs in THP-1 and HUVEC recipient cells through ROS-elicited modifications in mitochondrial RNA (Puhm et al., 2019).

Inflammatory signalling, especially through TNF-α and IL-6, can lead to the activation of endothelial cells. Endothelial cell activation can be divided into type I and type II activation. Type I activation takes place almost immediately in response to endothelial cell stimulation. It does not require gene transcription nor *de novo* protein synthesis. Instead, it involves the release of proteins such as von Willebrand factor (vWF), P-selectin, thrombin, and histamine. Type II activation, on the other hand, is delayed (over hours or even days). It requires gene transcription and protein synthesis, for example the generation of E-selectin, ICAM-1, Vascular Cell Adhesion Molecule 1 (VCAM-1), vWF, IL-1, MCP-1, and tissue factor (Zhang, 2022).

Indeed, it has been shown that EVs from 16 h long LPS-stimulated THP-1 monocytes induce inflammatory signalling and lead to endothelial cell activation: pathway enrichment analysis has shown that these EVs lead to type I IFN and TNF signalling pathway enrichment. Using qPCR, the authors confirmed the increase in expression of 2'-5'-Oligoadenylate Synthetase 2 (*OAS2)*, MX Dynamin Like GTPase 1 (*MX1)*, Interferon Induced Protein With Tetratricopeptide Repeats 1 (*IFIT1)*, and Radical S-Adenosyl Methionine Domain Containing 2 (*RSAD2)* (all induced through IFN type I signalling), the increase in expression of *CCL2*, *CXCL8*, *VCAM1*, and *ICAM1* (all induced through TNF signalling), and the increase in expression of *CXCL10* and *CXCL11* (both induced by TNF and type I IFN signalling). Looking at the contributions of both IFN and TNF-α signalling pathways, they demonstrated that, in their model of the EV-mediated effect,

TNF-α plays the primary role in endothelial cell activation and, in line with this, showed the presence of TNF-α in these EVs (Puhm *et al*, 2019). The activation of the endothelial cells was further shown to have *in vivo* relevance: they performed a low-grade endotoxemia model in healthy human volunteers who were injected 2 ng/kg LPS intravenously, identifying an increase in the EVs of interest (which in their case were $TOM22^{+}$ EVs), and mirroring the *in vitro* experimental results. They then took those EVs and used them to stimulate HUVEC cells. Indeed, they induced TNF-dependent genes and ISGs (Puhm *et al*, 2019).

Endothelial activation through THP-1 derived EVs has further been shown by Wang *et al.* They treated THP-1 monocytes with LPS for 24 h and subsequently isolated EVs using a 1,500 x g spin to pellet debris followed by a 20,000 x g centrifugation for 15 min to pellet EVs, which were then washed twice (Wang *et al*, 2011). Thus, while the isolation is different to the one employed in our experiments to isolate 10K EVs, they are still similar enough for a comparison. Additionally, instead of using canonical inflammasome activation (LPS for 2 h followed by nigericin for 90 min) as employed in our experiment, they used non-canonical inflammasome activation (24 h LPS stimulation). As discussed previously (section 3.1.3), the outcome of canonical and non-canonical inflammasome activation is still pretty much the same, so this would not make our data less comparable. As we did, they showed EV uptake by HUVECs after 4 h. They further showed engagement of the ERK1/2 and NF-κB signalling pathways in recipient HUVEC cells through an increased mRNA expression of *ICAM1*, *VCAM1*, and *SELE*—all being NF-κB dependent. Furthermore, as we have shown previously (Budden *et al*, 2021), they demonstrated that this is not due to LPS contamination still present on the EVs. They then went on to show that LPS-treated THP-1-derived EVs contained IL-1β and further contained ICAM-1 and VCAM-1. Finally, they showed that IL-1β secretion through EVs after LPS stimulation was NLRP3 dependent and that inhibiting IL-1 receptor signalling reversed the observed induction of VCAM-1 and E-selectin in recipient HUVEC cells (Wang *et al*, 2011). This is in line with studies reporting that IL-1β and other

inflammatory stimuli such as TNF-α or oxLDL induce the upregulation of adhesion molecules in endothelial cells (Szmitko *et al*, 2003).

Interestingly, all of the above studies have shown these effects with EVs isolated at around 20,000 x g, thus probably mainly microvesicles. This is in line with our finding, that 10KLN EVs and not SEC EVs lead to the inflammatory signalling in HUVECs.

So what are the effects of an activated endothelium? The induction of selectins such as E-selectin induces rolling of cells along the endothelium. Sialyl-Lewis^x on monocytes or neutrophils, for example, interacts with P-selectin and E-selectin (Murphy *et al*, 2017). CXCL8 (IL-8) and other chemokines bound to proteoglycan on endothelial cells further induce conformational changes in leukocyte integrins LFA-1 and complement receptor 3, increasing their adhesion to molecules such as ICAM-1. This interaction stops the rolling motion and instead cells firmly attach (Murphy *et al*, 2017). Subsequently, cells cross the endothelial layer and migrate to the inflamed tissue (Murphy *et al*, 2017). This migration is mediated through, for example, the interaction of the CCR2 receptor on migrating cells and a gradient of MCP-1 (Boring *et al*, 1998) or down a CXCL8 gradient (Murphy *et al*, 2017).

When endothelial cell activation becomes chronic, it can lead to endothelial dysfunction (Zhang, 2022). Endothelial dysfunction is described as a decrease in the endothelium's ability or the failure to perform its basal functions and is characterised by reduced availability of NO or the imbalance between other endothelium-derived relaxing and contracting factors (Szmitko *et al*, 2003). It also includes the inability to control coagulation, permeability, or quiesce leukocytes (Pober & Sessa, 2007).
For example, endothelial cell dysfunction is observed in atherosclerosis (Gimbrone & García-Cardeña, 2016), which has also been linked to the NLRP3 inflammasome (Duewell *et al*, 2010). Amongst the many genes of interest in the context of atherosclerosis, the IL-18 receptor was significantly upregulated in

HUVEC cells upon 10KLN EV treatment (Table 2), which can be explained by the fact that especially the combination of IL-1β, IFN-γ, and TNF-α, all of which have been implicated in our model, has been shown to lead to the upregulation of the IL-18 receptor (Szmitko *et al*, 2003). IL-18 drives atherosclerosis in several ways, for example by inducing IFN-γ production from several lymphocytes such as endothelial cells, smooth muscle cells, and MΦs—all prominent cells in atherosclerotic plaques. IFN-γ then promotes T_H1 immune response development, which further drive atherosclerosis (Szmitko *et al*, 2003).

Endothelial dysfunction has further been linked to type 2 diabetes (Zhang, 2022). This is especially of interest, as it is further known that NLRP3 plays a role in insulin resistance: proinflammatory cytokines such as IL-1β can disrupt insulin signalling, thus driving disease pathology. In addition to IL-1β, IL-18 and IFN-γ play a role and blocking of NLRP3 not only led to a reduction in IL-1β, but further in IL-18 and IFN-γ (Vandanmagsar *et al*, 2011). Considering that we see an increase in IFN signalling after 10KLN EV transfer (Figure 62) in addition to the known presence of IL-1β in EVs, one should definitely consider inflammasome-elicited EVs when looking at the involvement of NLRP3 in type 2 diabetes.

4.3.3 Effect of Inflammasome-Elicited EVs on Fibroblasts

Considering the increase in tissue accessibility caused by the activation of the endothelium, it can be deduced that, as a result, cells outside the circulatory system encounter an increase in proinflammatory cells such as MΦs and thus inflammasome-elicited EVs. Furthermore, NLRP3 in tissue-resident MΦs themselves might get activated, leading to local inflammasome-elicited EV release.

One of our initial questions was whether inflammasome-elicited MΦ-derived EVs play a role in the development of fibrosis, for example in tissues like the lung. As pro-fibrotic MΦs have been shown to coordinate scar formation through various interactions with fibroblasts (Adler *et al*, 2020), with fibroblasts being the major source of cellular, pathological ECM in fibrosis (Pakshir & Hinz, 2018; Shook *et*

al, 2018; Ramachandran *et al*, 2019), we set out to investigate the effect of NLRP3-elicited EVs on fibroblasts.

While we could demonstrate an increase in inflammatory signalling in fibroblasts (Figure 64), we did not find a general upregulation of fibrosis marker genes with *VIM* and *TGFB1* showing no upregulation and *MMP7* showing only an increase in qPCR, but not sequencing experiments (Figure 65). However, the low sequencing depth might not have allowed us to pick up changes in *MMP7*. Furthermore, in terms of fibrosis, a 15 h timepoint is very short. In those types of fibrosis that showed involvement of inflammation, such as in pulmonary fibrosis or silicosis, fibrosis developed over longer timeframes (Porter *et al*, 2002; White *et al*, 2022). Thus, the fact that EVs cause inflammation could mean that, if EV release occurs constantly over long time periods, 10KLN EVs could possibly contribute to the progression of pulmonary fibrosis or other types of fibrosis linked to inflammation.

4.3.4 Effect of Inflammasome-Elicited EVs on Naïve T cells

In T cells we observed the enrichment of MSigDB hallmark gene sets for MYC targets, oxidative phosphorylation, and MTORC1 signalling, along with enrichment of the inflammatory signalling gene sets for TNF-α and IFN-α/γ signalling (Figure 67B).

Resting T cells mainly rely on oxidative phosphorylation of glucose and fatty acids to generate their energy (Bishop *et al*, 2021): they employ glycolysis to convert glucose into pyruvate, which is then further shuttled from the cytoplasm into the mitochondrion, where it is then converted to acetyl-coenzyme A(CoA) for oxidative phosphorylation. During oxidative phosphorylation, acetyl-CoA is sequentially oxidised, yielding carbon dioxide, GTP, and water. Additionally, the two electron carriers NADH and FADH2 are reduced, which then drive the electron transport chain to produce ATP and ROS. Besides glucose, fatty acids and glutamine are also oxidised in the tricarboxylic acid (TCA) cycle to produce energy (Bishop *et al*, 2021).

Upon recognition of their respective antigen, T cells increase their rate of glucose and amino acid uptake and the conversion of glucose to pyruvate during glycolysis. This leads to high levels of pyruvate, the majority of which is not shuttled as usual to the mitochondria for oxidative phosphorylation, but instead the majority of pyruvate is reduced to lactate and subsequently secreted. Additionally, while T cell activation leads to a substantial increase of glucose uptake and the reduction of pyruvate to lactate, an increase in oxidative phosphorylation is still observed (Sena *et al*, 2013; Blagih *et al*, 2015).

Some of the key signalling pathways that drive these metabolic changes in T cells upon antigen recognition include the Phosphoinositide 3-kinase (PI3K)/Akt/mTOR axis as well as c-Myc signalling. mTOR is involved in the translation of key metabolic transcription factors and in regulating their stability. It plays such an important role that T cells deficient in mTOR can no longer engage in metabolic reprogramming once they have recognised their cognate antigen. They do not proliferate and cannot gain their effector functions (Delgoffe *et al*, 2009).

c-Myc is one of the transcription factors that is upregulated through Akt and mTOR signalling. It is involved in the increase of glucose and amino acid (involving glutamine) uptake and their metabolism (Bishop *et al*, 2021).

Thus, the fact that we observed an enrichment in the oxidative phosphorylation, the mTORC1, and the MYC pathways, points to a role of 10KLN EVs in metabolic reprogramming in T cells.

This metabolic reprogramming in T cells depends on several cytokines, such as IFN-γ, TNF-α, and even IL-1β (Bishop *et al*, 2021), that have so far been implicated in our experiments and whose pathways are also enriched in T cells themselves: we have seen an enrichment in IFN-α/γ and TNF-α signalling not only in T cells, but also in fibroblasts and endothelial cells. Furthermore, recipient MΦs have been shown to increase their IFN signalling and inflammasome-elicited EVs have been shown to contain IL-1β (Budden *et al*, 2021).

Of course, so far, this has not been confirmed in other experiments. A next step would for example be to perform a Seahorse assay to properly investigate if a change in naïve T cell metabolism is induced upon 10KLN stimulation.

Furthermore, quantifying naïve T cell proliferation and checking with flow cytometry for certain subpopulation of T cell types would be possible next steps.

4.3.5 The Role of IL-1β in the Mediation of These Effects

We know that IL-1β binding to its receptor leads to the induction of MyD88 and, as a result, to the activation of NF-κB, AP-1, JNK, several MAPKs such as p38, ERKs, and different IRFs (Murphy *et al*, 2017). Locally, this leads to the activation of the vascular endothelium, the activation of lymphocytes, local tissue destruction, and increased access for effector cells. Systemically, IL-1β induces fever and the production of IL-6 (Murphy *et al*, 2017). NF-κB leads for example to the induction of innate and inflammatory genes such as iNOS, TNF-α, IL-1, and IL-6 (Owen *et al*, 2019).

Considering the above-described effects of 10KLN EVs on the various recipient cells, it seems likely that at least part of these effects was mediated through IL-1β being present in 10KLN EVs.

As touched upon before, IL-1β and IL-18 have mainly been discussed to be released through GSDMD pores during pyroptosis (Monteleone *et al*, 2015). However, some scientists have reported IL-1β release in cells not undergoing pyroptosis: for example, murine neutrophils were shown to release IL-1β without dying of pyroptosis (Karmakar *et al*, 2015), as were murine DCs upon oxPAPC stimulation (Zanoni *et al*, 2016). In the case of human cells, monocytes have been shown to release IL-1 in the absence of pyroptosis in response to *S*. Typhimurium infection (Diamond *et al*, 2017) and when stimulated with LPS (alternative inflammasome activation) (Gaidt *et al*, 2016; Gaidt & Hornung, 2017).

While still in the presence of pyroptosis and GSDMD pore formation, EVs have been shown to be an alternative pathway for IL-1β release: for the first time in 2001, MacKenzie and colleagues showed the release of IL-1β in microvesicles after ATP stimulation of cells (MacKenzie *et al*, 2001): They reported that, upon stimulation of THP-1 monocytes with LPS and ATP, plasma membrane vesicles (<0.5 µm diameter) form. These EVs were shown to contain both unprocessed (32 kDa) and processed (17 kDa) IL-1β (MacKenzie *et al*, 2001). When

transferred to recipient HeLa cells transfected with an EGFP-reporter for IL-1 receptor activity, fluorescence was reported, indicating that IL-1β released from microvesicles engages the IL-1 receptor on recipient cells. This happened when applying EVs released within 2–10 min after stimulation. EVs collected later after inflammasome activation still led to EGFP expression in recipient cells; however, at later time points, treatment of recipient cells with supernatant was a stronger inducer of EGFP than treatment with vesicles (MacKenzie *et al*, 2001).
The presence of IL-1β in inflammasome-elicited EVs was later confirmed, for example by Pizzirani and colleagues (Pizzirani *et al*, 2007) but also in our lab: Dr. Christina Budden stimulated THP-1 MΦs with LPS + nigericin and isolated 2K, 10K, and SEC EVs. IL-1β levels were either measured directly (thus determining how much IL-1β was stuck to the outside of EVs), or after lysis of the EVs with 0.1 % Triton X-100. 2K and 10K EVs dose dependently showed the presence of IL-1β at low levels in samples without Triton addition and higher levels in EVs lysed with Triton. Levels of IL-1β in Triton lysed EVs were higher for 10K EVs than for 2K EVs (normalisation of EVs was performed based on donor cell number, not EV number) (Budden *et al*, 2021).

When it comes to the mechanism of how IL-1β ends up in microvesicles, much has been discovered in recent years: in 2018, Monteleone and colleagues showed that upon maturation, IL-1β relocates from the cytosol to the plasma membrane (Monteleone *et al*, 2018). At neutral pH, pre-IL-1β is negatively charged. Cleavage of pre-IL-1β to its active form reveals a polybasic motif within the cytokine. This allows mature IL-1β to interact with highly negatively charged PIP2. PIP2 is enriched at plasma membrane ruffles and a result of PIP2-IL-1β interactions, mature IL-1β is targeted to plasma membrane ruffles (Monteleone *et al*, 2018). What Monteleone and colleagues have shown for IL-1β is likely to be relevant for IL-18: they compared IL-1β and IL-18 and found conservation of the polybasic region (Monteleone *et al*, 2018). Being targeted to plasma membrane ruffles of course increases the likelihood of IL-1β ending up in EVs. As microvesicles form from plasma membranes (Cocucci *et al*, 2009), the IL-1β

is probably found in microvesicles. 10K EVs isolated in our experiments are probably mainly microvesicles. Thus, we would expect to find IL-1β in 10K EVs.

Combining this with the observation that GSDMD pores formed upon inflammasome activation lead to the influx of Ca^{2+}, which triggers microvesicle release at plasma membrane sites of GSDMD pores (Rühl *et al*, 2018), the model can further be expanded: we have both an increased relocation of mature IL-1β to plasma membrane ruffles and additional an induction of microvesicle release at plasma membrane sites.
Furthermore, knowing that microvesicles form at sites of GSDMD pores and actually have been shown to contain GSDMD pores (which was also indicated by the observation that we found N-terminal GSDMD in our inflammasome-elicited EVs), we can hypothesise that inflammasome-elicited EVs are leaky for certain molecules (mature IL-1β, due to its size and charge being amongst them), leading to the release of IL-1β from microvesicles. This would also explain the results observed in our lab when measuring IL-1β with or without previous EV lysis: if IL-1β can leak from vesicles, lysis is not necessary to be able to detect IL-1β. However, still some IL-1β remained within the EV lumen (or not all EVs contain GSDMD pores), and thus IL-1β levels were even higher in samples treated with Triton X-100. A way to further investigate this would be to isolate inflammasome-elicited EVs, keep them in media over a period of time, and then separate both media and EVs: the amount of IL-1β in the media itself should increase while the amount of EV associated IL-1β should decrease.

In conclusion, it can be said from previous experiments performed in our lab and from literature that we know that IL-1β is found in 10K EVs and microvesicles and that this might account for some of the effects mediated by 10KLN EVs.
For example, it might account for the induction of TNF and IL-6 signalling: our lab has previously shown that treatment of cells with the soluble IL-1 receptor antagonist anakinra lead to the abolishment of TNF and IL-6 expression (Budden *et al*, 2021).

An alternative source of IL-1β might be extracellular ASC specks. It has previously been shown that ASC specks are released during pyroptosis and are able to process IL-1β in the extracellular space (Franklin *et al*, 2014, 2018). ASC specks could theoretically be co-purified with EVs, depending on the centrifugation speed and isolation method chosen. However, taking into account the particle sizes measured using NTA, the particles isolated in our experiments are of smaller size (750 nm and smaller) than the average extracellular ASC speck, which is around 1 µm in size (Franklin *et al*, 2014; Fernandes-Alnemri *et al*, 2007), and thus, we do not expect significant ASC speck contaminations in our EV preparations. Nevertheless, considering that some smaller ASC specks could also be formed (Franklin *et al*, 2018), it cannot be excluded that extracellular ASC specks might, to a certain extent, contribute to some of the effects observed.

While it might account for those effects, it does not seem to mediate ISG induction. Instead, ISG induction was found to depend on IFN-β signalling through the type I IFN receptor. IFN-β was present within EVs and barely on the outside of EVs, as determined through EV lysis with Triton X-100 before IFN-β measurements (Budden *et al*, 2021). Being within EVs, this raises the question how IFN-β can engage in IFNAR binding. IFN-β-IFNAR binding is described to take place at the plasma membrane (Lazear *et al*, 2019). Upon receptor engagement, IFNAR re-localises to the endosome. This relocation is crucial for IFNAR signalling and signalling termination (Marchetti *et al*, 2006; Chmiest *et al*, 2016). Considering that, from the experiments described in this thesis, EV uptake seems to take place through endocytic mechanisms, it can be hypothesised that IFN-β binding to IFNAR takes place in the endosome. However, it is so far unclear if IFNAR signalling from the endosome can take place without previous ligand binding at the plasma membrane. Intriguingly, IFN-β binding to IFNAR and induction of signalling in the endosome might explain why we observed IFN signalling in cells that endocytosed EVs (MΦs, endothelial, and fibroblasts) but not in cells that did not take up 10K EVs (naïve T cells).

4.3.6 The Role of HMGB1 in the Mediation of These Effects

As discussed in the introduction (section 1.7.1), IL-1β and IL-18 release are not the only outcomes of inflammasome activation. Instead, other molecules, including the DAMP HMGB1, are also released. Fiuza and colleagues examined the effects of HMGB1 on endothelial cells and found that it induced the expression of VCAM-1, ICAM-1, and RAGE and led to the secretion of TNF-α, IL-8, MCP-1, and others, thus leading to the activation of the endothelium (Fiuza *et al*, 2003). These findings are similar to our results, which also point towards EC activation. Combining this knowledge with results published in 2021 by Wang and colleagues, who showed that macrophages release HMGB1-loaded EVs upon LPS stimulation (Wang *et al*, 2021), this suggests that some of the effects observed might be due to HMGB1 carried within inflammasome-elicited EVs. As HMGB1 release was shown to be downstream of GSDMD pore formation, mediated by NINJ1 (Kayagaki *et al*, 2021), these potential HMGB1-loaded EVs might also be released in other cases of lytic cell death and would not be specific to inflammasome activation.

4.4 Concluding Remarks

EVs were originally thought to be a way for cells to get rid of waste. Considering cells already have lysosomes to do so, researchers started to challenge this assumption and have since demonstrated that EVs contribute significantly to cell-to-cell communication throughout the body.

In this thesis, I have shown that this also holds true for inflammasome-elicited EVs. Indeed, inflammasome activation leads to a strong increase in EV release. These EVs carry a distinct RNA signature and can be identified by the presence of N-terminal GSDMD; they are thus specific to inflammasome-activated cells. This has implications for their use as potential biomarkers, as well as for their effect on different surrounding cells:

NCDs are as common as ever and a big burden on today's economy. NCD-related deaths are further expected to rise, thus making it a pressing issue to diagnose these diseases early to intervene before they become irreversible and

the cause of death for the affected individual. EVs have the potential to serve as biomarkers for inflammasome involvement—either through their distinct RNA signature or through the presence of N-terminal GSDMD.

While the prevention of diseases in the first place is in my opinion the most important way to approach the problem of rising numbers in deaths caused by NCDs, treatment must also be improved. To find suitable, specific treatment options, pathogenesis must be understood. I have analysed the content of inflammasome-elicited EVs and studied their effect on various cell types relevant to NLRP3-related diseases, such as atherosclerosis and type II diabetes, in order to understand the specific role these EVs could play. Not only are inflammasome-elicited EVs taken up by diverse recipient cells, including MΦs, endothelial cells, epithelial cells, fibroblasts, and T cells (primarily activated T cells), but they also affect various cells. They induce inflammatory signalling in endothelial cells and lead to the upregulation of marker genes of activated epithelial cells. An activated endothelium allows cells to leave the circulation and enter tissues where they can further affect cells such as fibroblasts. I have shown that inflammasome-elicited EVs have the potential to induce inflammatory signalling pathways in fibroblasts. Under prolonged exposure to inflammatory stimuli, including EVs released by inflammasome-elicited MΦs but also cytokines released by surrounding cells (possibly induced by inflammasome-elicited EVs), fibroblasts, together with further cells, may lead to the development of fibrosis, for example causing COPD. Taken together, these findings may not only help in the prevention of a broad spectrum of diseases, but also help to elucidate how systemic inflammation can spread and thus provide insights into possible treatment options.

References

Aarreberg LD, Esser-Nobis K, Driscoll C, Shuvarikov A, Roby JA & Gale M (2019) Interleukin-1β Induces mtDNA Release to Activate Innate Immune Signaling via cGAS-STING. *Molecular Cell* 74: 801-815.e6

Adler M, Mayo A, Zhou X, Franklin RA, Meizlish ML, Medzhitov R, Kallenberger SM & Alon U (2020) Principles of Cell Circuits for Tissue Repair and Fibrosis. *iScience* 23: 100841

Admyre C, Grunewald J, Thyberg J, Bripenäck S, Tornling G, Eklund A, Scheynius A & Gabrielsson S (2003) Exosomes with major histocompatibility complex class II and co-stimulatory molecules are present in human BAL fluid. *European Respiratory Journal* 22: 578–583

Admyre C, Johansson SM, Qazi KR, Filén J-J, Lahesmaa R, Norman M, Neve EPA, Scheynius A & Gabrielsson S (2007) Exosomes with Immune Modulatory Features Are Present in Human Breast Milk. *The Journal of Immunology* 179: 1969–1978

Aglietti RA, Estevez A, Gupta A, Ramirez MG, Liu PS, Kayagaki N, Ciferri C, Dixit VM & Dueber EC (2016) GsdmD p30 elicited by caspase-11 during pyroptosis forms pores in membranes. *Proceedings of the National Academy of Sciences* 113: 7858–7863

Agostini L, Martinon F, Burns K, McDermott MF, Hawkins PN & Tschopp J (2004) NALP3 forms an IL-1beta-processing inflammasome with increased activity in Muckle-Wells autoinflammatory disorder. *Immunity* 20: 319–25

Allen IC, Jania CM, Wilson JE, Tekeppe EM, Hua X, Brickey WJ, Kwan M, Koller BH, Tilley SL & Ting JP-Y (2012) Analysis of NLRP3 in the Development of Allergic Airway Disease in Mice. *The Journal of Immunology* 188: 2884–2893

Altman JB, Taft J, Wedeking T, Gruber CN, Holtmannspötter M, Piehler J & Bogunovic D (2020) Type I IFN is siloed in endosomes. *Proceedings of the National Academy of Sciences* 117: 17510–17512

Alvarez-Erviti L, Seow Y, Yin H, Betts C, Lakhal S & Wood MJA (2011) Delivery of siRNA to the mouse brain by systemic injection of targeted exosomes. *Nat Biotechnol* 29: 341–345

Andre F, Schartz NEC, Movassagh M, Flament C, Pautier P, Morice P, Pomel C, Lhomme C, Escudier B, Le Chevalier T, *et al* (2002) Malignant effusions and immunogenic tumour-derived exosomes. *Lancet* 360: 295–305

Andrews S, Pierre Lindenbaum, Brian Howard, & Phil Ewels (2017) FastQC: a quality control tool for high throughput sequence data.

Archer GT & Blackwood A (1965) Formation of Charcot-Leyden crystals in human eosinophils and basophils and study of the composition of isolated crystals. *Journal of Experimental Medicine* 122: 173–180

Atay S, Gercel-Taylor C & Taylor DD (2011) Human Trophoblast-Derived Exosomal Fibronectin Induces Pro-Inflammatory Il-1β Production by Macrophages. *American Journal of Reproductive Immunology* 66: 259–269

Atkin-Smith GK & Poon IKH (2017) Disassembly of the Dying: Mechanisms and Functions. *Trends in Cell Biology* 27: 151–162

Atkin-Smith GK, Tixeira R, Paone S, Mathivanan S, Collins C, Liem M, Goodall KJ, Ravichandran KS, Hulett MD & Poon IKH (2015) A novel mechanism of generating extracellular vesicles during apoptosis via a beads-on-a-string membrane structure. *Nature Communications* 6: 1–10

Bakele M, Joos M, Burdi S, Allgaier N, Pöschel S, Fehrenbacher B, Schaller M, Marcos V, Kümmerle-Deschner J, Rieber N, *et al* (2014) Localization and Functionality of the Inflammasome in Neutrophils*. *Journal of Biological Chemistry* 289: 5320–5329

Baker PJ, Boucher D, Bierschenk D, Tebartz C, Whitney PG, D'Silva DB, Tanzer MC, Monteleone M, Robertson AAB, Cooper MA, *et al* (2015) NLRP3 inflammasome activation downstream of cytoplasmic LPS recognition by both caspase-4 and caspase-5. *Eur J Immunol* 45: 2918–2926

Ball DP, Taabazuing CY, Griswold AR, Orth EL, Rao SD, Kotliar IB, Vostal LE, Johnson DC & Bachovchin DA (2020) Caspase-1 interdomain linker cleavage is required for pyroptosis. *Life Sci Alliance* 3: e202000664

Banerjee S & Bond JS (2008) Prointerleukin-18 Is Activated by Meprin β in Vitro and in Vivo in Intestinal Inflammation *. *Journal of Biological Chemistry* 283: 31371–31377

Barlan AU, Griffin TM, Mcguire KA & Wiethoff CM (2011) Adenovirus Membrane Penetration Activates the NLRP3 Inflammasome. *Journal of Virology* 85: 146–155

Barnett KC, Li S, Liang K & Ting JP-Y (2023) A 360° view of the inflammasome: Mechanisms of activation, cell death, and diseases. *Cell* 186: 2288–2312

Baroja-Mazo A, Martín-Sánchez F, Gomez AI, Martínez CM, Amores-Iniesta J, Compan V, Barberà-Cremades M, Yagüe J, Ruiz-Ortiz E, Antón J, *et al* (2014) The NLRP3 inflammasome is released as a particulate danger signal that amplifies the inflammatory response. *Nature immunology* 15: 738–48

Bauernfeind FG, Horvath G, Stutz A, Alnemri ES, MacDonald K, Speert D, Fernandes-Alnemri T, Wu J, Monks BG, Fitzgerald KA, *et al* (2009) Cutting edge: NF-kappaB activating pattern recognition and cytokine receptors license NLRP3

inflammasome activation by regulating NLRP3 expression. *Journal of immunology (Baltimore, Md : 1950)* 183: 787–91

Bazan JF, Timans JC & Kastelein RA (1996) A newly defined interleukin-1? *Nature* 379: 591–591

Berda-Haddad Y, Robert S, Salers P, Zekraoui L, Farnarier C, Dinarello CA, Dignat-George F & Kaplanski G (2011) Sterile inflammation of endothelial cell-derived apoptotic bodies is mediated by interleukin-1α. *Proceedings of the National Academy of Sciences* 108: 20684–20689

Berg S, Kutra D, Kroeger T, Straehle CN, Kausler BX, Haubold C, Schiegg M, Ales J, Beier T, Rudy M, *et al* (2019) ilastik: interactive machine learning for (bio)image analysis. *Nat Methods* 16: 1226–1232

Besnard A-G, Guillou N, Tschopp J, Erard F, Couillin I, Iwakura Y, Quesniaux V, Ryffel B & Togbe D (2011) NLRP3 inflammasome is required in murine asthma in the absence of aluminum adjuvant. *Allergy* 66: 1047–1057

Bhatnagar S & Schorey JS (2007) Exosomes released from infected macrophages contain Mycobacterium avium glycopeptidolipids and are proinflammatory. *Journal of Biological Chemistry* 282: 25779–25789

Bhowmick R & Gappa-Fahlenkamp H (2016) Cells and Culture Systems Used to Model the Small Airway Epithelium. *Lung* 194: 419–428

Bianco F, Pravettoni E, Colombo A, Schenk U, Möller T, Matteoli M & Verderio C (2005) Astrocyte-Derived ATP Induces Vesicle Shedding and IL-1β Release from Microglia. *The Journal of Immunology* 174: 7268–7277

Bibo-Verdugo B, Snipas SJ, Kolt S, Poreba M & Salvesen GS (2020) Extended subsite profiling of the pyroptosis effector protein gasdermin D reveals a region recognized by inflammatory caspase-11. *Journal of Biological Chemistry* 295: 11292–11302

Bishop EL, Gudgeon N & Dimeloe S (2021) Control of T Cell Metabolism by Cytokines and Hormones. *Frontiers in Immunology* 12: 1055

Bissig C & Gruenberg J (2014) ALIX and the multivesicular endosome: ALIX in Wonderland. *Trends in Cell Biology* 24: 19–25

Blagih J, Coulombe F, Vincent EE, Dupuy F, Galicia-Vázquez G, Yurchenko E, Raissi TC, van der Windt GJW, Viollet B, Pearce EL, *et al* (2015) The Energy Sensor AMPK Regulates T Cell Metabolic Adaptation and Effector Responses In Vivo. *Immunity* 42: 41–54

Bode JG, Albrecht U, Häussinger D, Heinrich PC & Schaper F (2012) Hepatic acute phase proteins – Regulation by IL-6- and IL-1-type cytokines involving

STAT3 and its crosstalk with NF-κB-dependent signaling. *European Journal of Cell Biology* 91: 496–505

Bolstad BM, Irizarry RA, Åstrand M & Speed TP (2003) A comparison of normalization methods for high density oligonucleotide array data based on variance and bias. *Bioinformatics (Oxford, England)* 19: 185–193

Bonsergent E, Grisard E, Buchrieser J, Schwartz O, Théry C & Lavieu G (2021) Quantitative characterization of extracellular vesicle uptake and content delivery within mammalian cells. *Nature Communications* 12

Bonsergent E & Lavieu G (2019) Content release of extracellular vesicles in a cell-free extract. *FEBS Letters* 593: 1983–1992

Boring L, Gosling J, Cleary M & Charo IF (1998) Decreased lesion formation in CCR2−/− mice reveals a role for chemokines in the initiation of atherosclerosis. *Nature* 394: 894–897

Bottino LZMF, Rodrigues-Junior DM, Farias IS de, Branco LM, Iyer NG, de Albuquerque GE, Vettore AL & Bortoluci KR (2021) Extracellular vesicles derived from head and neck squamous cells carcinoma inhibit NLRP3 inflammasomes. *Current Research in Immunology* 2: 175–183

Boucher D, Monteleone M, Coll RC, Chen KW, Ross CM, Teo JL, Gomez GA, Holley CL, Bierschenk D, Stacey KJ, *et al* (2018) Caspase-1 self-cleavage is an intrinsic mechanism to terminate inflammasome activity. *J Exp Med* 215: 827–840

Brenner SL & Korn ED (1979) Substoichiometric concentrations of cytochalasin D inhibit actin polymerization. Additional evidence for an F-actin treadmill. *Journal of Biological Chemistry* 254: 9982–9985

Broderick L & Hoffman HM (2022) IL-1 and autoinflammatory disease: biology, pathogenesis and therapeutic targeting. *Nat Rev Rheumatol* 18: 448–463

Broz P & Dixit VM (2016) Inflammasomes: mechanism of assembly, regulation and signalling. *Nature reviews Immunology* 16: 407–20

Brubaker SW, Bonham KS, Zanoni I & Kagan JC (2015) Innate immune pattern recognition: a cell biological perspective. *Annual review of immunology* 33: 257–90

Brydges SD, Broderick L, McGeough MD, Pena CA, Mueller JL & Hoffman HM (2013) Divergence of IL-1, IL-18, and cell death in NLRP3 inflammasomopathies. *The Journal of clinical investigation* 123: 4695–705

Brydges SD, Mueller JL, McGeough MD, Pena CA, Misaghi A, Gandhi C, Putnam CD, Boyle DL, Firestein GS, Horner AA, *et al* (2009) Inflammasome-Mediated

Disease Animal Models Reveal Roles for Innate but Not Adaptive Immunity. *Immunity* 30: 875–887

Budden CF (2020) Characterisation of Extracellular Vesicles Released upon NLRP3 Activation and Their Impact on Bystander Cells.

Budden CF, Gearing LJ, Kaiser R, Standke L, Hertzog PJ & Latz E (2021) Inflammasome-induced extracellular vesicles harbour distinct RNA signatures and alter bystander macrophage responses. *Journal of Extracellular Vesicles* 10: e12127

Bürckstümmer T, Baumann C, Blüml S, Dixit E, Dürnberger G, Jahn H, Planyavsky M, Bilban M, Colinge J, Bennett KL, *et al* (2009) An orthogonal proteomic-genomic screen identifies AIM2 as a cytoplasmic DNA sensor for the inflammasome. *Nature immunology* 10: 266–72

Busatto S, Yang Y, Iannotta D, Davidovich I, Talmon Y & Wolfram J (2022) Considerations for extracellular vesicle and lipoprotein interactions in cell culture assays. *Journal of Extracellular Vesicles* 11: e12202

Caby MP, Lankar D, Vincendeau-Scherrer C, Raposo G & Bonnerot C (2005) Exosomal-like vesicles are present in human blood plasma. *International Immunology* 17: 879–887

Cai X, Chen J, Xu H, Liu S, Jiang Q-X, Halfmann R & Chen ZJ (2014) Prion-like polymerization underlies signal transduction in antiviral immune defense and inflammasome activation. *Cell* 156: 1207–1222

Carpenter AE, Jones TR, Lamprecht MR, Clarke C, Kang IH, Friman O, Guertin DA, Chang JH, Lindquist RA, Moffat J, *et al* (2006) CellProfiler: image analysis software for identifying and quantifying cell phenotypes. *Genome Biology* 7: R100

Carvalho BS & Irizarry RA (2010) A framework for oligonucleotide microarray preprocessing. *Bioinformatics (Oxford, England)* 26: 2363–2367

Casella G, Colombo F, Finardi A, Descamps H, Ill-Raga G, Spinelli A, Podini P, Bastoni M, Martino G, Muzio L, *et al* (2018) Extracellular Vesicles Containing IL-4 Modulate Neuroinflammation in a Mouse Model of Multiple Sclerosis. *Molecular Therapy* 26: 2107–2118

Cassel SL, Eisenbarth SC, Iyer SS, Sadler JJ, Colegio OR, Tephly LA, Carter AB, Rothman PB, Flavell RA & Sutterwala FS (2008) The Nalp3 inflammasome is essential for the development of silicosis. *Proceedings of the National Academy of Sciences of the United States of America* 105: 9035–9040

Cavarra E, Carraro F, Fineschi S, Naldini A, Bartalesi B, Pucci A & Lungarella G (2004) Early response to bleomycin is characterized by different cytokine and cytokine receptor profiles in lungs. *American Journal of Physiology-Lung Cellular and Molecular Physiology* 287: L1186–L1192

Cermakian N, Westfall S & Kiessling S (2014) Circadian Clocks and Inflammation: Reciprocal Regulation and Shared Mediators. *Arch Immunol Ther Exp* 62: 303–318

Chang MY, Kang I, Gale M, Manicone AM, Kinsella MG, Braun KR, Wigmosta T, Parks WC, Altemeier WA, Wight TN, *et al* (2017) Versican is produced by Trif- and type I interferon-dependent signaling in macrophages and contributes to fine control of innate immunity in lungs. *American Journal of Physiology-Lung Cellular and Molecular Physiology* 313: L1069–L1086

Chen X, He W, Hu L, Li J, Fang Y, Wang X, Xu X, Wang Z, Huang K & Han J (2016a) Pyroptosis is driven by non-selective gasdermin-D pore and its morphology is different from MLKL channel-mediated necroptosis. *Cell Res* 26: 1007–1020

Chen Y, Lun ATL, Smyth GK, Burden CJ, Ryan DP, Khang TF & Lianoglou S (2016b) From reads to genes to pathways: differential expression analysis of RNA-Seq experiments using Rsubread and the edgeR quasi-likelihood pipeline. *F1000Research 2016 5:1438* 5: 1438

Cheng KT, Xiong S, Ye Z, Hong Z, Di A, Tsang KM, Gao X, An S, Mittal M, Vogel SM, *et al* (2017) Caspase-11-mediated endothelial pyroptosis underlies endotoxemia-induced lung injury. *Journal of Clinical Investigation* 127: 4124–4135

Chiang H-Y, Lu H-H, Sudhakar JN, Chen Y-W, Shih N-S, Weng Y-T & Shui J-W (2022) IL-22 initiates an IL-18-dependent epithelial response circuit to enforce intestinal host defence. *Nat Commun* 13: 874

Chivet M, Javalet C, Laulagnier K, Blot B, Hemming FJ & Sadoul R (2014) Exosomes secreted by cortical neurons upon glutamatergic synapse activation specifically interact with neurons. *Journal of Extracellular Vesicles* 3: 24722

Chmiest D, Sharma N, Zanin N, Viaris de Lesegno C, Shafaq-Zadah M, Sibut V, Dingli F, Hupé P, Wilmes S, Piehler J, *et al* (2016) Spatiotemporal control of interferon-induced JAK/STAT signalling and gene transcription by the retromer complex. *Nat Commun* 7: 13476

Choi D-S, Kim D-K, Kim Y-K & Gho YS (2013) Proteomics, transcriptomics and lipidomics of exosomes and ectosomes. *PROTEOMICS* 13: 1554–1571

Choi D-S, Kim D-K, Kim Y-K & Gho YS (2015) Proteomics of extracellular vesicles: Exosomes and ectosomes. *Mass Spectrometry Reviews* 34: 474–490

Christ A & Latz E (2019) The Western lifestyle has lasting effects on metaflammation. *Nat Rev Immunol* 19: 267–268

Christ A, Lauterbach M & Latz E (2019) Western Diet and the Immune System: An Inflammatory Connection. *Immunity* 51: 794–811

Christianson HC, Svensson KJ, van Kuppevelt TH, Li J-P & Belting M (2013) Cancer cell exosomes depend on cell-surface heparan sulfate proteoglycans for their internalization and functional activity. *Proceedings of the National Academy of Sciences* 110: 17380–17385

Cocucci E, Racchetti G & Meldolesi J (2009) Shedding microvesicles: artefacts no more. *Trends in Cell Biology* 19: 43–51

Coeshott C, Ohnemus C, Pilyavskaya A, Ross S, Wieczorek M, Kroona H, Leimer AH & Cheronis J (1999) Converting enzyme-independent release of tumor necrosis factor α and IL-1β from a stimulated human monocytic cell line in the presence of activated neutrophils or purified proteinase 3. *Proceedings of the National Academy of Sciences* 96: 6261–6266

Cohen I, Rider P, Carmi Y, Braiman A, Dotan S, White MR, Voronov E, Martin MU, Dinarello CA & Apte RN (2010) Differential release of chromatin-bound IL-1α discriminates between necrotic and apoptotic cell death by the ability to induce sterile inflammation. *Proceedings of the National Academy of Sciences* 107: 2574–2579

Coll RC, Robertson AAB, Chae JJ, Higgins SC, Muñoz-Planillo R, Inserra MC, Vetter I, Dungan LS, Monks BG, Stutz A, *et al* (2015) A small molecule inhibitior of the NLRP3 inflammasome is a potential therapeutic for inflammatory diseases. *Nat Med* 21: 248–255

Coll RC, Schroder K & Pelegrín P (2022) NLRP3 and pyroptosis blockers for treating inflammatory diseases. *Trends in Pharmacological Sciences* 43: 653–668

Colombo F, Norton EG & Cocucci E (2021) Microscopy approaches to study extracellular vesicles. *Biochim Biophys Acta Gen Subj* 1865: 129752

Colombo M, Raposo G & Théry C (2014) Biogenesis, Secretion, and Intercellular Interactions of Exosomes and Other Extracellular Vesicles. *Annual Review of Cell and Developmental Biology* 30: 255–289

Commisso C, Davidson SM, Soydaner-Azeloglu RG, Parker SJ, Kamphorst JJ, Hackett S, Grabocka E, Nofal M, Drebin JA, Thompson CB, *et al* (2013) Macropinocytosis of protein is an amino acid supply route in Ras-transformed cells. *Nature* 497: 633–637

del Conde I, Shrimpton CN, Thiagarajan P & López JA (2005) Tissue-factor–bearing microvesicles arise from lipid rafts and fuse with activated platelets to initiate coagulation. *Blood* 106: 1604–1611

Cordazzo C, Petrini S, Neri T, Lombardi S, Carmazzi Y, Pedrinelli R, Paggiaro P & Celi A (2014) Rapid shedding of proinflammatory microparticles by human mononuclear cells exposed to cigarette smoke is dependent on Ca2+ mobilization. *Inflammation Research* 63: 539–547

Costa Verdera H, Gitz-Francois JJ, Schiffelers RM & Vader P (2017) Cellular uptake of extracellular vesicles is mediated by clathrin-independent endocytosis and macropinocytosis. *Journal of Controlled Release* 266: 100–108

Craven RR, Gao X, Allen IC, Gris D, Wardenburg JB, McElvania-TeKippe E, Ting JP & Duncan JA (2009) Staphylococcus aureus α-Hemolysin Activates the NLRP3-Inflammasome in Human and Mouse Monocytic Cells. *PLOS ONE* 4: e7446

Crystal RG, Bitterman PB, Mossman B, Schwarz MI, Sheppard D, Almasy L, Chapman HA, Friedman SL, King TE, Leinwand LA, *et al* (2012) Future Research Directions in Idiopathic Pulmonary Fibrosis. *American Journal of Respiratory and Critical Care Medicine* 166: 236–246

Cuisset L, Jeru I, Dumont B, Fabre A, Cochet E, Bozec JL, Delpech M, Amselem S, Touitou I & Group and the FC study (2011) Mutations in the autoinflammatory cryopyrin-associated periodic syndrome gene: epidemiological study and lessons from eight years of genetic analysis in France. *Annals of the Rheumatic Diseases* 70: 495–499

Cunningham F, Allen JE, Allen J, Alvarez-Jarreta J, Amode MR, Armean IM, Austine-Orimoloye O, Azov AG, Barnes I, Bennett R, *et al* (2022) Ensembl 2022. *Nucleic Acids Research* 50: D988–D995

Czernek L, Chworos A & Duechler M (2015) The Uptake of Extracellular Vesicles is Affected by the Differentiation Status of Myeloid Cells. *Scandinavian Journal of Immunology* 82: 506–514

Dagvadorj J, Mikulska-Ruminska K, Tumurkhuu G, Ratsimandresey RA, Carriere J, Andres AM, Marek-Iannucci S, Song Y, Chen S, Lane M, *et al* (2021) Recruitment of pro-IL-1α to mitochondrial cardiolipin, via shared LC3 binding domain, inhibits mitophagy and drives maximal NLRP3 activation. *Proceedings of the National Academy of Sciences* 118: e2015632118

Davis MA, Fairgrieve MR, Den Hartigh A, Yakovenko O, Duvvuri B, Lood C, Thomas WE, Fink SL & Gale M (2019) Calpain drives pyroptotic vimentin cleavage, intermediate filament loss, and cell rupture that mediates immunostimulation. *Proceedings of the National Academy of Sciences* 116: 5061–5070

Dehghani M, Gulvin SM, Flax J & Gaborski TR (2020) Systematic Evaluation of PKH Labelling on Extracellular Vesicle Size by Nanoparticle Tracking Analysis. *Sci Rep* 10: 9533

Delenclos M, Trendafilova T, Mahesh D, Baine AM, Moussaud S, Yan IK, Patel T & McLean PJ (2017) Investigation of Endocytic Pathways for the Internalization of Exosome-Associated Oligomeric Alpha-Synuclein. *Frontiers in Neuroscience* 11

Delgoffe GM, Kole TP, Zheng Y, Zarek PE, Matthews KL, Xiao B, Worley PF, Kozma SC & Powell JD (2009) The mTOR Kinase Differentially Regulates Effector and Regulatory T Cell Lineage Commitment. *Immunity* 30: 832–844

Denhardt DT & Guo X (1993) Osteopontin: a protein with diverse functions. *The FASEB Journal* 7: 1475–1482

Denning N-L, Aziz M, Gurien SD & Wang P (2019) DAMPs and NETs in Sepsis. *Frontiers in Immunology* 10

Deretic V, Saitoh T & Akira S (2013) Autophagy in infection, inflammation and immunity. *Nature reviews Immunology* 13: 722–37

van Deuren RC, Arts P, Cavalli G, Jaeger M, Steehouwer M, van de Vorst M, Gilissen C, Joosten LAB, Dinarello CA, Mhlanga MM, *et al* (2021) Impact of rare and common genetic variation in the interleukin-1 pathway on human cytokine responses. *Genome Medicine* 13: 94

Di A, Xiong S, Ye Z, Malireddi RKS, Kometani S, Zhong M, Mittal M, Hong Z, Kanneganti TD, Rehman J, *et al* (2018) The TWIK2 Potassium Efflux Channel in Macrophages Mediates NLRP3 Inflammasome-Induced Inflammation. *Immunity* 49: 56-65.e4

Di Paolo NC & Shayakhmetov DM (2016) Interleukin 1α and the inflammatory process. *Nat Immunol* 17: 906–913

Di Stefano A, Caramori G, Barczyk A, Vicari C, Brun P, Zanini A, Cappello F, Garofano E, Padovani A, Contoli M, *et al* (2014) Innate immunity but not NLRP3 inflammasome activation correlates with severity of stable COPD. *Thorax* 69: 516–524

Diamond CE, Leong KWK, Vacca M, Rivers-Auty J, Brough D & Mortellaro A (2017) Salmonella typhimurium-induced IL-1 release from primary human monocytes requires NLRP3 and can occur in the absence of pyroptosis. *Scientific Reports* 7

Dinarello CA (2009) Immunological and inflammatory functions of the interleukin-1 family. *Annu Rev Immunol* 27: 519–550

Dinarello CA (2018) Overview of the IL-1 family in innate inflammation and acquired immunity. *Immunol Rev* 281: 8–27

Dinarello CA, Goldin NP & Wolff SM (1974) DEMONSTRATION AND CHARACTERIZATION OF TWO DISTINCT HUMAN LEUKOCYTIC PYROGENS. *J Exp Med* 139: 1369–1381

Dinarello CA, Ikejima T, Warner SJ, Orencole SF, Lonnemann G, Cannon JG & Libby P (1987) Interleukin 1 induces interleukin 1. I. Induction of circulating

interleukin 1 in rabbits in vivo and in human mononuclear cells in vitro. *The Journal of Immunology* 139: 1902–1910

Dinarello CA, Renfer L & Wolff SM (1977) Human leukocytic pyrogen: purification and development of a radioimmunoassay. *Proceedings of the National Academy of Sciences* 74: 4624–4627

Donaldson JG (2019) Macropinosome formation, maturation and membrane recycling: lessons from clathrin-independent endosomal membrane systems. *Philos Trans R Soc Lond B Biol Sci* 374: 20180148

Dor PJ, Ackerman SJ & Gleich GJ (1984) Charcot-Leyden Crystal Protein and Eosinophil Granule Major Basic Protein in Sputum of Patients with Respiratory Diseases. *Am Rev Respir Dis* 130: 1072–1077

Dörsam B, Bösl T, Reiners KS, Barnert S, Schubert R, Shatnyeva O, Zigrino P, Engert A, Hansen HP & von Strandmann EP (2018) Hodgkin Lymphoma-Derived Extracellular Vesicles Change the Secretome of Fibroblasts Toward a CAF Phenotype. *Frontiers in Immunology* 9

Dostert C, Pétrilli V, Van Bruggen R, Steele C, Mossman BT & Tschopp J (2008) Innate immune activation through Nalp3 inflammasome sensing of asbestos and silica. *Science* 320: 674–677

Downs KP, Nguyen H, Dorfleutner A & Stehlik C (2020) An overview of the non-canonical inflammasome. *Molecular Aspects of Medicine* 76: 100924

Doz E, Noulin N, Boichot E, Guénon I, Fick L, Le Bert M, Lagente V, Ryffel B, Schnyder B, Quesniaux VFJ, *et al* (2008) Cigarette Smoke-Induced Pulmonary Inflammation Is TLR4/MyD88 and IL-1R1/MyD88 Signaling Dependent. *The Journal of Immunology* 180: 1169–1178

Driedonks T, Jiang L, Carlson B, Han Z, Liu G, Queen SE, Shirk EN, Gololobova O, Liao Z, Nyberg LH, *et al* (2022) Pharmacokinetics and biodistribution of extracellular vesicles administered intravenously and intranasally to Macaca nemestrina. *Journal of Extracellular Biology* 1: e59

Driedonks TAP, Nijen Twilhaar MK & Nolte-'t Hoen ENM (2019) Technical approaches to reduce interference of Fetal calf serum derived RNA in the analysis of extracellular vesicle RNA from cultured cells. *Journal of Extracellular Vesicles* 8

Duewell P, Kono H, Rayner KJ, Sirois CM, Vladimer G, Bauernfeind FG, Abela GS, Franchi L, Nuñez G, Schnurr M, *et al* (2010) NLRP3 inflammasomes are required for atherogenesis and activated by cholesterol crystals. *Nature* 464: 1357–1361

Duncan JA, Bergstralh DT, Wang Y, Willingham SB, Ye Z, Zimmermann AG & Ting JPY (2007) Cryopyrin/NALP3 binds ATP/dATP, is an ATPase, and requires

ATP binding to mediate inflammatory signaling. *Proceedings of the National Academy of Sciences of the United States of America* 104: 8041–8046

Durinck S, Moreau Y, Kasprzyk A, Davis S, De Moor B, Brazma A & Huber W (2005) BioMart and Bioconductor: A powerful link between biological databases and microarray data analysis. *Bioinformatics* 21: 3439–3440

Durinck S, Spellman PT, Birney E & Huber W (2009) Mapping identifiers for the integration of genomic datasets with the R/Bioconductor package biomaRt. *Nature protocols* 4: 1184–1191

Eisenberg SP, Evans RJ, Arend WP, Verderber E, Brewer MT, Hannum CH & Thompson RC (1990) Primary structure and functional expression from complementary DNA of a human interleukin-1 receptor antagonist. *Nature* 343: 341–346

Eitan E, Green J, Bodogai M, Mode NA, Bæk R, Jørgensen MM, Freeman DW, Witwer KW, Zonderman AB, Biragyn A, *et al* (2017) Age-Related Changes in Plasma Extracellular Vesicle Characteristics and Internalization by Leukocytes. *Sci Rep* 7: 1342

Elinav E, Strowig T, Henao-Mejia J & Flavell RA (2011) Regulation of the Antimicrobial Response by NLR Proteins. *Immunity* 34: 665–679

Elliott JM, Rouge L, Wiesmann C & Scheer JM (2009) Crystal Structure of Procaspase-1 Zymogen Domain Reveals Insight into Inflammatory Caspase Autoactivation. *J Biol Chem* 284: 6546–6553

Eltom S, Stevenson CS, Rastrick J, Dale N, Raemdonck K, Wong S, Catley MC, Belvisi MG & Birrell MA (2011) P2x7 receptor and caspase 1 activation are central to airway inflammation observed after exposure to tobacco smoke. *PLoS ONE* 6

Emam SE, Ando H, Lila ASA, Shimizu T, Ukawa M, Okuhira K, Ishima Y, Mahdy MA, Ghazy FS & Ishida T (2018) A Novel Strategy to Increase the Yield of Exosomes (Extracellular Vesicles) for an Expansion of Basic Research. *Biological and Pharmaceutical Bulletin* 41: 733–742

Escola JM, Kleijmeer MJ, Stoorvogel W, Griffith JM, Yoshie O & Geuze HJ (1998) Selective enrichment of tetraspan proteins on the internal vesicles of multivesicular endosomes and on exosomes secreted by human B-lymphocytes. *Journal of Biological Chemistry* 273: 20121–20127

Escrevente C, Keller S, Altevogt P & Costa J (2011) Interaction and uptake of exosomes by ovarian cancer cells. *BMC Cancer* 11

Espósito DLA, Nguyen JB, DeWitt DC, Rhoades E & Modis Y (2015) Physico-chemical requirements and kinetics of membrane fusion of flavivirus-like particles. *Journal of General Virology* 96: 1702–1711

Evavold CL, Ruan J, Tan Y, Xia S, Wu H & Kagan JC (2018) The Pore-Forming Protein Gasdermin D Regulates Interleukin-1 Secretion from Living Macrophages. *Immunity* 48: 35-44.e6

Ewels P, Magnusson M, Lundin S & Käller M (2016) MultiQC: summarize analysis results for multiple tools and samples in a single report. *Bioinformatics* 32: 3047–3048

Fantuzzi G, Puren AJ, Harding MW, Livingston DJ & Dinarello CA (1998) Interleukin-18 Regulation of Interferon γ Production and Cell Proliferation as Shown in Interleukin-1β–Converting Enzyme (Caspase-1)-Deficient Mice. *Blood* 91: 2118–2125

Faustin B, Lartigue L, Bruey J-M, Luciano F, Sergienko E, Bailly-Maitre B, Volkmann N, Hanein D, Rouiller I & Reed JC (2007) Reconstituted NALP1 inflammasome reveals two-step mechanism of caspase-1 activation. *Molecular cell* 25: 713–24

Feng D, Zhao W-L, Ye Y-Y, Bai X-C, Liu R-Q, Chang L-F, Zhou Q & Sui S-F (2010) Cellular Internalization of Exosomes Occurs Through Phagocytosis. *Traffic* 11: 675–687

Fernandes-Alnemri T, Wu J, Yu J-W, Datta P, Miller B, Jankowski W, Rosenberg S, Zhang J & Alnemri ES (2007) The pyroptosome: a supramolecular assembly of ASC dimers mediating inflammatory cell death via caspase-1 activation. *Cell Death Differ* 14: 1590–1604

Fernandes-Alnemri T, Yu J-W, Datta P, Wu J & Alnemri ES (2009) AIM2 activates the inflammasome and cell death in response to cytoplasmic DNA. *Nature* 458: 509–513

Filipe V, Hawe A & Jiskoot W (2010) Critical evaluation of nanoparticle tracking analysis (NTA) by NanoSight for the measurement of nanoparticles and protein aggregates. *Pharmaceutical Research* 27: 796–810

Fisch D, Clough B, Domart M-C, Encheva V, Bando H, Snijders AP, Collinson LM, Yamamoto M, Shenoy AR & Frickel E-M (2020) Human GBP1 Differentially Targets Salmonella and Toxoplasma to License Recognition of Microbial Ligands and Caspase-Mediated Death. *Cell Reports* 32: 108008

Fitzner D, Schnaars M, van Rossum D, Krishnamoorthy G, Dibaj P, Bakhti M, Regen T, Hanisch U-K & Simons M (2011) Selective transfer of exosomes from oligodendrocytes to microglia by macropinocytosis. *Journal of Cell Science* 124: 447–458

Fiuza C, Bustin M, Talwar S, Tropea M, Gerstenberger E, Shelhamer JH & Suffredini AF (2003) Inflammation-promoting activity of HMGB1 on human microvascular endothelial cells. *Blood* 101: 2652–2660

Franchi L, Amer A, Body-Malapel M, Kanneganti T-D, Ozören N, Jagirdar R, Inohara N, Vandenabeele P, Bertin J, Coyle A, *et al* (2006) Cytosolic flagellin requires Ipaf for activation of caspase-1 and interleukin 1beta in salmonella-infected macrophages. *Nature immunology* 7: 576–82

Franchi L, Eigenbrod T & Núñez G (2009) Cutting Edge: TNF-α Mediates Sensitization to ATP and Silica via the NLRP3 Inflammasome in the Absence of Microbial Stimulation1. *The Journal of Immunology* 183: 792–796

Franklin BS, Bossaller L, De Nardo D, Ratter JM, Stutz A, Engels G, Brenker C, Nordhoff M, Mirandola SR, Al-Amoudi A, *et al* (2014) The adaptor ASC has extracellular and 'prionoid' activities that propagate inflammation. *Nature immunology* 15: 727–37

Franklin BS, Latz E & Schmidt FI (2018) The intra- and extracellular functions of ASC specks. *Immunol Rev* 281: 74–87

Friker LL, Scheiblich H, Hochheiser IV, Brinkschulte R, Riedel D, Latz E, Geyer M & Heneka MT (2020) β-Amyloid Clustering around ASC Fibrils Boosts Its Toxicity in Microglia. *Cell Rep* 30: 3743-3754.e6

Fujimoto LM, Roth R, Heuser JE & Schmid SL (2000) Actin Assembly Plays a Variable, but not Obligatory Role in Receptor-Mediated Endocytosis. *Traffic* 1: 161–171

Gaidt MM, Ebert TS, Chauhan D, Schmidt T, Schmid-Burgk JL, Rapino F, Robertson AAB, Cooper MA, Graf T & Hornung V (2016) Human Monocytes Engage an Alternative Inflammasome Pathway. *Immunity* 44: 833–846

Gaidt MM & Hornung V (2017) Alternative inflammasome activation enables IL-1β release from living cells. *Current opinion in immunology* 44: 7–13

Gasse P, Riteau N, Charron S, Girre S, Fick L, Pétrilli V, Tschopp J, Lagente V, Quesniaux VFJ, Ryffel B, *et al* (2009) Uric Acid Is a Danger Signal Activating NALP3 Inflammasome in Lung Injury Inflammation and Fibrosis. *Am J Respir Crit Care Med* 179: 903–913

Gatti S, Beck J, Fantuzzi G, Bartfai T & Dinarello CA (2002) Effect of interleukin-18 on mouse core body temperature. *American Journal of Physiology-Regulatory, Integrative and Comparative Physiology* 282: R702–R709

Gemmell CH, Sefton MV & Yeo EL (1993) Platelet-derived microparticle formation involves glycoprotein IIb-IIIa. Inhibition by RGDS and a Glanzmann's thrombasthenia defect. *Journal of Biological Chemistry* 268: 14586–14589

Ghayur T, Banerjee S, Hugunin M, Butler D, Herzog L, Carter A, Quintal L, Sekut L, Talanian R, Paskind M, *et al* (1997) Caspase-1 processes IFN-γ-inducing factor and regulates LPS-induced IFN- γ production. *Nature* 386: 619–623

Gimbrone MA & García-Cardeña G (2016) Endothelial Cell Dysfunction and the Pathobiology of Atherosclerosis. *Circ Res* 118: 620–636

Global Burden of Disease (2019) Non-communicable diseases — Level 1 cause.

Global Burden of Disease (2020) Health systems must adapt to rapid shift in disease burden.

Golightly LM, Thomas LL, Dvorak AM & Ackerman SJ (1992) Charcot-Leyden crystal protein in the degranulation and recovery of activated basophils. *Journal of Leukocyte Biology* 51: 386–392

Gonda A, Kabagwira J, Senthil GN, Bennit HRF, Neidigh JW, Khan S & Wall NR (2018) Exosomal survivin facilitates vesicle internalization. *Oncotarget* 9: 34919–34934

Grange C, Tapparo M, Bruno S, Chatterjee D, Quesenberry PJ, Tetta C & Camussi G (2014) Biodistribution of mesenchymal stem cell-derived extracellular vesicles in a model of acute kidney injury monitored by optical imaging. *International Journal of Molecular Medicine* 33: 1055–1063

Grebe A, Hoss F & Latz E (2018) NLRP3 Inflammasome and the IL-1 Pathway in Atherosclerosis. *Circulation Research* 122: 1722–1740

Grigor'eva AE, Tamkovich SN, Eremina AV, Tupikin AE, Kabilov MR, Chernykh VV, Vlassov VV, Laktionov PP & Ryabchikova EI (2016) Characteristics of exosomes andmicroparticles discovered in human tears. *Biomeditsinskaya Khimiya* 62: 99–106

Groß CJ & Groß O (2016) PKA Has the Gall to Oppose NLRP3. *Immunity* 45: 707–709

Groß CJ, Mishra R, Schneider KS, Médard G, Wettmarshausen J, Dittlein DC, Shi H, Gorka O, Koenig PA, Fromm S, *et al* (2016) K+ Efflux-Independent NLRP3 Inflammasome Activation by Small Molecules Targeting Mitochondria. *Immunity* 45: 761–773

Gu Y, Kuida K, Tsutsui H, Ku G, Hsiao K, Fleming MA, Hayashi N, Higashino K, Okamura H, Nakanishi K, *et al* (1997) Activation of Interferon-γ Inducing Factor Mediated by Interleukin-1β Converting Enzyme. *Science* 275: 206–209

Guescini M, Genedani S, Stocchi V & Agnati LF (2010) Astrocytes and Glioblastoma cells release exosomes carrying mtDNA. *Journal of Neural Transmission* 117: 1–4

Gupta D, Liang X, Pavlova S, Wiklander OPB, Corso G, Zhao Y, Saher O, Bost J, Zickler AM, Piffko A, *et al* (2020) Quantification of extracellular vesicles in vitro and in vivo using sensitive bioluminescence imaging. *Journal of Extracellular Vesicles* 9

Ha KD, Bidlingmaier SM & Liu B (2016) Macropinocytosis Exploitation by Cancers and Cancer Therapeutics. *Front Physiol* 7: 381

Hammad H & Lambrecht BN (2021) The basic immunology of asthma. *Cell* 184: 1469–1485

Han Z, Liu S, Pei Y, Ding Z, Li Y, Wang X, Zhan D, Xia S, Driedonks T, Witwer KW, *et al* (2021) Highly efficient magnetic labelling allows MRI tracking of the homing of stem cell-derived extracellular vesicles following systemic delivery. *Journal of Extracellular Vesicles* 10: e12054

Hannum CH, Wilcox CJ, Arend WP, Joslin FG, Dripps DJ, Heimdal PL, Armes LG, Sommer A, Eisenberg SP & Thompson RC (1990) Interleukin-1 receptor antagonist activity of a human interleukin-1 inhibitor. *Nature* 343: 336–340

Hao S, Bai O, Li F, Yuan J, Laferte S & Xiang J (2007) Mature dendritic cells pulsed with exosomes stimulate efficient cytotoxic T-lymphocyte responses and antitumour immunity. *Immunology* 120: 90–102

Harding C, Heuser J & Stahl P (1983) Receptor-mediated endocytosis of transferrin and recycling of the transferrin receptor in rat reticulocytes. *The Journal of cell biology* 97: 329–339

Harding C, Heuser J & Stahl P (1984) Endocytosis and intracellular processing of transferrin and colloidal gold-transferrin in rat reticulocytes: Demonstration of a pathway for receptor shedding. *European Journal of Cell Biology* 35: 256–263

Håversen L, Danielsson KN, Fogelstrand L & Wiklund O (2009) Induction of proinflammatory cytokines by long-chain saturated fatty acids in human macrophages. *Atherosclerosis* 202: 382–393

He W, Wan H, Hu L, Chen P, Wang X, Huang Z, Yang Z-H, Zhong C-Q & Han J (2015) Gasdermin D is an executor of pyroptosis and required for interleukin-1β secretion. *Cell research* 25: 1285–98

Heilig R, Dick MS, Sborgi L, Meunier E, Hiller S & Broz P (2018) The Gasdermin-D pore acts as a conduit for IL-1β secretion in mice. *European Journal of Immunology* 48: 584–592

Herzog C, Haun RS, Kaushal V, Mayeux PR, Shah SV & Kaushal GP (2009) Meprin A and meprin α generate biologically functional IL-1β from pro-IL-1β. *Biochemical and Biophysical Research Communications* 379: 904–908

Heusermann W, Hean J, Trojer D, Steib E, von Bueren S, Graff-Meyer A, Genoud C, Martin K, Pizzato N, Voshol J, *et al* (2016) Exosomes surf on filopodia to enter cells at endocytic hot spots, traffic within endosomes, and are targeted to the ER. *Journal of Cell Biology* 213: 173–184

Hiemstra PS, Grootaers G, van der Does AM, Krul CAM & Kooter IM (2018) Human lung epithelial cell cultures for analysis of inhaled toxicants: Lessons learned and future directions. *Toxicology in Vitro* 47: 137–146

Hikita T, Miyata M, Watanabe R & Oneyama C (2018) Sensitive and rapid quantification of exosomes by fusing luciferase to exosome marker proteins. *Scientific Reports* 8

Hochheiser IV, Pilsl M, Hagelueken G, Moecking J, Marleaux M, Brinkschulte R, Latz E, Engel C & Geyer M (2022) Structure of the NLRP3 decamer bound to the cytokine release inhibitor CRID3. *Nature* 604: 184–189

Hoekstra D, De Boer T, Klappe K & Wilschut J (1984) Fluorescence method for measuring the kinetics of fusion between biological membranes. *Biochemistry* 23: 5675–5681

Hoffman HM, Mueller JL, Broide DH, Wanderer AA & Kolodner RD (2001a) Mutation of a new gene encoding a putative pyrin-like protein causes familial cold autoinflammatory syndrome and Muckle–Wells syndrome. *Nat Genet* 29: 301–305

Hoffman HM, Wanderer AA & Broide DH (2001b) Familial cold autoinflammatory syndrome: Phenotype and genotype of an autosomal dominant periodic fever. *Journal of Allergy and Clinical Immunology* 108: 615–620

Holme PA, Ørvim U, Hamers MJAG, Solum NO, Brosstad FR, Barstad RM & Sakariassen KS (1997) Shear-Induced Platelet Activation and Platelet Microparticle Formation at Blood Flow Conditions as in Arteries With a Severe Stenosis. *Arteriosclerosis, Thrombosis, and Vascular Biology* 17: 646–653

Hornung V, Ablasser A, Charrel-Dennis M, Bauernfeind F, Horvath G, Caffrey DR, Latz E & Fitzgerald KA (2009) AIM2 recognizes cytosolic dsDNA and forms a caspase-1-activating inflammasome with ASC. *Nature* 458: 514–8

Hornung V, Bauernfeind F, Halle A, Samstad EO, Kono H, Rock KL, Fitzgerald KA & Latz E (2008) Silica crystals and aluminum salts activate the NALP3 inflammasome through phagosomal destabilization. *Nature Immunology* 9: 847–856

Hoshino A, Costa-Silva B, Shen TL, Rodrigues G, Hashimoto A, Tesic Mark M, Molina H, Kohsaka S, Di Giannatale A, Ceder S, *et al* (2015) Tumour exosome integrins determine organotropic metastasis. *Nature* 527: 329–335

Houali K, Wang X, Shimizu Y, Djennaoui D, Nicholls J, Fiorini S, Bouguermouh A & Ooka T (2007) A new diagnostic marker for secreted Epstein-Barr virus-encoded LMP1 and BARF1 oncoproteins in the serum and saliva of patients with nasopharyngeal carcinoma. *Clinical Cancer Research* 13: 4993–5000

Hu B, Jin C, Li H-B, Tong J, Ouyang X, Cetinbas NM, Zhu S, Strowig T, Lam FC, Zhao C, *et al* (2016) The DNA-sensing AIM2 inflammasome controls radiation-induced cell death and tissue injury. *Science* 354: 765–768

Hu Y, Jiang Y, Li S, Ma X, Chen M, Yang R, Wen S, Moynagh PN, Wang B, Hu G, *et al* (2022) The Gasdermin D N-terminal fragment acts as a negative feedback system to inhibit inflammasome-mediated activation of Caspase-1/11. *Proceedings of the National Academy of Sciences* 119: e2210809119

Huber W, Carey VJ, Gentleman R, Anders S, Carlson M, Carvalho BS, Bravo HC, Davis S, Gatto L, Girke T, *et al* (2015) Orchestrating high-throughput genomic analysis with Bioconductor. *Nature methods* 12: 115–121

Hulsmans M & Holvoet P (2013) MicroRNA-containing microvesicles regulating inflammation in association with atherosclerotic disease. *Cardiovascular Research* 100: 7–18

Hunt L, Hacker DL, Grosjean F, De Jesus M, Uebersax L, Jordan M & Wurm FM (2005) Low-temperature pausing of cultivated mammalian cells. *Biotechnology and Bioengineering* 89: 157–163

Icer MA & Gezmen-Karadag M (2018) The multiple functions and mechanisms of osteopontin. *Clinical Biochemistry* 59: 17–24

Imai T, Takahashi Y, Nishikawa M, Kato K, Morishita M, Yamashita T, Matsumoto A, Charoenviriyakul C & Takakura Y (2015) Macrophage-dependent clearance of systemically administered B16BL6-derived exosomes from the blood circulation in mice. *Journal of Extracellular Vesicles* 4: 26238

Irizarry RA, Bolstad BM, Collin F, Cope LM, Hobbs B & Speed TP (2003a) Summaries of Affymetrix GeneChip probe level data. *Nucleic acids research* 31: e15

Irizarry RA, Hobbs B, Collin F, Beazer-Barclay YD, Antonellis KJ, Scherf U & Speed TP (2003b) Exploration, normalization, and summaries of high density oligonucleotide array probe level data. *Biostatistics (Oxford, England)* 4: 249–264

Ismail N, Wang Y, Dakhlallah D, Moldovan L, Agarwal K, Batte K, Shah P, Wisler J, Eubank TD, Tridandapani S, *et al* (2013) Macrophage microvesicles induce macrophage differentiation and miR-223 transfer. *Blood* 121: 984–995

Ivashkiv LB & Donlin LT (2014) Regulation of type I interferon responses. *Nat Rev Immunol* 14: 36–49

Jakobs C, Perner S & Hornung V (2015) AIM2 Drives Joint Inflammation in a Self-DNA Triggered Model of Chronic Polyarthritis. *PLOS ONE* 10: e0131702

de Jesus AA, Canna SW, Liu Y & Goldbach-Mansky R (2015) Molecular Mechanisms in Genetically Defined Autoinflammatory Diseases: Disorders of Amplified Danger Signaling. *Annu Rev Immunol* 33: 823–874

Johnstone RM, Adam M, Hammond JR, Orr L & Turbide C (1987) Vesicle formation during reticulocyte maturation. Association of plasma membrane activities with released vesicles (exosomes). *Journal of Biological Chemistry* 262: 9412–9420

Joosten LAB, Netea MG, Fantuzzi G, Koenders MI, Helsen MMA, Sparrer H, Pham CT, van der Meer JWM, Dinarello CA & van den Berg WB (2009) Inflammatory arthritis in caspase 1 gene-deficient mice: contribution of proteinase 3 to caspase 1-independent production of bioactive interleukin-1beta. *Arthritis Rheum* 60: 3651–3662

Jorgensen I, Lopez JP, Laufer SA & Miao EA (2016a) IL-1β, IL-18, and eicosanoids promote neutrophil recruitment to pore-induced intracellular traps following pyroptosis. *European Journal of Immunology* 46: 2761–2766

Jorgensen I, Rayamajhi M & Miao EA (2017) Programmed cell death as a defence against infection. *Nat Rev Immunol* 17: 151–164

Jorgensen I, Zhang Y, Krantz BA & Miao EA (2016b) Pyroptosis triggers pore-induced intracellular traps (PITs) that capture bacteria and lead to their clearance by efferocytosis. *Journal of Experimental Medicine* 213: 2113–2128

Joshi BS, de Beer MA, Giepmans BNG & Zuhorn IS (2020) Endocytosis of Extracellular Vesicles and Release of Their Cargo from Endosomes. *ACS Nano* 14: 4444–4455

Juliana C, Fernandes-Alnemri T, Kang S, Farias A, Qin F & Alnemri ES (2012) Non-transcriptional priming and deubiquitination regulate NLRP3 inflammasome activation. *The Journal of biological chemistry* 287: 36617–22

Jurgielewicz BJ, Yao Y & Stice SL (2020) Kinetics and Specificity of HEK293T Extracellular Vesicle Uptake using Imaging Flow Cytometry. *Nanoscale Res Lett* 15: 170

Kadota T, Fujita Y, Araya J, Watanabe N, Fujimoto S, Kawamoto H, Minagawa S, Hara H, Ohtsuka T, Yamamoto Y, *et al* (2021) Human bronchial epithelial cell-derived extracellular vesicle therapy for pulmonary fibrosis via inhibition of TGF-β-WNT crosstalk. *Journal of Extracellular Vesicles* 10: e12124

Kalia M & Jameel S (2011) Virus entry paradigms. *Amino Acids* 41: 1147–1157

Kalluri R & LeBleu VS (2020) The biology, function, and biomedical applications of exosomes. *Science* 367

Kalra H, Drummen GPC & Mathivanan S (2016) Focus on extracellular vesicles: Introducing the next small big thing. *International Journal of Molecular Sciences* 17

Kalra H, Simpson RJ, Ji H, Aikawa E, Altevogt P, Askenase P, Bond VC, Borràs FE, Breakefield X, Budnik V, *et al* (2012) Vesiclepedia: A Compendium for Extracellular Vesicles with Continuous Community Annotation. *PLoS Biology* 10: e1001450

Kang M, Jordan V, Blenkiron C & Chamley LW (2021) Biodistribution of extracellular vesicles following administration into animals: A systematic review. *J Extracell Vesicles* 10: e12085

Karimi N, Cvjetkovic A, Jang SC, Crescitelli R, Hosseinpour Feizi MA, Nieuwland R, Lötvall J & Lässer C (2018) Detailed analysis of the plasma extracellular vesicle proteome after separation from lipoproteins. *Cellular and molecular life sciences : CMLS* 75: 2873–2886

Karlsson M, Zhang C, Méar L, Zhong W, Digre A, Katona B, Sjöstedt E, Butler L, Odeberg J, Dusart P, *et al* (2021) A single–cell type transcriptomics map of human tissues. *Science Advances* 7: eabh2169

Karmakar M, Katsnelson M, Malak HA, Greene NG, Howell SJ, Hise AG, Camilli A, Kadioglu A, Dubyak GR & Pearlman E (2015) Neutrophil IL-1β Processing Induced by Pneumolysin Is Mediated by the NLRP3/ASC Inflammasome and Caspase-1 Activation and Is Dependent on K+ Efflux. *The Journal of Immunology* 194: 1763–1775

Kaur M, Chandel J, Malik J & Naura AS (2022) Particulate matter in COPD pathogenesis: an overview. *Inflamm Res* 71: 797–815

Kayagaki N, Kornfeld OS, Lee BL, Stowe IB, O'Rourke K, Li Q, Sandoval W, Yan D, Kang J, Xu M, *et al* (2021) NINJ1 mediates plasma membrane rupture during lytic cell death. *Nature* 591: 131–136

Kayagaki N, Stowe IB, Lee BL, O'Rourke K, Anderson K, Warming S, Cuellar T, Haley B, Roose-Girma M, Phung QT, *et al* (2015) Caspase-11 cleaves gasdermin D for non-canonical inflammasome signalling. *Nature* 526: 666–71

Kayagaki N, Wong MT, Stowe IB, Ramani SR, Gonzalez LC, Akashi-Takamura S, Miyake K, Zhang J, Lee WP, Muszyński A, *et al* (2013) Noncanonical inflammasome activation by intracellular LPS independent of TLR4. *Science (New York, NY)* 341: 1246–9

Keller S, Rupp C, Stoeck A, Runz S, Fogel M, Lugert S, Hager HD, Abdel-Bakky MS, Gutwein P & Altevogt P (2007) CD24 is a marker of exosomes secreted into urine and amniotic fluid. *Kidney International* 72: 1095–1102

Kennedy CR, Goya Grocin A, Kovačič T, Singh R, Ward JA, Shenoy AR & Tate EW (2021) A Probe for NLRP3 Inflammasome Inhibitor MCC950 Identifies Carbonic Anhydrase 2 as a Novel Target. *ACS Chem Biol* 16: 982–990

Kim B, Lee Y, Kim E, Kwak A, Ryoo S, Bae S, Azam T, Kim S & Dinarello C (2013a) The Interleukin-1α Precursor is Biologically Active and is Likely a Key Alarmin in the IL-1 Family of Cytokines. *Frontiers in Immunology* 4

Kim CW, Lee HM, Lee TH, Kang C, Kleinman HK & Gho YS (2002) Extracellular membrane vesicles from tumor cells promote angiogenesis via sphingomyelin. *Cancer Research* 62: 6312–6317

Kim DK, Kang B, Kim OY, Choi DS, Lee J, Kim SR, Go G, Yoon YJ, Kim JH, Jang SC, *et al* (2013b) EVpedia: An integrated database of high-throughput data for systemic analyses of extracellular vesicles. *Journal of Extracellular Vesicles* 2

Kim DK, Lee J, Kim SR, Choi DS, Yoon YJ, Kim JH, Go G, Nhung D, Hong K, Jang SC, *et al* (2015) EVpedia: A community web portal for extracellular vesicles research. *Bioinformatics* 31: 933–939

Kim HY, Lee HJ, Chang YJ, Pichavant M, Shore SA, Fitzgerald KA, Iwakura Y, Israel E, Bolger K, Faul J, *et al* (2014a) Interleukin-17-producing innate lymphoid cells and the NLRP3 inflammasome facilitate obesity-associated airway hyperreactivity. *Nature Medicine* 20: 54–61

Kim RY, Pinkerton JW, Essilfie AT, Robertson AAB, Baines KJ, Brown AC, Mayall JR, Ali MK, Starkey MR, Hansbro NG, *et al* (2017) Role for NLRP3 Inflammasome–mediated, IL-1β–Dependent Responses in Severe, Steroid-Resistant Asthma. *Am J Respir Crit Care Med* 196: 283–297

Kim SR, Kim DI, Kim SH, Lee H, Lee KS, Cho SH & Lee YC (2014b) NLRP3 inflammasome activation by mitochondrial ROS in bronchial epithelial cells is required for allergic inflammation. *Cell Death Dis* 5: e1498–e1498

Kitasato Y, Hoshino T, Okamoto M, Kato S, Koda Y, Nagata N, Kinoshita M, Koga H, Yoon DY, Asao H, *et al* (2004) Enhanced expression of interleukin-18 and its receptor in idiopathic pulmonary fibrosis. *American Journal of Respiratory Cell and Molecular Biology* 31: 619–625

Knodler LA, Crowley SM, Sham HP, Yang H, Wrande M, Ma C, Ernst RK, Steele-Mortimer O, Celli J & Vallance BA (2014) Noncanonical Inflammasome Activation of Caspase-4/Caspase-11 Mediates Epithelial Defenses against Enteric Bacterial Pathogens. *Cell Host & Microbe* 16: 249–256

Kolahian S, Fernandez IE, Eickelberg O & Hartl D (2016) Immune mechanisms in pulmonary fibrosis. *American Journal of Respiratory Cell and Molecular Biology* 55: 309–322

Kolb M, Margetts PJ, Anthony DC, Pitossi F & Gauldie J (2001) Transient expression of IL-1beta induces acute lung injury and chronic repair leading to pulmonary fibrosis. *J Clin Invest* 107: 1529–1536

Konno S, Eckman JA, Plunkett B, Li X, Berman JS, Schroeder J & Huang S-K (2006) Interleukin-10 and Th2 Cytokines Differentially Regulate Osteopontin Expression in Human Monocytes and Dendritic Cells. *Journal of Interferon & Cytokine Research* 26: 562–567

Kool M, Willart MAM, van Nimwegen M, Bergen I, Pouliot P, Virchow JC, Rogers N, Osorio F, Reis e Sousa C, Hammad H, *et al* (2011) An unexpected role for uric acid as an inducer of T helper 2 cell immunity to inhaled antigens and inflammatory mediator of allergic asthma. *Immunity* 34: 527–540

Kowal J, Arras G, Colombo M, Jouve M, Morath JP, Primdal-Bengtson B, Dingli F, Loew D, Tkach M & Théry C (2016) Proteomic comparison defines novel markers to characterize heterogeneous populations of extracellular vesicle subtypes. *Proceedings of the National Academy of Sciences* 113: E968–E977

Kuemmerle-Deschner JB (2015) CAPS — pathogenesis, presentation and treatment of an autoinflammatory disease. *Semin Immunopathol* 37: 377–385

Kurt-Jones EA, Beller DI, Mizel SB & Unanue ER (1985) Identification of a membrane-associated interleukin 1 in macrophages. *Proceedings of the National Academy of Sciences* 82: 1204–1208

Kutsch M, Sistemich L, Lesser CF, Goldberg MB, Herrmann C & Coers J (2020) Direct binding of polymeric GBP1 to LPS disrupts bacterial cell envelope functions. *EMBO Journal* 39

Labrecque N & Cermakian N (2015) Circadian Clocks in the Immune System. *J Biol Rhythms* 30: 277–290

Lai CP, Kim EY, Badr CE, Weissleder R, Mempel TR, Tannous BA & Breakefield XO (2015) Visualization and tracking of tumour extracellular vesicle delivery and RNA translation using multiplexed reporters. *Nat Commun* 6: 7029

Lamkanfi M, Sarkar A, Vande Walle L, Vitari AC, Amer AO, Wewers MD, Tracey KJ, Kanneganti T-D & Dixit VM (2010) Inflammasome-Dependent Release of the Alarmin HMGB1 in Endotoxemia. *The Journal of Immunology* 185: 4385–4392

Lammert CR, Frost EL, Bellinger CE, Bolte AC, McKee CA, Hurt ME, Paysour MJ, Ennerfelt HE & Lukens JR (2020) AIM2 inflammasome surveillance of DNA damage shapes neurodevelopment. *Nature* 580: 647–652

Lässer C, O'Neil SE, Ekerljung L, Ekström K, Sjöstrand M & Lötvall J (2011) RNA-containing exosomes in human nasal secretions. *American Journal of Rhinology and Allergy* 25: 89–93

Latz E, Xiao TS & Stutz A (2013) Activation and regulation of the inflammasomes. *Nature Reviews Immunology* 13: 397–411

Law CW, Chen Y, Shi W & Smyth GK (2014) voom: precision weights unlock linear model analysis tools for RNA-seq read counts. *Genome Biology* 15: R29

Lazear HM, Schoggins JW & Diamond MS (2019) Shared and Distinct Functions of Type I and Type III Interferons. *Immunity* 50: 907–923

Lee CQE, Kerouanton B, Chothani S, Zhang S, Chen Y, Mantri CK, Hock DH, Lim R, Nadkarni R, Huynh VT, *et al* (2021) Coding and non-coding roles of MOCCI (C15ORF48) coordinate to regulate host inflammation and immunity. *Nat Commun* 12: 2130

Lee J-K, Kim S-H, Lewis EC, Azam T, Reznikov LL & Dinarello CA (2004) Differences in signaling pathways by IL-1β and IL-18. *Proceedings of the National Academy of Sciences of the United States of America* 101: 8815–8820

Levy M, Thaiss CA, Zeevi D, Dohnalová L, Zilberman-Schapira G, Mahdi JA, David E, Savidor A, Korem T, Herzig Y, *et al* (2015) Microbiota-Modulated Metabolites Shape the Intestinal Microenvironment by Regulating NLRP6 Inflammasome Signaling. *Cell* 163: 1428–1443

Levy O, Zarember KA, Roy RM, Cywes C, Godowski PJ & Wessels MR (2004) Selective Impairment of TLR-Mediated Innate Immunity in Human Newborns: Neonatal Blood Plasma Reduces Monocyte TNF-α Induction by Bacterial Lipopeptides, Lipopolysaccharide, and Imiquimod, but Preserves the Response to R-8481. *The Journal of Immunology* 173: 4627–4634

Li S, Goorha S, Ballou LR & Blatteis CM (2003a) Intracerebroventricular interleukin-6, macrophage inflammatory protein-1β and IL-18: pyrogenic and PGE2-mediated? *Brain Research* 992: 76–84

Li X, O'Regan AW & Berman JS (2003b) IFN-γ Induction of Osteopontin Expression in Human Monocytoid Cells. *Journal of Interferon & Cytokine Research* 23: 259–265

Li Y, Oosting M, Deelen P, Ricaño-Ponce I, Smeekens S, Jaeger M, Matzaraki V, Swertz MA, Xavier RJ, Franke L, *et al* (2016a) Inter-individual variability and genetic influences on cytokine responses to bacteria and fungi. *Nat Med* 22: 952–960

Li Y, Oosting M, Smeekens SP, Jaeger M, Aguirre-Gamboa R, Le KTT, Deelen P, Ricaño-Ponce I, Schoffelen T, Jansen AFM, *et al* (2016b) A Functional Genomics Approach to Understand Variation in Cytokine Production in Humans. *Cell* 167: 1099-1110.e14

Liao Y, Smyth GK & Shi W (2014) FeatureCounts: An efficient general purpose program for assigning sequence reads to genomic features. *Bioinformatics* 30: 923–930

Liao Y, Smyth GK & Shi W (2019) The R package Rsubread is easier, faster, cheaper and better for alignment and quantification of RNA sequencing reads. *Nucleic acids research* 47

Liberzon A, Birger C, Thorvaldsdóttir H, Ghandi M, Mesirov JP & Tamayo P (2015) The Molecular Signatures Database Hallmark Gene Set Collection. *Cell Systems* 1: 417–425

Lieber M, Todaro G, Smith B, Szakal A & Nelson-Rees W (1976) A continuous tumor-cell line from a human lung carcinoma with properties of type II alveolar epithelial cells. *International Journal of Cancer* 17: 62–70

Linder A, Bauernfried S, Cheng Y, Albanese M, Jung C, Keppler OT & Hornung V (2020) CARD8 inflammasome activation triggers pyroptosis in human T cells. *The EMBO Journal* 39: e105071

Lindskog S & Coleman JE (1973) The Catalytic Mechanism of Carbonic Anhydrase. *Proc Natl Acad Sci U S A* 70: 2505–2508

Lipinski S, Pfeuffer S, Arnold P, Treitz C, Aden K, Ebsen H, Falk-Paulsen M, Gisch N, Fazio A, Kuiper J, *et al* (2019) Prdx4 limits caspase-1 activation and restricts inflammasome-mediated signaling by extracellular vesicles. *The EMBO Journal* 38: e101266

Liston A & Masters SL (2017) Homeostasis-altering molecular processes as mechanisms of inflammasome activation. *Nature reviews Immunology* 17: 208–214

Liu J, Du S, Kong Q, Zhang X, Jiang S, Cao X, Li Y, Li C, Chen H, Ding Z, *et al* (2020) HSPA12A attenuates lipopolysaccharide-induced liver injury through inhibiting caspase-11-mediated hepatocyte pyroptosis via PGC-1α-dependent acyloxyacyl hydrolase expression. *Cell Death Differ* 27: 2651–2667

Liu X, Zhang Z, Ruan J, Pan Y, Magupalli VG, Wu H & Lieberman J (2016) Inflammasome-activated gasdermin D causes pyroptosis by forming membrane pores. *Nature* 535: 153–158

Logozzi M, Mizzoni D, Angelini DF, Di Raimo R, Falchi M, Battistini L & Fais S (2018) Microenvironmental pH and Exosome Levels Interplay in Human Cancer Cell Lines of Different Histotypes. *Cancers (Basel)* 10: 370

Lötvall J, Hill AF, Hochberg F, Buzás EI, Vizio DD, Gardiner C, Gho YS, Kurochkin IV, Mathivanan S, Quesenberry P, *et al* (2014) Minimal experimental requirements for definition of extracellular vesicles and their functions: A position

statement from the International Society for Extracellular Vesicles. *Journal of Extracellular Vesicles* 3

Lu A, Magupalli V, Ruan J, Yin Q, Atianand MK, Vos M, Schröder GF, Fitzgerald KA, Wu H & Egelman EH (2014) Unified Polymerization Mechanism for the Assembly of ASC-dependent Inflammasomes. *Cell* 156: 1193–1206

Lu B, Nakamura T, Inouye K, Li J, Tang Y, Lundbäck P, Valdes-Ferrer SI, Olofsson PS, Kalb T, Roth J, *et al* (2012) Novel role of PKR in inflammasome activation and HMGB1 release. *Nature* 488: 670–674

MacDonald JW (2021) clariomdhumantranscriptcluster.db: Affymetrix clariomdhuman annotation data (chip clariomdhumantranscriptcluster).

MacKenzie A, Wilson HL, Kiss-Toth E, Dower SK, North RA & Surprenant A (2001) Rapid secretion of interleukin-1β by microvesicle shedding. *Immunity* 15: 825–835

Madouri F, Guillou N, Fauconnier L, Marchiol T, Rouxel N, Chenuet P, Ledru A, Apetoh L, Ghiringhelli F, Chamaillard M, *et al* (2015) Caspase-1 activation by NLRP3 inflammasome dampens IL-33-dependent house dust mite-induced allergic lung inflammation. *J Mol Cell Biol* 7: 351–365

Malik A & Kanneganti T-D (2018) Function and regulation of IL-1α in inflammatory diseases and cancer. *Immunological Reviews* 281: 124–137

Mallegol J, Van Niel G, Lebreton C, Lepelletier Y, Candalh C, Dugave C, Heath JK, Raposo G, Cerf–Bensussan N & Heyman M (2007) T84-Intestinal Epithelial Exosomes Bear MHC Class II/Peptide Complexes Potentiating Antigen Presentation by Dendritic Cells. *Gastroenterology* 132: 1866–1876

Mangan MSJ, Olhava EJ, Roush WR, Seidel HM, Glick GD & Latz E (2018) Targeting the NLRP3 inflammasome in inflammatory diseases. *Nat Rev Drug Discov* 17: 588–606

Mankan AK, Dau T, Jenne D & Hornung V (2012) The NLRP3/ASC/Caspase-1 axis regulates IL-1β processing in neutrophils. *European Journal of Immunology* 42: 710–715

Mantovani A, Dinarello CA, Molgora M & Garlanda C (2019) Interleukin-1 and Related Cytokines in the Regulation of Inflammation and Immunity. *Immunity* 50: 778–795

Marchetti M, Monier M-N, Fradagrada A, Mitchell K, Baychelier F, Eid P, Johannes L & Lamaze C (2006) Stat-mediated Signaling Induced by Type I and Type II Interferons (IFNs) Is Differentially Controlled through Lipid Microdomain Association and Clathrin-dependent Endocytosis of IFN Receptors. *Mol Biol Cell* 17: 2896–2909

Mariathasan S, Weiss DS, Newton K, McBride J, O'Rourke K, Roose-Girma M, Lee WP, Weinrauch Y, Monack DM & Dixit VM (2006) Cryopyrin activates the inflammasome in response to toxins and ATP. *Nature* 440: 228–232

Martens S & McMahon HT (2008) Mechanisms of membrane fusion: disparate players and common principles. *Nat Rev Mol Cell Biol* 9: 543–556

Martinon F, Burns K & Tschopp J (2002) The inflammasome: a molecular platform triggering activation of inflammatory caspases and processing of proIL-beta. *Molecular cell* 10: 417–26

Masumoto J, Taniguchi S, Ayukawa K, Sarvotham H, Kishino T, Niikawa N, Hidaka E, Katsuyama T, Higuchi T & Sagara J (1999) ASC, a novel 22-kDa protein, aggregates during apoptosis of human promyelocytic leukemia HL-60 cells. *J Biol Chem* 274: 33835–33838

Masyuk AI, Huang BQ, Ward CJ, Gradilone SA, Banales JM, Masyuk TV, Radtke B, Splinter PL & LaRusso NF (2010) Biliary exosomes influence cholangiocyte regulatory mechanisms and proliferation through interaction with primary cilia. *American Journal of Physiology - Gastrointestinal and Liver Physiology* 299

Mathieu M, Martin-Jaular L, Lavieu G & Théry C (2019) Specificities of secretion and uptake of exosomes and other extracellular vesicles for cell-to-cell communication. *Nature Cell Biology 2019 21:1* 21: 9–17

Mathivanan S & Simpson RJ (2009) ExoCarta: A compendium of exosomal proteins and RNA. *Proteomics* 9: 4997–5000

Matsumoto A, Takahashi Y, Nishikawa M, Sano K, Morishita M, Charoenviriyakul C, Saji H & Takakura Y (2017) Accelerated growth of B16BL6 tumor in mice through efficient uptake of their own exosomes by B16BL6 cells. *Cancer Science* 108: 1803–1810

Mazzali M, Kipari T, Ophascharoensuk V, Wesson JA, Johnson R & Hughes J (2002) Osteopontin-A molecule for all seasons. *QJM - Monthly Journal of the Association of Physicians* 95: 3–13

McCarthy DJ, Chen Y & Smyth GK (2012) Differential expression analysis of multifactor RNA-Seq experiments with respect to biological variation. *Nucleic Acids Research* 40: 4288–4297

Mccarthy DJ & Smyth GK (2009) Testing significance relative to a fold-change threshold is a TREAT. *Bioinformatics* 25: 765–771

McNew JA, Weber T, Parlati F, Johnston RJ, Melia TJ, Söllner TH & Rothman JE (2000) Close Is Not Enough: Snare-Dependent Membrane Fusion Requires an Active Mechanism That Transduces Force to Membrane Anchors. *Journal of Cell Biology* 150: 105–118

Miao EA, Alpuche-Aranda CM, Dors M, Clark AE, Bader MW, Miller SI & Aderem A (2006) Cytoplasmic flagellin activates caspase-1 and secretion of interleukin 1beta via Ipaf. *Nature immunology* 7: 569–75

Miao EA, Leaf IA, Treuting PM, Mao DP, Dors M, Sarkar A, Warren SE, Wewers MD & Aderem A (2010) Caspase-1-induced pyroptosis is an innate immune effector mechanism against intracellular bacteria. *Nature Immunology* 11: 1136–1142

Milhavet F, Cuisset L, Hoffman HM, Slim R, El-Shanti H, Aksentijevich I, Lesage S, Waterham H, Wise C, Sarrauste de Menthiere C, *et al* (2008) The infevers autoinflammatory mutation online registry: update with new genes and functions. *Human Mutation* 29: 803–808

Miyazaki Y, Tashiro T, Higuchi Y, Setoguchi M, Yamamoto S, Nagai H, Nasu M & Vassalli P (1995) Expression of Osteopontin in a Macrophage Cell Line and in Transgenic Mice with Pulmonary Fibrosis Resulting from the Lung Expression of a Tumor Necrosis Factor-α Transgene. *Annals of the New York Academy of Sciences* 760: 334–341

Montecalvo A, Larregina AT, Shufesky WJ, Stolz DB, Sullivan MLG, Karlsson JM, Baty CJ, Gibson GA, Erdos G, Wang Z, *et al* (2012) Mechanism of transfer of functional microRNAs between mouse dendritic cells via exosomes. *Blood* 119: 756–766

Monteleone M, Stanley AC, Chen KW, Brown DL, Bezbradica JS, von Pein JB, Holley CL, Boucher D, Shakespear MR, Kapetanovic R, *et al* (2018) Interleukin-1β Maturation Triggers Its Relocation to the Plasma Membrane for Gasdermin-D-Dependent and -Independent Secretion. *Cell Reports* 24: 1425–1433

Monteleone M, Stow JL & Schroder K (2015) Mechanisms of unconventional secretion of IL-1 family cytokines. *Cytokine* 74: 213–218

Morales-Kastresana A, Telford B, Musich TA, McKinnon K, Clayborne C, Braig Z, Rosner A, Demberg T, Watson DC, Karpova TS, *et al* (2017) Labeling Extracellular Vesicles for Nanoscale Flow Cytometry. *Sci Rep* 7: 1878

Morel JCM, Park CC, Woods JM & Koch AE (2001) A Novel Role for Interleukin-18 in Adhesion Molecule Induction through NFκB and Phosphatidylinositol (PI) 3-Kinase-dependent Signal Transduction Pathways. *Journal of Biological Chemistry* 276: 37069–37075

Morelli AE, Larregina AT, Shufesky WJ, Sullivan MLG, Stolz DB, Papworth GD, Zahorchak AF, Logar AJ, Wang Z, Watkins SC, *et al* (2004) Endocytosis, intracellular sorting, and processing of exosomes by dendritic cells. *Blood* 104: 3257–3266

Mossman BT & Churg A (1998) Mechanisms in the Pathogenesis of Asbestosis and Silicosis. *Am J Respir Crit Care Med* 157: 1666–1680

Mulcahy LA, Pink RC & Carter DRF (2014) Routes and mechanisms of extracellular vesicle uptake. *Journal of Extracellular Vesicles* 3: 24641

Muller L, Mitsuhashi M, Simms P, Gooding WE & Whiteside TL (2016) Tumor-derived exosomes regulate expression of immune function-related genes in human T cell subsets. *Sci Rep* 6: 20254

Muller L, Simms P, Hong C-S, Nishimura MI, Jackson EK, Watkins SC & Whiteside TL (2017) Human tumor-derived exosomes (TEX) regulate Treg functions via cell surface signaling rather than uptake mechanisms. *OncoImmunology* 6: e1261243

Murgia N & Gambelunghe A (2022) Occupational COPD—The most under-recognized occupational lung disease? *Respirology* 27: 399–410

Murphy KM, Weaver C, Janeway C 1943-2003 & Seidler L (2017) Janeway Immunologie

Nabar NR, Shi C-S & Kehrl JH (2017) Chapter 16 - Autophagy Accompanies Inflammasome Activation to Moderate Inflammation by Eliminating Active Inflammasomes. In *Autophagy: Cancer, Other Pathologies, Inflammation, Immunity, Infection, and Aging*, Hayat MA (ed) pp 343–357. Academic Press

Nachmias N, Langier S, Brzezinski RY, Siterman M, Stark M, Etkin S, Avriel A, Schwarz Y, Shenhar-Tsarfaty S & Bar-Shai A (2019) NLRP3 inflammasome activity is upregulated in an in-vitro model of COPD exacerbation. *PLOS ONE* 14: e0214622

Nagata S & Tanaka M (2017) Programmed cell death and the immune system. *Nature reviews Immunology* 17: 333–340

Nakamura K, Okamura H, Wada M, Nagata K & Tamura T (1989) Endotoxin-induced serum factor that stimulates gamma interferon production. *Infect Immun* 57: 590–595

Nakanishi K, Yoshimoto T, Tsutsui H & Okamura H (2001) Interleukin-18 is a unique cytokine that stimulates both Th1 and Th2 responses depending on its cytokine milieu. *Cytokine & Growth Factor Reviews* 12: 53–72

Nakase I, Ueno N, Matsuzawa M, Noguchi K, Hirano M, Omura M, Takenaka T, Sugiyama A, Bailey Kobayashi N, Hashimoto T, *et al* (2021) Environmental pH stress influences cellular secretion and uptake of extracellular vesicles. *FEBS Open Bio* 11: 753–767

Neri T, Armani C, Pegoli A, Cordazzo C, Carmazzi Y, Brunelleschi S, Bardelli C, Breschi MC, Paggiaro P & Celi A (2011) Role of NF-κB and PPAR-γ in lung inflammation induced by monocyte-derived microparticles. *European Respiratory Journal* 37: 1494–1502

Netea MG, Nold-Petry CA, Nold MF, Joosten LAB, Opitz B, van der Meer JHM, van de Veerdonk FL, Ferwerda G, Heinhuis B, Devesa I, *et al* (2009) Differential requirement for the activation of the inflammasome for processing and release of IL-1β in monocytes and macrophages. *Blood* 113: 2324–2335

Netea MG, Simon A, Veerdonk F van de, Kullberg B-J, Meer JWMV der & Joosten LAB (2010) IL-1β Processing in Host Defense: Beyond the Inflammasomes. *PLOS Pathogens* 6: e1000661

Netea MG, van de Veerdonk FL, van der Meer JWM, Dinarello CA & Joosten LAB (2015) Inflammasome-Independent Regulation of IL-1-Family Cytokines. *Annual Review of Immunology* 33: 49–77

Nguyen DG, Booth A, Gould SJ & Hildreth JEK (2003) Evidence That HIV Budding in Primary Macrophages Occurs through the Exosome Release Pathway. *Journal of Biological Chemistry* 278: 52347–52354

Nichols BJ & Lippincott-Schwartz J (2001) Endocytosis without clathrin coats. *Trends in Cell Biology* 11: 406–412

Nilsson J, Skog J, Nordstrand A, Baranov V, Mincheva-Nilsson L, Breakefield XO & Widmark A (2009) Prostate cancer-derived urine exosomes: A novel approach to biomarkers for prostate cancer. *British Journal of Cancer* 100: 1603–1607

Noels H, Lehrke M, Vanholder R & Jankowski J (2021) Lipoproteins and fatty acids in chronic kidney disease: molecular and metabolic alterations. *Nature reviews Nephrology* 17: 528–542

Nolte-'t Hoen ENM, Buermans HPJ, Waasdorp M, Stoorvogel W, Wauben MHM & 't Hoen PAC (2012) Deep sequencing of RNA from immune cell-derived vesicles uncovers the selective incorporation of small non-coding RNA biotypes with potential regulatory functions. *Nucleic Acids Research* 40: 9272–9285

Nolte-'t Hoen ENM, Buschow SI, Anderton SM, Stoorvogel W & Wauben MHM (2009) Activated T cells recruit exosomes secreted by dendritic cells via LFA-1. *Blood* 113: 1977–1981

Novick D, Elbirt D, Dinarello CA, Rubinstein M & Sthoeger ZM (2009) Interleukin-18 Binding Protein in the Sera of Patients with Wegener's Granulomatosis. *J Clin Immunol* 29: 38–45

Novick D, Elbirt D, Miller G, Dinarello CA, Rubinstein M & Sthoeger ZM (2010) High circulating levels of free interleukin-18 in patients with active SLE in the presence of elevated levels of interleukin-18 binding protein. *Journal of Autoimmunity* 34: 121–126

Novick D, Kim S, Kaplanski G & Dinarello CA (2013) Interleukin-18, more than a Th1 cytokine. *Seminars in Immunology* 25: 439–448

Novick D, Kim S-H, Fantuzzi G, Reznikov LL, Dinarello CA & Rubinstein M (1999) Interleukin-18 Binding Protein: A Novel Modulator of the Th1 Cytokine Response. *Immunity* 10: 127–136

Novick D, Schwartsburd B, Pinkus R, Suissa D, Belzer I, Sthoeger Z, Keane WF, Chvatchko Y, Kim SH, Fantuzzi G, *et al* (2001) A novel IL-18BP ELISA shows elevated serum IL-18BP in sepsis and extensive decrease of free IL-18. *Cytokine* 14: 334–342

Obregon C, Rothen-Rutishauser B, Gerber P, Gehr P & Nicod LP (2009) Active Uptake of Dendritic Cell-Derived Exovesicles by Epithelial Cells Induces the Release of Inflammatory Mediators through a TNF-α-Mediated Pathway. *The American Journal of Pathology* 175: 696–705

Ohki S, Flanagan TD & Hoekstra D (1998) Probe Transfer with and without Membrane Fusion in a Fluorescence Fusion Assay. *Biochemistry* 37: 7496–7503

Okamura H, Tsutsui H, Komatsu T, Yutsudo M, Hakura A, Tanimoto T, Torigoe K, Okura T, Nukada Y, Hattori K, *et al* (1995) Cloning of a new cytokine that induces IFN-γ production by T cells. *Nature* 378: 88–91

Omoto Y, Tokime K, Yamanaka K, Habe K, Morioka T, Kurokawa I, Tsutsui H, Yamanishi K, Nakanishi K & Mizutani H (2006) Human Mast Cell Chymase Cleaves Pro-IL-18 and Generates a Novel and Biologically Active IL-18 Fragment1. *The Journal of Immunology* 177: 8315–8319

Omoto Y, Yamanaka K, Tokime K, Kitano S, Kakeda M, Akeda T, Kurokawa I, Gabazza EC, Tsutsui H, Katayama N, *et al* (2010) Granzyme B is a novel interleukin-18 converting enzyme. *Journal of Dermatological Science* 59: 129–135

Orzalli MH, Smith A, Jurado KA, Iwasaki A, Garlick JA & Kagan JC (2018) An Antiviral Branch of the IL-1 Signaling Pathway Restricts Immune-Evasive Virus Replication. *Molecular Cell* 71: 825-840.e6

Owen JA, Punt J, Stranford SA & Jones PP (2019) Kuby Immunology Seventh Edition. New York: W.H. Freeman and Company

Oyama Y, Akuzawa N, Nagai R & Kurabayashi M (2002) PPARγ Ligand Inhibits Osteopontin Gene Expression Through Interference With Binding of Nuclear Factors to A/T-Rich Sequence in THP-1 Cells. *Circulation Research* 90: 348–355

Oyama Y, Kurabayashi M, Akuzawa N & Nagai R (2000) Troglitazone, a PPARγ Ligand, Inhibits Osteopontin Gene Expression in Human Monocytes/macrophage THP-1 Cells. *Journal of Atherosclerosis and Thrombosis* 7: 77–82

Pakshir P & Hinz B (2018) The big five in fibrosis: Macrophages, myofibroblasts, matrix, mechanics, and miscommunication. *Matrix Biology* 68–69: 81–93

Pan BT & Johnstone RM (1983) Fate of the transferrin receptor during maturation of sheep reticulocytes in vitro: Selective externalization of the receptor. *Cell* 33: 967–978

Pan BT, Teng K, Wu C, Adam M & Johnstone RM (1985) Electron microscopic evidence for externalization of the transferrin receptor in vesicular form in sheep reticulocytes. *Journal of Cell Biology* 101: 942–948

Pan LH, Ohtani H, Yamauchi K & Nagura H (1996) Co-expression of TNFα and IL-1β in human acute pulmonary fibrotic diseases: An immunohistochemical analysis. *Pathology International* 46: 91–99

Park T-S, Hu Y, Noh H-L, Drosatos K, Okajima K, Buchanan J, Tuinei J, Homma S, Jiang X-C, Abel ED, *et al* (2008) Ceramide is a cardiotoxin in lipotoxic cardiomyopathy*s. *Journal of Lipid Research* 49: 2101–2112

Parolini I, Federici C, Raggi C, Lugini L, Palleschi S, De Milito A, Coscia C, Iessi E, Logozzi M, Molinari A, *et al* (2009) Microenvironmental pH Is a Key Factor for Exosome Traffic in Tumor Cells*. *Journal of Biological Chemistry* 284: 34211–34222

Peeters PM, Perkins TN, Wouters EFM, Mossman BT & Reynaert NL (2013) Silica induces NLRP3 inflammasome activation in human lung epithelial cells. *Particle and Fibre Toxicology* 10

Pegtel DM, Cosmopoulos K, Thorley-Lawson DA, van Eijndhoven MAJ, Hopmans ES, Lindenberg JL, de Gruijl TD, Würdinger T & Middeldorp JM (2010) Functional delivery of viral miRNAs via exosomes. *Proceedings of the National Academy of Sciences* 107: 6328–6333

Pelkmans L & Helenius A (2003) Insider information: what viruses tell us about endocytosis. *Current Opinion in Cell Biology* 15: 414–422

Perez GI, Broadbent D, Zarea AA, Dolgikh B, Bernard MP, Withrow A, McGill A, Toomajian V, Thampy LK, Harkema J, *et al* (2022) In Vitro and In Vivo Analysis of Extracellular Vesicle-Mediated Metastasis Using a Bright, Red-Shifted Bioluminescent Reporter Protein. *Adv Genet (Hoboken)* 3: 2100055

Perregaux D & Gabel CA (1994) Interleukin-1β maturation and release in response to ATP and nigericin. Evidence that potassium depletion mediated by these agents is a necessary and common feature of their activity. *Journal of Biological Chemistry* 269: 15195–15203

Perregaux DG, McNiff P, Laliberte R, Hawryluk N, Peurano H, Stam E, Eggler J, Griffiths R, Dombroski MA & Gabel CA (2001) Identification and characterization of a novel class of interleukin-1 post-translational processing inhibitors. *J Pharmacol Exp Ther* 299: 187–197

Phipson B, Lee S, Majewski IJ, Alexander WS & Smyth GK (2016) Robust hyperparameter estimation protects against hypervariable genes and improves power to detect differential expression. *The Annals of Applied Statistics* 10: 946–963

Pierrakos C, Velissaris D, Bisdorff M, Marshall JC & Vincent J-L (2020) Biomarkers of sepsis: time for a reappraisal. *Critical Care* 24: 287

Pisitkun T, Shen RF & Knepper MA (2004) Identification and proteomic profiling of exosomes in human urine. *Proceedings of the National Academy of Sciences of the United States of America* 101: 13368–13373

Pizzirani C, Ferrari D, Chiozzi P, Adinolfi E, Sandonà D, Savaglio E & Di Virgilio F (2007) Stimulation of P2 receptors causes release of IL-1β-loaded microvesicles from human dendritic cells. *Blood* 109: 3856–3864

Pober JS & Sessa WC (2007) Evolving functions of endothelial cells in inflammation. *Nat Rev Immunol* 7: 803–815

Polasek J (1982) The appearance of multivesicular structures during platelet activation as observed by scanning electron microscopy. *Thrombosis Research* 28: 433–437

Poliakov A, Spilman M, Dokland T, Amling CL & Mobley JA (2009) Structural heterogeneity and protein composition of exosome-like vesicles (prostasomes) in human semen. *The Prostate* 69: 159–167

Pope JE & Choy EH (2021) C-reactive protein and implications in rheumatoid arthritis and associated comorbidities. *Seminars in Arthritis and Rheumatism* 51: 219–229

Porter DW, Ye J, Ma J, Barger M, Robinson VA, Ramsey D, McLaurin J, Khan A, Landsittel D, Teass A, *et al* (2002) TIME COURSE OF PULMONARY RESPONSE OF RATS TO INHALATION OF CRYSTALLINE SILICA: NF-kappa B ACTIVATION, INFLAMMATION, CYTOKINE PRODUCTION, AND DAMAGE. *Inhalation Toxicology* 14: 349–367

Poyet JL, Srinivasula SM, Tnani M, Razmara M, Fernandes-Alnemri T & Alnemri ES (2001) Identification of Ipaf, a human caspase-1-activating protein related to Apaf-1. *The Journal of biological chemistry* 276: 28309–13

Pradeu T (2020) Philosophy of Immunology. *Elements in the Philosophy of Biology*

Prieur X, Rőszer T & Ricote M (2010) Lipotoxicity in macrophages: evidence from diseases associated with the metabolic syndrome. *Biochimica et Biophysica Acta (BBA) - Molecular and Cell Biology of Lipids* 1801: 327–337

Primiano MJ, Lefker BA, Bowman MR, Bree AG, Hubeau C, Bonin PD, Mangan M, Dower K, Monks BG, Cushing L, *et al* (2016) Efficacy and Pharmacology of the NLRP3 Inflammasome Inhibitor CP-456,773 (CRID3) in Murine Models of Dermal and Pulmonary Inflammation. *The Journal of Immunology* 197: 2421–2433

Puhm F, Afonyushkin T, Resch U, Obermayer G, Rohde M, Penz T, Schuster M, Wagner G, Rendeiro AF, Melki I, *et al* (2019) Mitochondria Are a Subset of Extracellular Vesicles Released by Activated Monocytes and Induce Type I IFN and TNF Responses in Endothelial Cells. *Circulation research* 125: 43–52

Puren AJ, Fantuzzi G & Dinarello CA (1999) Gene expression, synthesis, and secretion of interleukin 18 and interleukin 1β are differentially regulated in human blood mononuclear cells and mouse spleen cells. *Proceedings of the National Academy of Sciences* 96: 2256–2261

Qi L, Ge W, Pan C, Jiang W, Lin D & Zhang L (2023) Compromised osteogenic effect of exosomes internalized by senescent bone marrow stem cells via endocytoses involving clathrin, macropinocytosis and caveolae. *Frontiers in Bioengineering and Biotechnology* 10

Qu Y, Franchi L, Nunez G & Dubyak GR (2007) Nonclassical IL-1β Secretion Stimulated by P2X7 Receptors Is Dependent on Inflammasome Activation and Correlated with Exosome Release in Murine Macrophages. *The Journal of Immunology* 179: 1913–1925

Qu Y, Ramachandra L, Mohr S, Franchi L, Harding CV, Nunez G & Dubyak GR (2009) P2X7 Receptor-Stimulated Secretion of MHC Class II-Containing Exosomes Requires the ASC/NLRP3 Inflammasome but Is Independent of Caspase-1. *The Journal of Immunology* 182: 5052–5062

R Core Team (2022) R: A Language and Environment for Statistical Computing.

Raivo K (2019) pheatmap: Pretty Heatmaps.

Rajamäki K, Lappalainen J, Öörni K, Välimäki E, Matikainen S, Kovanen PT & Eklund KK (2010) Cholesterol Crystals Activate the NLRP3 Inflammasome in Human Macrophages: A Novel Link between Cholesterol Metabolism and Inflammation. *PLOS ONE* 5: e11765

Ramachandra L, Qu Y, Wang Y, Lewis CJ, Cobb BA, Takatsu K, Boom WH, Dubyak GR & Harding CV (2010) Mycobacterium tuberculosis synergizes with ATP to induce release of microvesicles and exosomes containing major histocompatibility complex class II molecules capable of antigen presentation. *Infect Immun* 78: 5116–5125

Ramachandran P, Dobie R, Wilson-Kanamori JR, Dora EF, Henderson BEP, Luu NT, Portman JR, Matchett KP, Brice M, Marwick JA, *et al* (2019) Resolving the fibrotic niche of human liver cirrhosis at single-cell level. *Nature* 575: 512–518

Ramirez MLG, Poreba M, Snipas SJ, Groborz K, Drag M & Salvesen GS (2018) Extensive peptide and natural protein substrate screens reveal that mouse caspase-11 has much narrower substrate specificity than caspase-1. *Journal of Biological Chemistry* 293: 7058–7067

Raposo G, Nijman HW, Stoorvogel W, Leijendekker R, Harding CV, Melief CJM & Geuze HJ (1996) B lymphocytes secrete antigen-presenting vesicles. *Journal of Experimental Medicine* 183: 1161–1172

Ratajczak J, Miekus K, Kucia M, Zhang J, Reca R, Dvorak P & Ratajczak MZ (2006) Embryonic stem cell-derived microvesicles reprogram hematopoietic progenitors: Evidence for horizontal transfer of mRNA and protein delivery. *Leukemia* 20: 847–856

Rathinam VAK, Zhao Y & Shao F (2019) Innate immunity to intracellular LPS. *Nat Immunol* 20: 527–533

Reddel RR, Ke Y, Gerwin BI, McMenamin MG, Lechner JF, Su RT, Brash DE, Park JB, Rhim JS & Harris CC (1988) Transformation of Human Bronchial Epithelial Cells by Infection with SV40 or Adenovirus-12 SV40 Hybrid Virus, or Transfection via Strontium Phosphate Coprecipitation with a Plasmid Containing SV40 Early Region Genes. *Cancer Research* 48: 1904–1909

Rennick JJ, Johnston APR & Parton RG (2021) Key principles and methods for studying the endocytosis of biological and nanoparticle therapeutics. *Nat Nanotechnol* 16: 266–276

Riazanski V, Mauleon G, Lucas K, Walker S, Zimnicka AM, McGrath JL & Nelson DJ (2022) Real time imaging of single extracellular vesicle pH regulation in a microfluidic cross-flow filtration platform. *Commun Biol* 5: 1–13

Richards N, Schaner P, Diaz A, Stuckey J, Shelden E, Wadhwa A & Gumucio DL (2001) Interaction between Pyrin and the Apoptotic Speck Protein (ASC) Modulates ASC-induced Apoptosis*. *Journal of Biological Chemistry* 276: 39320–39329

Ridker PM, Everett BM, Thuren T, MacFadyen JG, Chang WH, Ballantyne C, Fonseca F, Nicolau J, Koenig W, Anker SD, *et al* (2017) Antiinflammatory Therapy with Canakinumab for Atherosclerotic Disease. *N Engl J Med* 377: 1119–1131

Ripa I, Andreu S, López-Guerrero JA & Bello-Morales R (2021) Membrane Rafts: Portals for Viral Entry. *Frontiers in Microbiology* 12

Ritchie ME, Phipson B, Wu D, Hu Y, Law CW, Shi W & Smyth GK (2015) limma powers differential expression analyses for RNA-sequencing and microarray studies. *Nucleic Acids Research* 43: e47–e47

Rittling SR (2011) Osteopontin in macrophage function. *Expert Reviews in Molecular Medicine* 13: e15

Roberts TL, Idris A, Dunn JA, Kelly GM, Burnton CM, Hodgson S, Hardy LL, Garceau V, Sweet MJ, Ross IL, *et al* (2009) HIN-200 proteins regulate caspase activation in response to foreign cytoplasmic DNA. *Science (New York, NY)* 323: 1057–60

Robertson MJ, Mier JW, Logan T, Atkins M, Koon H, Koch KM, Kathman S, Pandite LN, Oei C, Kirby LC, *et al* (2006) Clinical and Biological Effects of Recombinant Human Interleukin-18 Administered by Intravenous Infusion to Patients with Advanced Cancer. *Clinical Cancer Research* 12: 4265–4273

Robinson MD, McCarthy DJ & Smyth GK (2010) edgeR: a Bioconductor package for differential expression analysis of digital gene expression data. *Bioinformatics* 26: 139–140

Robinson MD & Oshlack A (2010) A scaling normalization method for differential expression analysis of RNA-seq data. *Genome Biology* 11: 1–9

Rodríguez-Alcázar JF, Ataide MA, Engels G, Schmitt-Mabmunyo C, Garbi N, Kastenmüller W, Latz E & Franklin BS (2019) Charcot–Leyden Crystals Activate the NLRP3 Inflammasome and Cause IL-1β Inflammation in Human Macrophages. *The Journal of Immunology* 202: 550–558

Rogers C, Erkes DA, Nardone A, Aplin AE, Fernandes-Alnemri T & Alnemri ES (2019) Gasdermin pores permeabilize mitochondria to augment caspase-3 activation during apoptosis and inflammasome activation. *Nat Commun* 10: 1689

Rolfes V, Ribeiro LS, Hawwari I, Böttcher L, Rosero N, Maasewerd S, Santos MLS, Próchnicki T, Silva CM de S, Wanderley CW de S, *et al* (2020) Platelets Fuel the Inflammasome Activation of Innate Immune Cells. *Cell Rep* 31: 107615

Roth GA, Mensah GA, Johnson CO, Addolorato G, Ammirati E, Baddour LM, Barengo NC, Beaton AZ, Benjamin EJ, Benziger CP, *et al* (2020) Global Burden of Cardiovascular Diseases and Risk Factors, 1990–2019. *Journal of the American College of Cardiology* 76: 2982–3021

Roth-Isigkeit A, Hasselbach L, Ocklitz E, Brückner S, Ros A, Gehring H, Schmucker P, Rink L & Seyfarth M (2001) Inter-individual differences in cytokine release in patients undergoing cardiac surgery with cardiopulmonary bypass. *Clin Exp Immunol* 125: 80–88

RStudio Team (2022) RStudio: Integrated Development Environment for R.

Rubartelli A, Cozzolino F, Talio M & Sitia R (1990) A novel secretory pathway for interleukin-1 beta, a protein lacking a signal sequence. *The EMBO Journal* 9: 1503–1510

Rühl S, Shkarina K, Demarco B, Heilig R, Santos JC & Broz P (2018) ESCRT-dependent membrane repair negatively regulates pyroptosis downstream of GSDMD activation. *Science (New York, NY)* 362: 956–960

Russell AE, Sneider A, Witwer KW, Bergese P, Bhattacharyya SN, Cocks A, Cocucci E, Erdbrügger U, Falcon-Perez JM, Freeman DW, *et al* (2019) Biological membranes in EV biogenesis, stability, uptake, and cargo transfer: an ISEV position paper arising from the ISEV membranes and EVs workshop. *Journal of Extracellular Vesicles* 8: 1684862

Saberi M, Woods N-B, de Luca C, Schenk S, Lu JC, Bandyopadhyay G, Verma IM & Olefsky JM (2009) Hematopoietic Cell-Specific Deletion of Toll-like Receptor 4 Ameliorates Hepatic and Adipose Tissue Insulin Resistance in High-Fat-Fed Mice. *Cell Metabolism* 10: 419–429

Sahdo B, Fransén K, Asfaw Idosa B, Eriksson P, Söderquist B, Kelly A & Särndahl E (2013) Cytokine profile in a cohort of healthy blood donors carrying polymorphisms in genes encoding the NLRP3 inflammasome. *PloS one* 8

Sancho-Albero M, Navascués N, Mendoza G, Sebastián V, Arruebo M, Martín-Duque P & Santamaría J (2019) Exosome origin determines cell targeting and the transfer of therapeutic nanoparticles towards target cells. *Journal of Nanobiotechnology* 17: 16

Sanman LE, Qian Y, Eisele NA, Ng TM, van der Linden WA, Monack DM, Weerapana E & Bogyo M (2016) Disruption of glycolytic flux is a signal for inflammasome signaling and pyroptotic cell death. *eLife* 5: e13663

Santos JC, Boucher D, Schneider LK, Demarco B, Dilucca M, Shkarina K, Heilig R, Chen KW, Lim RYH & Broz P (2020) Human GBP1 binds LPS to initiate assembly of a caspase-4 activating platform on cytosolic bacteria. *Nature Communications* 11

Sarkar A, Mitra S, Mehta S, Raices R & Wewers MD (2009) Monocyte derived microvesicles deliver a cell death message via encapsulated caspase-1. *PLoS ONE* 4

Sborgi L, Rühl S, Mulvihill E, Pipercevic J, Heilig R, Stahlberg H, Farady CJ, Müller DJ, Broz P & Hiller S (2016) GSDMD membrane pore formation constitutes the mechanism of pyroptotic cell death. *The EMBO Journal* 35: 1766–1778

Scheiermann C, Kunisaki Y & Frenette PS (2013) Circadian control of the immune system. *Nat Rev Immunol* 13: 190–198

van Scheppingen J, Mills JD, Zimmer TS, Broekaart DWM, Iori V, Bongaarts A, Anink JJ, Iyer AM, Korotkov A, Jansen FE, *et al* (2018) miR147b: A novel key regulator of interleukin 1 beta-mediated inflammation in human astrocytes. *Glia* 66: 1082–1097

Schindler R, Ghezzi P & Dinarello CA (1990a) IL-1 induces IL-1. IV. IFN-gamma suppresses IL-1 but not lipopolysaccharide-induced transcription of IL-1. *The Journal of Immunology* 144: 2216–2222

Schindler R, Mancilla J, Endres S, Ghorbani R, Clark SC & Dinarello CA (1990b) Correlations and Interactions in the Production of Interleukin-6 (IL-6), IL-1, and Tumor Necrosis Factor (TNF) in Human Blood Mononuclear Cells: IL-6 Suppresses IL-1 and TNF. *Blood* 75: 40–47

Schnittler H, Taha M, Schnittler MO, Taha AA, Lindemann N & Seebach J (2014) Actin filament dynamics and endothelial cell junctions: the Ying and Yang between stabilization and motion. *Cell and tissue research* 355: 529–543

Schroder K, Sagulenko V, Zamoshnikova A, Richards AA, Cridland JA, Irvine KM, Stacey KJ & Sweet MJ (2012) Acute lipopolysaccharide priming boosts inflammasome activation independently of inflammasome sensor induction. *Immunobiology* 217: 1325–9

Seckinger P, Lowenthal JW, Williamson K, Dayer JM & MacDonald HR (1987) A urine inhibitor of interleukin 1 activity that blocks ligand binding. *The Journal of Immunology* 139: 1546–1549

Segura E, Amigorena S & Théry C (2005) Mature dendritic cells secrete exosomes with strong ability to induce antigen-specific effector immune responses. *Blood Cells, Molecules, and Diseases* 35: 89–93

Sena LA, Li S, Jairaman A, Prakriya M, Ezponda T, Hildeman DA, Wang C-R, Schumacker PT, Licht JD, Perlman H, *et al* (2013) Mitochondria Are Required for Antigen-Specific T Cell Activation through Reactive Oxygen Species Signaling. *Immunity* 38: 225–236

Sender R, Fuchs S & Milo R (2016) Are We Really Vastly Outnumbered? Revisiting the Ratio of Bacterial to Host Cells in Humans. *Cell* 164: 337–340

Shah C, Yang G, Lee I, Bielawski J, Hannun YA & Samad F (2008) Protection from High Fat Diet-induced Increase in Ceramide in Mice Lacking Plasminogen Activator Inhibitor 1. *J Biol Chem* 283: 13538–13548

Shi C-S, Shenderov K, Huang N-N, Kabat J, Abu-Asab M, Fitzgerald KA, Sher A & Kehrl JH (2012) Activation of autophagy by inflammatory signals limits IL-1β production by targeting ubiquitinated inflammasomes for destruction. *Nat Immunol* 13: 255–263

Shi H, Kokoeva MV, Inouye K, Tzameli I, Yin H & Flier JS (2006) TLR4 links innate immunity and fatty acid–induced insulin resistance. *J Clin Invest* 116: 3015–3025

Shi J, Zhao Y, Wang K, Shi X, Wang Y, Huang H, Zhuang Y, Cai T, Wang F & Shao F (2015) Cleavage of GSDMD by inflammatory caspases determines pyroptotic cell death. *Nature* 526: 660–5

Shi J, Zhao Y, Wang Y, Gao W, Ding J, Li P, Hu L & Shao F (2014) Inflammatory caspases are innate immune receptors for intracellular LPS. *Nature* 514: 187–192

Shi L, Song L, Maurer K, Dou Y, Patel VR, Su C, Leonard ME, Lu S, Hodge KM, Torres A, *et al* (2020) IL-1 transcriptional responses to LPS are regulated by a complex of RNA-binding proteins. *J Immunol* 204: 1334–1344

Shook BA, Wasko RR, Rivera-Gonzalez GC, Salazar-Gatzimas E, López-Giráldez F, Dash BC, Muñoz-Rojas AR, Aultman KD, Zwick RK, Lei V, *et al* (2018) Myofibroblast proliferation and heterogeneity are supported by macrophages during skin repair. *Science* 362: eaar2971

Sidhu SS, Mengistab AT, Tauscher AN, LaVail J & Basbaum C (2004) The microvesicle as a vehicle for EMMPRin in tumor-stromal interactions. *Oncogene* 23: 956–963

Sims PJ, Wiedmer T, Esmon CT, Weiss HJ & Shattil SJ (1989) Assembly of the Platelet Prothrombinase Complex Is Linked to Vesiculation of the Platelet Plasma Membrane: Studies in scott syndrome: an isolated defect in platelet procoagulant activity. *Journal of Biological Chemistry* 264: 17049–17057

Singh PP, Li L & Schorey JS (2015) Exosomal RNA from Mycobacterium tuberculosis-Infected Cells Is Functional in Recipient Macrophages. *Traffic* 16: 555–571

Skokos D, Botros HG, Demeure C, Morin J, Peronet R, Birkenmeier G, Boudaly S & Mécheri S (2003) Mast Cell-Derived Exosomes Induce Phenotypic and Functional Maturation of Dendritic Cells and Elicit Specific Immune Responses In Vivo. *The Journal of Immunology* 170: 3037–3045

Skriner K, Adolph K, Jungblut PR & Burmester GR (2006) Association of citrullinated proteins with synovial exosomes. *Arthritis and Rheumatism* 54: 3809–3814

Sneezum L, Eislmayr K, Dworak H, Sedlyarov V, Le Heron A, Ebner F, Fischer I, Iwakura Y & Kovarik P (2020) Context-Dependent IL-1 mRNA-Destabilization by TTP Prevents Dysregulation of Immune Homeostasis Under Steady State Conditions. *Front Immunol* 11: 1398

Song N & Li T (2018) Regulation of NLRP3 Inflammasome by Phosphorylation. *Frontiers in Immunology* 9: 2305

Song N, Liu Z-S, Xue W, Bai Z-F, Wang Q-Y, Dai J, Liu X, Huang Y-J, Cai H, Zhan X-Y, *et al* (2017) NLRP3 Phosphorylation Is an Essential Priming Event for Inflammasome Activation. *Molecular cell* 68: 185-197.e6

Sproston NR & Ashworth JJ (2018) Role of C-Reactive Protein at Sites of Inflammation and Infection. *Front Immunol* 9: 754

Stein JM & Luzio JP (1991) Ectocytosis caused by sublytic autologous complement attack on human neutrophils. The sorting of endogenous plasma-membrane proteins and lipids into shed vesicles. *Biochemical Journal* 274: 381–386

Stewart CE, Torr EE, Mohd Jamili NH, Bosquillon C & Sayers I (2012) Evaluation of Differentiated Human Bronchial Epithelial Cell Culture Systems for Asthma Research. *Journal of Allergy* 2012: 1–11

Stewart CR, Stuart LM, Wilkinson K, van Gils JM, Deng J, Halle A, Rayner KJ, Boyer L, Zhong R, Frazier WA, *et al* (2010) CD36 ligands promote sterile inflammation through assembly of a Toll-like receptor 4 and 6 heterodimer. *Nat Immunol* 11: 155–161

Strowitzki MJ, Nelson R, Garcia MP, Tuffs C, Bleul MB, Fitzsimons S, Navas J, Uzieliene I, Ritter AS, Phelan D, *et al* (2022) Carbon Dioxide Sensing by Immune Cells Occurs through Carbonic Anhydrase 2–Dependent Changes in Intracellular pH. *The Journal of Immunology* 208: 2363–2375

Stutz A, Horvath GL, Monks BG & Latz E (2013) ASC speck formation as a readout for inflammasome activation. *Methods Mol Biol* 1040: 91–101

Subra C, Grand D, Laulagnier K, Stella A, Lambeau G, Paillasse M, De Medina P, Monsarrat B, Perret B, Silvente-Poirot S, *et al* (2010) Exosomes account for vesicle-mediated transcellular transport of activatable phospholipases and prostaglandins. *Journal of Lipid Research* 51: 2105–2120

Subramanian A, Tamayo P, Mootha VK, Mukherjee S, Ebert BL, Gillette MA, Paulovich A, Pomeroy SL, Golub TR, Lander ES, *et al* (2005) Gene set enrichment analysis: A knowledge-based approach for interpreting genome-wide expression profiles. *Proceedings of the National Academy of Sciences* 102: 15545–15550

Subramanian SL, Kitchen RR, Alexander R, Carter BS, Cheung KH, Laurent LC, Pico A, Roberts LR, Roth ME, Rozowsky JS, *et al* (2015) Integration of extracellular RNA profiling data using metadata, biomedical ontologies and Linked Data technologies. *Journal of Extracellular Vesicles* 4

Sugawara S, Uehara A, Nochi T, Yamaguchi T, Ueda H, Sugiyama A, Hanzawa K, Kumagai K, Okamura H & Takada H (2001) Neutrophil Proteinase 3-Mediated Induction of Bioactive IL-18 Secretion by Human Oral Epithelial Cells1. *The Journal of Immunology* 167: 6568–6575

Sung BH, Ketova T, Hoshino D, Zijlstra A & Weaver AM (2015) Directional cell movement through tissues is controlled by exosome secretion. *Nature Communications* 6

Sung BH, von Lersner A, Guerrero J, Krystofiak ES, Inman D, Pelletier R, Zijlstra A, Ponik SM & Weaver AM (2020) A live cell reporter of exosome secretion and uptake reveals pathfinding behavior of migrating cells. *Nature Communications* 11

Sur S, Steele R, Isbell TS, Ray R & Ray RB (2022) Circulatory Exosomes from COVID-19 Patients Trigger NLRP3 Inflammasome in Endothelial Cells. *mBio* 13: e00951-22

Sutterwala FS, Ogura Y, Szczepanik M, Lara-Tejero M, Lichtenberger GS, Grant EP, Bertin J, Coyle AJ, Galán JE, Askenase PW, *et al* (2006) Critical Role for NALP3/CIAS1/Cryopyrin in Innate and Adaptive Immunity through Its Regulation of Caspase-1. *Immunity* 24: 317–327

Suzuki H, Forrest ARR, van Nimwegen E, Daub CO, Balwierz PJ, Irvine KM, Lassmann T, Ravasi T, Hasegawa Y, de Hoon MJL, *et al* (2009) The transcriptional network that controls growth arrest and differentiation in a human myeloid leukemia cell line. *Nat Genet* 41: 553–562

Svensson KJ, Christianson HC, Wittrup A, Bourseau-Guilmain E, Lindqvist E, Svensson LM, Mörgelin M & Belting M (2013) Exosome Uptake Depends on ERK1/2-Heat Shock Protein 27 Signaling and Lipid Raft-mediated Endocytosis Negatively Regulated by Caveolin-1*. *Journal of Biological Chemistry* 288: 17713–17724

Swanson KV, Deng M & Ting JPY (2019) The NLRP3 inflammasome: molecular activation and regulation to therapeutics. *Nature Reviews Immunology* 19: 477–489

Szmitko PE, Wang CH, Weisel RD, De Almeida JR, Anderson TJ & Verma S (2003) New Markers of Inflammation and Endothelial Cell Activation Part I. *Circulation* 108: 1917–1923

Takahashi Y, Nishikawa M, Shinotsuka H, Matsui Y, Ohara S, Imai T & Takakura Y (2013) Visualization and in vivo tracking of the exosomes of murine melanoma B16-BL6 cells in mice after intravenous injection. *J Biotechnol* 165: 77–84

Takeda K, Tsutsui H, Yoshimoto T, Adachi O, Yoshida N, Kishimoto T, Okamura H, Nakanishi K & Akira S (1998) Defective NK Cell Activity and Th1 Response in IL-18–Deficient Mice. *Immunity* 8: 383–390

Tang X, Lu H, Dooner M, Chapman S, Quesenberry PJ & Ramratnam B (2018) Exosomal Tat protein activates latent HIV-1 in primary, resting $CD4^+$ T lymphocytes. *JCI Insight* 3

Temchura VV, Tenbusch M, Nchinda G, Nabi G, Tippler B, Zelenyuk M, Wildner O, Überla K & Kuate S (2008) Enhancement of immunostimulatory properties of exosomal vaccines by incorporation of fusion-competent G protein of vesicular stomatitis virus. *Vaccine* 26: 3662–3672

Thakur BK, Zhang H, Becker A, Matei I, Huang Y, Costa-Silva B, Zheng Y, Hoshino A, Brazier H, Xiang J, *et al* (2014) Double-stranded DNA in exosomes: A novel biomarker in cancer detection. *Cell Research* 24: 766–769

Théry C, Regnault A, Garin J, Wolfers J, Zitvogel L, Ricciardi-Castagnoli P, Raposo G & Amigorena S (1999) Molecular characterization of dendritic cell-derived exosomes: Selective accumulation of the heat shock protein hsc73. *Journal of Cell Biology* 147: 599–610

Théry C, Witwer KW, Aikawa E, Alcaraz MJ, Anderson JD, Andriantsitohaina R, Antoniou A, Arab T, Archer F, Atkin-Smith GK, *et al* (2018) Minimal information for studies of extracellular vesicles 2018 (MISEV2018): a position statement of the International Society for Extracellular Vesicles and update of the MISEV2014 guidelines. *Journal of Extracellular Vesicles* 7

Thornberry NA, Bull HG, Calaycay JR, Chapman KT, Howard AD, Kostura MJ, Miller DK, Molineaux SM, Weidner JR & Aunins J (1992) A novel heterodimeric cysteine protease is required for interleukin-1 beta processing in monocytes. *Nature* 356: 768–74

Tian T, Wang Y, Wang H, Zhu Z & Xiao Z (2010) Visualizing of the cellular uptake and intracellular trafficking of exosomes by live-cell microscopy. *Journal of Cellular Biochemistry* 111: 488–496

Tian T, Zhu Y-L, Zhou Y-Y, Liang G-F, Wang Y-Y, Hu F-H & Xiao Z-D (2014) Exosome Uptake through Clathrin-mediated Endocytosis and Macropinocytosis and Mediating miR-21 Delivery*. *Journal of Biological Chemistry* 289: 22258–22267

Tkach M, Kowal J, Zucchetti AE, Enserink L, Jouve M, Lankar D, Saitakis M, Martin-Jaular L & Théry C (2017) Qualitative differences in T-cell activation by dendritic cell-derived extracellular vesicle subtypes. *The EMBO Journal* 36: 3012–3028

Toribio V, Morales S, López-Martín S, Cardeñes B, Cabañas C & Yáñez-Mó M (2019) Development of a quantitative method to measure EV uptake. *Sci Rep* 9: 10522

Tóth EÁ, Turiák L, Visnovitz T, Cserép C, Mázló A, Sódar BW, Försönits AI, Petővári G, Sebestyén A, Komlósi Z, *et al* (2021) Formation of a protein corona on the surface of extracellular vesicles in blood plasma. *Journal of Extracellular Vesicles* 10: e12140

Tran TAT, Grievink HW, Lipinska K, Kluft C, Burggraaf J, Moerland M, Tasev D & Malone KE (2019) Whole blood assay as a model for in vitro evaluation of inflammasome activation and subsequent caspase-mediated interleukin-1 beta release. *PLOS ONE* 14: e0214999

Turchinovich A, Drapkina O & Tonevitsky A (2019) Transcriptome of Extracellular Vesicles: State-of-the-Art. *Frontiers in Immunology* 10

Valadi H, Ekström K, Bossios A, Sjöstrand M, Lee JJ & Lötvall JO (2007) Exosome-mediated transfer of mRNAs and microRNAs is a novel mechanism of genetic exchange between cells. *Nature Cell Biology* 9: 654–659

Van Niel G, D'Angelo G & Raposo G (2018) Shedding light on the cell biology of extracellular vesicles. *Nature Reviews Molecular Cell Biology* 19: 213–228

Van Niel G, Raposo G, Candalh C, Boussac M, Hershberg R, Cerf-Bensussan N & Heyman M (2001) Intestinal epithelial cells secrete exosome-like vesicles. *Gastroenterology* 121: 337–349

Vandanmagsar B, Youm Y-H, Ravussin A, Galgani JE, Stadler K, Mynatt RL, Ravussin E, Stephens JM & Dixit VD (2011) The NLRP3 inflammasome instigates obesity-induced inflammation and insulin resistance. *Nat Med* 17: 179–188

Vella LJ, Greenwood DLV, Cappai R, Scheerlinck JPY & Hill AF (2008) Enrichment of prion protein in exosomes derived from ovine cerebral spinal fluid. *Veterinary Immunology and Immunopathology* 124: 385–393

Verweij FJ, Revenu C, Arras G, Dingli F, Loew D, Pegtel DM, Follain G, Allio G, Goetz JG, Zimmermann P, *et al* (2019) Live Tracking of Inter-organ Communication by Endogenous Exosomes In Vivo. *Developmental Cell* 48: 573-589.e4

Vickers KC, Palmisano BT, Shoucri BM, Shamburek RD & Remaley AT (2011) MicroRNAs are transported in plasma and delivered to recipient cells by high-density lipoproteins. *Nature Cell Biology* 13: 423–435

Viganò E, Diamond CE, Spreafico R, Balachander A, Sobota RM & Mortellaro A (2015) Human caspase-4 and caspase-5 regulate the one-step non-canonical inflammasome activation in monocytes. *Nat Commun* 6: 8761

Volchuk A, Ye A, Chi L, Steinberg BE & Goldenberg NM (2020) Indirect regulation of HMGB1 release by gasdermin D. *Nat Commun* 11: 4561

Vos T, Lim SS, Abbafati C, Abbas KM, Abbasi M, Abbasifard M, Abbasi-Kangevari M, Abbastabar H, Abd-Allah F, Abdelalim A, *et al* (2020) Global burden of 369 diseases and injuries in 204 countries and territories, 1990–2019: a systematic analysis for the Global Burden of Disease Study 2019. *The Lancet* 396: 1204–1222

Wandel MP, Kim B-H, Park E-S, Boyle KB, Nayak K, Lagrange B, Herod A, Henry T, Zilbauer M, Rohde J, *et al* (2020) Guanylate-binding proteins convert cytosolic bacteria into caspase-4 signaling platforms. *Nat Immunol* 21: 880–891

Wang A, Zheng N, Jia Q, Chen Y & Xu S (2022) S100A9-containing serum exosomes obtained from patients with burn injuries promote myocardial cell pyroptosis through NLRP3. *Exp Ther Med* 24: 646

Wang G, Jin S, Huang W, Li Y, Wang J, Ling X, Huang Y, Hu Y, Li C, Meng Y, *et al* (2021) LPS-induced macrophage HMGB1-loaded extracellular vesicles trigger hepatocyte pyroptosis by activating the NLRP3 inflammasome. *Cell Death Discov* 7: 1–11

Wang H, Bloom O, Zhang M, Vishnubhakat JM, Ombrellino M, Che J, Frazier A, Yang H, Ivanova S, Borovikova L, *et al* (1999) HMG-1 as a late mediator of endotoxin lethality in mice. *Science* 285: 248–251

Wang J-G, Williams JC, Davis BK, Jacobson K, Doerschuk CM, Ting JP-Y & Mackman N (2011) Monocytic microparticles activate endothelial cells in an IL-1β–dependent manner. *Blood* 118: 2366–2374

Warner SJ, Auger KR & Libby P (1987a) Human interleukin 1 induces interleukin 1 gene expression in human vascular smooth muscle cells. *Journal of Experimental Medicine* 165: 1316–1331

Warner SJ, Auger KR & Libby P (1987b) Interleukin 1 induces interleukin 1. II. Recombinant human interleukin 1 induces interleukin 1 production by adult human vascular endothelial cells. *The Journal of Immunology* 139: 1911–1917

Warren BA & Vales O (1972) The Release of Vesicles from Platelets Following Adhesion to Vessel Walls In Vitro. *British Journal of Experimental Pathology* 53: 206

Watson DC, Bayik D, Srivatsan A, Bergamaschi C, Valentin A, Niu G, Bear J, Monninger M, Sun M, Morales-Kastresana A, *et al* (2016) Efficient production and enhanced tumor delivery of engineered extracellular vesicles. *Biomaterials* 105: 195–205

Wen H, Gris D, Lei Y, Jha S, Zhang L, Huang MT-H, Brickey WJ & Ting JP-Y (2011) Fatty acid–induced NLRP3-ASC inflammasome activation interferes with insulin signaling. *Nat Immunol* 12: 408–415

Werman A, Werman-Venkert R, White R, Lee J-K, Werman B, Krelin Y, Voronov E, Dinarello CA & Apte RN (2004) The precursor form of IL-1α is an intracrine proinflammatory activator of transcription. *Proceedings of the National Academy of Sciences* 101: 2434–2439

Wessendorf JH, Garfinkel S, Zhan X, Brown S & Maciag T (1993) Identification of a nuclear localization sequence within the structure of the human interleukin-1 alpha precursor. *Journal of Biological Chemistry* 268: 22100–22104

White ES, Thomas M, Stowasser S & Tetzlaff K (2022) Challenges for Clinical Drug Development in Pulmonary Fibrosis. *Frontiers in Pharmacology* 13

White JM & Whittaker GR (2016) Fusion of Enveloped Viruses in Endosomes. *Traffic* 17: 593–614

Wieland T, Faulstich H & Fiume L (2008) Amatoxins, Phallotoxins, Phallolysin, and Antamanide: The Biologically Active Components of Poisonous Amanita Mushroom. *http://dx.doi.org/103109/10409237809149870* 5: 185–260

Wight TN, Kang I, Evanko SP, Harten IA, Chang MY, Pearce OMT, Allen CE & Frevert CW (2020) Versican—A Critical Extracellular Matrix Regulator of Immunity and Inflammation. *Frontiers in Immunology* 11: 512

Wight TN, Kinsella MG, Evanko SP, Potter-Perigo S & Merrilees MJ (2014) Versican and the regulation of cell phenotype in disease. *Biochimica et Biophysica Acta (BBA) - General Subjects* 1840: 2441–2451

Wilson KP, Black J-AF, Thomson JA, Kim EE, Griffith JP, Navia MA, Murcko MA, Chambers SP, Aldape RA, Raybuck SA, *et al* (1994) Structure and mechanism of interleukin-lβ converting enzyme. *Nature* 370: 270–275

Wolf AJ, Reyes CN, Liang W, Becker C, Shimada K, Wheeler ML, Cho HC, Popescu NI, Coggeshall KM, Arditi M, *et al* (2016) Hexokinase Is an Innate Immune Receptor for the Detection of Bacterial Peptidoglycan. *Cell* 166: 624–636

Wolf P (1967) The nature and significance of platelet products in human plasma. *British journal of haematology* 13: 269–288

World Health Organisation (2022) Noncommunicable diseases.

Wozniak AL, Adams A, King KE, Dunn W, Christenson LK, Hung W-T & Weinman SA (2020) The RNA binding protein FMR1 controls selective exosomal miRNA cargo loading during inflammation. *Journal of Cell Biology* 219: e201912074

Wu D, Dinh TL, Bausk BP & Walt DR (2017) Long-Term Measurements of Human Inflammatory Cytokines Reveal Complex Baseline Variations between Individuals. *The American Journal of Pathology* 187: 2620–2626

Wu D & Smyth GK (2012) Camera: a competitive gene set test accounting for inter-gene correlation. *Nucleic Acids Research* 40: e133

Wu Y, Di X, Zhao M, Li H, Bai L & Wang K (2022) The role of the NLRP3 inflammasome in chronic inflammation in asthma and chronic obstructive pulmonary disease. *Immunity, Inflammation and Disease* 10: e750

Wulf E, Deboben A, Bautz FA, Faulstich H & Wieland T (1979) Fluorescent phallotoxin, a tool for the visualization of cellular actin. *Proceedings of the National Academy of Sciences of the United States of America* 76: 4498–4502

Wynn TA (2011) Integrating mechanisms of pulmonary fibrosis. *Journal of Experimental Medicine* 208: 1339–1350

Xia S, Zhang Z, Magupalli VG, Pablo JL, Dong Y, Vora SM, Wang L, Fu T-M, Jacobson MP, Greka A, *et al* (2021) Gasdermin D pore structure reveals preferential release of mature interleukin-1. *Nature* 593: 607–611

Xiang M, Shi X, Li Y, Xu J, Yin L, Xiao G, Scott MJ, Billiar TR, Wilson MA & Fan J (2011) Hemorrhagic Shock Activation of NLRP3 Inflammasome in Lung Endothelial Cells. *The Journal of Immunology* 187: 4809–4817

Xiao J, Wang C, Yao J-C, Alippe Y, Xu C, Kress D, Civitelli R, Abu-Amer Y, Kanneganti T-D, Link DC, *et al* (2018) Gasdermin D mediates the pathogenesis of neonatal-onset multisystem inflammatory disease in mice. *PLOS Biology* 16: e3000047

Xu H, Yang J, Gao W, Li L, Li P, Zhang L, Gong Y-N, Peng X, Xi JJ, Chen S, *et al* (2014) Innate immune sensing of bacterial modifications of Rho GTPases by the Pyrin inflammasome. *Nature* 513: 237–241

Xu J & Núñez G (2022) The NLRP3 inflammasome: activation and regulation. *Trends in Biochemical Sciences*

Xu Z-H, Miao Z-W, Jiang Q-Z, Gan D-X, Wei X-G, Xue X-Z, Li J-Q, Zheng F, Qin X-X, Fang W-G, *et al* (2019) Brain microvascular endothelial cell exosome–mediated S100A16 up-regulation confers small-cell lung cancer cell survival in brain. *The FASEB Journal* 33: 1742–1757

Yamauchi Y & Helenius A (2013) Virus entry at a glance. *Journal of Cell Science* 126: 1289–1295

Yang D, He Y, Muñoz-Planillo R, Liu Q & Núñez G (2015) Caspase-11 Requires the Pannexin-1 Channel and the Purinergic P2X7 Pore to Mediate Pyroptosis and Endotoxic Shock. *Immunity* 43: 923–932

Yang H, Hreggvidsdottir HS, Palmblad K, Wang H, Ochani M, Li J, Lu B, Chavan S, Rosas-Ballina M, Al-Abed Y, *et al* (2010) A critical cysteine is required for HMGB1 binding to Toll-like receptor 4 and activation of macrophage cytokine release. *Proceedings of the National Academy of Sciences* 107: 11942–11947

Yang H, Ochani M, Li J, Qiang X, Tanovic M, Harris HE, Susarla SM, Ulloa L, Wang H, DiRaimo R, *et al* (2004) Reversing established sepsis with antagonists of endogenous high-mobility group box 1. *Proceedings of the National Academy of Sciences* 101: 296–301

Yasuda K, Nakanishi K & Tsutsui H (2019) Interleukin-18 in Health and Disease. *International Journal of Molecular Sciences* 20: 649

Ye S-B, Zhang H, Cai T-T, Liu Y-N, Ni J-J, He J, Peng J-Y, Chen Q-Y, Mo H-Y, Jun-Cui, *et al* (2016) Exosomal miR-24-3p impedes T-cell function by targeting FGF11 and serves as a potential prognostic biomarker for nasopharyngeal carcinoma. *The Journal of Pathology* 240: 329–340

Yi G, Liang M, Li M, Fang X, Liu J, Lai Y, Chen J, Yao W, Feng X, Hu L, *et al* (2018) A large lung gene expression study identifying IL1B as a novel player in airway inflammation in COPD airway epithelial cells. *Inflamm Res* 67: 539–551

Yoon Y-K, Kim H-P, Han S-W, Oh DY, Im S-A, Bang Y-J & Kim T-Y (2010) KRAS mutant lung cancer cells are differentially responsive to MEK inhibitor due to AKT or STAT3 activation: Implication for combinatorial approach. *Molecular Carcinogenesis* 49: 353–362

Yu J-W, Wu J, Zhang Z, Datta P, Ibrahimi I, Taniguchi S, Sagara J, Fernandes-Alnemri T & Alnemri ES (2006a) Cryopyrin and pyrin activate caspase-1, but not NF-kappaB, via ASC oligomerization. *Cell death and differentiation* 13: 236–49

Yu M, Wang H, Ding A, Golenbock DT, Latz E, Czura CJ, Fenton MJ, Tracey KJ & Yang H (2006b) HMGB1 SIGNALS THROUGH TOLL-LIKE RECEPTOR (TLR) 4 AND TLR2. *Shock* 26: 174

Zanin N, Viaris de Lesegno C, Lamaze C & Blouin CM (2021) Interferon Receptor Trafficking and Signaling: Journey to the Cross Roads. *Front Immunol* 11: 615603

Zanin N, Viaris de Lesegno C, Podkalicka J, Meyer T, Gonzalez Troncoso P, Bun P, Danglot L, Chmiest D, Urbé S, Piehler J, *et al* (2023) STAM and Hrs interact sequentially with IFN-α Receptor to control spatiotemporal JAK–STAT endosomal activation. *Nat Cell Biol* 25: 425–438

Zanoni I, Tan Y, Di Gioia M, Broggi A, Ruan J, Shi J, Donado CA, Shao F, Wu H, Springstead JR, *et al* (2016) An endogenous caspase-11 ligand elicits interleukin-1 release from living dendritic cells. *Science* 352: 1232–1236

Zasłona Z, Flis E, Wilk MM, Carroll RG, Palsson-McDermott EM, Hughes MM, Diskin C, Banahan K, Ryan DG, Hooftman A, *et al* (2020) Caspase-11 promotes allergic airway inflammation. *Nature Communications* 11

Zech D, Rana S, Büchler MW & Zöller M (2012) Tumor-exosomes and leukocyte activation: an ambivalent crosstalk. *Cell Communication and Signaling* 10: 37

Zhang J (2022) Biomarkers of endothelial activation and dysfunction in cardiovascular diseases. *Reviews in Cardiovascular Medicine* 23

Zhang L, Yu J, Pan H, Hu P, Hao Y, Cai W, Zhu H, Yu AD, Xie X, Ma D, *et al* (2007) Small molecule regulators of autophagy identified by an image-based high-throughput screen. *Proceedings of the National Academy of Sciences* 104: 19023–19028

Zhang M-Y, Jiang Y-X, Yang Y-C, Liu J-Y, Huo C, Ji X-L & Qu Y-Q (2021) Cigarette smoke extract induces pyroptosis in human bronchial epithelial cells through the ROS/NLRP3/caspase-1 pathway. *Life Sciences* 269: 119090

Zhang S, Reljić B, Liang C, Kerouanton B, Francisco JC, Peh JH, Mary C, Jagannathan NS, Olexiouk V, Tang C, *et al* (2020) Mitochondrial peptide BRAWNIN is essential for vertebrate respiratory complex III assembly. *Nat Commun* 11: 1312

Zhang Y, Lee TC, Guillemin B, Yu MC & Rom WN (1993) Enhanced IL-1 beta and tumor necrosis factor-alpha release and messenger RNA expression in macrophages from idiopathic pulmonary fibrosis or after asbestos exposure. *Journal of immunology (Baltimore, Md : 1950)* 150: 4188–96

Zhou T, Damsky W, Weizman O-E, McGeary MK, Hartmann KP, Rosen CE, Fischer S, Jackson R, Flavell RA, Wang J, *et al* (2020) IL-18BP is a secreted immune checkpoint and barrier to IL-18 immunotherapy. *Nature* 583: 609–614

Zhu Z, Zhang D, Lee H, Menon AA, Wu J, Hu K & Jin Y (2017) Macrophage-derived apoptotic bodies promote the proliferation of the recipient cells via shuttling microRNA-221/222. *Journal of Leukocyte Biology* 101: 1349–1359

Zitvogel L, Regnault A, Lozier A, Wolfers J, Flament C, Tenza D, Ricciardi-Castagnoli P, Raposo G & Amigorena S (1998) Eradication of established murine tumors using a novel cell-free vaccine: Dendritic cell-derived exosomes. *Nature Medicine* 4: 594–600